

**NUMERICAL OPTIMIZATION OF  
LONGITUDINAL MAGNETIC FIELD PROFILES  
OF A DIPOLE IN A LOW EMITTANCE LATTICE  
CELL**

*By*

**SURAJ PRAKASH  
PHYS03201802001**

**Raja Ramanna Centre for Advanced Technology, Indore**

*A thesis submitted to the  
Board of Studies in Physical Sciences  
In partial fulfillment of requirements*

*for the Degree of*

**MASTER OF PHILOSOPHY**

*of*

**HOMI BHABHA NATIONAL INSTITUTE**

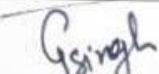
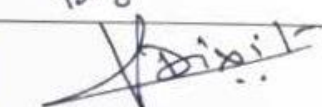
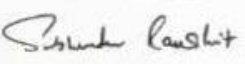
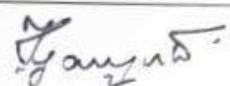
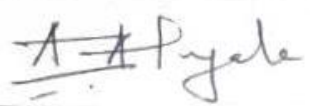


**January, 2021**

# Homi Bhabha National Institute

## Recommendations of the Thesis Examining Committee

As members of the Thesis Examining Committee, we recommend that the thesis prepared by **Suraj Prakash** entitled **Numerical optimization of longitudinal magnetic field profiles of a dipole in a low emittance lattice cell** be accepted as fulfilling the thesis requirement for the Degree of Master of Technology.

	Name	Signature
Mamber-1	Dr. Om Prakash	
Member-2	Dr. Gurvinderjit Singh	
Member-3	Dr. Vijay Kumar Dixit	
External Expert	Prof. Shubhendu Rakshit, Dept. of Physics, IIT Indore	
Technical Advisor	Dr. Riyasat Husain	
Guide/Convener	Dr. Tapas Ganguli	
Chairperson	Dr. Alka A. Ingale	

Final approval and acceptance of this thesis is contingent upon the candidate's submission of the final copies of the thesis to HBNI.

I hereby certify that I have read this thesis prepared under my direction and recommend that it may be accepted as fulfilling the thesis requirement.

**Date:** 04/02/2021

**Guide**

**Place:** RRCAT, Indore

**Dr. Tapas Ganguli**

## **DECLARATION**

I, hereby declare that the investigation presented in the thesis has been carried out by me. The work is original and has not been submitted earlier as a whole or in part for a degree / diploma at this or any other Institution / University.

Date:

Suraj Prakash

Dedicated  
To  
My Loving Parents

## **ACKNOWLEDGEMENTS**

It is my pleasure to convey my gratitude to all the people who helped me a lot for the completion of my M.Phil. Project work at Raja Ramanna Centre for Advanced Technology (RRCAT).

First and foremost, my heartfelt thanks goes to my guide Dr. Tapas Ganguli (Head, Synchrotron Utilization Section, RRCAT) who despite his busy schedules offered invaluable and immeasurable guidance and constructive criticisms for this work.

I am grateful to thank my technology advisor Dr. Riyasat Husain (Accelerator Physics Section, RRCAT), without whom this work could have not been completed. He helps in analyzing and reporting the work in a presentable shape. Under his guidance, I successfully overcame many difficulties and learned a lot. I am highly indebted to him and no words can explain this.

I also express my gratitude to Shri A. D. Ghodke (Head, Accelerator Physics Section, RRCAT) for his valuable suggestion and inspiration.

I would like to express my gratitude to Prof. Shubhendu Rakshit (Dept. of Physics, IIT Indore) for his meticulous reading of this thesis and synopsis, which helped me a lot to present the research work in effective way.

I would also like to express my gratitude to the members of my M.Phil. Committee for their valuable and constructive comments, guidance and support. In addition, I also thank to HBNI, for their academic support. I specially thank Dr. Arup Banerjee (Head, Human Resource Development Section, RRCAT).

I would also like to convey my thanks to the members of my section for their valuable suggestion and inspiration. I specially thank Dr. Pradeep Kumar Sharma (Accelerator Physics Section, RRCAT). His dedication towards work motivates me a lot.

I have no words to express my feelings and gratitude to my family for their love, care and support to complete my work.

I like to mention my friends Ashutosh Mohan and Sanhita Parihar. Their hard work and dedication always inspire me.

**Suraj Prakash**

# Contents

<b>Synopsis</b>	<b>v</b>
<b>List of Figures</b>	<b>viii</b>
<b>List of Tables</b>	<b>xv</b>
<b>1 Basic Accelerator Physics</b>	<b>1</b>
1.1 Synchrotron radiation sources . . . . .	2
1.2 Coordinate system used in circular accelerators . . . . .	5
1.3 Motion of a charged particle in an electromagnetic field . . . . .	6
1.4 Basic magnetic elements used in accelerators . . . . .	8
1.4.1 Dipole magnets . . . . .	8
1.4.2 Quadrupole . . . . .	9
1.4.3 Sextupole . . . . .	11
1.5 Equation of motion of a charged particle in a given magnetic field . . . . .	12
1.5.1 Transfer matrix for a drift space . . . . .	15
1.5.2 Transfer matrix for a quadrupole . . . . .	16
1.5.3 Transfer matrix for a dipole . . . . .	17

1.6	Dispersion and trajectory of an off-momentum particle . . . . .	19
1.7	Parametric solution of equation of motion and Courant- -Snyder parameters . . . . .	21
1.8	Beam dynamics in terms of Courant-Snyder variables . . . . .	25
1.9	Betatron tune . . . . .	28
1.10	Chromaticity . . . . .	29
1.11	Momentum compaction factor . . . . .	31
1.12	Effect of synchrotron radiation on electron beam in the storage ring . . . . .	32
1.13	Different types of magnetic lattices and equilibrium emittance . . . . .	38
1.13.1	Theoretical minimum emittance (TME) lattice . . . . .	39
1.13.2	Double bend achromat (DBA)lattice . . . . .	41
1.13.3	Multi bend achromat (MBA) lattice . . . . .	42
1.14	RMS beam sizes . . . . .	43
1.15	Advance methods to improve beam emittance . . . . .	43
1.16	Indus-2 storage ring lattice . . . . .	46
1.17	Indus-3 storage ring lattice . . . . .	49
<b>2</b>	<b>Optimization techniques used in accelerators</b>	<b>53</b>
2.1	Single objective optimization problem . . . . .	54
2.1.1	Nelder-Mead method . . . . .	55
2.2	Multi-objective optimization . . . . .	60
2.3	Classical methods for multi-objective optimization problems (MOOP) . . . . .	61
2.4	Evolutionary algorithm for optimization problems . . . . .	63

2.4.1	Genetic algorithm . . . . .	64
2.4.2	Multi-objective genetic algorithm . . . . .	67
<b>3</b>	<b>Optimization of longitudinal gradient bend profiles in dipole magnet</b>	<b>70</b>
3.1	LGB profiles in dipoles for achromatic and TME lattices . . . . .	70
3.2	Objective function to generate LGB profiles . . . . .	74
3.3	Optimization of LGB profiles in dipole for achromat lattice . . . . .	75
3.3.1	Optimization using Nelder-Mead algorithm . . . . .	77
3.3.2	Optimization using genetic algorithm . . . . .	79
3.4	Optimization of LGB profiles in dipole for TME lattices . . . . .	90
<b>4</b>	<b>Indus-2 and Indus-3 storage ring lattice performance with LGBs</b>	<b>95</b>
4.1	DBA lattice of Indus-2 with LGBs . . . . .	96
4.1.1	Optimization of lattice function with LGBs . . . . .	97
4.1.2	Dynamic aperture . . . . .	104
4.2	Comparative study of beam emittance with and without LGBs . . . . .	106
4.3	MBA lattice of Indus-3 with LGBs . . . . .	108
4.3.1	Matching of lattice function with quadrupoles . . . . .	110
4.3.2	Dynamic aperture . . . . .	116
<b>5</b>	<b>Conclusion and future scope</b>	<b>118</b>
	<b>Appendix</b>	<b>120</b>
<b>A</b>	<b>Derivations</b>	<b>120</b>
A.1	Equation of motion of an electron in a moving coordinate system . . . . .	120
A.2	Closed form solution . . . . .	123

A.3 Energy Loss . . . . . 125

**References** . . . . . **128**

# Synopsis

Synchrotron light sources, based on an electron storage ring have many characteristic advantages over conventional x-ray sources such as wide energy range, higher flux, high brightness etc. The high brightness of synchrotron radiation from electron storage ring is the result of high quality of stored electron beam in the storage ring. The quality of electron beam is represented by an important figure of merit of the electron storage ring called beam emittance. The magnetic lattice of the storage ring controls the beam and the brightness of photon beam is inversely proportional to the product of two transverse beam emittances of electron beam. Beam emittance signifies how well collimated and divergent the electron beam is. Smaller its value brighter is the emitted synchrotron radiation. Thus, in storage ring lattice design, one of the important criteria for increasing the brightness is to minimize the beam emittance. The beam emittance at fixed electron energy has a cubic dependence on the bending angle. Therefore, to reduce the beam emittance, bending magnets in large numbers are required in given circumference of the storage ring.

In last few decades, several methods have been evolved to improve the beam emittance. Now a days, an innovative method using multi bend achromat (MBA) instead of double or triple bend achromat is being considered and studied, which leads to ultra low emittance. Using MBA lattice, few hundreds of pm.rad beam emittance can be achieved which leads to brightness of the photon beam of the order of  $10^{20}$  to  $10^{22}$  *photons per second per unit area per unit solid*

*angle in 0.1% bandwidth of considered wavelength* with fully loaded insertion devices. MAX IV, a 3 GeV electron storage ring, is an example of this kind of machine, which uses seven bend achromat lattice.

In order to improve beam emittance further, other technologically challenging techniques like transverse gradient, longitudinal gradient bend (LGB), introduction of anti or reverse bend in dipoles of the lattice are being used to get more aggressive design of new synchrotron radiation sources and upgrade existing/running facility to facilitate users with ever increasing brightness. Beam emittance reduction is desirable, however for successful operation of the facility, various other lattice parameters need to be optimized or constrained. For example, betatron tunes should be far away from dangerous resonances, horizontal beta function should be large at injection point and large value of dispersion is desirable at sextupole locations for effective chromaticity correction etc. These aspects make lattice design of a storage ring a complex optimization problem. In order to handle such complex optimization problem, one has to use available numerical optimization techniques.

In this thesis, extensive optimization studies to minimize the beam emittance in an electron storage ring using LGBs are discussed. We have optimized the magnetic field profile along the beam direction in a dipole magnet in general and for dipole magnet of Indus-2 storage ring, in particular. Detailed comparative studies of a storage ring lattice cell utilizing LGB and constant field dipoles are presented and merits and demerits are highlighted. The studies indicate that the beam emittance of a storage ring is much lower with dipoles utilizing LGB compared to dipoles with constant field. In addition, LGB also helps in shaping lattice parameters at sextupole location to correct chromaticity with reduced strength of sextupoles. Maintaining same circumference of the Indus-2 storage ring and matching other lattice parameters with quadrupole magnets, beam emittance can be reduced to  $\sim 40$  nm.rad with LGB compar-

ed to 58 nm.rad with constant field dipole. The studies are extended to minimize the beam emittance of baseline lattice of Indus-3, a 6 GeV electron storage ring with beam emittance 150 pm.rad. Satisfying the operational constraints, the beam emittance can further be reduced to  $\sim 135$  pm.rad by replacing four dipoles out of seven with LGBs.

This whole thesis is organized in the following way. In the first Chapter, basic physics of circular accelerators and some important parameters, such as Courant-Snyder variables, dispersion, betatron tune, chromaticity, emittance etc., are discussed, which are important in view of lattice design of a storage ring. In addition, some of the advanced techniques to reduce the beam emittance are also discussed in this Chapter. Lattice design of a storage ring and its analysis is a complex optimization problem. Different types of optimization techniques, which are capable to handle these complex optimization problem, are introduced in Chapter 2. In Chapter 3, extensive studies on optimization of LGB profiles in a dipole taking emittance and synchrotron radiation loss in consideration have been discussed. These optimization studies of LGB profiles then applied to Indus-2 storage ring lattice. The application of LGB profile changes the distribution of dispersion function which needs to be matched with original lattice. Therefore, optimization of quadrupole strengths with LGBs are carried out and important parameters are compared with original lattice of Indus-2 storage ring. Further, this study is extended to the base line design of Indus-3. These studies are presented in Chapter 4. In the last Chapter, conclusion and future scope of this thesis work has been discussed.

# List of Figures

1.1	Coordinate system used in a circular accelerators. . . . .	6
1.2	(a) Sector (black) and Rectangular (parallel edges with red color) type dipoles. (b) Vertical magnetic field along x-direction. . . . .	8
1.3	(a) Pole faces and field direction in a quadrupole magnet. A positive charged particle coming out of the page will experience a focusing force in x direction and a defocusing force in y direction. (b) Variation of vertical magnetic field along x-direction. . . . .	10
1.4	(a) Pole faces and field direction in a sextupole magnet. Force on a positively charge particle on the x axis and coming out side of the page is shown by arrow. (b) Variation of vertical magnetic field along x-direction. . . . .	12
1.5	Position and slope (with respect to longitudinal direction) of the charged particle before and after traversing the magnetic element. . . . .	15
1.6	Position and slope (with respect to longitudinal direction) of the charged particle after passing through a drift space. . . . .	16
1.7	Particle position (with respect to longitudinal direction) after passing through a focusing quadrupole. O is the centre of the quadrupole and F is focal point. . .	17

1.8	An example of arrangement of different magnetic elements. Elements 1, 3, 5, 7, 9, 11 are drift spaces. Elements 2 and 12 are focusing quadrupole, 4 and 8 are defocusing quadrupole. Elements 6 and 10 are dipole magnets. . . . .	19
1.9	Motion of different energy particles in a sector type dipole magnet. . . . .	19
1.10	Emittance as a phase space area for a single particle. Maximum position and maximum slope are also shown. . . . .	24
1.11	Position and slope of a particle after passing through a magnetic element. $(\beta_0, \alpha_0, \gamma_0)'$ and $(\beta, \alpha, \gamma)'$ are CS variables at entrance and exit of the magnetic element. . . . .	25
1.12	CS variables at the entrance and exit of the magnetic element. . . . .	27
1.13	Tune diagram for fractional betatron tune up to fourth order resonance. . . . .	28
1.14	Radiation damping phenomenon in horizontal plane. $p_x$ and $p_s$ are the momentum of electron in horizontal and longitudinal direction respectively. $p_{RF}$ is the momentum provided by RF cavity. $x'_0$ is the initial slope of electron and $x'_1$ is the slope of electron after passing through RF cavity. . . . .	33
1.15	Quantum Excitation phenomenon. . . . .	36
1.16	Variation of horizontal beta and dispersion function in case TME lattice. Both functions have minima at the centre of the bending magnet. . . . .	40
1.17	Variation of horizontal beta and dispersion function in the first dipole of DBA lattice. Dispersion and its derivative are zero at the entrance of the dipole. . . .	42
1.18	(a) Linear variation of magnetic field along x-direction (black) and compared with homogeneous field (blue). (b) Shape of dipole to get linearly decreasing magnetic field. . . . .	44
1.19	Variation of longitudinal field profile in the dipole magnet of a DBA lattice . . .	45

1.20	Variation of longitudinal field profile in the dipole of TME lattice . . . . .	46
1.21	Schematic layout of Indus Accelerator complex [3,5]. . . . .	47
1.22	Variation of beta and dispersion functions in Indus-2 unit lattice cell. Bending magnets are shown by green boxes, quadrupoles are in red and blue boxes and sextupoles are in yellow and black boxes. . . . .	48
1.23	Beta Functions of Indus-3 lattice cell. Boxes in red colour are dipole magnet, boxes in green colour are quadrupoles and boxes in blue colour are sextupole magnets. . . . .	50
2.1	Reflection (left) and expansion (right) of Nelder-Mead simplex. . . . .	59
2.2	Outside contraction (left), inside contraction (middle) and shrink (right) of Nelder-Mead simplex. . . . .	59
2.3	Various steps involved in Genetic Algorithm. . . . .	65
2.4	NSGA-II procedure for one iteration [25]. . . . .	68
3.1	Variation of dispersion function in DBA lattice. The green rectangular boxes are homogeneous dipoles, blue rectangular boxes are focusing quadrupoles, red rectangular boxes are defocusing quadrupoles, yellow ones are focusing sextupoles and the black ones are defocusing sextupoles. . . . .	71
3.2	Variation of dispersion function in TME lattice. Dispersion function is symmetric in the dipole and minima occurs at the center of the dipole. Two quadrupoles, one focusing (blue) and other defocusing (red), at both side of the dipole are used to control the lattice functions. . . . .	71
3.3	Breaking of a homogeneous dipole (left) into $n$ dipoles (right). The dipole (left) has parameters, length ( $L$ ), magnetic field ( $B$ ), bending angle ( $\theta$ ), local bending radius ( $\rho$ ). Same parameters can be defined for each section of dipole (right). . . . .	72

3.4	Variation of longitudinal field profile in the dipole magnet (DBA). (b) Comparison of Horizontal dispersion function for LGB dipole (solid curve) with homogeneous dipole (dashed curve). . . . .	73
3.5	(a) Variation of longitudinal field profile in the dipole magnet (TME). (b) Comparison of Horizontal dispersion function for LGB dipole (solid curve) with homogeneous dipole (dashed curve). . . . .	74
3.6	Values of CS variables at points A, B, ..., E, which are entrance of each dipole section and F is the exit of last section. . . . .	76
3.7	Variation of $\Delta\theta$ with successive simulation run. . . . .	77
3.8	LGB profiles after each simulation run using Nelder-Mead algorithm. . . . .	78
3.9	Variation of objective function after 8th simulation run. . . . .	78
3.10	Variation of $\rho$ after final simulation run. . . . .	78
3.11	Variation of dispersion function in the dipole. . . . .	78
3.12	Variation of objective function in different generations. Best fitness shows the value of objective function at current generation and maximum constraint shows how constraints are more satisfied in each generation. . . . .	81
3.13	Variation of magnetic field and $\rho$ . For homogeneous dipole magnetic field and $\rho$ are 1.503 Tesla and 5.55 m respectively. . . . .	81
3.14	Variation of dispersion function in the dipole. . . . .	81
3.15	Variation of objective function in each generation for the case where no initial guess is provided. . . . .	82
3.16	Variation of magnetic field and $\rho$ . For homogeneous dipole magnetic field and $\rho$ are 1.503 Tesla and 5.55 m respectively. . . . .	83
3.17	Variation of dispersion function in the dipole. . . . .	83

3.18	Different LGB profiles generated by genetic algorithm. . . . .	84
3.19	Emittance for different LGB profiles with objective function and SR loss (color bar). . . . .	84
3.20	Different LGB profiles using GA with maximum magnetic field in the first section 2.65 Tesla. . . . .	85
3.21	LGB profile for the 10 section case with hard constraint on maximum magnetic field. . . . .	86
3.22	LGB profile for the 15 section case with hard constraint on total magnetic field.	87
3.23	Pareto optimal front between first and second objective. SR loss is given by color at each point of Pareto optimal front. . . . .	89
3.24	Different LGB profiles for A, B and C. . . . .	89
3.25	Different magnetic elements of Indus-2 lattice in TME configuration. . . . .	90
3.26	Variation of different lattice functions. . . . .	91
3.27	LGB profiles for different chosen maximum magnetic field. . . . .	92
3.28	Comparison of lattice functions with and without LGB. . . . .	93
4.1	Basic elements in Indus-2 unit lattice (not to scale). Here, QF: focusing quadrupole, QD: defocusing quadrupole, SF: focusing sextupole, SD: defocusing quadrupole. Number indicates family of that element, e.g. Q1D shows first family of defocusing quadrupoles. . . . .	97
4.2	Variation of beta and dispersion functions in Indus-2 unit lattice. . . . .	97
4.3	LGB profile compared with homogeneous dipole field in the dipole magnet. . .	98
4.4	Variation of dispersion function with LGB. . . . .	98
4.5	Variation of horizontal beta function with LGB. . . . .	99
4.6	Variation of vertical beta function with LGB. . . . .	99

4.7	Variation of objective function. . . . .	101
4.8	Variation of dispersion function with LGB and matching. . . . .	101
4.9	Variation of horizontal beta function with LGB and matching. . . . .	101
4.10	Variation of vertical beta function with LGB and matching. . . . .	101
4.11	Variation of horizontal beta function with LGB, matching, and betatron tune correction. . . . .	104
4.12	Variation of vertical beta function with LGB, matching and betatron tune correction.	104
4.13	Dynamic aperture comparison for on momentum charged particles. . . . .	105
4.14	Comparison of Pareto optimal front. . . . .	107
4.15	Comparison of beta functions at injection for each solution. . . . .	108
4.16	Maximum beta functions comparison for each solution. . . . .	108
4.17	Betatron tune comparison for each solution. . . . .	108
4.18	Natural chromaticity comparison for each solution. . . . .	108
4.19	Different magnetic elements of Indus-3 lattice (not to scale). Magnetic elements which are above base line are focusing in nature and below the base line are defocusing in nature. . . . .	109
4.20	Designed lattice functions of Indus-3 lattice. . . . .	109
4.21	Optimized LGB profile. . . . .	110
4.22	Pareto optimal front for emittance with dispersion at straight section. . . . .	112
4.23	Horizontal and vertical beta functions comparison for each solution. . . . .	112
4.24	Maximum horizontal and vertical beta functions comparison for each solution. .	112
4.25	Horizontal and vertical betatron tune comparison for each solution. . . . .	113
4.26	Horizontal and vertical natural chromaticity comparison for each solution. . . .	113
4.27	Comparison of dispersion function. . . . .	114

4.28	Comparison of horizontal beta function. . . . .	114
4.29	Comparison of vertical beta function. . . . .	114
4.30	Comparison of dynamic aperture for 1000 turns. . . . .	116
A.1	Frenet-Serret coordinate system. $\hat{x}$ , $\hat{y}$ and $\hat{s}$ are unit vectors in horizontal, vertical and longitudinal direction respectively. . . . .	121
A.2	Change in unit vector in horizontal direction. . . . .	121

# List of Tables

1.1	Important mathematical relations [2,22] . . . . .	37
1.2	Different design parameters of Indus-2 storage ring . . . . .	47
1.3	Different magnetic elements of the Indus-2 storage ring. . . . .	48
1.4	Different design parameters of Indus-3 storage ring. . . . .	50
1.5	Different magnetic elements of the Indus-3 lattice. . . . .	51
3.1	Comparison of parameters with original lattice. . . . .	79
3.2	Comparison of parameters with original lattice in case of genetic algorithm. . .	81
3.3	Comparison of parameters with original lattice. . . . .	83
3.4	Comparison of different parameter with original lattice for 15 section case. . . .	87
3.5	Comparison of different LGB profiles in case of MOGA. . . . .	89
3.6	Comparison of different parameter with original lattice in case of TME. . . . .	92
4.1	Comparison of Indus-2 lattice with LGB, Indus-2 lattice with LGB and betatron tune correction and original lattice. . . . .	102
4.2	Comparison of Indus-3 lattice with LGB with original Indus-3 lattice. . . . .	115

# Chapter 1

## Basic Accelerator Physics

The synchrotron radiation (SR), emitted by transverse acceleration of ultra relativistic electron under applied magnetic field, is in much demand for various science experiments due to wide photon energy range and high brightness. To achieve high brightness SR, the dedicated electron storage rings have been built and are further being designed for further enhancing it. The brightness is governed by the beam emittance, which is the design criteria for any storage ring magnetic lattice. In order to design a magnetic lattice of a electron storage ring, deep understanding of beam dynamics of circular accelerators is required. In this Chapter, beam dynamics of circular accelerators and important concepts relevant to the thesis are presented.

In Section 1.1, a brief introduction to evolution of accelerators dedicated to produce SR are discussed. Various parameters based on linear beam dynamics of circular accelerators are discussed in Sections 1.2-1.8. Important phenomenon that govern the beam emittance in a storage ring, which highly affects the brightness of SR, is introduced in Section 1.12. Various types of low emittance magnetic lattices, which are used to build storage rings, are discussed in Section 1.13. In addition, advanced methods to improve the beam emittance is described in Section 1.15. At the end, features of Indus-2 and proposed Indus-3 storage ring lattices

are discussed in Section 1.16 and 1.17. These lattices are considered to study the effect of longitudinal variation of magnetic field in the dipoles on the beam emittance.

## 1.1 Synchrotron radiation sources

E. McMillan and independently V. Veksler, invented the synchrotron in 1945 [1]. Synchrotron, basically, is a circular accelerator in which radius of the accelerating charged particle is fixed by applying magnetic field and acceleration is provided by radio frequency (RF) cavities at one or more places in the circular ring. It is well known from special relativity equations that as particle achieves higher and higher velocity, its mass increases. Therefore, under applied magnetic field, orbit of the charged particle changes. To stabilize the orbit, magnetic field has to be synchronized with energy of the charged particle. This concept is the basic principle of a synchrotron.

First synchrotron was made for the purpose of accelerating charged particle with ever increased energy for the particle physics research [1]. Electron, a very light charged particle, achieves ultrarelativistic speed in energy range of few MeV. In electron synchrotrons, at these energies electron emits SR while going through transverse acceleration under applied magnetic force in the bending magnet. The SR was first time detected at 70 MeV synchrotron at GE in the year 1947 [1].

The energy loss per turn by an electron in the form of SR increases as fourth power of energy of an electron [2], which was the main limitation in high energy circular electron accelerators and it requires very high RF power to compensate this energy loss. Soon it was realized that SR emitted from electrons has better characteristics than conventional X-rays sources like high brightness, high flux, broad energy spectrum etc., which became boon for various science experiments. At that time, scientist started to use SR produced from high energy

electron synchrotrons parasitically. These synchrotrons, where SR was used parasitically are called first generation synchrotron radiation sources (SRSs). Since then, rigorous study on the design of dedicated SRSs based on electron storage ring, in which electron beam is stored for a long time, had been carried out in various synchrotron accelerator facilities. These synchrotrons or storage rings, which were fully dedicated to produce synchrotron radiation are called second generation SRSs. In second generation SRSs, bending magnets were primary source to get uninterrupted high brightness SR for many beam line users at a time. This is the great advantage over X-rays facility where only one user at a time can use the X-ray facility. Indus-1, a 450 MeV electron storage ring located at RRCAT, is an example of second generation SRS [3]. After successful operation of second-generation electron storage rings, insertion devices (IDs) like undulators, wigglers, wavelength shifter etc. were introduced to increase brightness, flux and energy range of SR. These devices are external to the well design lattice of the storage ring. Therefore, more spaces are to be provided to install them. These spaces, i.e. magnet free zones, therefore, become part of the design of storage ring lattices. These SRSs are called third generation SRSs. Indus-2, a 2.5 GeV electron storage ring is an example of third generation SRS [3–5].

One of the main purpose of designing a new electron storage ring or upgrading an existing electron storage ring is the demand of high brightness of the photon beam. The brightness of photon beam is defined as photon flux per unit area per unit solid angle and is mathematically expressed as [6]

$$B = \frac{F}{4\pi^2 \Sigma_x \Sigma_y \Sigma_{x'} \Sigma_{y'}}, \quad (1.1)$$

where  $F$  is the flux, defined as number of photons produced per second in 0.1% bandwidth of considered wavelength.  $\Sigma_{x,y}$  and  $\Sigma_{x',y'}$  are effective beam size and divergence of photon beam,

which are related to electron beam size and divergence as [6]

$$\Sigma_{x,y} = \sqrt{\sigma_{x,y}^2 + \sigma_r^2}, \quad (1.2)$$

$$\Sigma_{x',y'} = \sqrt{\sigma_{x',y'}^2 + \sigma_{r'}^2}. \quad (1.3)$$

Here  $\sigma_{x,y}$  and  $\sigma_{x',y'}$  are horizontal and vertical electron beam size and divergence respectively, and  $\sigma_r$  and  $\sigma_{r'}$  are the photon beam size and divergence, respectively.  $\sigma_{x,y}$  and  $\sigma_{x',y'}$  are related to beam emittance of the storage ring which is an important criteria in storage ring design. Beam sizes and its relation to beam emittance is discussed in Section 1.14.

Flux of photon beam depends on number of photons produced, which depends on stored beam current. But, one cannot fill large current due to many limitations such as vacuum, load on RF, intra beam scattering issues related to lifetime etc. In addition, high current does not lead to improvement of quality of stored beam, e.g. beam size. From eq.(1.1) brightness of the photon beam is inversely proportional to product of two beam emittances in transverse plane. Therefore, as a lattice designer, one focuses on beam emittances to increase brightness with improved beam quality.

Beam emittance, roughly, scales as cubic power of bending angle, therefore more number of dipole magnets in the lattice are required to reduce the beam emittance. Now a days, scientist are focusing on fourth generation SRSs, utilizing the concept of multi bend achromat (MBA) lattice, instead of double or triple bend achromat, and IDs to build or upgrade existing storage rings to achieve ultra low emittance [7]. The requirement of more number of dipoles make storage ring large in size and consequently increases the cost of the machine. MAX IV is the first operating machine based on MBA concept [7, 8]. Further, to push beam emittance towards more lower side, technologically challenging, advanced methods were introduced such as transverse gradient [9], longitudinal gradient bend (LGB) [10, 11], reverse or anti bend [12]. LGB was first introduced by J. Gau, T. Raubenheimer in 2002 [10]. They applied the LGB

in NLC damping storage ring and found sufficient beam emittance reduction. Now a days, magnet design technology has been improved much and LGB has been widely accepted in lattice design to upgrade of an existing facility and new storage ring lattices [11]. MAX IV, a 3 GeV storage ring, is a running example of it [13]. Some examples of high energy and large circumference SRSs to produce hard X-rays are ESRF, France (6 GeV) [14], Spring-8, Japan (8 GeV) [15], APS, USA (7 GeV) [16]. Also, there are some facilities which are build to get soft X-rays like ALS, USA (1.9 GeV) [17], ELLETRA, Italy (2-2.4 GeV) [18] etc.

## 1.2 Coordinate system used in circular accelerators

It is always desirable to study the dynamics of a particle in a coordinate system in which equation of motion of the particle takes a simple form. In circular accelerators, study of charged particle dynamics is preferred in moving or Frenet-Serret coordinate system instead of conventional coordinate system.

As shown in Fig. 1.1, this coordinate system consists a designed orbit at which reference or designed charged particle moves. Coordinate axes of the coordinate system are denoted by  $X$ ,  $Y$  and  $S$  and origin is co-moving with reference charged particle which has coordinates  $(0, 0, 0)$ . Coordinates of any other charged particle is defined as deviation from the designed orbit and are denoted by  $x$ ,  $y$  and  $s$ . Here,  $x$  and  $y$  are deviations in radial and vertical direction from the designed orbit, respectively, and  $s$  is the deviation of the charged particle with respect to reference charged particle in the direction of motion. Unit vectors along  $X$ ,  $Y$  and  $S$  direction are shown in Fig. 1.1. Also, it is notable that unit vector in  $Y$  direction does not change.

Most of the large circular accelerators in the world are build to keep designed orbit in the horizontal plane. Therefore,  $X - S$  plane is known as horizontal or median plane and  $Y - S$  plane is known as vertical plane. Motion of charged particles in these two planes defines the

transverse properties of the beam of charged particles.

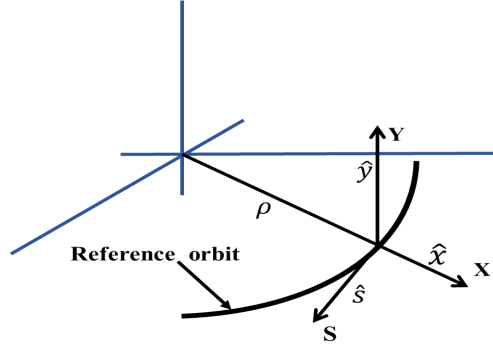


Fig. 1.1: Coordinate system used in a circular accelerators.

Local radius of curvature  $\rho$ , in general, is a function of path length  $s$ , i.e.,  $\rho = \rho(s)$ . For a straight section  $\rho = \infty$  and  $\rho$  is finite where path is curved. The  $X, Y$  and  $S$  form a right-handed coordinate system, i.e.,  $\hat{x} \times \hat{y} = \hat{s}$ . Generally, transverse deviations of a charged particle are very small, i.e.,  $x, y \ll \rho$ . Therefore, paraxial approximation can be used in study of motion of charged particle. Motion of a charged particle in an electromagnetic field is discussed in the following section.

### 1.3 Motion of a charged particle in an electromagnetic field

Motion of a charged particle in an electromagnetic field is governed by Lorentz force law and is mathematically given by [2]

$$\vec{F} = \frac{d\vec{p}}{dt} = q(\vec{E} + \vec{v} \times \vec{B}), \quad (1.4)$$

where  $\vec{p}$ ,  $q$ , and  $\vec{v}$  are momentum, charge, and velocity of the charged particle, respectively.  $\vec{E}$  and  $\vec{B}$  are electric and magnetic fields, respectively. To govern an ultrarelativistic charged particle, magnetic field is much more effective than electric field. Therefore, the transverse dynamics of the charged particle at ultrarelativistic speed can be controlled by magnetic field

only. Equation of motion for such charged particle can be written as

$$\vec{F} = \frac{d(m_0\gamma\vec{R})}{dt} = q(\vec{v} \times \vec{B}), \quad (1.5)$$

where  $m_0$  and  $\vec{R}$  are rest mass and velocity of the charged particle, respectively, and  $\gamma$  is the Lorentz factor which is given by  $\gamma = 1 + \frac{E}{E_{rest}}$ ;  $E$  and  $E_{rest}$  are the kinetic energy and rest mass energy of the charged particle respectively.

From eq.(1.5), in a normal magnetic field, one can derive following relation for a circular orbit [2]

$$\frac{p}{q} = B\rho, \quad (1.6)$$

where  $p = |\vec{p}| = \gamma m_0 |\vec{v}|$  and  $\rho$  are the momentum and bending radius of charged particle, respectively. The result in eq.(1.6) is also true for relativistic velocities. The quantity  $B\rho$ , called "Beam rigidity", is an important quantity in a circular accelerator which depends only on the momentum and given charge of the particle. For an ultrarelativistic charged particle, energy and momentum are related by  $E = cp$ ;  $c$  is the speed of light in vacuum. It means that, energy and momentum can be used interchangeably. In a storage ring, energy of reference charged particle is constant and therefore, beam rigidity of storage ring is a constant quantity.

Beam rigidity is often used to define normalized quantities for storage ring like strength of the quadrupole, sextupole etc. which are discussed in Section 1.4. For an electron storage ring  $q = e$ , eq.(1.6) can be written in terms of energy as [2]

$$B\rho(T.m) = \frac{10}{2.998}\beta E(GeV). \quad (1.7)$$

For ultrarelativistic particles, this expression is further simplified as  $\beta$  is almost equal to 1.

In a circular accelerator, magnetic fields are generated by different types of magnetic elements which are discussed in the following Section.

## 1.4 Basic magnetic elements used in accelerators

To guide the charge particles in a circular accelerator, different magnetic elements like dipoles, quadrupoles and sextupoles are used. In case of storage ring, usually a periodic unit lattice cell, an arrangement of magnetic elements in a particular fashion, is designed and is repeated to make a complete storage ring. The different magnetic elements are discussed in the following Sections [5].

### 1.4.1 Dipole magnets

An ideal dipole magnet (constant field  $\vec{B}$  in space) is used to generate a curvature (bending) in the design trajectory of an accelerator and therefore is also known as bending magnet or dipole magnet. An ideal dipole has infinite long pole faces parallel to each other and produces homogeneous (constant) field irrespective of position, i.e.,  $|\vec{B}(x, y, s)| = b$ , where  $b$  is a constant. However, practical dipole magnet has finite size. Due to finite length, fringe fields are generated which contain higher order multipoles.

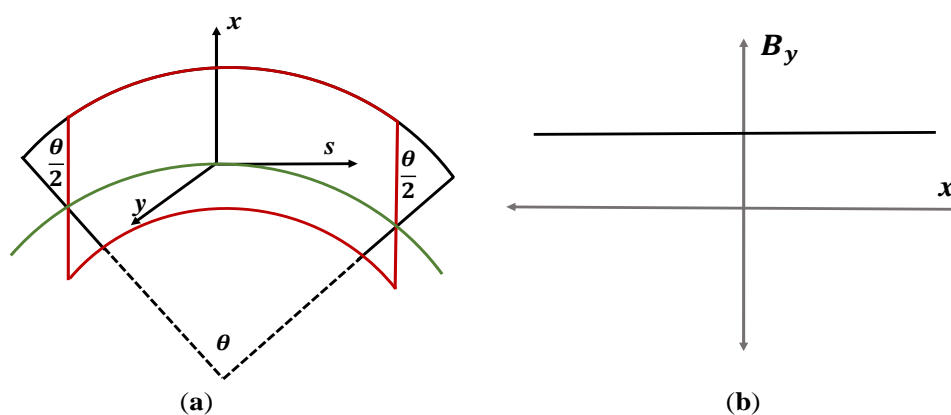


Fig. 1.2: (a) Sector (black) and Rectangular (parallel edges with red color) type dipoles.

(b) Vertical magnetic field along  $x$ -direction.

Magnetic field in a normal dipole is defined as

$$\vec{B}(x, y, s) = \pm b\hat{y}, \quad (1.8)$$

where  $\hat{y}$  is the unit vector in the vertical direction and  $b$  is a constant. However, skew dipole is defined as  $\vec{B}(x, y, s) = \pm b\hat{x}$ , where  $\hat{x}$  is the unit vector in horizontal or radial direction. It means that a normal dipole becomes a skew dipole after rotation of  $90^\circ$  about longitudinal direction.

Two types of dipole magnets are generally used in lattice design of a storage ring namely sector and rectangular, which are shown in Fig. 1.2. In a sector type dipole, the design trajectory enters and leaves the magnet edges at right angles, whereas in rectangular type, end faces are parallel to each other and design trajectory enters and leaves the magnet edges at equal angle but different from  $90^\circ$ . The transverse gradient and the longitudinal gradient can also be introduced in the bending magnets to make the size of a storage ring compact and minimise the beam emittance.

## 1.4.2 Quadrupole

A quadrupole magnet has a linearly varying magnetic field with the transverse distance ( $x$  or  $y$ ) from the design orbit, resulting in a restoring force on the charged particle passing through it, which can be used as a focusing magnet. Normal quadrupole magnet has four pole faces as shown Fig. 1.3. These pole faces are hyperbolic in shape to provide linear variation of fields with distances. Field lines originate perpendicularly from North pole and terminate on South pole. Variation of magnetic fields in a quadrupole are given as

$$B_x = gy \quad \text{and} \quad B_y = gx, \quad (1.9)$$

where  $g = \frac{dB_y}{dx}$ . At the centre of quadrupole, i.e.,  $x = 0, y = 0$ , the net magnetic field is zero. Therefore, charged particle which passes through the centre of quadrupole does not experience

any force. Also, force on the charged particle increases with the increase of the distance from the center. Hence, more distant particle experiences more force towards or away from the centre of the quadrupole magnet. Quadrupoles are mainly used for focusing or defocusing action on the charged particles. Normalized quadrupole strength  $k$  is defined as [2]

$$k = \left( \frac{e}{p} \right) g = \frac{g}{B\rho}. \quad (1.10)$$

Eq.(1.10) can be written in terms of energy as

$$k(\text{m}^{-2}) = 0.2998 \frac{g(\text{Tm}^{-1})}{\beta E(\text{GeV})}. \quad (1.11)$$

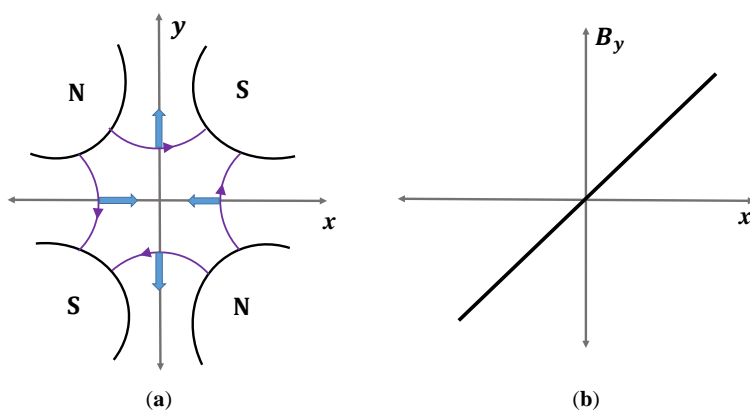


Fig. 1.3: (a) Pole faces and field direction in a quadrupole magnet. A positive charged particle coming out of the page will experience a focusing force in x direction and a defocusing force in y direction. (b)

Variation of vertical magnetic field along x-direction.

As shown in Fig. 1.3, positive charged particle coming out of the page and having different position on x-axis focuses towards centre of the quadrupole. Also, if a quadrupole focuses in one plane then in another plane it always defocuses. Therefore, to achieve overall focusing in both the transverse planes, at least two quadrupoles separated by some distance are normally used in the lattice design. Conventionally, a quadrupole focusing in horizontal plane is called focusing quadrupole and a quadrupole focusing in vertical plane is called defocusing

quadrupole. If a normal quadrupole is rotated through  $45^\circ$  about longitudinal direction, then it is called skew quadrupole. Skew quadrupoles are used to correct coupling in the machine. To build a tight focusing storage ring high gradient in the quadrupole is required.

Dipole and quadrupole magnets generate magnetic force on the particle that is either independent or linear to the charged particle position. The dynamics, which includes only dipole, quadrupole and drift space with zero magnetic fields, is known as the linear beam dynamics. Various optics characteristics and parameters of the storage rings are determined by linear beam dynamics. These parameters are introduced in Sections 1.5, 1.7 and 1.9.

### 1.4.3 Sextupole

The electron beam contains many charged particles, each may have small energy deviation from the energy of the reference or central particle. These particles when pass through the quadrupole, they focus away from the focal point. This phenomenon is known as chromatic aberration or chromaticity (discussed in Section 1.10). To correct chromaticity, the sextupole magnets are included in a storage ring and are placed near a quadrupole. A sextupole has six pole faces with North and South poles placed alternatively as shown in Fig. 1.4. The orientation of the poles are in such a way that magnetic field variation in the sextupole has following form

$$B_y = \frac{1}{2}g'(x^2 - y^2) \quad \text{and} \quad B_x = g'xy. \quad (1.12)$$

Variation of  $y$  component of magnetic field, i.e.,  $B_y$  along  $x$ -axis is shown in Fig. 1.4. The sextupole strength is defined as [2]

$$S[\text{m}^{-3}] = \frac{e}{p}g' = 0.2998 \frac{g'}{\beta E(\text{GeV})}. \quad (1.13)$$

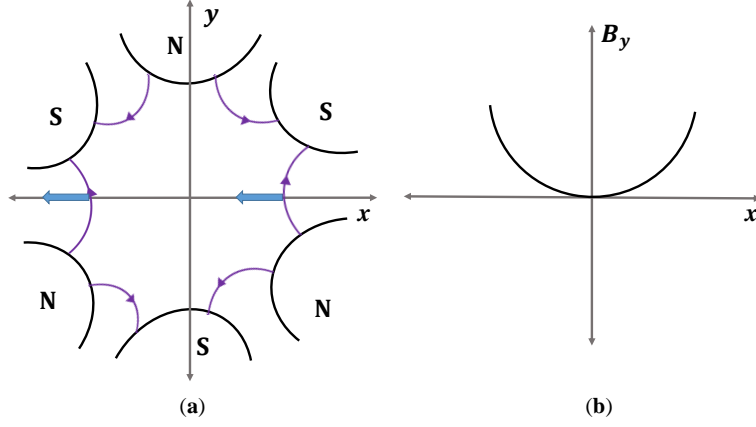


Fig. 1.4: (a) Pole faces and field direction in a sextupole magnet. Force on a positively charge particle on the  $x$  axis and coming out side of the page is shown by arrow. (b) Variation of vertical magnetic field along  $x$ -direction.

Fields in the sextupole are non-linear, as the strength of the sextupoles increase, non-linearity in the machine also increases. In addition,  $B_x$  component of sextupole field is the product of  $x$  and  $y$ , it will generate coupling in the charged particle motion.

## 1.5 Equation of motion of a charged particle in a given magnetic field

Equation of motion of a charged particle moving in a general magnetic field  $\vec{B}$  with velocity  $\vec{v}$  is given by eq.(1.5). In a storage ring, kinetic energy of the charged particle is constant, consequently,  $\gamma$  will be a constant and rest mass,  $m_0$ , is a constant, too. Therefore, eq.(1.5) becomes

$$\frac{d^2 \vec{R}}{dt^2} = q \frac{\vec{v} \times \vec{B}}{\gamma m_0}. \quad (1.14)$$

General position of the charged particle can be written as  $\vec{R} = r\hat{x} + y\hat{y}$  and general radius of curvature as  $r = \rho + x$ . Considering uncoupled motion in both transverse directions, general equation of transverse motion of a charged particle in a given magnetic field can be

written in terms of path length  $s$  as [A.1]

$$\frac{d^2x}{ds^2} - \left( \frac{\rho + x}{\rho^2} \right) = -\frac{B_y}{B\rho} \left( 1 + \frac{x}{\rho} \right)^2, \quad (1.15)$$

$$\frac{d^2y}{ds^2} = \frac{B_x}{B\rho} \left( 1 + \frac{x}{\rho} \right)^2. \quad (1.16)$$

Here, it is assumed that energy of the charged particle is constant and magnetic field component in  $s$  direction, i.e.,  $B_s$ , is zero. Magnetic field components  $B_x$  and  $B_y$  can be expanded as a Taylor's series about reference orbit as

$$B_x = B_x(0) + \frac{\partial B_x}{\partial y} y + \frac{1}{2!} \frac{\partial^2 B_x}{\partial y^2} y^2 + \dots, \quad (1.17)$$

$$B_y = B_y(0) + \frac{\partial B_y}{\partial x} x + \frac{1}{2!} \frac{\partial^2 B_y}{\partial x^2} x^2 + \dots. \quad (1.18)$$

Here,  $B_x(0)$  and  $B_y(0)$  are constant and derivatives of magnetic fields are calculated at reference orbit. For small deviations, i.e.,  $x, y \ll \rho$ , higher order terms in expansion of magnetic fields can be neglected. Using fourth Maxwell relation in the pole gap of a magnetic element where current and charges are zero, we have  $\nabla \times \vec{B} = 0 \rightarrow \frac{\partial B_x}{\partial y} = \frac{\partial B_y}{\partial x}$ . Since bending of the charged particle is considered in horizontal plane. Therefore, for horizontal motion  $B_x(0) = 0$ . Using these results, eq.(1.15) and eq.(1.16) can be further simplified as

$$\frac{d^2x}{ds^2} + \left( \frac{1}{\rho^2} + \frac{1}{B\rho} \frac{\partial B_y}{\partial x} \right) x = 0, \quad (1.19)$$

$$\frac{d^2y}{ds^2} - \left( \frac{1}{B\rho} \frac{\partial B_y}{\partial x} \right) y = 0. \quad (1.20)$$

Expression  $\frac{1}{B\rho} \frac{\partial B_y}{\partial x}$  is denoted by  $k$ . This is an important quantity which is normalized with beam rigidity and has units  $[\text{m}^{-2}]$ . In general, equation of motion in transverse planes can

be written in a single equation as

$$u'' + K(s)u = 0, \quad \text{with} \quad \begin{cases} K = \frac{1}{\rho^2} + \frac{1}{B\rho} \frac{\partial B_y}{\partial x}, & \text{for } u = x \\ K = -\frac{1}{B\rho} \frac{\partial B_y}{\partial x}, & \text{for } u = y \end{cases} \quad (1.21)$$

Eq.(1.21) is called ‘‘Hill’s equation’’ and is similar to equation of simple harmonic motion with variable spring constant. From this equation, position and slope of a charged particle can be found at any position  $s$ . In general,  $K$  is the function of path-length  $s$ . But for a magnetic element,  $K(s)$  can be treated as a constant, i.e.,  $K(s) = K$ . Assuming  $K$  positive and constant, the solution of eq.(1.21) can be written as [2, 19]

$$u(s) = A \cos(\sqrt{K}s) + B \sin(\sqrt{K}s). \quad (1.22)$$

Then slope of the particle trajectory is given by

$$u'(s) = -A\sqrt{K} \sin(\sqrt{K}s) + B\sqrt{K} \cos(\sqrt{K}s), \quad (1.23)$$

here  $A$  and  $B$  are constant. For  $K < 0$ , hyperbolic sine and cosine terms will appear instead of sine and cosine. For a given length of a magnetic element and initial position of a charged particle at the entrance of magnetic element, constants  $A$  and  $B$  can be found. After finding these two constants, eq.(1.22) and (1.23) can be written in matrix form as

$$\begin{pmatrix} u \\ u' \end{pmatrix}_{out} = \begin{pmatrix} \cos(\phi) & \frac{1}{\sqrt{K}} \sin(\phi) \\ -\sqrt{K} \sin(\phi) & \cos(\phi) \end{pmatrix} \begin{pmatrix} u \\ u' \end{pmatrix}_{in}, \quad (1.24)$$

where  $\phi = \sqrt{K}L$ . Here, *in* and *out* shows entrance and exit of the magnetic element as shown in Fig. 1.5.

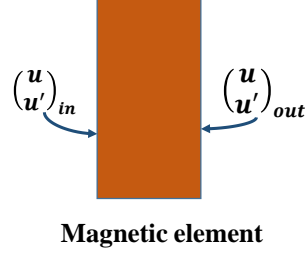


Fig. 1.5: Position and slope (with respect to longitudinal direction) of the charged particle before and after traversing the magnetic element.

The matrix

$$M = \begin{pmatrix} \cos(\phi) & \frac{1}{\sqrt{K}} \sin(\phi) \\ -\sqrt{K} \sin(\phi) & \cos(\phi) \end{pmatrix} = \begin{pmatrix} C(S) & S(s) \\ C'(s) & S'(s) \end{pmatrix} = \begin{pmatrix} M_{11} & M_{12} \\ M_{21} & M_{22} \end{pmatrix} \quad (1.25)$$

is called transfer matrix for the magnetic element, and it is different for different type of magnetic elements. Here,  $C(s) = M_{11} = \cos(\phi)$ ,  $S(s) = M_{12} = \frac{1}{\sqrt{K}} \sin(\phi)$ .  $C'(s)$  and  $S'(s)$  are derivatives of  $C(s)$  and  $S(s)$ , respectively. This transfer matrix transports position and slope of a charged particle from entrance to exit point of the magnetic element. Transfer matrix for different type of magnetic element are in following Section.

### 1.5.1 Transfer matrix for a drift space

For a drift space, i.e., no magnetic field,  $K = 0$ . Transfer matrix for a drift space is given by [19]

$$M_{Drift} = \begin{pmatrix} 1 & L \\ 0 & 1 \end{pmatrix}, \quad (1.26)$$

where  $L$  is the length of the drift space. As shown in Fig. 1.6, when a charged particle passes through a drift space its position changes, but slope remains constant.

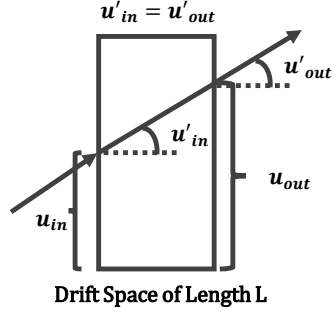


Fig. 1.6: Position and slope (with respect to longitudinal direction) of the charged particle after passing through a drift space.

Drift spaces play an important role in lattice design. Mostly all magnetic elements in the storage ring are electromagnetic in nature. Magnetic elements have coils wrapped on the iron core. One must provide some space between two magnetic element for these coils. Also, vacuum pumps and cooling systems, beam position monitors, dipole correctors, beam profile monitors require spaces. In addition, installation of IDs also require large spaces.

### 1.5.2 Transfer matrix for a quadrupole

For a pure quadrupole,  $K = k = \frac{1}{B\rho} \frac{\partial B_y}{\partial x}$  and transfer matrix for a focusing quadrupole is given by [19]

$$M_{Q, focusing} = \begin{pmatrix} \cos \phi & \frac{1}{\sqrt{|k|}} \sin \phi \\ -\sqrt{|k|} \sin \phi & \cos \phi \end{pmatrix}, \quad (1.27)$$

where  $\phi = \sqrt{k}L$  and  $k > 0$  (focusing quadrupole) and for a defocusing quadrupole transfer matrix is given by

$$M_{Q, defocusing} = \begin{pmatrix} \cosh \phi & \frac{1}{\sqrt{|k|}} \sinh \phi \\ \sqrt{|k|} \sinh \phi & \cosh \phi \end{pmatrix}, \quad (1.28)$$

where  $\phi = \sqrt{|k|}L$  and  $k < 0$  (defocusing quadrupole).

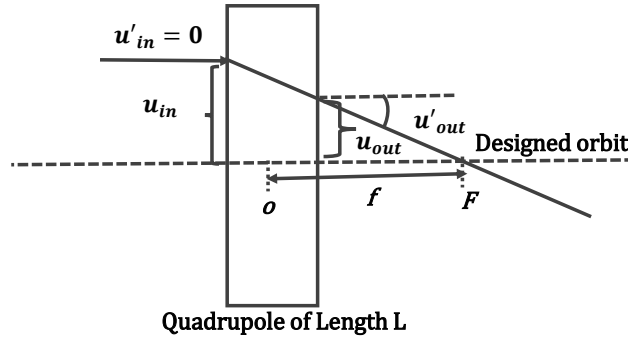


Fig. 1.7: Particle position (with respect to longitudinal direction) after passing through a focusing quadrupole. O is the centre of the quadrupole and F is focal point.

Quadrupole is a focusing element. In Fig. 1.7, action of a focusing quadrupole is shown.

Focal length of a quadrupole is given by [19]

$$f = \begin{cases} \frac{1}{\sqrt{k}L \tan(\sqrt{k}L)}, & \text{for } k > 0 \\ \frac{1}{\sqrt{-k}L \tanh(\sqrt{-k}L)}, & \text{for } k < 0 \end{cases} \quad (1.29)$$

If  $f \ll L$  (thin lens approximation), eq.(1.29) becomes

$$f = \frac{1}{kL} \quad (1.30)$$

### 1.5.3 Transfer matrix for a dipole

For a sector type dipole  $K(s) = \frac{1}{\rho^2}$ . Transfer matrix for horizontal plane is given by [19]

$$M_x = \begin{pmatrix} \cos \theta & \rho \sin \theta \\ -\frac{1}{\rho} \sin \theta & \cos \theta \end{pmatrix}, \quad (1.31)$$

where  $\theta = \frac{L}{\rho}$  is the bending angle of the dipole magnet. In vertical plane sector type dipole magnet behaves like a drift space with length  $L = \theta\rho$ , because there is no any bending in vertical plane. In thin lens approximation  $\theta \rightarrow 0$ , transfer matrix  $M_x$  can be written as

$$M_x = \begin{pmatrix} 1 & 0 \\ -\frac{L}{\rho^2} & 1 \end{pmatrix} \quad (1.32)$$

Here, one can see that dipole act as a focusing element. This focusing originates from the fact that the different energy charged particle has different  $\rho$  in the dipole. This type of focusing is called geometrical focusing.

For a rectangular type dipole magnet, transfer matrices for both transverse planes are given as [19]

$$M_x = \begin{pmatrix} 1 & \rho \sin \theta \\ 0 & 1 \end{pmatrix}, \quad M_y = \begin{pmatrix} \cos \theta & \rho \sin \theta \\ -\frac{1}{\rho} \sin \theta & \cos \theta \end{pmatrix}. \quad (1.33)$$

Transfer matrix for horizontal plane has the form like a drift space with length  $L = \rho \sin \theta$ . This is because, the weak geometrical focusing in horizontal plane is exactly compensated by the defocusing at the entrance and exit faces [2, 5].

In a magnetic lattice of a storage ring, there are large number of magnetic elements to guide a charged particle. In matrix formulation one can compute transfer matrix for a given arrangement of magnetic elements. In Fig. 1.8, an example of an arrangement of magnetic elements is shown. If transfer matrices for different magnetic elements are  $M_1, M_2, M_3, \dots, M_{12}$  and a charged particle enters from the entrance of the first element and exits from the last element, then transfer matrix for this arrangement is given by the product of individual transfer matrix as

$$M = M_{12}.M_{11}.M_{10} \dots M_2 M_1 \quad (1.34)$$

This result can be generalized for  $n$  number of magnetic elements provided transfer matrix for each element is known.

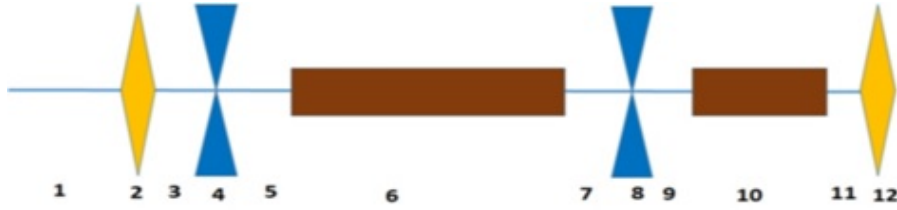


Fig. 1.8: An example of arrangement of different magnetic elements. Elements 1, 3, 5, 7, 9, 11 are drift spaces. Elements 2 and 12 are focusing quadrupole, 4 and 8 are defocusing quadrupole. Elements 6 and 10 are dipole magnets.

## 1.6 Dispersion and trajectory of an off-momentum particle

In a dipole, an off-momentum or off-energy charged particle does not follow the same path as reference charged particle even if it is launched on the designed path. This is shown in Fig. 1.9, higher energy charged particle follows longer path, however, lower energy particle follow shorter path and trajectories of different energy particles get dispersed. This phenomenon is called dispersion.

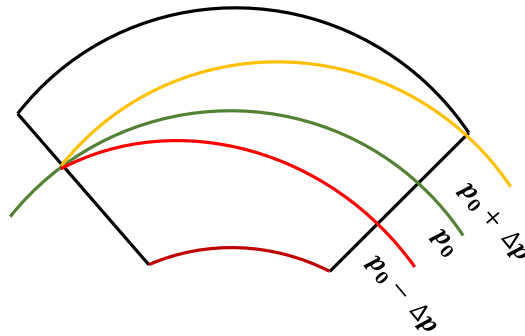


Fig. 1.9: Motion of different energy particles in a sector type dipole magnet.

Position or deviation from designed orbit of such particles is given by [2]

$$x(s) = \eta(s) \frac{\Delta p}{p_0} = \eta(s) \delta, \quad x'(s) = \eta'(s) \delta, \quad (1.35)$$

here,  $p_0$  is the momentum of reference charged particle and  $\delta p = p - p_0$  is the change in

momentum of a charged particle from reference charged particle.  $\Delta = \frac{\Delta p}{p_0}$  and  $\eta(s)$  are relative momentum deviation and dispersion function, respectively. Eq.(1.35) shows that dipole separates off different momentum or energy charged particles in position, i.e., if  $\Delta p < 0$  then  $x < 0$  and if  $\Delta p > 0$  then  $x > 0$ .

In an ideal lattice dispersion is generated by the dipole magnet in horizontal direction only. However, vertical dispersion can be present in the machine due to various errors in the machine. For example, skew quadrupole (rotated quadrupole) and rotational error in the dipole magnet can generate dispersion in vertical plane. Phenomenon of dispersion plays an important role in the consideration of lattice design of a storage ring.

Considering ideal dipole, after including dispersion and considering small momentum deviation, new equations of motion in both transverse planes can be written as [2, 19]

$$\frac{d^2x}{ds^2} + \left( \frac{1}{\rho^2} + \frac{1}{B\rho} \frac{\partial B_y}{\partial x} \right) x = \frac{\delta}{\rho}, \quad (1.36)$$

$$\frac{d^2y}{ds^2} - \left( \frac{1}{B\rho} \frac{\partial B_y}{\partial x} \right) y = 0. \quad (1.37)$$

Eq.(1.36) is an inhomogeneous differential equation while eq.(1.37) is a homogeneous differential equation. Therefore, solution of eq.(1.36) will contain homogeneous solution with particular integral and is given by [2]

$$x(s) = A.C(s) + B.S(s) + \delta.\eta(s), \quad (1.38)$$

where  $\eta(s)$  is given by

$$\eta(s) = \int_0^s \frac{1}{\rho(s')} [S(s)C(s') - C(s)S(s')] ds'. \quad (1.39)$$

After including dispersion term one can write solution of equation of motion in matrix formulation

and in terms of dispersion function as [19]

$$\begin{pmatrix} \eta \\ \eta' \\ 1 \end{pmatrix}_{out} = \begin{pmatrix} M_{11} & M_{12} & M_{13} \\ M_{21} & M_{22} & M_{23} \\ M_{31} & M_{32} & M_{33} \end{pmatrix} \begin{pmatrix} \eta \\ \eta' \\ 1 \end{pmatrix}_{in}. \quad (1.40)$$

For a sector type dipole, eq.(1.40) can be written as [19]

$$\begin{pmatrix} \eta \\ \eta' \\ 1 \end{pmatrix}_{out} = \begin{pmatrix} \cos \theta & \sin \theta & \rho(1 - \cos \theta) \\ -\frac{1}{\rho} \sin \theta & \cos \theta & \sin \theta \\ 0 & 0 & 1 \end{pmatrix} \begin{pmatrix} \eta \\ \eta' \\ 1 \end{pmatrix}_{in}, \quad (1.41)$$

Similarly for a rectangular type dipole

$$\begin{pmatrix} \eta \\ \eta' \\ 1 \end{pmatrix}_{out} = \begin{pmatrix} \cos \theta & \sin \theta & \rho(1 - \cos \theta) \\ -\frac{1}{\rho} \sin \theta & \cos \theta & 2 \tan \frac{\theta}{2} \\ 0 & 0 & 1 \end{pmatrix} \begin{pmatrix} \eta \\ \eta' \\ 1 \end{pmatrix}_{in}. \quad (1.42)$$

In Section 1.5, equation of motion is solved considering  $K$  as a constant. In the following Section, solution of equation of motion is given for a more general case, in which  $K$  is a periodic function.

## 1.7 Parametric solution of equation of motion and Courant-Snyder parameters

For circular accelerators, i.e., a periodic system, general equation of motion of a charged particle with reference energy can be written as [A.2]

$$u''(s) + K(s)u(s) = 0, \quad (1.43)$$

here  $u$  stands for  $x$  or  $y$  and  $K$  is a periodic function of path length  $s$  with period  $C$ . The period  $C$  may be either full circumference of circular accelerator or one super period in the circular

accelerator. The charged particle in the circular accelerator has to make millions of revolutions and will experience a periodic potential in every turn. Solution of such differential equation is given by Floquet's theorem and can be written in the form [2]

$$u(s) = A\sqrt{\beta(s)} \cos[\phi(s) + \phi_0], \quad (1.44)$$

here  $\phi_0$  and  $A$  are constant and  $\phi$  is the phase of the charged particle. This form of amplitude is chosen for specific problem of circular accelerators. Any general function which depends on  $s$  can be chosen for amplitude function. Amplitude function  $\beta(s)$  is also a periodic function with same period of  $K$ , i.e.,  $C$ . Solution in eq.(1.44) confirms that after each turn charged particle acquires a positive phase, which means, particle will not have same position after travelling a complete turn or a super period.

After substituting solution in eq.(1.43), an equation in terms of sine and cosine can be obtained. After equating the coefficient of sine and cosine terms equal to zero, two equations can be obtained as [A.2]

$$\frac{1}{2} \left( \beta\beta'' - \frac{1}{2}(\beta'')^2 \right) - \beta^2(\phi')^2 + k\beta^2 = 0 \quad (1.45)$$

$$\beta'\phi' + \beta\phi'' = 0. \quad (1.46)$$

Eq.(1.46) can be rearranged as  $(\beta\phi')' = 0$  or  $\beta\phi' = \text{Constant}$ . Value of this constant is just a scaling factor and can be chosen as 1 for simplicity. Further,

$$\phi'(s) = \frac{1}{\beta(s)} \rightarrow \phi(s) = \int_0^s \frac{ds'}{\beta(s')}. \quad (1.47)$$

In a circular accelerator, one is free to choose our reference point of integration from 0 to  $s$ . Therefore, integration constant is chosen as 0 for simplicity.  $\phi(s)$  is called phase advance of charged particle after travelling a distance  $s$  and it depends on amplitude function  $\beta(s)$ . Using result for phase advance, eq.(1.45) becomes

$$\frac{1}{2}\beta\beta'' - \frac{1}{4}(\beta')^2 + \beta^2k = 1. \quad (1.48)$$

This is an important relation called envelope equation. Because it represent the envelope of the beam. Also, it may happen that for some values of quadrupole strength  $k$ , solution of envelope equation may not exist. This leads to resonances for such values of  $k$ .

With the introduction of new variables, which are given as

$$\alpha = -\frac{1}{2}\beta', \quad \gamma = \frac{1 + \alpha^2}{\beta} \quad (1.49)$$

eq.(1.45) becomes

$$\alpha' = k\beta - \gamma. \quad (1.50)$$

The variables  $\alpha(s), \beta(s), \gamma(s)$  are called Courant-Snyder variables or Twiss parameters. Twiss parameters and the phase function  $\phi(s)$  are called betatron functions or lattice functions and oscillatory motion of a charged particle along longitudinal direction or beam line is called the betatron oscillation [2].

One can find an invariant of motion between solution  $u(s)$  and Courant-Snyder variables by eliminating  $(\phi(s) + \phi_0)$  from solution  $u(s)$ , which is given by

$$\gamma u^2 + 2\alpha u u' + \beta u'^2 = A^2. \quad (1.51)$$

A quantity  $\epsilon$ , called emittance, is defined as  $A^2 = \epsilon$ . Relation in eq.(1.51) is the equation of general ellipse with area  $\pi\epsilon$ , i.e., emittance is directly related to the phase space area. General ellipse as shown in Fig.1.10, denotes motion of single particle in phase space. After passing through different magnetic elements this ellipse will change its shape and size but area will remain constant if forces are conservative and linear. In circular accelerators, there are large number of charged particles and form the beam. Charged particles having same emittance but different in phase will lie on this ellipse at different locations. If this is the ellipse for outermost charged particle which survives i.e. stable in the storage ring, then all charged particles whose emittance are lower than outermost charged particle will surely survive.

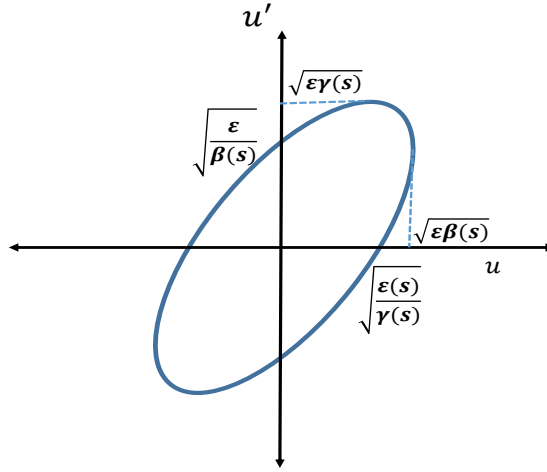


Fig. 1.10: Emittance as a phase space area for a single particle. Maximum position and maximum slope are also shown.

The beam emittance of whole beam can equivalently be describe by the emittance of the outermost charged particle in a beam. Trajectories of charged particles on the ellipse is described by

$$u_i(s) = \sqrt{\epsilon} \sqrt{\beta(s)} \cos[\phi(s) + \phi_{0i}], \quad (1.52)$$

where  $\phi_{0i}$  is an arbitrary phase constant of the  $i^{th}$  charged particle. Selecting every point along the beam line for which  $\cos[\phi(s) + \phi_{0i}] = \pm 1$ , one can get an envelope of the beam containing all charged particles as

$$u_{max} = \pm \sqrt{\epsilon \beta(s)}. \quad (1.53)$$

This is the maximum amplitude that a charged particle can have at any position  $s$ . Beam envelope changes with path length  $s$  and depends only on beam emittance and betatron functions.

Courant-Snyder variables plays important role in beam dynamics and one can study beam dynamics in terms of Courant-Snyder variables.

## 1.8 Beam dynamics in terms of Courant-Snyder variables

If, initial position and slope at the entrance of a magnetic element are known, then position and slope can be found at the exit of the magnetic element provided that Courant-Snyder (CS) are known at entrance and exit of the magnetic element. one can write matrix equation for position and slope of a charged particle in term of CS variables as [20]

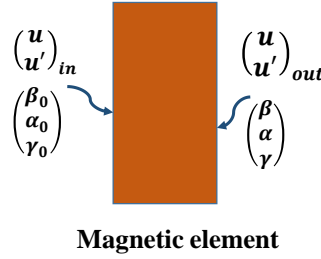


Fig. 1.11: Position and slope of a particle after passing through a magnetic element.  $(\beta_0, \alpha_0, \gamma_0)'$  and  $(\beta, \alpha, \gamma)'$  are CS variables at entrance and exit of the magnetic element.

$$\begin{pmatrix} u \\ u' \end{pmatrix}_{out} = \begin{pmatrix} \sqrt{\frac{\beta}{\beta_0}}(\cos \phi + \alpha_0 \sin \phi) & \sqrt{\beta\beta_0} \sin \phi \\ \frac{(\alpha_0 - \alpha) \cos \phi - (1 + \alpha\alpha_0) \sin \phi}{\sqrt{\beta\beta_0}} & \frac{\beta_0}{\beta}(\cos \phi - \alpha \sin \phi) \end{pmatrix} \begin{pmatrix} u \\ u' \end{pmatrix}_{in}. \quad (1.54)$$

Here, *in* and *out* denote entrance and exit of the magnetic element. Eq.(1.54) is true for any charged particle trajectory. CS variables are properties of magnetic element and each charged particle having different position and slope will experience same values of these variables.

For a periodic system  $\beta = \beta_0$  and  $\alpha = \alpha_0$ , eq.(1.54) reduces to

$$\begin{pmatrix} u \\ u' \end{pmatrix}_{out} = M \begin{pmatrix} u \\ u' \end{pmatrix}_{in}, \quad (1.55)$$

where matrix  $M$  is the transfer matrix which is given by

$$M = \begin{pmatrix} \cos \mu + \alpha \sin \mu & \beta \sin \mu \\ \gamma \sin \mu & \cos \mu - \alpha \sin \mu \end{pmatrix}, \quad (1.56)$$

here  $\mu$  is the phase advance for one turn or one super period [A.2]. This  $2 \times 2$  matrix is called one turn or one period matrix and further, it can be written as

$$M = I \cos \mu + J \sin \mu, \quad (1.57)$$

where  $I$  is the  $2 \times 2$  identity matrix and  $J$  is given by

$$J = \begin{pmatrix} \alpha & \beta \\ -\gamma & -\alpha \end{pmatrix}; \quad \text{with property } J^2 = -I. \quad (1.58)$$

Transfer matrix in this form has an advantage that it can be written as  $M = \exp(J\mu)$ .

If charged particle makes  $n$  turns in the ring then for stability of this charged particle in the whole ring, there must be a stability criteria. In any large circular accelerator, a unit periodic structure is repeatedly used to make complete structure of circular accelerator. Number of repetition of this periodic structure is called super period. If  $M_p$  is the transfer matrix for one super period and charged particles makes  $n$  turns in a storage ring then transfer matrix for  $p$  super period and  $n$  turns is given as follows

$$M = ((M_p)^p)^n = (M_p)^{np} = \exp(npJ\mu). \quad (1.59)$$

To ensure stability of particles after  $n$  turns,  $\mu$  must be real and matrix element of  $M$  must be finite. From eq.(1.56), a necessary condition for stability of charged particles can be derived as [20]

$$|\text{Trace}(M)| = |2 \cos \mu| \leq 2. \quad (1.60)$$

In addition, CS variables at the entrance and exit can be related for a magnetic element if transfer matrix  $M$  for a magnetic element is known. Consider CS variables at the entrance

of the magnetic element, are  $(\beta, \alpha, \gamma)_{in} = (\beta_0, \alpha_0, \gamma_0)$ , then CS variables at the exit is given

by [19]

$$\begin{pmatrix} \beta \\ \alpha \\ \gamma \end{pmatrix}_{in} = \begin{pmatrix} M_{11}^2 & -2M_{11}M_{12} & M_{12}^2 \\ -M_{11}M_{21} & M_{11}M_{22} + M_{12}M_{21} & -M_{12}M_{22} \\ M_{21}^2 & -2M_{21}M_{22} & M_{22}^2 \end{pmatrix} \begin{pmatrix} \beta_0 \\ \alpha_0 \\ \gamma_0 \end{pmatrix} \quad (1.61)$$

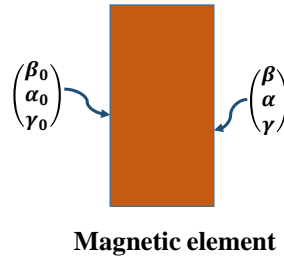


Fig. 1.12: CS variables at the entrance and exit of the magnetic element.

Eq.(1.61) is an important relation to see the behaviour of CS variables in different magnetic elements e.g. for a drift space, the transfer matrix  $M$  can be given in terms of path length,  $s$ , as

$$M = \begin{pmatrix} 1 & s \\ 0 & 1 \end{pmatrix}. \quad (1.62)$$

Therefore,

$$\begin{pmatrix} \beta \\ \alpha \\ \gamma \end{pmatrix} = \begin{pmatrix} 1 & -2s & s^2 \\ 0 & 1 & -s \\ 0 & 0 & 1 \end{pmatrix} \begin{pmatrix} \beta_0 \\ \alpha_0 \\ \gamma_0 \end{pmatrix}. \quad (1.63)$$

Hence,

$$\begin{aligned} \beta(s) &= \beta_0 - 2\alpha_0 s + s^2 \gamma_0 \\ \alpha(s) &= \alpha_0 - s \gamma_0 \\ \gamma(s) &= \gamma_0. \end{aligned} \quad (1.64)$$

From eq.(1.64),  $\beta(s)$  follows a parabolic nature in drift space,  $\alpha(s)$  is linear with  $s$  and  $\gamma(s)$  is constant throughout drift space.

Some concepts like betatron tune, chromaticity, momentum compaction factor play important role in operation of practical storage ring. These are discussed in the Sections 1.9, 1.10 and 1.11.

## 1.9 Betatron tune

Off axis particle oscillates about designed orbit due to focusing nature of the quadrupoles. The number of oscillations per revolution is called betatron tune and denoted by  $\nu_x$  for horizontal plane and  $\nu_y$  in vertical plane. Expression for betatron tune is given by [A.2]

$$\nu_{x,y} = \frac{\mu_{x,y}}{2\pi} = \frac{1}{2\pi} \oint \frac{1}{\beta_{x,y}(s)} ds, \quad (1.65)$$

where  $\mu_{x,y} = \oint \frac{1}{\beta_{x,y}(s)} ds$  is the phase advance for complete ring.

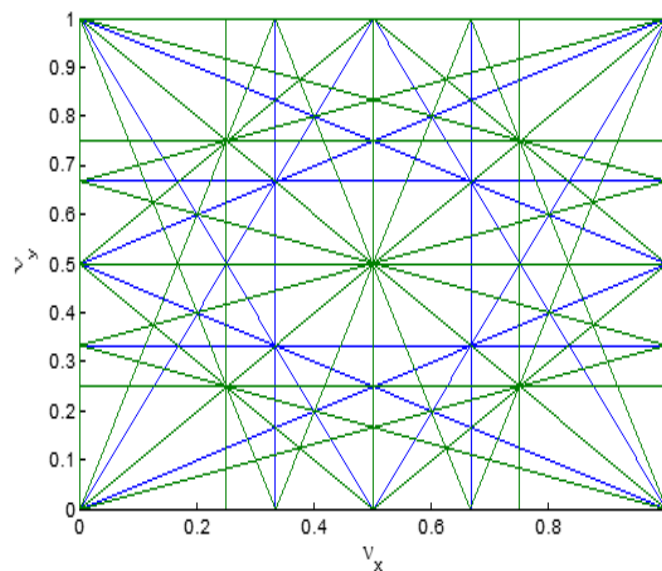


Fig. 1.13: Tune diagram for fractional betatron tune up to fourth order resonance.

Any practical storage ring is not ideal, errors, either systematic or random, always are present in the practical machine. Imperfections in the machine, e.g. dipolar error, quadrupolar

error, sextupolar error, excite resonances in the storage ring. Therefore, for stable oscillations, there are restriction on the betatron tunes. For example betatron tune should not be integer or half integer or one third integer. Dipolar error generates first order resonances or integer tune resonances, quadrupolar error generates second order or half integer tune resonances and sextupole error generates third order resonances. General condition for resonance can be written as  $m\nu_x + n\nu_y = l$ , where  $m, n, l$  are integers. This is the equation of straight line in a 2-D plane, called tune space. This is shown in Fig.1.13 up to fourth order. Each line is a resonance line and  $|m| + |n|$  is called order of resonance. In order to operate a storage ring, the fractional betatron tunes in both planes should be far away from the resonance lines.

## 1.10 Chromaticity

Generally, in a storage ring there are bunches instead of a single charged particle and these bunches have large number of charged particles. In addition, single bunch has spread in energy, i.e., each charged particle has small energy deviation from the reference charged particle. After passing through the quadrupole, these different energy charged particles experience different focusing force, and as a result, they focus at different points. This phenomenon is called chromaticity.

Momentum dependent quadrupole strength is given as [2]

$$k(p) = \frac{e}{p}g, \quad (1.66)$$

here  $e$  is the charge on charged particle. Then change in quadrupole strength will be

$$\Delta k = \frac{dk}{dp}\Delta p = \frac{eg}{p_0} \left( \frac{\Delta p}{p_0} \right) = -k\delta \quad (1.67)$$

$$\Delta k = \begin{cases} k\delta, & \text{for horizontal motion } (k > 0) \\ -k\delta, & \text{for vertical motion } (k < 0) \end{cases} \quad (1.68)$$

For horizontal focusing quadrupole, higher momentum charged particle experiences weaker quadrupole strength and vice versa for lower momentum charged particles. These effects introduce shift in betatron tune, which may cross the resonance line and may lead to loss of the beam. Total betatron tune shift can be given as [5, 6]

$$\Delta\nu_{x,y} = \frac{1}{4\pi} \int \beta_{x,y}(s) \Delta k_{x,y}(s) ds = \mp \frac{1}{4\pi} \int \beta_{x,y} \frac{\Delta p}{p_0} k(s) ds. \quad (1.69)$$

Taking  $k$  positive, naturally occurring chromaticities for both planes of the machine are defined as [5]

$$\xi_{x,y} = \frac{\Delta\nu_{x,y}}{\frac{\Delta p}{p_0}} = -\frac{1}{4\pi} \oint \beta_{x,y} k(s) ds. \quad (1.70)$$

For a strong focusing machine, natural chromaticity is always negative [5]. Natural chromaticity depends on betatron function and strength of the quadrupoles only, i.e., higher strength quadrupole placed at higher beta functions will lead to higher natural chromaticity. Correction of natural chromaticity is done by using sextupoles. Expression for chromaticity correction for horizontal and vertical planes are given by [5]

$$\xi_{x,y} = -\frac{1}{4\pi} \oint \beta_{x,y}(s) [k(s) \mp S(s)\eta(s)] ds, \quad (1.71)$$

where  $S(s)$  is the sextupole strength. Using appropriate strength of the sextupole, one can achieve desired value of chromaticity in the machine. To efficiently correct the chromaticity in each plane, chromatic sextupoles should be placed at the location where dispersion is non-zero and betatron functions are well separated. Horizontal chromaticity correction needs large horizontal and small vertical beta function and vice versa for the vertical chromaticity correction. Sextupole having a strength  $S$ , compensate the focusing error by deflecting higher momentum charged particle and lower momentum charged particle towards the focusing point.

In a storage ring, there are two types of aperture: (i) physical aperture, which is defined by boundary of vacuum chamber, and (ii) dynamic aperture, which is a completely theoretical

phenomenon. Dynamic aperture is defined as "stable area of a boundary under non-linear forces". Non-linear forces arise due to non-linear magnetic fields e.g. fields of sextupoles, octupoles and multipoles due to errors in the practical electron storage ring. Multipole fields excite various higher order resonances and leads to particle loss in the beam. Therefore, area available for stable oscillation of charged particles gets reduced.

Dynamic aperture of an electron beam in the storage ring is a hypothetical aperture beyond which any charged particle will not survive. This means that if a charged particle is inside of dynamic aperture, then it has stable oscillations for sufficient number of turns. It is always experienced that large dynamic aperture provides good operating condition for a any electron storage ring. It is very challenging to increase the dynamic aperture. Dynamic aperture can be calculated by tracking of charged particle through the storage ring. The plot of all maximum stable initial amplitude gives dynamic aperture boundary.

## 1.11 Momentum compaction factor

The path length of a closed off-momentum charged particle will differ from the path length of the reference charged particle (which is defined to be the circumference,  $C$ ). Momentum compaction is defined as relative change in circumference per unit relative momentum off-set and denoted by  $\alpha_c$  [2].

$$\alpha_c = \frac{\frac{\Delta L}{L}}{\frac{\Delta p}{p}} = \frac{\Delta L}{L} \frac{p}{\delta}. \quad (1.72)$$

This quantity tells us about how orbits are closely packed for different off-energy charged particles.  $\alpha_c$  can be negative, positive or zero depending on the energy deviation of the particle.

$\alpha_c$  is related with dispersion as

$$\alpha_c = \frac{1}{C} \oint \frac{\eta(s)}{\rho(s)} ds. \quad (1.73)$$

In a storage ring, a low value of  $\alpha$  is desired to make beam close to reference orbit, which is also a challenging task for a storage ring lattice designer.

In an electron storage ring, emission of synchrotron radiation affects the dynamics of electron beam which is discussed below.

## 1.12 Effect of synchrotron radiation on electron beam in the storage ring

A relativistic charged particle when accelerated in a macroscopic electromagnetic field emits radiation which is called synchrotron radiation (SR). Instantaneous power radiated by such a charged particle is given by [21]

$$P = \frac{2e^2}{3c} \gamma^6 \left( (\dot{\vec{\beta}})^2 - (\vec{\beta} \times \dot{\vec{\beta}})^2 \right), \quad (1.74)$$

where  $e$  is the charge of the charged particle,  $\gamma$  is the Lorentz factor,  $c$  is the speed of the light,  $\vec{\beta} = \frac{\vec{v}}{c}$  is the velocity and  $\dot{\vec{\beta}} = \frac{\dot{\vec{v}}}{c}$  is the acceleration of the charged particle. In terms of accelerating forces, the rate of radiated energy is proportional to the square of the accelerating force. Also, the rate depends on the angle between the force and the charged particle's velocity and is larger by the factor  $\gamma^2 = \left( \frac{E}{m_0 c^2} \right)^2$  when the force is perpendicular to the velocity than when the force is parallel to the velocity. In a circular accelerator the typical longitudinal forces (from the accelerating system) are much weaker than the typical transverse magnetic forces. Therefore, one needs to consider the radiation effects that accompanied by the magnetic forces only.

Energy lost by an electron, having energy  $E$ , in one turn in an electron storage ring is given by [22]

$$U = \frac{C_\gamma \beta_0 E^4}{2\pi} \oint \frac{ds}{[\rho(s)]^2} = \frac{c_\gamma E^4}{2\pi} \oint \frac{ds}{[\rho(s)]^2}, \quad (1.75)$$

here  $\beta_0 = 1$  (at ultrarelativistic speed),  $C_\gamma = \frac{e^2}{3\epsilon_0(m_0c^2)^4}$  is a constant and for electrons this constant has a numerical value equal to  $8.846 \times 10^{-5}$  [m.GeV<sup>-3</sup>].  $I_2$  is the second radiation integral and is defined as [22]

$$I_2 = \oint \frac{ds}{[\rho(s)]^2} \quad (1.76)$$

Second radiation integral is inversely proportional to square of the local radius of curvature and for an isomagnet (constant field dipole), it is a constant and has value  $\frac{2\pi}{\rho}$ . Thus, for an isomagnet energy loss per turn can be given as [A.3]

$$U_0 = 88.575 \frac{[E(\text{GeV})]^4}{\rho}. \quad (1.77)$$

Eq.(1.77) shows that, electron storage rings with small radius of curvature (high magnetic field) have higher energy loss per turn.

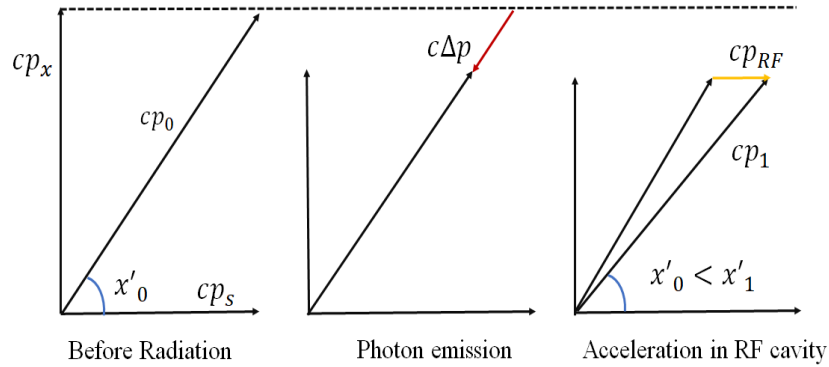


Fig. 1.14: Radiation damping phenomenon in horizontal plane.  $p_x$  and  $p_s$  are the momentum of electron in horizontal and longitudinal direction respectively.  $p_{RF}$  is the momentum provided by RF cavity.  $x'_0$  is the initial slope of electron and  $x'_1$  is the slope of electron after passing through RF cavity.

In an electron storage ring, emission of SR has damping effect on betatron oscillations as well as synchrotron oscillations (oscillations in longitudinal direction). This damping effect is called radiation damping. Fig.1.14 explains the phenomenon of radiation damping in the horizontal plane. To understand this, consider an electron oscillating about a closed orbit in horizontal plane having momentum  $p_0$ , after emission of SR in bending magnet, the momentum

of an electron reduced by  $\Delta p$  in the direction of SR emission. The loss of momentum is compensated by RF cavity. But, as shown in Fig. 1.14, after passing through the RF cavity only longitudinal component of momentum,  $p_s$ , is compensated and energy is restored. As a result, slope of the electron is decreased. As electron moves in the ring, slope of electron decreases turn by turn. This radiation damping phenomenon is true for each electron in the beam which emits radiation and it leads to reduction in beam emittance. Also, this radiation damping happens in each plane, i.e., horizontal, vertical and longitudinal planes. The rate equation of damping of horizontal beam emittance is given by [22]

$$\frac{d\epsilon_x}{dt} = -\frac{2}{\tau_x}\epsilon_x. \quad (1.78)$$

Similarly, for vertical beam emittance

$$\frac{d\epsilon_y}{dt} = -\frac{2}{\tau_y}\epsilon_y. \quad (1.79)$$

Damping times in horizontal, vertical and longitudinal planes are given by [22]

$$\tau_x = \frac{2E_0}{j_x U_0} T_0, \quad (1.80)$$

$$\tau_y = \frac{2E_0}{j_y U_0} T_0, \quad (1.81)$$

$$\tau_s = \frac{2E_0}{j_s U_0} T_0, \quad (1.82)$$

where  $T_0$  is the time period for one revolution and  $j_{i=x,y,s}$  is called damping partition number and are given as [22]

$$j_x = 1 - \frac{I_4}{I_2}, \quad j_y = 1, \quad j_s = 2 + \frac{I_4}{I_2}. \quad (1.83)$$

Here,  $j_x$ ,  $j_y$ , and  $j_s$  are called horizontal, vertical and longitudinal damping partition number, respectively.  $I_4$  is the fourth radiation integral and is defined as [22]

$$I_4 = \oint \frac{\eta_x(s)}{\rho(s)} \left( \frac{1}{[\rho(s)]^2} + 2k_1 \right) ds, \quad (1.84)$$

where  $k_1$  is the normalized quadrupole strength in the dipole magnet. This type of magnets are called combined function magnet. For a homogeneous field dipole magnet  $k_1$  becomes zero. The damping partition numbers satisfy an important relation called Robinson theorem which is given as [22]

$$j_x + j_y + j_s = 4. \quad (1.85)$$

Significance of Robinson theorem is this, damping in a particular plane can be influenced by damping in the other planes, because total damping number must be constant.

After so many turns, slope of electrons in the beam must go to zero, consequently beam emittance will reduce to zero if only radiation damping phenomenon occurs. However, there exist finite value of beam emittance called equilibrium or natural beam emittance. This is because of counter effect that occurs in the electron storage ring, called quantum excitation.

It is well established that emission of SR radiation is discrete and quantum in nature. As shown in Fig.1.15, after emission of photon from an on energy closed orbit electron, there is a sudden change in energy of the electron and it oscillates about an off-energy closed energy. In addition, electron beam consist of large number of electrons in the form of bunches. There is energy spread in these electron bunches. Therefore, photons emitted from different electrons are of different energy and also, random in nature [22, 23]. These sudden change in energies of electrons act as noise or fluctuation source in the phase space and act opposite to the radiation damping, which prevent the betatron amplitude of oscillations to be damped to zero. Due to quantum excitation, oscillations grow up unless they are balanced by radiation damping. Including these two phenomena a rate equation for horizontal emittance can be written as [22]

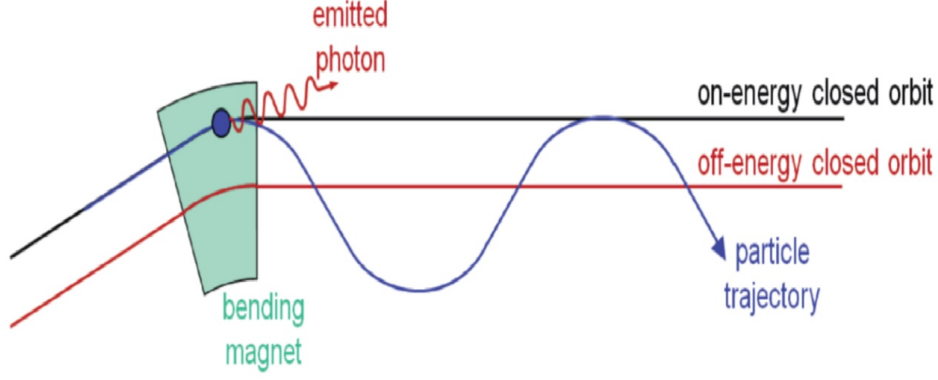


Fig. 1.15: Quantum Excitation phenomenon.

$$\frac{d\epsilon_x}{dt} = -\frac{2}{\tau_x}\epsilon_x + \frac{2}{\tau_x}C_q\gamma^2\frac{I_5}{j_x I_2}. \quad (1.86)$$

In eq.(1.86), first term arises from radiation damping and second term arises from quantum excitation. In the equilibrium condition,  $\frac{d\epsilon_x}{dt} = 0$ , and emittance is given by

$$\epsilon_{x0} = C_q\gamma^2\frac{I_5}{j_x I_2}. \quad (1.87)$$

$\epsilon_{x0}$  is called natural emittance and  $C_q = \frac{55}{32\sqrt{3}}\frac{\hbar}{m_0c}$ ,  $\hbar$  is the Plank constant divided by  $2\pi$ . For electron storage rings, its value is equal to  $C_q = 3.832 \times 10^{-12}\text{m}$ .  $I_5$  is the fifth radiation integral and is defined as [22]

$$I_5 = \oint \frac{\mathcal{H}_x(s)}{[\rho(s)]^3} ds. \quad (1.88)$$

$I_5$  depends on  $\mathcal{H}$  function and inversely proportional to cubic power of local radius of curvature.

The  $\mathcal{H}$  function is defined as [22]

$$\mathcal{H}_x = \gamma_x\eta_x^2 + 2\alpha_x\eta_x\eta_x' + \beta_x\eta_x'^2. \quad (1.89)$$

The  $\mathcal{H}_x(s)$  function depends on twiss parameters, dispersion and its derivative. There are two more radiation integral which are defined as [22]

$$I_1 = \oint \frac{\eta_x(s)}{\rho(s)} ds, \quad (1.90)$$

$$I_3 = \oint \frac{ds}{|\dot{\rho}(s)|^3}. \quad (1.91)$$

$I_1$  is related to the momentum compaction factor  $\alpha_c$ , which plays an important role in the longitudinal dynamics and  $I_3$  is related to equilibrium energy spread in a bunch, which is given by

$$\sigma_{\delta 0} = C_q \gamma^2 \frac{I_3}{j_s I_2}. \quad (1.92)$$

For y-direction, ideally there should not be any dispersion. Therefore,  $\mathcal{H}$  and hence fifth radiation integral must be zero. This implies that the vertical emittance must be zero. However, in deriving equation for the natural emittance, it is assumed that all photons were emitted directly along the instantaneous direction of motion of electron. In fact, photons are emitted with a distribution with angular width  $\frac{1}{\gamma}$  about the direction of motion of the electron [22]. This leads to some vertical recoil that excite vertical betatron motion, resulting a non-zero vertical emittance. An expression for lower limit of the vertical beam emittance, called quantum limit, is given by [22].

$$\epsilon_{y,min} = \frac{12}{55} \frac{C_q}{I_2} \oint \frac{\beta_y(s)}{|\dot{\rho}(s)|^3} ds. \quad (1.93)$$

Though vertical beam emittance has finite value, but, still it is much smaller than the natural beam emittance. Also, errors and betatron coupling in the practical electron storage ring, increase the vertical beam emittance. It is always desirable to make errors in the practical machine as small as possible to achieve quantum limit of vertical beam emittance.

Important mathematical relations are summarized in Table 1.1.

Table 1.1: Important mathematical relations [2, 22]

Radiation integral $I_1$	$\oint \frac{\eta_x(s)}{\rho(s)} ds$
Radiation integral $I_2$	$\oint \frac{ds}{[\rho(s)]^2}$

Radiation integral $I_3$	$\oint \frac{1}{ \rho^3 }$
Radiation integral $I_4$	$\oint \frac{\eta_x(s)}{\rho(s)} \left( \frac{1}{[\rho(s)]^2} + 2k_1 \right) ds$
Radiation integral $I_5$	$\oint \frac{\mathcal{H}_x(s)}{[\rho(s)]^3} ds$
Energy loss per turn	$88.575 \frac{[E(\text{GeV})]^4}{\rho}$
Natural emittance $\epsilon_x$	$C_q \gamma^2 \frac{I_5}{j_x I_2}$
Damping partition numbers	$j_x = 1 - \frac{I_4}{I_2}, j_y = 1, j_s = 2 + \frac{I_4}{I_2}$
Horizontal damping time $\tau_x$	$\frac{2E_0}{j_x U_0} T_0$
Vertical damping time $\tau_y$	$\frac{2E_0}{j_y U_0} T_0$
Longitudinal damping time $\tau_s$	$\frac{2E_0}{j_s U_0} T_0$
Robinson's theorem	$j_x + j_y + j_s = 4$
$\mathcal{H}$ function	$\gamma\eta^2 + 2\alpha\eta\eta' + \beta\eta'^2$
Equilibrium energy spread $\sigma_{\delta 0}$	$C_q \gamma^2 \frac{I_3}{j_s I_2}$

## 1.13 Different types of magnetic lattices and equilibrium emittance

In order to achieve low emittance different type of lattices are proposed such as theoretical minimum emittance (TME), double bend achromat (DBA), and triple bend achromat (TBA),

a combination of TME and DBA. Now a days multi bend achromat (MBA) lattice are used to achieve ultra low emittance in electron storage rings. Natural beam emittance can be written as averaged quantities as [20]

$$\epsilon_{x0} = C_q \gamma^2 \frac{I_5}{j_x I_2} = C_q \gamma^2 \frac{\langle \frac{\mathcal{H}_x(s)}{\rho^3(s)} \rangle}{\langle \frac{1}{\rho^2(s)} \rangle}. \quad (1.94)$$

For a lattice which utilizes isomagnetic dipole,  $\rho$  is constant and beam emittance is given by

$$\epsilon_{x0} = C_q \gamma^2 \frac{I_5}{j_x I_2} = C_q \gamma^2 \frac{\langle \mathcal{H}_x(s) \rangle}{j_x \rho}. \quad (1.95)$$

Storage ring having isomagnetic dipoles, the horizontal damping partition number  $j_x \sim 1$  and  $\langle \mathcal{H}_x \rangle$  is the average over the dipoles [20]. Therefore, to minimize emittance is equivalent to minimize  $\langle \mathcal{H}_x \rangle$  over the dipole with respect to  $\eta_x$  and  $\beta_x$ .

The theoretical minimum beam emittance in the isomagnetic lattice is given by [5]

$$\epsilon_{x,min} = F_{lat} C_q \gamma^2 \theta^3, \quad (1.96)$$

where  $\theta$  is the bending angle of the dipole.  $F_{lat}$  is called form factor, which depends on the particular magnetic cell structure. From eq.(1.96), it can be seen that beam emittance depends on third power of the bending angle. For a fixed energy electron storage ring  $C_q \gamma^2$  is constant. Therefore, emittance in a given storage ring with fixed energy can be reduced with dipoles with smaller bending angle. But small bending will lead to large number of dipoles to bend the electron by 360 deg and this leads to large size of storage ring, consequently cost of the storage ring will increase.

### 1.13.1 Theoretical minimum emittance (TME) lattice

In a TME lattice, there is a single dipole in the unit lattice cell. Dispersion and beta functions are symmetric with respect to centre of the dipole magnet as shown in Fig.1.16. After

minimizing  $\mathcal{H}_x$  with respect to horizontal beta function and horizontal dispersion function  $\eta_x$  over the dipole, the minimum of the average of  $\mathcal{H}_x$  function is given by [5, 20]

$$\langle \mathcal{H}_x \rangle = \frac{1}{12\sqrt{15}} \rho \theta^3, \quad (1.97)$$

where  $\rho$  and  $\theta$  are the radius of curvature and bending angle of the dipole. Values of  $\beta_x$  and  $\eta_x$  at the entrance and at centre of the dipole magnet are given as

$$\text{at the entrance of the dipole : } (\beta_0, \alpha_0, \eta_0, \eta'_0) = \left( \frac{8}{\sqrt{15}}L, \sqrt{15}, 6L\theta, -2\theta \right), \quad (1.98)$$

$$\text{at the centre of the dipole : } (\beta_c, \eta_c)_{TME} = \left( \frac{1}{\sqrt{60}}L, \frac{L\theta}{24} \right), \quad (1.99)$$

here  $L$  is the length of the dipole. Theoretical minimum emittance is given by

$$\epsilon_{x,TME} = \frac{1}{12\sqrt{15}} C_q \frac{\gamma^2 \theta^3}{j_x}. \quad (1.100)$$

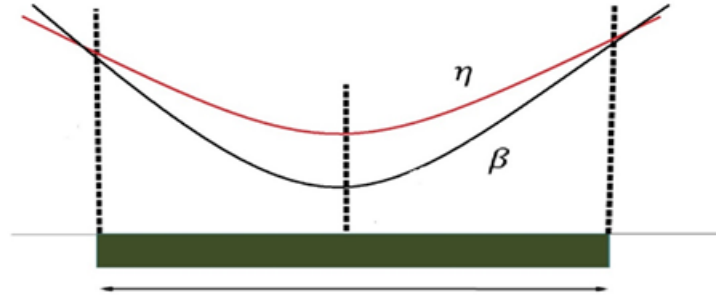


Fig. 1.16: Variation of horizontal beta and dispersion function in case TME lattice. Both functions have minima at the centre of the bending magnet.

For a TME lattice form factor is taken as 1. Though TME lattice has lowest minimum emittance. But they cannot be used for third generation synchrotron radiation sources due to requirement of zero dispersion at the location of IDs. Both horizontal beta function and dispersion function attain higher value in the quadrupoles, therefore, generate large negative

natural chromaticity. Therefore, much stronger sextupoles are required to correct the chromaticity. In addition, dispersion is nonzero at the ID straight section, which is not desirable. Hence, TME lattice is not the proper choice for the storage ring lattice. Therefore, a lattice called DBA is used which provide zero dispersion at location of IDs.

### 1.13.2 Double bend achromat (DBA)lattice

This type of lattice consists two bending magnets in the unit lattice cell to make an achromat. If dispersion and it derivative are zero at the entrance of the dipole magnet, it is called achromatic condition and lattice which provide achromatic condition is called achromat. The dispersion free region is utilized for installation of IDs. This type of lattice is most widely used in electron storage rings. In Fig.1.17, part of the achromat is shown. In this type of lattice minimum of beta function is not at the centre of the bending magnet. After minimizing  $\langle \mathcal{H}_x(s) \rangle$  with respect to  $\beta_x$  and  $\alpha_x$ , minimum of  $\langle \mathcal{H}_x \rangle$  is given by [20]

$$\langle \mathcal{H}_x \rangle_{MEDBA} = \frac{1}{4\sqrt{15}} \rho \theta^3, \quad (1.101)$$

with the condition on  $\beta_x$  and  $\alpha_x$  at the entrance as [20]

$$\beta_0 = \frac{6}{\sqrt{15}} L \quad \alpha_0 = \sqrt{15} \quad \gamma_0 = \frac{8\sqrt{5}}{\sqrt{3}}. \quad (1.102)$$

Minimum beam emittance is given by [5, 20]

$$\epsilon_{x,DBA} = \frac{1}{4\sqrt{15}} C_q \frac{\gamma^2 \theta^3}{j_x}. \quad (1.103)$$

After choosing optimum values of  $\beta_0 = \frac{6}{\sqrt{15}} L$  and  $\alpha_0 = \sqrt{15}$  at the entrance of the dipole, beta function achieves minimum value  $\beta_{x,minimum} = \frac{3}{4\sqrt{60}} L$  at  $s_0 = \frac{3}{8} L$  in the dipole magnet. From eq.(1.100) and eq.(1.103) we found that

$$\epsilon_{x,DBA} = 3\epsilon_{x,TME} \quad (1.104)$$

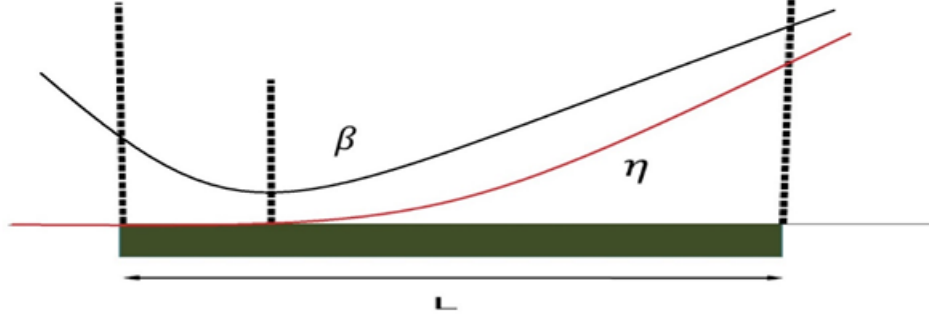


Fig. 1.17: Variation of horizontal beta and dispersion function in the first dipole of DBA lattice.

Dispersion and its derivative are zero at the entrance of the dipole.

Though form factor for DBA is three time higher than the TME, a practical storage ring in DBA configuration acquires even higher form factor than 3, generally, in the range of 3-10 [24]. For some storage rings, it may be higher than 10.

### 1.13.3 Multi bend achromat (MBA) lattice

To achieve much lower natural emittance, concept of MBA lattice was introduced. In MBA lattice more than two dipole magnets are normally used. In a MBA lattice, more number of TME dipoles are introduced between the two dipoles of DBA lattice. The minimum emittance in a MBA lattice is given by [5]

$$\epsilon_{x,MBA} = \frac{1}{12\sqrt{15}} \left( \frac{M+1}{M-1} \right) C_q \frac{\gamma^2 \theta^3}{j_x}, \quad (1.105)$$

where  $M$  is the number of dipole in the MBA lattice and for equal bending angle in all dipole used,  $\theta$  is the average angle of all dipoles. Now a days, MBA lattice is more preferred to achieve ultra low emittance in the electron storage rings.

## 1.14 RMS beam sizes

In dispersion free region, the RMS beam sizes and beam divergences in the transverse plane are defined by only betatron function and are given as [22]

$$\text{Horizontal plane: } \sqrt{\epsilon_x \beta_x(s)}, \quad \sqrt{\epsilon_x \gamma_x(s)}, \quad (1.106)$$

$$\text{Vertical plane: } \sqrt{\epsilon_y \beta_y(s)}, \quad \sqrt{\epsilon_y \gamma_y(s)}, \quad (1.107)$$

For a region where dispersion is finite, the RMS beam sizes and divergences are given by

$$\text{Horizontal plane: } \sqrt{\epsilon_x \beta_x(s) + (\eta_x \sigma_\delta)^2}, \quad \sqrt{\epsilon_x \gamma_x(s) + (\eta'_x \sigma_\delta)^2}, \quad (1.108)$$

$$\text{Vertical plane: } \sqrt{\epsilon_y \beta_y(s) + (\eta_y \sigma_\delta)^2}, \quad \sqrt{\epsilon_y \gamma_y(s) + (\eta'_y \sigma_\delta)^2}, \quad (1.109)$$

where  $\epsilon_x$  and  $\sigma_\delta$  are RMS beam emittance and RMS momentum spread.

## 1.15 Advance methods to improve beam emittance

In last few decades, new advance methods were introduced to reduce the beam emittance further, like transverse gradient, longitudinal gradient bend (LGB), and anti bend etc. in the dipole magnet. Here, we have discussed transverse gradient and LGB in a dipole.

Natural horizontal beam emittance as given in eq.(1.87) is

$$\epsilon_{x0} = C_q \gamma^2 \frac{I_5}{j_x I_2}. \quad (1.110)$$

Here, the first term  $C_q$  is constant and second term  $\gamma^2$  is also a constant as energy in the storage ring is fixed. Therefore, in order to reduce the beam emittance, only radiation integrals and horizontal damping partition number are to be optimized. This can be done in following two ways.

**Maximize  $j_x$ :** From eq.(1.84), if we introduce negative quadrupole gradient in dipole magnet in such a way that the quantity  $\frac{I_4}{I_2}$  becomes  $-ve$ , then  $j_x$  can be made greater than 1 and beam emittance will reduce. As Robinson's theorem puts a limit on  $j_x$ , the value of  $j_x$  can be increased up to 2 only. Also, if one increase the  $j_x$  above 2 by increasing  $k_1$ , the dipole will loose its dipole nature and behaves like a pure quadrupole and it is also difficult task to provide such gradient in the dipole magnet. It means, improving horizontal damping partition number, one can reduce beam emittance by a factor of 2. Physically, increasing horizontal damping partition number means rate of radiation damping will increase, i.e., electron beam will damp fast for the same quantum excitation.

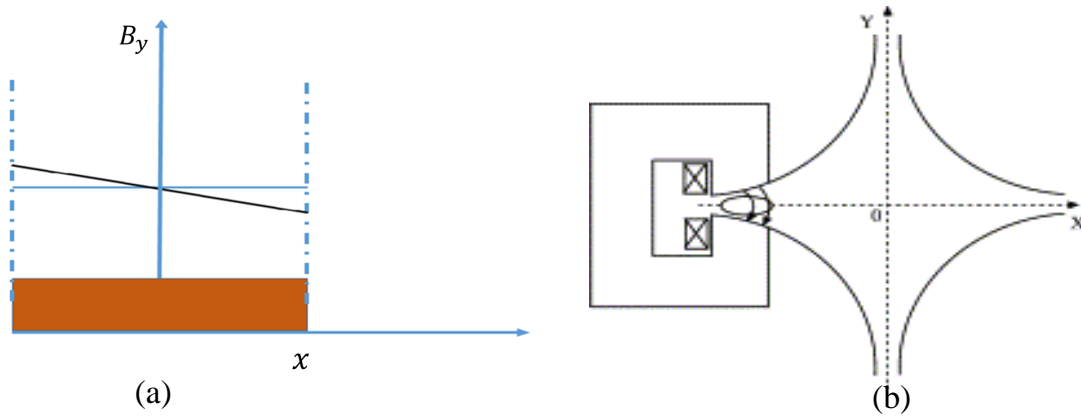


Fig. 1.18: (a) Linear variation of magnetic field along  $x$ -direction (black) and compared with homogeneous field (blue). (b) Shape of dipole to get linearly decreasing magnetic field.

Since bending of electron is in horizontal plane, there will not be any effect on  $j_y$ . Therefore,  $j_s$  will increase due to Robinson theorem. Also,  $j_s$  is inversely proportional to energy spread in the bunch [24], energy spread of bunch will increase and this leads to increase in bunch length that is not desirable in electron storage rings. In Fig. 1.18, a linearly decreasing magnetic field compared with homogeneous magnetic field is shown. At the center of dipole both have same value of field. The linearly decreasing magnetic field will provide quadrupole gradient in the dipole. Also, a curved shape of dipole is shown to produce linearly decreasing

magnetic field.

**Minimize the term  $\frac{I_5}{I_2}$ :**  $I_5$  contains  $\mathcal{H}$  function in the numerator which is defined in eq.(1.89) and  $\rho^3$  in the denominator. If, one is able to reduce the  $\mathcal{H}$  function or increase the radius of curvature or both in the dipole magnet, emittance will decreased naturally. To achieve this goal, a longitudinal variation in dipole field profile was introduced [10]. These dipoles then termed as longitudinal gradient bend (LGB). The LGB field profile instead of homogeneous magnetic field in the dipole causes  $\mathcal{H}$  function and radius of curvature to vary differently. In recent studies, it was established that LGB profile follows parabolic decay [24] of the magnetic field over the length of the dipole magnet. For achromat case, magnetic field decreases from high value at one end to low value at other end as shown in Fig. 1.19 [24]. This LGB profile helps in providing two major beam dynamical advantages: (i) reduction of beam emittance, and (ii) large dispersion at the sextupole location.

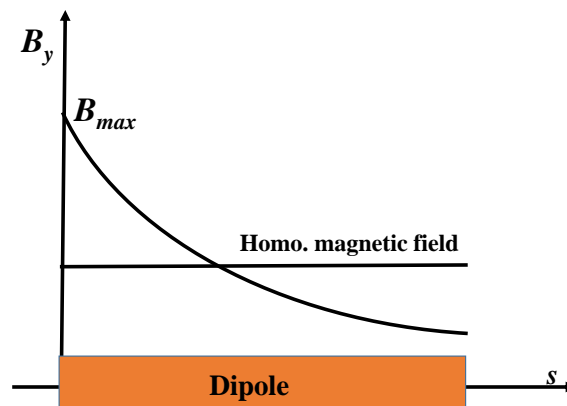


Fig. 1.19: Variation of longitudinal field profile in the dipole magnet of a DBA lattice

For a TME lattice, the magnetic field profile is such that its maximum occurs at the center of the dipole and field reduces symmetrically to lower value on either side as shown in Fig. 1.20 [24]. This LGB profile satisfy only one purpose, i.e., reduction of beam emittance.

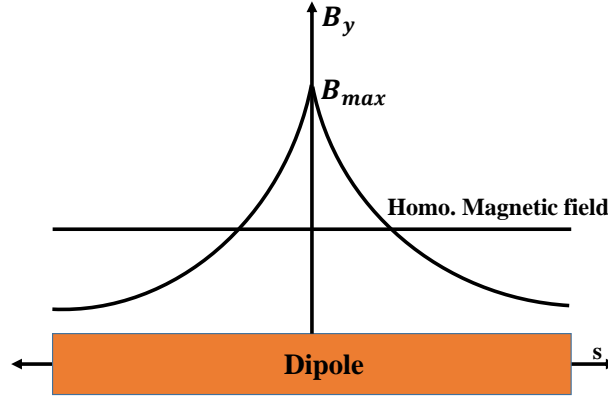


Fig. 1.20: Variation of longitudinal field profile in the dipole of TME lattice

Using this type of LGB profile dispersion will reduce at the centre of dipole and consequently  $\mathcal{H}$  function will reduce. This leads to reduction in beam emittance. Physically in both cases i.e achromat and TME, we are reducing the quantum excitation in the dipole magnet.

## 1.16 Indus-2 storage ring lattice

In India, there are two electron storage ring based SRSs namely Indus-1 and Indus-2, located at RRCAT, Indore. Indus-1, a 450 MeV energy synchrotron radiation source has circumference of 18 m, which provides SR in the vacuum ultraviolet range. Indus-2, which is a third generation electron storage ring, has energy 2.5 GeV and provides synchrotron radiation in the hard x-rays regime [3,4]. This radiation is very useful for variety of material study. A schematic layout of Indus-1 and Indus-2 synchrotron radiation source facility is shown in Fig. 1.21. The base line lattice of Indus-2 was designed for beam emittance of 58 nm.rad.

Both storage rings share a common injector system consisting of a 20 MeV microtron and 20-450/550 MeV booster synchrotron [3–5]. Unit lattice cell of Indus-2 is based on DBA or Chessman Green lattice. In unit lattice cell, there are 2 dipole magnets for bending of beam, 9 quadrupoles (4 focusing type and 5 defocusing type) for focusing and defocusing action of beam, 4 sextupoles (2 focusing and 2 defocusing) for chromaticity correction.

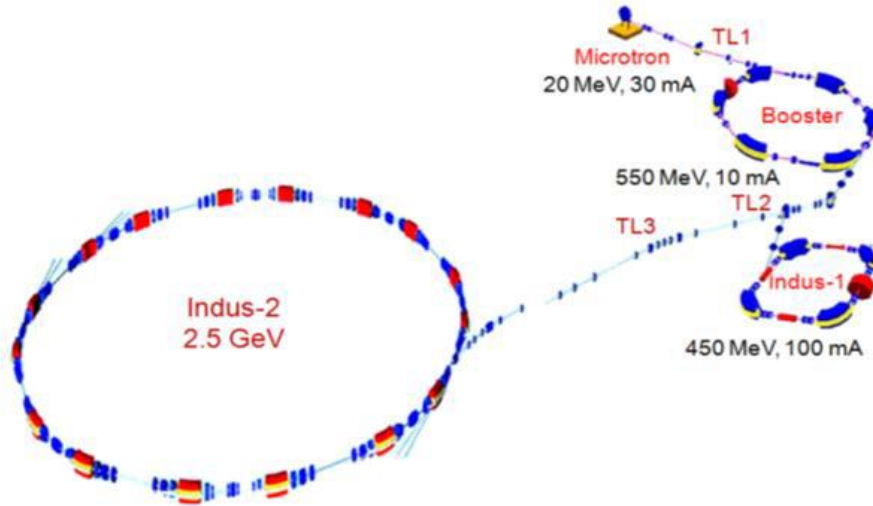


Fig. 1.21: Schematic layout of Indus Accelerator complex [3, 5].

In Table 1.2 different designed parameters of Indus-2 lattice are given and different magnetic elements with their maximum available strength are shown in Table 1.3.

Table 1.2: Different design parameters of Indus-2 storage ring

Beam Energy	2.5 GeV
Beam current	200-300 mA
Circumference	172.47 m
Beam Emittance, $\epsilon_x$	58 nm.rad
Betatron tune [ $\nu_x, \nu_y$ ]	[9.2, 5.2]
Natural chromaticity [ $\xi_x, \xi_y$ ]	[-19, -12]
Corrected chromaticity [ $\xi_x, \xi_y$ ]	[2, 2]
Momentum compaction factor, $\alpha_c$	$5.2 \times 10^{-3}$
Energy spread, $\sigma_\delta$	$9 \times 10^{-4}$
Damping time [ $\tau_x, \tau_y, \tau_s$ ]	[4.74, 4.62, 2.28] ms
Energy loss per turn	623 keV
Power loss	186.6 kW(BM)@ 300 mA

Table 1.3: Different magnetic elements of the Indus-2 storage ring.

S.No.	Name	Type	Length [m]	Max. Available Field	Total Number
1.	BM	Dipole (Rectangular type)	2.18	1.503 T	16
2.	Q1D	Defocusing Quadrupole	0.30	16 T m <sup>-1</sup>	16
3.	Q2F	Focusing Quadrupole	0.55	16 T m <sup>-1</sup>	16
4.	Q3D	Defocusing Quadrupole	0.40	16 T m <sup>-1</sup>	16
5.	Q4F	Focusing Quadrupole	0.40	16 T m <sup>-1</sup>	16
6.	Q5D	Defocusing Quadrupole	0.40	16 T.m <sup>-1</sup>	8
7.	SF	Focusing Sextupole	0.2	400 T m <sup>-2</sup>	16
8.	SD	Defocusing Sextupole	0.2	400 T m <sup>-2</sup>	16

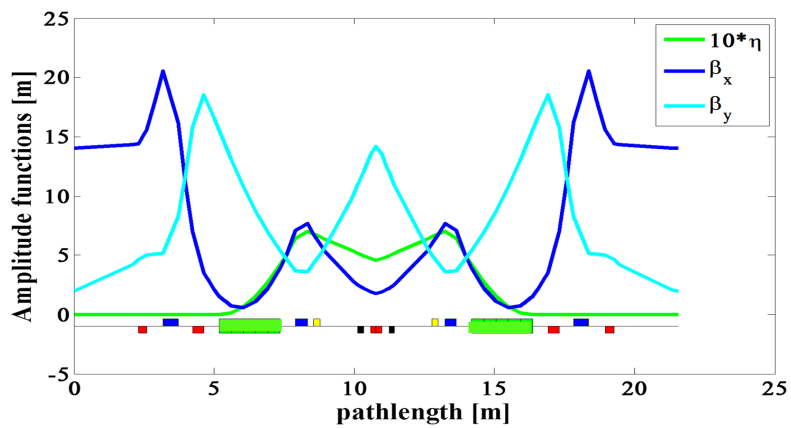


Fig. 1.22: Variation of beta and dispersion functions in Indus-2 unit lattice cell. Bending magnets are shown by green boxes, quadrupoles are in red and blue boxes and sextupoles are in yellow and black boxes.

Lattice functions for one unit lattice cell of Indus-2 are shown in Fig.1.22. This lattice is designed in such a way that dispersion acquires high value at sextupole location, maximum beta functions are less than 21 m through out the lattice cell.

Indus-2 is in regular operation. Therefore no changes in position and lengths of any magnetic element of Indus-2 lattice can be done. Beam emittance of Indus-2 lattice can be reduced by replacing homogeneous dipole with dipoles with LGBs. In this thesis work, studies with LGB in the dipole magnet has been done with two purposes, (i) lower the beam emittance, (ii) increase dispersion at sextupole location. In addition, building constraints are to be satisfied, i.e. all other hardware need not be shifted.

## 1.17 Indus-3 storage ring lattice

Indus-3, a 6 GeV electron storage ring, is a proposed high brightness synchrotron radiation source (HBSRS) at RRCAT. Baseline lattice has been designed to achieve emittance of  $\sim 150$  pm.rad. Indus-3 uses hybrid seven bend achromat lattice cell with ring circumference  $\sim 911.7$  m. The ultra low emittance of Indus-3 leads to brightness of the order of  $10^{20} - 10^{22}$  photons per second per unit angle per unit area in 0.1% bandwidth of considered wavelength with fully loaded IDs. In Fig. 1.23, the lattice functions for one unit lattice cell are shown with position of different magnetic elements. In the Table 1.4, different designed parameters are shown and the Table 1.5 shows numbers and strengths of different magnetic elements in Indus-3 lattice. A transverses quadrupole gradient have been provided in BM3 and BM4. That is why this lattice is a hybrid lattice. The strengths of quadrupoles are quite high. This leads to tight focusing of beam in the machine. The aperture size of Indus-3 is quite small compared to Indus-2 lattice.

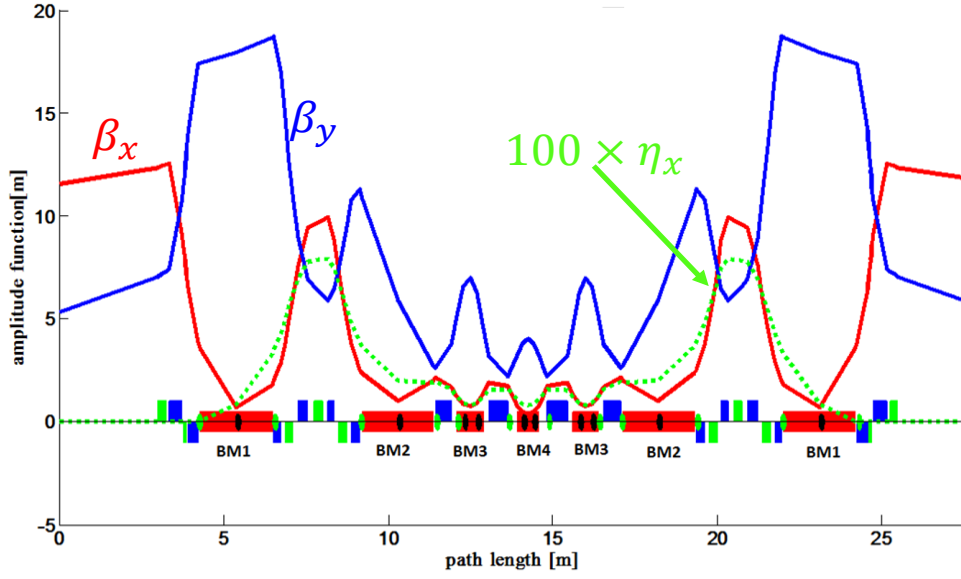


Fig. 1.23: Beta Functions of Indus-3 lattice cell. Boxes in red colour are dipole magnet, boxes in green colour are quadrupoles and boxes in blue colour are sextupole magnets.

Table 1.4: Different design parameters of Indus-3 storage ring.

Beam Energy	6.0 GeV
Beam current	200 mA
Circumference	911.798 m
Beam Emittance, $\epsilon_x$	149 pm.rad
Betatron tune $[\nu_x, \nu_y]$	[74.15, 24.22]
Natural chromaticity $[\xi_x, \xi_y]$	[-109.6, -80.9]
Corrected chromaticity $[\xi_x, \xi_y]$	[4, 4]
Momentum compaction factor, $\alpha_c$	$1 \times 10^{-4}$
Energy spread, $\sigma_\delta$	$1.02 \times 10^{-3}$
Damping time $[\tau_x, \tau_y, \tau_s]$	[8.72, 14.84, 11.44] ms
Energy loss per turn	2.46 MeV
Power loss per turn	491.7 kW(BM)@ 200 mA

Table 1.5: Different magnetic elements of the Indus-3 lattice.

S.No.	Name	Element	Length [m]	Required Field	Total Number
1.	BM1	Dipole	2.17	0.28 T	64
2.	BM2	Dipole	2.17	0.28 T	64
3.	BM3	Dipole	0.4	0.63 T	64
4.	BM4	Dipole	0.325	0.75 T	32
5.	Q1F	Quadrupole	0.40	40.8 T m <sup>-1</sup>	16
6.	Q2D	Quadrupole	0.30	42.8 T m <sup>-1</sup>	64
7.	Q3D	Quadrupole	0.20	42.2 T m <sup>-1</sup>	64
8.	Q4F	Quadrupole	0.30	71.2 T m <sup>-1</sup>	64
9.	Q5F	Quadrupole	0.20	54.8 T m <sup>-1</sup>	64
10.	Q6D	Quadrupole	0.25	60.6 T m <sup>-1</sup>	64
11.	Q7D	Quadrupole	0.50	36.4 T m <sup>-1</sup>	64
12.	Q8F	Quadrupole	0.60	73.6 T m <sup>-1</sup>	64
14.	S1 (D)	Sextupole	0.25	3580 T m <sup>-2</sup>	64
15.	S2 (F)	Sextupole	0.25	4752 T m <sup>-2</sup>	64
16.	S3 (D)	Sextupole	0.250	2880 T m <sup>-2</sup>	64
17.	SH1 (F)	Harmonic Sextupole	0.25	1462 T m <sup>-2</sup>	64
18.	SH2 (D)	Harmonic Sextupole	0.1	2748 T m <sup>-2</sup>	64

F: Focusing, D: Defocusing

As there are transverse gradient in BM3 and BM4, therefore, only BM1 and BM2 are left which have homogeneous field. These dipoles can be chosen to study LGB profiles.

In this Chapter, a brief introduction of accelerator physics relevant to this thesis work is presented which are very important in storage ring design. Many concepts like, lattice functions, betatron tune, beam emittance, chromaticity etc are discussed. In addition, effect of SR on the beam emittance and concept of radiation damping and quantum excitation which leads to equilibrium emittance are also discussed. Different types of low emittance lattice cell and advanced method to reduce the beam emittance are also described. Though, beam emittance reduction is desirable in any storage ring, however for successful operation of the facility, various other lattice parameters need to be optimized or constrained. For example, betatron tunes should be far away from dangerous resonances, horizontal beta function should be large at injection point, large value of dispersion is desirable at sextupole locations for effective chromaticity correction, large dynamic aperture for good beam life time and injection efficiency etc. These aspects make lattice design of a storage ring a complex optimization problem. This requires a better understanding of optimization techniques. Various optimization techniques are discussed in Chapter 2 and optimized result for Indus-2 and Indus-3 are presented in Chapter 3 and 4.

## **Chapter 2**

# **Optimization techniques used in accelerators**

As discussed in Chapter 1, in lattice design of a storage ring, many conflicting objectives like beam emittance, dynamic aperture, desired lattice parameters, with large number of variables such as strengths of different magnetic elements, position of different magnetic elements etc., and many constraints like maximum achievable strengths of magnetic elements, constraints on lattice functions, betatron tune etc., are needed to be optimized. These aspects make the storage ring lattice design a complicated multi-objective optimization problem. Therefore, numerical techniques that can handle these complicated optimization problem are required. In recent past, classical, like simplex method, as well as modern methods, which are evolutionary methods, were used to handle these optimization problems. Evolutionary algorithms were introduced in the field of accelerator design in recent years [5]. These evolutionary methods found to be very efficient in designing of lattice of storage ring and set a new trend in optimizing the accelerator performance in simulations as well as in real operation. In this Chapter, two non gradient optimization methods, Nelder-Mead algorithm, a classical method and genetic

algorithm, an evolutionary method are discussed in detail. These methods will be used to perform numerical optimization of LGB profiles in a dipole magnet and the studies are presented in Chapter 3.

The meaning of optimization of an objective function, which depends on one or more independent variables, is to find the values of the independent variables for which the objective function has extremum (either minima or maxima). If there is only one objective function that needs to be optimized, then this optimization problem is called **single objective optimization problem** [25], which is discussed in Section 2.1. On the other hand, if there are more than one objective function that need to be optimized, then this optimization problem is called **multi-objective optimization problem**, which is discussed in Section 2.2.

## 2.1 Single objective optimization problem

In a single objective optimization problem, an objective function  $f(\vec{x})$ , is needed to be optimized which depends on one or more independent variables  $\vec{x} = (x_1, x_2, x_3, \dots, x_n) = x_i$ ; where  $i = 1, 2, 3, \dots, n$ ;  $n$  is the number of independent variables. Single objective optimization problem can be written, mathematically, as [25]

$$\begin{aligned}
 & \text{Minimize or Maximize } f(\vec{x}) \\
 & \text{Subject to } \quad g_j(\vec{x}) \geq 0, \quad j = 1, 2, 3, \dots, J, \\
 & \quad \quad \quad h_k(\vec{x}) = 0, \quad k = 1, 2, 3, \dots, K, \\
 & \quad \quad \quad x_i^L \leq x_i \leq x_i^U, \quad i = 1, 2, 3, \dots, n,
 \end{aligned} \tag{2.1}$$

where  $g_j$ 's are  $J$  inequality constraints,  $h_k$ 's are  $K$  equality constraints,  $x_i^L$  and  $x_i^U$  are lower and upper bound for  $i^{\text{th}}$  independent variable, respectively. To optimize such single objective function  $f(\vec{x})$ , one needs to find those values of independent variables for which  $f(\vec{x})$  has extremum (maximum or minimum) value. Most of the algorithms were developed to solve

either minimization or maximization of objective functions. Hence, it was a difficult task to handle mixed optimization problems. Therefore, to handle such optimization problems, duality principle [25] was introduced, where any maximization problem can be converted into minimization problem by multiplying the objective function by -1.

To solve single objective optimization problems, various classical methods, also called derivative based methods, like Newton's method, steepest descent method, and quasi-Newton's method, were developed [5]. In these methods, the objective function must be differentiable upto first order (gradient) and sometimes, second partial derivatives (hessian) are required. But in most of the real world problem, the first or second partial derivatives of the objective functions are not always possible. Therefore, other methods called direct search methods, were developed to solve single optimization problem.

The simplest direct search method is the "Brute Force Method". Here, the search domain is divided into grids, which are visited point by point, and whenever best one is found, best found minimizer is updated. This method is also called sampling method. But this method has several drawbacks like there is strong dependence of grid size on the problem and exponential growth with grid size. Also search time increases exponentially. Another search method that tries to avoid these difficulties is **Nelder-Mead method**. In the following Section, the Nelder-Mead algorithm is discussed.

### 2.1.1 Nelder-Mead method

Nelder-Mead algorithm is designed to solve the classical unconstrained single objective optimization problem. It uses a variable shape simplex. A simplex in  $\mathbb{R}^n$  space is a convex hull of  $n + 1$  vertices, for example, in two dimensions, the simplex is a triangle and in three dimensions, it is a tetrahedron.

A simplex based direct search method begins with a set of  $n+1$  points  $\vec{x}_1, \vec{x}_2, \dots, \vec{x}_{n+1} \in$

$\mathbb{R}^n$  that are considered as the vertices of working simplex  $S$ . Here, each  $\vec{x}_i; i = 1, 2, \dots, n + 1$  is an initial solution of objective function. There are many methods to create initial simplex like Spendley's et al regular simplex, axis by axis simplex, Pfeffer's method etc [26]. Pfeffer's method for generating initial simplex is described below.

In the Pfeffer's method, two positive quantity  $\tau_u$  and  $\tau_z$  are defined, where  $\tau_u$  is used for usual components of  $\vec{x}_0$ , where  $\vec{x}_0$  is the user defined initial guess of solutions, and  $\tau_z$  is used for the case where one component of  $\vec{x}_0$  is zero. The standard values of  $\tau_u$  and  $\tau_z$  are

$$\tau_u = 0.05 \quad \text{and} \quad \tau_z = 0.00025.$$

The first vertex of the initial simplex is chosen as initial guess  $\vec{x}_0$  and can be written as

$$\vec{x}_1 = \vec{x}_0. \tag{2.2}$$

The other vertices are defined as

$$(\vec{x}_i)_j = \begin{cases} (\vec{x}_0)_j + \tau_u(\vec{x}_0), & \text{if } j = i - 1 \quad \text{and} \quad (\vec{x}_0)_j \neq 0, \\ \tau_z, & \text{if } j = i - 1 \quad \text{and} \quad (\vec{x}_0)_j = 0, \\ (\vec{x}_0)_j, & \text{if } j \neq i - 1, \end{cases} \tag{2.3}$$

for vertices  $i = 2, \dots, n + 1$  and components of initial guess  $j = 1, \dots, n$ . After calculating initial simplex, this algorithm perform some operation for one iteration which are discussed below [5, 27]

1. **Ordering:** In order to perform the algorithm, the vertices of  $S$  are ordered with respect to the function values as

$$f(\vec{x}_1) \leq f(\vec{x}_2) \leq f(\vec{x}_3) \leq \dots \leq f(\vec{x}_n) \leq f(\vec{x}_{n+1}).$$

Objective function values  $f(\vec{x}_{n+1})$ ,  $f(\vec{x}_n)$  and  $f(\vec{x}_1)$  are called worst, second worst and best points.

2. **Centroid:** After ordering function values at vertices, centroid  $\vec{c}$  of all vertices, except worst vertex, is calculated.

$$\vec{c} = \frac{1}{n} \sum_{i=1}^n \vec{x}_i. \quad (2.4)$$

3. **Transformation:** After calculating centroid, new working simplex is found from the current one by replacing only the worst vertex  $\vec{x}_{n+1}$  with a better point by using reflection, expansion and contraction. If iteration succeeds, the accepted point becomes the new vertex of the working simplex. If this fails, shrink the simplex towards the best vertex  $\vec{x}_1$ . In this case,  $n$  new vertices are computed.

- **Reflection:** In reflection, reflection point,  $\vec{x}_r$ , is calculated as

$$\vec{x}_r = \vec{c} + \alpha(\vec{c} - \vec{x}_{n+1}), \quad \text{and} \quad f_r = f(\vec{x}_r). \quad (2.5)$$

Here,  $\alpha$  is reflection coefficient. If  $f_1 \leq f(\vec{x}_r) < f(\vec{x}_n)$ , accept point  $\vec{x}_r$  and terminate the iteration here and go to the step 1 for next iteration.

- **Expansion:** If  $f_r < f_1$ , i.e., objective function has lower value at reflection point than the best point, then expansion operation is performed and expansion point  $\vec{x}_e$  is calculated as

$$\vec{x}_e = \vec{c} + \gamma(\vec{x}_r - \vec{c}) = \vec{c} + \alpha\gamma(\vec{c} - \vec{x}_{n+1}) \quad \text{and} \quad f_e = f(\vec{x}_e). \quad (2.6)$$

Here,  $\gamma$  is expansion coefficient. If  $f_e < f_r$ , accept  $\vec{x}_e$  and terminate the iteration. Otherwise, if  $f_e \geq f_r$ , accept  $\vec{x}_r$  and terminate the iteration here and go to the step 1 for next iteration. The expansion of the simplex is applied only if  $f_e < f_r < f_1$ .

- **Contraction:** if  $f_r \geq f_n$ , contraction is performed between best point and better of  $\vec{c}$  and  $\vec{x}_{n+1}$ , then contraction point,  $\vec{x}_c$  is calculated, which can be either outside or inside.

– **Outside:** If  $f_n \leq f_r < f_{n+1}$  (i.e.,  $\vec{x}_r$  is strictly better than  $\vec{x}_{n+1}$ ). In this case, outside contraction is performed and contraction point,  $\vec{x}_c$ , is calculated as

$$\vec{x}_c = \vec{c} + \beta(\vec{x}_r - \vec{c}) = \vec{c} + \beta\alpha(\vec{c} - \vec{x}_{n+1}) \quad \text{and} \quad f_c = f(\vec{x}_c). \quad (2.7)$$

Here,  $\beta$  is contraction coefficient. If  $f_c \leq f_r$ , accept  $\vec{x}_c$  and terminate the iteration and go to the step 1 for next iteration. Otherwise, shrink operation is performed.

– **Inside:** If  $f_r \geq f_{n+1}$ , inside contraction is performed and calculated as

$$\vec{x}_c = \vec{c} - \beta(\vec{c} - \vec{x}_{n+1}) \quad \text{and} \quad f_c = f(\vec{x}_c). \quad (2.8)$$

If  $f_c < f_{n+1}$ ,  $\vec{x}_c$  is accepted and terminate the iteration. Otherwise, perform the shrink operation.

• **Shrink:** In this operation,  $n$  vertices are computed as

$$\vec{x}_j = \vec{x}_l + \delta(\vec{x}_j - \vec{x}_l) \quad \text{and} \quad f_j = f(\vec{x}_j), \text{ for } j = 1, 2, \dots, n + 1 \text{ with } j \neq 1. \quad (2.9)$$

Here,  $\delta$  is shrink coefficient. The shrink transformation was introduced to prevent the algorithm from failing in the following case.

A failed contraction is much rarer, but it can occur when a valley is curved and one point of the simplex is much farther from the valley bottom than the others. Contraction may then cause the reflected point to move away from the valley bottom instead of towards it. Further contractions are then useless. The action proposed, contracts the simplex towards the lowest point, and will eventually bring all points into the valley.

In Fig. 2.1 and Fig. 2.2, different operation of Nelder-Mead algorithm for 2-D case are shown. In these figures,  $\vec{x}_3$  is the worst vertex for the simplex.

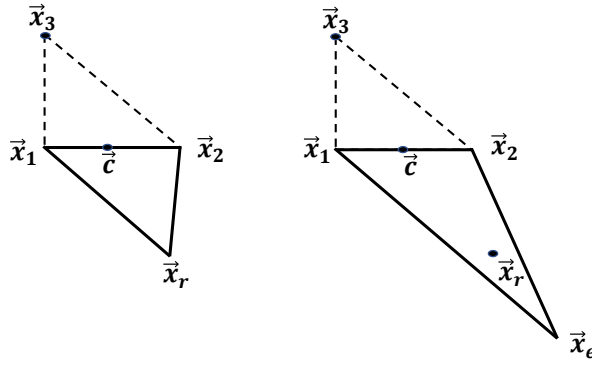


Fig. 2.1: Reflection (left) and expansion (right) of Nelder-Mead simplex.

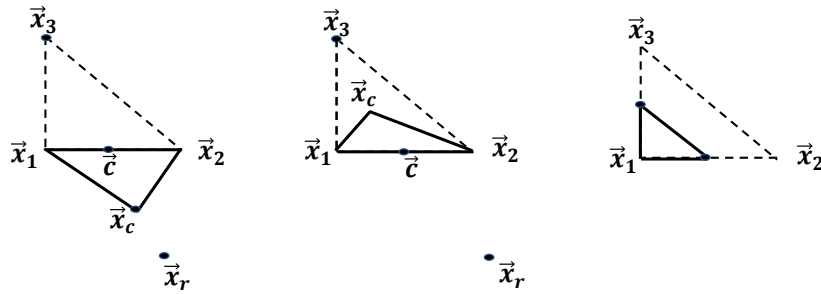


Fig. 2.2: Outside contraction (left), inside contraction (middle) and shrink (right) of Nelder-Mead simplex.

Different coefficients should satisfy the following constraints [27]

$$\alpha > 0, \gamma > 1, \gamma > \alpha, 0 < \beta < 1, 0 < \delta < 1.$$

The standard values of these parameters are

$$\alpha = 1, \gamma = 2, \beta = \frac{1}{2}, \delta = \frac{1}{2}.$$

For a practical implementation of the Nelder-Mead algorithm, it must include a test that ensures termination in a finite amount of time [28]. (i) Domain convergence or termination test: It becomes true when the working simplex  $S$  is sufficiently small in some sense. (ii) Function value convergence test: It become true when function values  $f_j$  are close enough in

some sense. (iii) No convergence test: It become true if the number of iteration or function evaluation exceeds some prescribed maximum allowed value.

In MATLAB, Nelder-Mead algorithm is coded with the name *fminsearch* and has been used in the present thesis for the optimization of LGB profile in a dipole magnet of a low emittance lattice cell.

## 2.2 Multi-objective optimization

In multi-objective optimization problems, a set of objective functions,  $f_m$ ;  $m = 1, 2, 3, \dots$ ,  $M$ , need to be optimized simultaneously. These objective functions can be defined in a vector form as

$$\vec{f}(\vec{x}) = (f_1, f_2, f_3, \dots, f_M), \quad (2.10)$$

here  $M$  is the number of objective function. Each  $f_m$  is a function of  $\vec{x} = (x_1, x_2, x_3, \dots, x_n)$ . Vector objective function  $\vec{f}$  has to be optimized with linear or non-linear constraints within variable bounds [25]. In mathematical form, optimization problem becomes

$$\begin{aligned} \text{Minimize} \quad & f_m(\vec{x}), \quad m = 1, 2, 3, \dots, M, \\ \text{Subject to} \quad & g_j(\vec{x}) \geq 0, \quad j = 1, 2, 3, \dots, J, \\ & h_k(\vec{x}) = 0, \quad k = 1, 2, 3, \dots, K, \\ & x_i^L \leq x_i \leq x_i^U, \quad i = 1, 2, 3, \dots, n, \end{aligned} \quad (2.11)$$

$J$  and  $K$  are the number of inequality and equality constraints respectively.  $x_i^L$  and  $x_i^U$  are lower and upper bounds for  $i^{th}$  independent variable. One must find vector  $\vec{x}$  such that each objective function achieves minimum value.

In real world multi-objective optimization, there may be conflicting nature of objective functions, i.e., one function can only be improved at the cost of deteriorating the other functions. In such cases, there does not exist unique optimal solution. There exist a number of solutions

which all are optimal. But, for a practical point of view user always needs a single optimal solution, no matter whether the associated optimization problem is single objective or multi-objective. Therefore, in multi-objective problem one must find a set of all optimal solution by considering all objectives equally important. After a set of all optimal solution is found, one can use higher level qualitative information associated with each objective to make a choice. Therefore, there is a two step process for an ideal multi-objective optimization procedure [25].

**Step 1** Find multiple trade-off optimal solutions with a wide range of values for objectives.

**Step 2** Choose one of the obtained solution using higher level information.

But, if for a particular problem a preference factor is known for each objective, then, there is no need to follow above two step process. One can assign preference factor to each objective and form a composite single objective [see Section 2.3]. This procedure is called a preference based multi-objective optimization. Using different preference vector, one can find many optimal solutions. But, it is important to realize that the trade-off solution is largely sensitive to preference vector used in forming composite function. A change in preference vector will result in a different trade-off solution and any arbitrary preference vector may not result in a trade-off optimal solution to all problems. Besides this difficulty, finding a relative preference vector itself is highly subjective and not straightforward. One of the classical method to solve multi-objective optimization problem is discussed in the following Section.

## **2.3 Classical methods for multi-objective optimization problems (MOOP)**

Many classical methods were developed to solve MOOP like weighted sum method, epsilon constraint Method, weighted matric methods, rotated matric methods etc. [25]. Weighted sum method, a preference based approach for solving MOOP, is described here.

Weighted sum method is useful if one knows about weight factors that must be given to each objective function. One can write optimization problem with composite function as [25]

$$\begin{aligned}
 f(\vec{x}) &= \sum_{m=1}^M w_m f_m \\
 \text{Subject to } \quad g_j(\vec{x}) &\geq 0, \quad j = 1, 2, 3, \dots, J, \\
 h_k(\vec{x}) &= 0, \quad k = 1, 2, 3, \dots, K, \\
 x_i^L &\leq x_i \leq x_i^U, \quad i = 1, 2, 3, \dots, n,
 \end{aligned} \tag{2.12}$$

where  $\sum_{m=1}^M w_m = 1$  and  $w_m$  is the weight factor for  $m^{\text{th}}$  objective function, which satisfy

$$0 \leq w_m \leq 1.$$

This method is the simplest way to solve MOOP. In this method, each objective  $f_m$  must have same functional behaviour, i.e., each function must have minima. Otherwise this method will not work.

Most of the classical methods use a deterministic procedure for approaching the optimum solution. These classical algorithms start from a random guess solution. After that, based on pre-specified transition rules, the algorithm finds a search direction, which is often arrived at by considering local information. Now, an unidirectional search is performed along the search direction to find the best solution. This best solution becomes the new solution and the above procedure is continued for a number of times. These methods are fast converging, however, they may converge to local minima. It is, therefore, recommended to run the method for few times to achieve a reasonable solution. In addition, these methods have many user defined parameters, for example in weighted sum method each weight factor,  $w_i$  must be defined and it is difficult to decide for an arbitrary optimization problem.

To avoid these difficulties, the evolutionary algorithms (EA) were introduced in MOOP. One of the most striking difference between classical search and EA is that in each iteration,

EA uses a population or set of random solutions. Therefore, the outcome of an EA is also a population of solution. If there is a single optimum in an optimization problem, all EA population will converge to that optimum solution. However, if there are multiple optimal solution for an optimization problem, then EA can capture all optimal solution in its final population. This ability makes EA an unique method in solving multi-objective optimization problem.

## **2.4 Evolutionary algorithm for optimization problems**

In 1975, Holland introduced the genetic algorithms (GA), a modern optimization method, to handle MOOP which allows optimization algorithm to find global optimal solutions [25]. After that many methods were developed. In 1983, the simulated annealing algorithm was introduced by Kirkpatrick et al. [29] and in 1995, Kennedy and Eberhart introduces another recipe in the optimization, a particle swarm optimization (PSO) [30, 31]. In 1995, differential evolution (DE) algorithm was introduced by Storn and Price [32]. These advance optimization methods belong to population based optimization methods, which are a class of evolutionary algorithms. These methods for optimization have proven their effectiveness in real world problem where the objective functions and the constraints are discontinuous and non differentiable.

The working of GA is based on the natural evolution and governed by Darwin's principle of survival of fittest which says that [5]

1. If above-average offspring is generated by genetic processing, usually it survives longer than an ordinary individuals survives. Therefore, it has more chances to produce offspring which have some of its qualities better than an average individual.
2. On the other hand, if a below-average offspring is created by a genetic processing, it

generally does not survive longer and eliminated quickly from the population.

This suggest that individuals in the population that are most fit amongst all others will survive in the next generation. This is the principle of genetic algorithm which is implemented in mathematical form and used as the global search algorithms and is discussed below.

### **2.4.1 Genetic algorithm**

The genetic algorithm (GA) is well established in the field of accelerator design. Since, GA uses population based approach, therefore, constraints can be handle in much better way than classical methods.

In all real optimization problems, there may be the case where domain of the problem is not known. In that case, GA initiates its search from a random population of the solution. If a termination criterion is not satisfied, different operators like reproduction, crossover and mutation are applied to update solutions. One iteration of these operators is called one generation. A flow chart for one iteration of genetic algorithm is shown in the Fig. 2.3 and various steps involved in genetic algorithm is discussed in the following Sections [5]

#### **1. Population initialization (P)**

According to the problem range and constraints at any generation, initial population is initialized. Familiar way to generate initial population is uniform distribution or Gaussian distribution of the variables. This distribution must be generated within the upper and lower limits of the variables. After the first population is created, GA assign fitness to each solution. If the termination criteria is not satisfied then GA performs reproduction, crossover and mutation operations to create population, called children or offsprings, for the next generation which are discussed below.

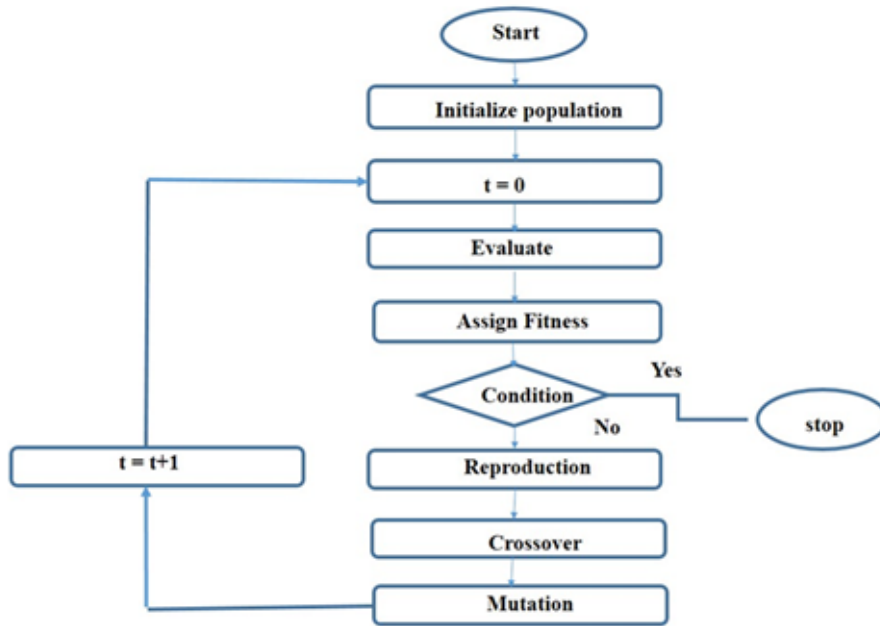


Fig. 2.3: Various steps involved in Genetic Algorithm.

## 2. **Reproduction or selection**

In the reproduction or selection method, more copies of a solution, which has highest fitness, are reproduced. There are many selection methods for example tournament selection, roulette wheel selection, ranking selection etc. Tournament selection is more popular among other selection methods due to its simple implementation. In this selection method  $n$  number of solutions are picked randomly and they compete with each other. The solution which has highest fitness, wins. This solution goes into next generation. The number of solutions which compete each other in the tournament is called as tournament size. Normally, the tournament size is taken to be two and the tournament selection method is called a binary tournament selection.

## 3. **Crossover**

Crossover operator in GA utilizes two or more parent solutions to generate offspring of the reproduced population which is based on selection method. Simulated binary crossover (SBX) is widely used among the available crossover operators [25]. Two

offspring  $(x_{o1}, x_{o2})$  solutions from two distinct parent solution  $(x_{p1}, x_{p2})$  are generate by SBX method using following set of equations [25]

$$\begin{aligned} x_{o1} &= \frac{1}{2}[(1 + \beta_i)x_{p1} + (1 - \beta_i)x_{p2}], \\ x_{o2} &= \frac{1}{2}[(1 - \beta_i)x_{p1} + (1 + \beta_i)x_{p2}], \end{aligned} \quad (2.13)$$

where  $\beta_i$  can be calculated using following relation [5]

$$\beta_i = \begin{cases} (2q_i)^{-(\eta_c+1)} & ; \quad q_i \leq 0.5, \\ \left(\frac{1}{2-2q_i}\right)^{-(\eta_c+1)} & ; \quad \text{otherwise,} \end{cases} \quad (2.14)$$

where  $q_i \in (0, 1)$  is a random number.  $\eta_c$  is a parameter that controls the crossover process. Generated offspring solution are close to the parent solution if value of  $\eta_c$  is high, and a small value of  $\eta_c$  allows the distant solution to be selected as offspring.

#### 4. Mutation

Mutation in GA has same meaning as in natural evolution, i.e., changes in genes. Here, a small change in a solution is done to mutate it. Mutation operation is performed after selection and crossover operations. One of the mutation method is polynomial mutation. It is given as [25]

$$x_{om} = x_o + \Delta_{max}\bar{\delta}_i, \quad (2.15)$$

where  $\Delta_{max} = (x_i^{(U)} - x_i^{(L)})$  and parameter  $\bar{\delta}_i$  is calculated as

$$\bar{\delta}_i = \begin{cases} (2r_i)^{-(\eta_m+1)} & ; \quad r_i < 0.5, \\ 1 - [2(1 - r_i)]^{-(\eta_m+1)} & ; \quad r_i \geq 0.5, \end{cases} \quad (2.16)$$

where  $r_i \in (0, 1)$  is a random number and  $\eta_m$  is a parameter that controls the mutation process. If  $\eta_m = 0$ , the independent variation  $-\Delta_{max}\bar{\delta}_i$  are uniformly distributed between  $\Delta_{max}$  to  $\Delta_{max}$ . As  $\eta_m$  is increased largely,  $\bar{\delta}_i$  approaches towards zero. It means that no mutation is applied. Therefore  $x_{0m} = x_0$

These operations generates the population for the next generation  $t + 1$ . This process continues until the stopping criteria is satisfied.

Genetic algorithms can be used to solve single as well as multi-objective optimization problems. Single objective optimization problem is defined in Section 2.1. In MATLAB, single objective genetic algorithm is implemented as a code "ga" and widely used in accelerator design.

## 2.4.2 Multi-objective genetic algorithm

Most of the multi-objective optimization problem contains conflicting objectives, for example, in lattice design of a storage ring one need small beam emittance and sizeable dynamic aperture. These two objectives are example of conflicting objectives. one cannot achieve lower emittance without worsening the dynamic aperture [5].

One of the goal of an ideal multi-objective is to find many trade-off solutions. Solutions which satisfy all constraints and non dominated by each others are called Pareto optimal solution and trade-off of Pareto optimal solutions is called Pareto optimal front [25]. A single objective GA can be converted into a multi-objective optimizer with following steps: (i) emphasize is given to the non-dominated solution in order to progress the solution towards the optimal solution, (ii) to maintain diversity in the solution, emphasize is given to less-crowded solution, (iii) to achieve fast convergence close to the true Pareto optimal front, emphasize is given to best solutions.

To address these three issues, elitist non dominated sorting GA is developed to convert single objective GA to multi-objective GA [5, 25]. Its working principle is shown in Fig. (2.4). The parent population ( $P_t$ ) of size  $N$  is generated randomly and off-springs ( $Q_t$ ) of size  $N$  are generated using GA operators at generation  $t$ . Together  $P_t$  and  $Q_t$  makes a population  $R_t$  of size  $2N$ . This combined population is sorted into number of Pareto optimal fronts using non

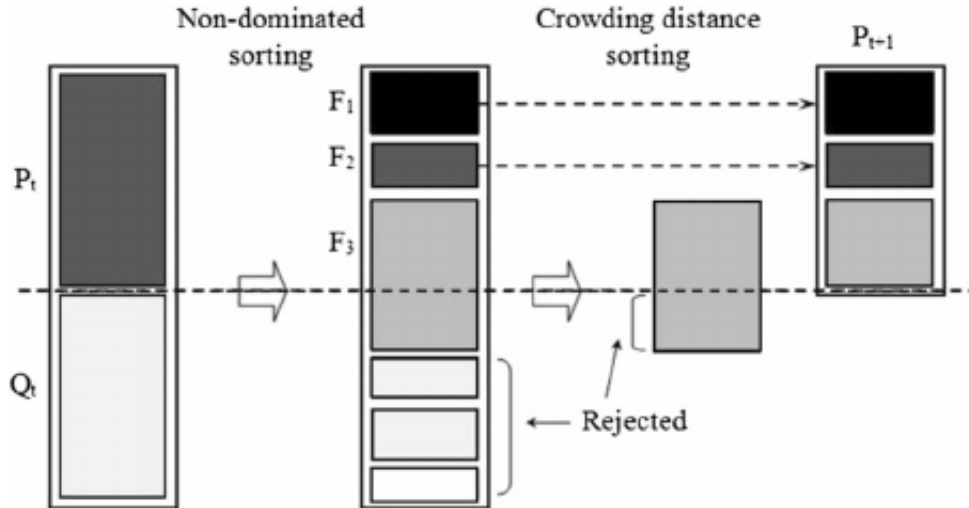


Fig. 2.4: NSGA-II procedure for one iteration [25].

dominated sorting. The first front  $F_1$  is completely non dominated set. The second front  $F_2$  is dominated by members of  $F_1$  only. This process is continued to get more and more optimal fronts. We assign fitness value 1 to  $F_1$ , fitness value 2 to  $F_2$ , and so on. A new parameter known as crowding distance, which measures how close the individual is to its neighbour individual, is calculated for each individuals. Large value of crowding distance provides better diversity in the population [5].

The parent population  $P_{t+1}$  of size  $N$  in the next generation are selected from non dominated solution starting from the best solutions or best optimal fronts and so on. When the number of population become  $N$ , rest of the solutions are simply rejected. This process of selecting parent population from previous generation continued until termination criteria is not satisfied. In MATLAB multi-objective GA is implemented with the code name *gamultiobj*.

In MATLAB, a complete package of simulation code with name Accelerator Toolbox (AT) [33], has been developed at SLAC worldwide. This code calculates all lattice parameters of a storage ring like emittance, momentum compaction factor, damping times, damping partition numbers, energy loss per turn etc. Also transfer matrix for an element or whole ring can be calculated. A program using AT can be written for a lattice design. AT generates data for plot

of beta function, dispersion function etc. and tracking can also be done to calculate dynamic aperture.

In this Chapter, different optimization techniques, in particular Nelder-Mead algorithm and genetic algorithm, have been discussed. These optimization techniques are very useful in handling optimization problems where derivatives of objective function are not possible. These techniques can handle complex optimization problems and are widely used in accelerator design. Both algorithms have been used in the study of optimization of LGB profiles in a dipole, which is presented in Chapter 3.

## Chapter 3

# Optimization of longitudinal gradient bend profiles in dipole magnet

As discussed in Chapter 1, longitudinal gradient bend (LGB) is an advance technique to reduce the beam emittance. First study of LGB in a storage ring was presented by J. Guo and T. Raubenheimer in 2002. In their paper [10], they applied the LGB in NLC damping storage ring and found a satisfactory reduction of beam emittance than the homogeneous dipoles. Now a days, magnet design technology has been improved much and most of the storage ring lattice designer are using LGB in place of constant filed dipoles to reduce beam emittance further. In this Chapter, optimization studies of LGB profiles in a dipole for two type of lattices namely achromat and theoretical minimum emittance (TME) is presented which is discussed in the following Section.

### 3.1 LGB profiles in dipoles for achromatic and TME lattices

In storage rings, mostly achromat type lattices are used, for example, double bend achromat (DBA), triple bend achromat (TBA) or multi bend achromat (MBA), due to requirement

of horizontal dispersion,  $\eta$ , and its derivative,  $\eta'$ , to be zero at the locations of IDs. A unit cell of a DBA lattice, similar to Indus-2 storage ring, is shown in Fig. 3.1. It consist of two homogeneous dipole magnets to bend the electron, nine quadrupoles to control lattice functions and four sextupoles to correct chromaticity in both transverse planes. Using combination of quadrupoles between the two dipoles, one can achieve achromatic condition, i.e.,  $\eta$  and  $\eta'$  are zero at the entrance of the first dipole and symmetrically at the exit of the second dipole. This lattice is designed to get large dispersion at sextupole locations.

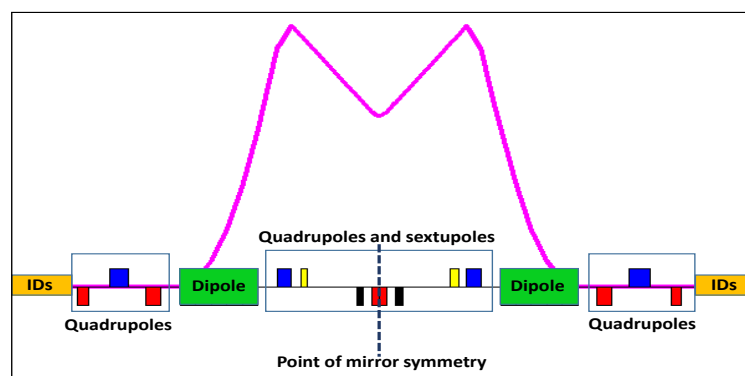


Fig. 3.1: Variation of dispersion function in DBA lattice. The green rectangular boxes are homogeneous dipoles, blue rectangular boxes are focusing quadrupoles, red rectangular boxes are defocusing quadrupoles, yellow ones are focusing sextupoles and the black ones are defocusing sextupoles.

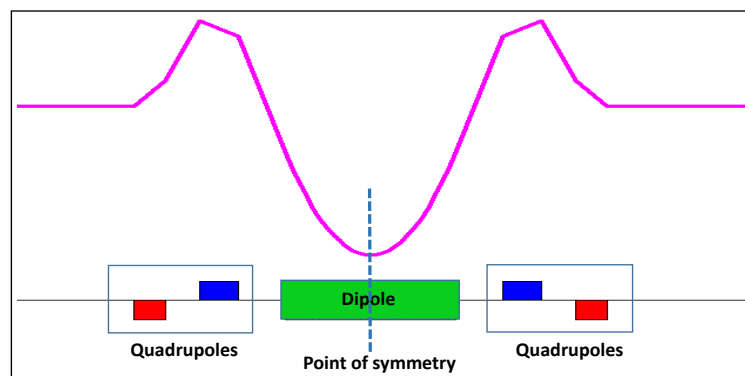


Fig. 3.2: Variation of dispersion function in TME lattice. Dispersion function is symmetric in the dipole and minima occurs at the center of the dipole. Two quadrupoles, one focusing (blue) and other defocusing (red), at both side of the dipole are used to control the lattice functions.

In Fig. 3.2, an unit cell of TME lattice with homogeneous dipoles is shown. Here, achromatic condition is not satisfied. Though, TME lattice can not be used for third generation storage rings due to requirement of zero dispersion at location of IDs, but, it is useful in designing of TBA or MBA lattices, where more than one dipole satisfying TME condition are used. In order to reduce beam emittance further in the same lattice, the homogeneous dipoles can be replaced with dipoles having LGB profile in both type of lattices. LGB profiles for DBA and TME lattices have been discussed in Section 1.15, Chapter 1. For a DBA lattice, a parabolic decaying LGB profile is required. On the other hand, for a TME lattice, LGB profile is such that its maxima occurs at centre of the dipole and reduces symmetrically on either side. Though, continuous LGB field profile are desirable, but, design of continuous decay profile is very complicated [11, 34]. Therefore, stair like parabolic decay profile is modeled instead of continuous parabolic decay profile.



Fig. 3.3: Breaking of a homogeneous dipole (left) into  $n$  dipoles (right). The dipole (left) has parameters, length ( $L$ ), magnetic field ( $B$ ), bending angle ( $\theta$ ), local bending radius ( $\rho$ ). Same parameters can be defined for each section of dipole (right).

In order to generate stair like LGB profile, dipole magnet is divided into  $n$  sections (Fig. 3.3) in such a way that total length is same as homogeneous dipole. After that, magnetic field in each section is chosen in such a way that, it fits the continuous parabolic decay profile with the condition that total bending angle must be same as homogeneous dipole. For DBA and TME lattices, stair like parabolic decay profiles are shown in Fig. 3.4 and Fig. 3.5.

As shown in Fig. 3.4, magnetic field in the first section is high (low local radius of curvature  $\rho$ ), which generates higher slope of horizontal dispersion,  $\eta'_x$ , than the homogeneous dipole, but almost same horizontal dispersion,  $\eta_x$ . In the next dipole section, magnetic field is lower than the first section, but still higher than the homogeneous dipole, it will also generate higher  $\eta'_x$  and  $\eta_x$  will have higher value than homogeneous dipole. This behaviour of  $\eta_x$  is shown in Fig. 3.4. Also, at the exit of the dipole,  $\eta_x$  and  $\eta'_x$  are higher than the homogeneous dipole, which leads to high dispersion at sextupole location. In each section,  $\mathcal{H}$  function and bending radius,  $\rho$ , will have different values than the homogeneous dipole. This leads to different values of  $I_5 \left( = \left\langle \frac{\mathcal{H}}{\rho^3} \right\rangle; \mathcal{H} = \gamma_x \eta_x^2 + 2\alpha_x \eta_x \eta'_x + \beta_x \eta_x'^2 \right)$  in each section and average of  $I_5$  will have smaller value than the homogeneous dipole magnet due to dominating nature of  $\rho^3$  in sections having magnetic field lower than the homogeneous dipole fields. In this way, emittance will reduce.

After introducing LGB in the dipole magnet, one can achieve lower emittance in the same circumference of the storage ring or one can design a compact ring for the same emittance. Also, large dispersion at the sextupole location leads to low sextupole strength to correct the same level of chromaticity in the machine. These are the major advantage of LGBs.

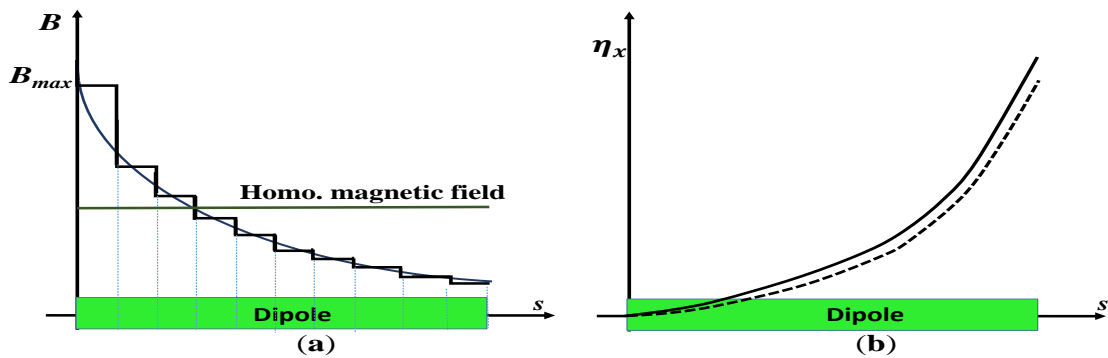


Fig. 3.4: Variation of longitudinal field profile in the dipole magnet (DBA). (b) Comparison of Horizontal dispersion function for LGB dipole (solid curve) with homogeneous dipole (dashed curve).

For a TME lattice, purpose of introducing LGB is to minimize beam emittance only. As shown in Fig. 3.5, a symmetric decaying LGB profile reduces the dispersion at the center of the dipole. Therefore, area under the curve, i.e.,  $\langle \frac{\mathcal{H}}{\rho^3} \rangle$  reduces, which leads to lower emittance. But, higher magnetic field will increase the SR loss, i.e., in order to reduce beam emittance, one has to compromise high SR loss.

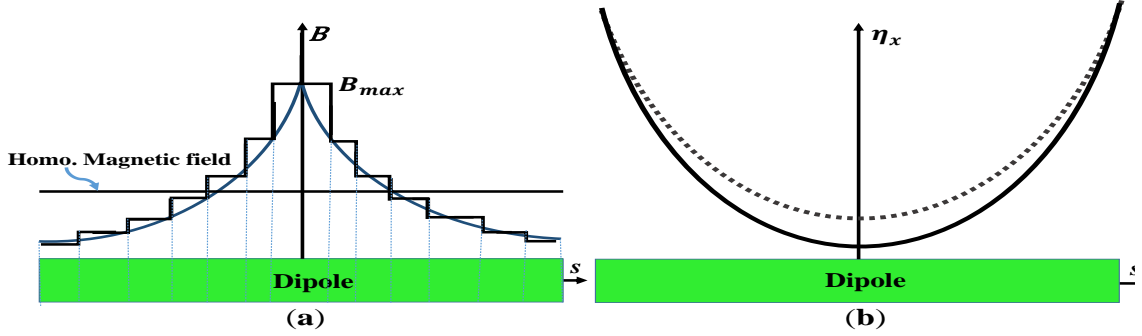


Fig. 3.5: (a) Variation of longitudinal field profile in the dipole magnet (TME). (b) Comparison of Horizontal dispersion function for LGB dipole (solid curve) with homogeneous dipole (dashed curve).

## 3.2 Objective function to generate LGB profiles

Expression for the horizontal natural beam emittance is given by eq.(1.95) as

$$\epsilon_{x0} = C_q \gamma^2 \frac{\langle \frac{\mathcal{H}_x(s)}{\rho^3(s)} \rangle}{\langle \frac{1}{\rho^2} \rangle}, \quad (3.1)$$

here,  $\mathcal{H}_x = \gamma_x \eta_x^2 + 2\alpha_x \eta_x \eta_x' + \beta_x \eta_x'^2$ , i.e.,  $\mathcal{H}_x = f(\alpha_x, \beta_x, \gamma_x, \eta_x, \eta_x')$  and  $\rho$  is the local radius of curvature of the dipole. For a storage ring with fixed energy, one can choose

$$f = \left\langle \frac{\mathcal{H}_x(s)}{\rho^3(s)} \right\rangle / \left\langle \frac{1}{\rho^2} \right\rangle, \quad (3.2)$$

as an objective function which, in principle, is a function of magnetic field and length in each section of dipole. Therefore, optimization problem will be; minimize  $f(\vec{B}, \vec{L})$  with constraints on total length, total bending angle and maximum magnetic field. One more constraint on

magnetic field in each section is that magnetic field should be of decreasing nature, i.e.,  $B_i > B_{i+1}$ ;  $i = 1, 2 \dots, n - 1$ ;  $n$  is the number of dipole sections. If dipole is divided into equal sections such that total length is equal to length of homogeneous dipole magnet, then objective function will be a function of magnetic fields only.

Variation in Courant-Snyder (CS) variables  $\alpha_x$ ,  $\beta_x$  and  $\gamma_x$  is governed by quadrupole strengths. Therefore, LGB profile will introduce only marginal change (due to geometrical focusing in dipoles) in these variables and CS variables of original lattice can be taken in calculation of  $\mathcal{H}_x$  function. It means that,  $\mathcal{H}_x$  is independent of CS variables and only function of  $\eta_x$  and  $\eta'_x$ . A case study, where dipole magnet is divided into 5 equal sections, is discussed in the following Section.

### 3.3 Optimization of LGB profiles in dipole for achromat lattice

To study LGB profiles for an achromat lattice, dipole of Indus-2 (a DBA lattice) is taken. The length of the dipole is 2.175 m and maximum magnetic field is 1.503 Tesla. This dipole magnet bends a charged particle by  $22.5^\circ$  with  $\rho = 5.55$  m. To generate LGB profiles, dipole is divided into 5 equal section such that total length of the dipole is unchanged. The objective function to minimize beam emittance can be chosen as

$$f = \left\langle \frac{\mathcal{H}_x(s)}{\rho^3(s)} \right\rangle. \quad (3.3)$$

The  $\langle \frac{1}{\rho^2} \rangle$  term will be taken care by the  $\rho^3$  in the  $\langle \frac{\mathcal{H}_x}{\rho^3} \rangle$ .

Let  $\theta_i$  and  $L_i$  are the angle length of  $i^{th}$  section of dipole magnet, where  $i = 1, 2, \dots, 5$ .

Therefore, optimization problem becomes

$$\begin{aligned}
 & \text{Minimize } f(\vec{B}) = \left\langle \frac{\mathcal{H}_x}{\rho^3} \right\rangle \\
 & \text{with constraints } \Delta\theta = \left| \sum_{i=1}^{i=5} \theta_i - \theta_{original} \right| = 0, \\
 & \max(\vec{B})_i < 2.65. \\
 & (\vec{B})_i > (\vec{B})_{i+1}; \quad i = 1, 2, \dots, 4,
 \end{aligned} \tag{3.4}$$

here  $\vec{B} = (B_1, B_2, B_3, B_4, B_5)$ ,  $\theta_{original} = 22.5^\circ$  and length,  $L = 2.1795$  m. The maximum magnetic field, 2.65 T, is chosen based on SR loss and emittance reduction. Since  $\Delta\theta$  can not be made to zero, therefore, if  $\Delta\theta$  is less than  $10^{-3}$ , then solution can be acceptable.

	Point A	Point B	Point C	Point D	Point E	Point F
$\alpha$	1.2462	0.5308	-0.1976	-0.9213	-1.6222	-2.2832
$\beta$ [m]	1.5357	0.7595	0.6139	1.1027	2.2136	3.9195
$\gamma$ [m <sup>-1</sup> ]	1.6625	1.6877	1.6924	1.6766	1.6405	1.5851

Fig. 3.6: Values of CS variables at points A, B, ..., E, which are entrance of each dipole section and F is the exit of last section.

In Fig. 3.6, values of CS variables are given at points A, B, ..., F. At each point,  $\mathcal{H}$ -function is calculated. After that, taking average of the  $\mathcal{H}$  function at entrance and exit of each dipole section,  $\mathcal{H}$  function is calculated at the centre of each dipole section. Then objective function can be calculated as

$$f = \frac{1}{5} \sum_{i=1}^5 \frac{\mathcal{H}_{xi}}{(\rho_i)^3}. \tag{3.5}$$

Here, hard edge model of dipole [2] is assumed, i.e. fringe fields between two dipole sections are completely ignored. Two optimization methods, Nelder-Mead algorithm and single objective genetic algorithm, have been used to generate LGB profiles.

### 3.3.1 Optimization using Nelder-Mead algorithm

The optimization problem is defined in eq. (3.4). The primary requirement of Nelder Mead method is that it requires an initial guess to create initial simplex. Therefore, 1.5 Tesla in each section of dipole magnet, which is the field of a homogeneous dipole, is chosen as an initial guess. For this initial guess, the value of objective function is  $2.07 \times 10^{-4}$ . Here, default stopping criteria of the algorithm are chosen, i.e., the algorithm will be stopped if objective function does not change in successive iteration or the objective function is less than  $10^{-4}$ . Though initial guess is provided for the first simulation run, but, it requires more relaxation on the constraint of total angle to run the program. In the second simulation run, optimized values of magnetic field from first simulation run can be used as initial guess and constraint on total angle is made more tight than the first simulation run.

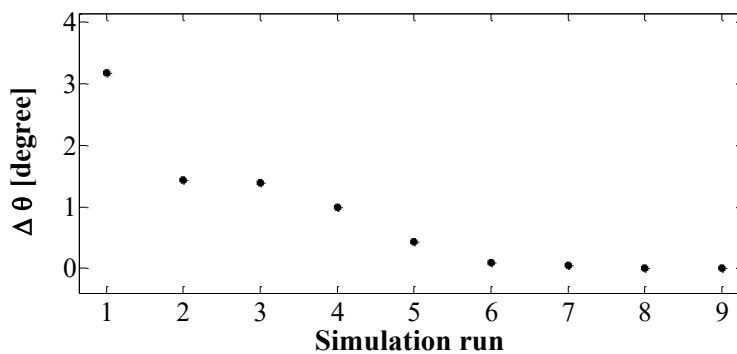


Fig. 3.7: Variation of  $\Delta\theta$  with successive simulation run.

After 9 successive simulation runs, a solution for which  $\Delta\theta$  is  $6.4 \times 10^{-4}$  is achieved, and solution is accepted. Variation of  $\Delta\theta$  for different simulation runs is shown in Fig 3.7 which shows that using improved initial guess, constraint on  $\Delta\theta$  can be satisfied in few simulation

runs. Different LGB profiles after each simulation run are shown in Fig. 3.8 and Variation of objective function for 9<sup>th</sup> simulation run is shown in Fig.3.11.

After final simulation run, optimized values of magnetic fields in each section are

$$B = [2.0991 \quad 1.6772 \quad 1.4414 \quad 1.2539 \quad 1.0740][\text{Tesla}],$$

with objective function value  $1.64 \times 10^{-4}$ .

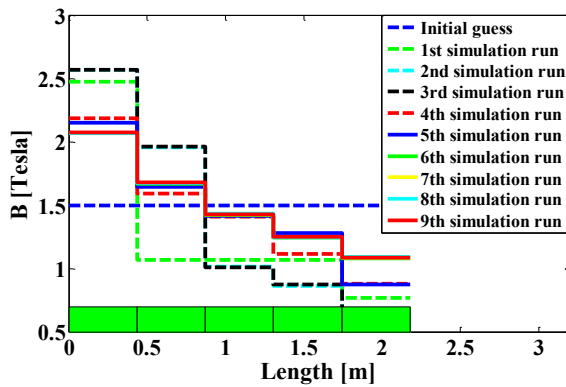


Fig. 3.8: LGB profiles after each simulation run using Nelder-Mead algorithm.

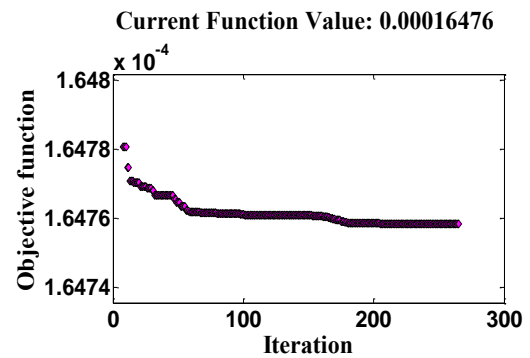


Fig. 3.9: Variation of objective function after 8th simulation run.

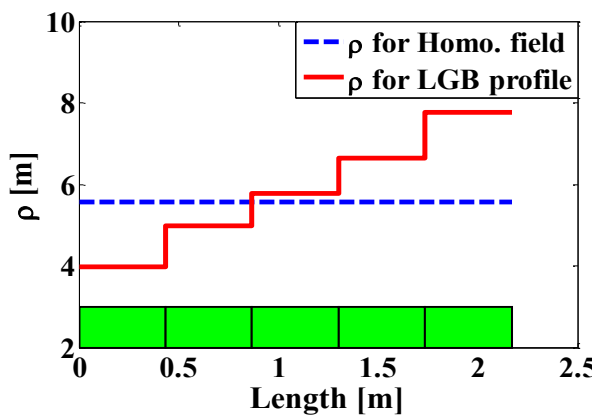


Fig. 3.10: Variation of  $\rho$  after final simulation run.

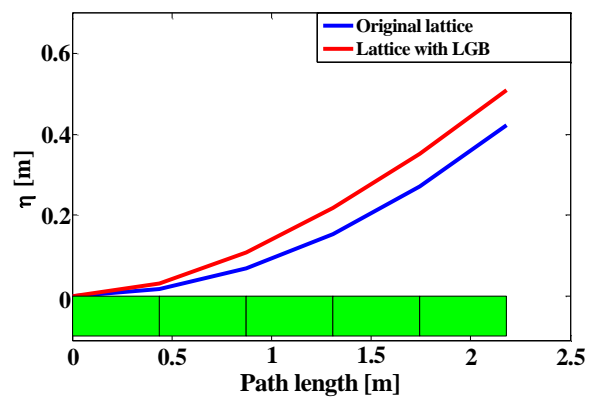


Fig. 3.11: Variation of dispersion function in the dipole.

After assuming LGB profile in all dipole magnets of Indus-2 lattice, different parameters in achromatic condition are shown in Table 3.1. In calculating the beam emittance (using

eq.(3.1)), electron energy is considered to be 2.5 GeV, which is the designed energy for Indus-2. For calculation of SR loss per turn, it is assumed that there are total 16 dipoles (each 22.5 deg) to complete the full storage ring i.e. ring of Indus-2.

Table 3.1: Comparison of parameters with original lattice.

S.No.	Parameter	original lattice	Lattice with LGB and achromatic condition
1.	Emittance [nm.rad]	58	41.5
2.	SR loss per turn [keV]	623	656

The emittance for this case is less than  $\sim 30\%$  from the nominal lattice, i.e., lattice with constant field dipole with a little increase in SR loss (30 keV).

This study shows that Nelder-Mead algorithm requires good initial guess to find an optimal solution in reasonable simulation runs. If initial guess is not good, it will need more relaxation on the constraints and requires more simulation runs to find an optimal solution. This is the major drawback of this method. To avoid these difficulties posed by Nelder-Mead method, GA technique can be used. In the Section below, a study with GA is presented.

### 3.3.2 Optimization using genetic algorithm

The genetic algorithm uses a random population of initial solutions. In successive generation, it try find a search direction in which solutions satisfy more constraints. The objective function for this case can be defined in a similar way as,

$$\text{Minimize } f(\vec{B}) = \left\langle \frac{\mathcal{H}_x}{\rho^3} \right\rangle$$

with constraints

Variable space range  $LB : 0.5$  Tesla in each section

$UB : 2.65$  Tesla in each section (3.6)

$$\Delta\theta = \left| \sum_{i=1}^{i=5} \theta_i - \theta_{original} \right| \leq 10^{-3},$$

$$\max(\vec{B})_i \leq 2.65.$$

$$(\vec{B})_i > (\vec{B})_{i+1}; \quad i = 1, 2, \dots, 4,$$

here,  $UB$  and  $LB$  are lower and upper bounds of independent variables.

### 3.3.2.1 Optimization using GA with initial guess

In order to provide a search direction to GA, initial guess for this method is provided same as in previous case, i.e., 1.5 Tesla in each section of the dipole. The number of generation and population size are chosen as 50 and 100, respectively. In a single simulation run, GA gives result with satisfying all constraints which is shown in Fig. 3.12.

After optimization the optimized values of the magnetic fields in each section of the dipole are

$$B = [2.0982 \quad 1.6111 \quad 1.4742 \quad 1.2926 \quad 1.0676][\text{Tesla}],$$

which is shown in the Fig.3.13. The obtained LGB profile is almost similar to the profile obtained using Nelder-Mead algorithm. The variation of dispersion function in the dipole is shown in Fig. 3.14. The calculated values of the beam emittance and SR loss per turn are also equivalent.

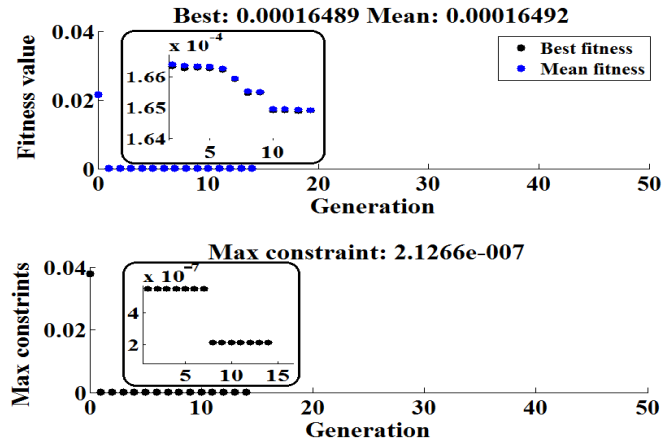


Fig. 3.12: Variation of objective function in different generations. Best fitness shows the value of objective function at current generation and maximum constraint shows how constraints are more satisfied in each generation.

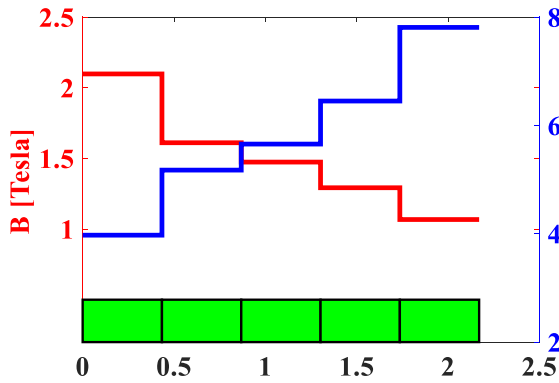


Fig. 3.13: Variation of magnetic field and  $\rho$ .

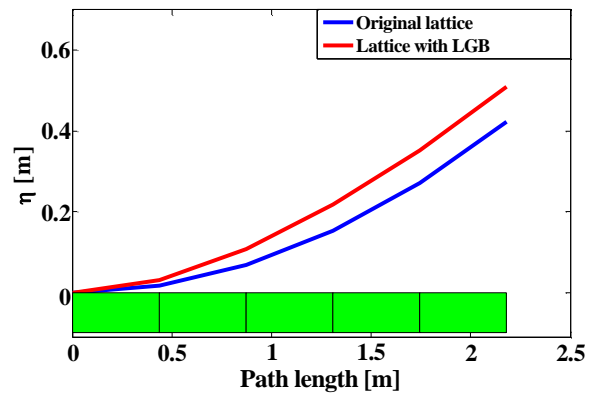


Fig. 3.14: Variation of dispersion function in the dipole.

For homogeneous dipole magnetic field and  $\rho$  are 1.503 Tesla and 5.55 m respectively.

Table 3.2: Comparison of parameters with original lattice in case of genetic algorithm.

S.No.	Parameter	original lattice	Lattice with LGB and achromatic condition
1.	Emittance [nm.rad]	58	42
2.	SR loss per turn [keV]	623	655

Though, an initial guess is provided here (a bad solution for GA), GA can give results without any initial guess in a single simulation run. This is the great advantage of GA over Nelder-Mead method. One result without any initial guess is presented in the following Section.

### 3.3.2.2 Optimization using GA without initial guess

For this case, GA algorithm is used with same objective function defined in eq.(3.6) without any initial guess. The variation of objective function and LGB profile are shown in Fig. 3.15 and Fig. 3.16. The objective function reduces to almost same value as previous case and a similar LGB profile is also generated. Emittance and SR loss are compared in Table 3.3, which shows almost same result i.e. there is no need to provide initial guess to run the GA code. After optimization the optimized values of the magnetic field in each section of the dipole are

$$B = [2.1701 \quad 1.6630 \quad 1.4979 \quad 1.0912 \quad 1.0904][\text{Tesla}]$$

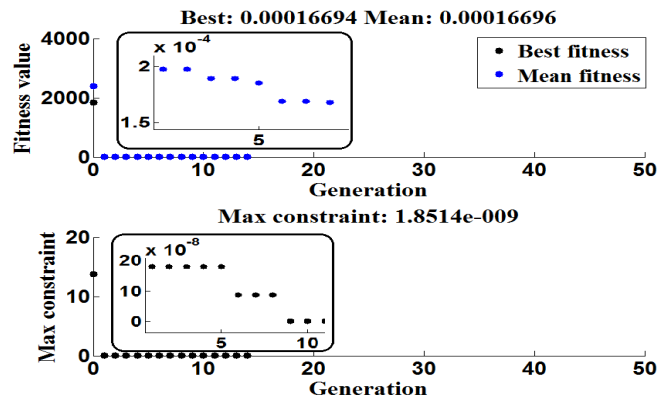


Fig. 3.15: Variation of objective function in each generation for the case where no initial guess is provided.

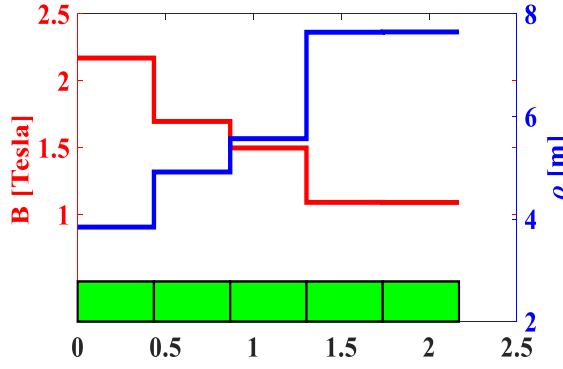


Fig. 3.16: Variation of magnetic field and  $\rho$ .  
For homogeneous dipole magnetic field and  $\rho$  are 1.503 Tesla and 5.55 m respectively.

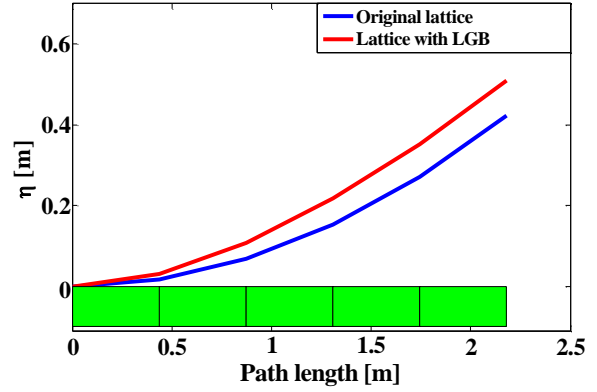


Fig. 3.17: Variation of dispersion function in the dipole.

Table 3.3: Comparison of parameters with original lattice.

S.No.	Parameter	original lattice	Lattice with LGB and achromatic condition
1.	Emittance [nm.rad]	58	41
2.	SR loss per turn [keV]	623	667.7

Based on these studies, it can be concluded that GA produces much better results compared to Nelder-Mead algorithm in view of getting optimal solution in a single run of the simulation. It can also be highlighted that the over all emittance in both the optimization is almost similar. Emittance in each case reduced to  $\sim 41 - 42$  nm.rad from 58 nm.rad and SR loss per turn is almost same.

### 3.3.2.3 Convergence test of GA

Simulation studies to test the convergence of GA algorithm in producing the LGB profiles and the objective function is also carried out. The results of generated LGB profiles for

fourteen simulation runs considering same lower and upper bounds of the magnetic fields are shown in Fig.3.18. The objective function converges to the same value almost in all simulation runs. There are very small variations in each profile except 13<sup>th</sup> and 14<sup>th</sup> profile. The small variation in the profile is due to randomness in the initial population in each GA simulation run.

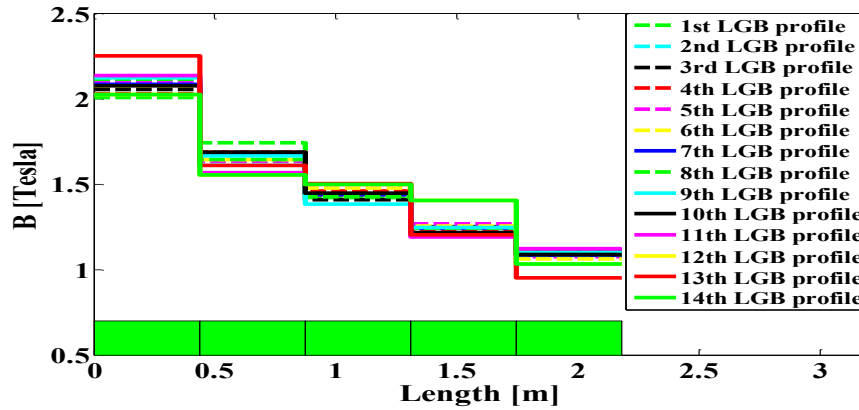


Fig. 3.18: Different LGB profiles generated by genetic algorithm.

As shown in Fig. 3.19, though, there is a little variation in the field profiles and objective functions in each case, but emittance is almost same which is  $\sim 40-42$  nm.rad. In addition, SR loss in each case is also same except one case (13<sup>th</sup> LGB profile), in which SR loss is  $\sim 675$  keV. It is because of increased magnetic field in the first section. This shows the advantage of LGB dipole over homogeneous dipole, i.e., using dipoles with LGB, one can significantly reduce beam emittance in the same circumference of storage ring.

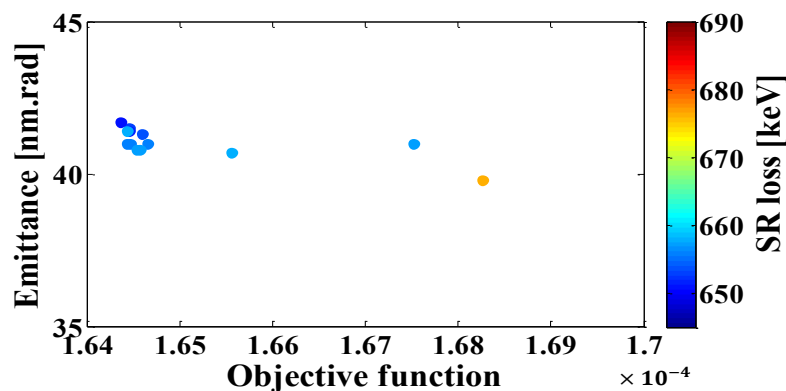


Fig. 3.19: Emittance for different LGB profiles with objective function and SR loss (color bar).

### 3.3.2.4 Optimization using GA with hard constraint

Another study with hard constraint on maximum field is also presented, in which maximum field in first section is strictly desired to be 2.65 Tesla. This maximum field will shift the critical wavelength of SR towards much harder X-rays [2], which is the requirement of many material research. Using objective function of eq.(3.6) with one more constraint, i.e.,  $\max(\vec{B})_1 = 2.65$  Tesla, different LGB profiles have been generated which are shown in Fig.3.20.

In this case, the value of objective function after optimization are  $1.840 \times 10^{-4}$  –  $1.879 \times 10^{-4}$  and emittance in achromatic condition are 38 – 39 nm.rad. Though, value of objective function is increased, emittance in achromatic condition get reduced a little bit more than previous cases, i.e.,  $\sim 38 - 39$  nm.rad, due to increased SR loss, which is increased from 623 keV to  $\sim 720 - 727$  keV, because of increased magnetic field. The increase in SR loss enhances the radiation damping which ultimately reduce the beam emittance. The increased SR loss can be compensated by increasing the RF power.

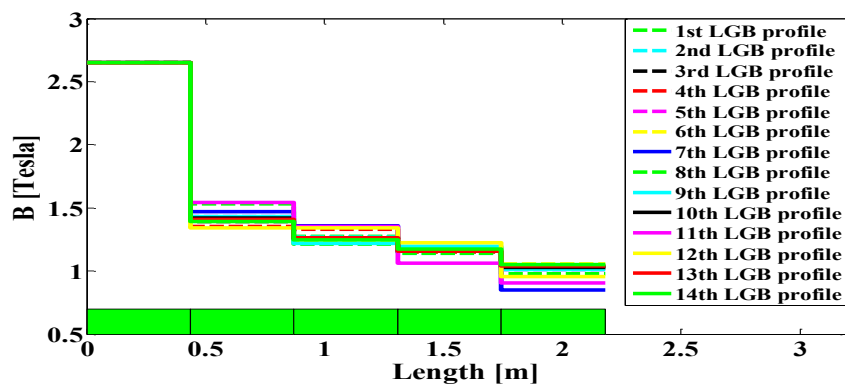


Fig. 3.20: Different LGB profiles using GA with maximum magnetic field in the first section 2.65 Tesla.

In the previous studies, dipole magnet is divided into 5 sections. In the following Section, we will explore the effect on beam emittance and SR loss by optimizing the LGB

profiles in a dipole magnet, divided in more number of sections. Motivation of this case is to achieve LGB profile close to true parabolic profile, and to see the effect on beam emittance. In the following Section, studies with dipole divided into 10 and 15 sections are presented.

### 3.3.2.5 Selection of number of dipole sections

If a dipole is divided into 10 or 15 sections, the number of independent variables will be 10 or 15 respectively. Here, same objective function with more number of variables and hard constrains on maximum magnetic field in first section has been used.

**Case I:** Dipole magnet is divided into 10 sections.

Optimization problem is given in eq.(3.6) and hard constraint on the magnetic field in first section is taken. After optimization, optimized LGB profile is shown in Fig.3.21.

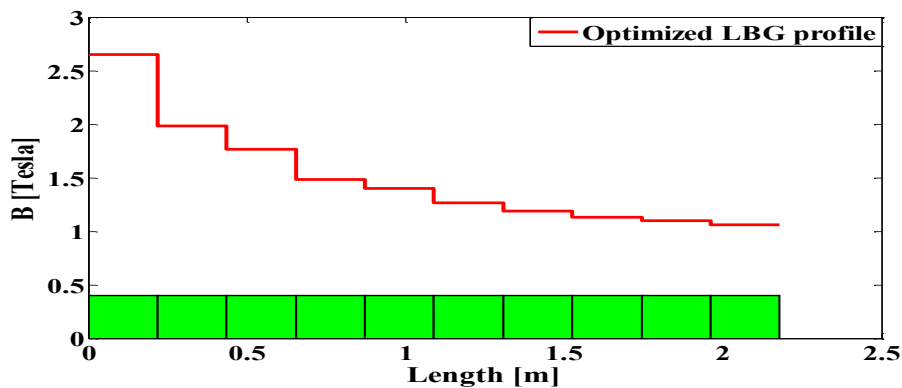


Fig. 3.21: LGB profile for the 10 section case with hard constraint on maximum magnetic field.

**Case II:** Dipole magnet is divided into 15 sections.

In a similar way, dipole can be divided into 15 sections to get more converged profile towards parabola. After optimization, the optimized profile is shown in Fig. 3.22.

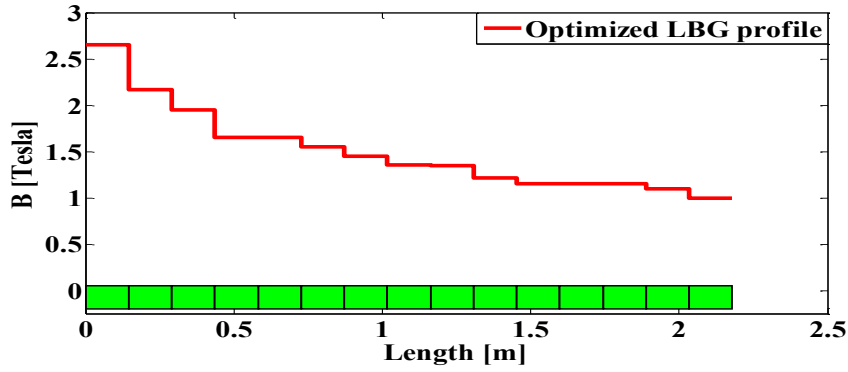


Fig. 3.22: LGB profile for the 15 section case with hard constraint on total magnetic field.

In Table 3.4, different parameters are compared for both the cases with 5 sections case.

Table 3.4: Comparison of different parameter with original lattice for 15 section case.

S.No.	Parameter	5 section case	10 section case	15 section case
1.	Emittance [nm.rad]	38.5	38.8	39.5
2.	SR loss per turn [keV]	722	685	677

In both cases, emittance reduces from 58 to  $\sim 39$  nm.rad. This study shows that more number of section in dipole does not lead to considerable reduction in beam emittance. It is also challenging to design and manufacture the dipole with LGB profile for more and small lengths of the sections, and it will increase the cost of magnet. For further studies, the case in which dipole is divided into 5 sections is considered, which is an acceptable trend in low emittance ring designs [34].

So far we have discussed the optimization of LGB profiles to minimize the beam emittance based on single objective Nelder-Mead and GA algorithm. Various other objectives are considered as the constraints. In the following Section, the optimization of the LGB profiles using MOGA to minimize the beam emittance, maximize the dispersion at sextupole location,

and minimize the SR loss will be discussed.

### 3.3.2.6 Optimization using multi objective genetic algorithm (MOGA)

The LGB profile optimization considering three conflicting objectives is performed using MOGA algorithm. First objective is to minimize emittance (minimize  $I_5$ ), maximize the dispersion at sextupole (in chromatic section) and minimize the SR loss. The second objective of maximizing the dispersion can be converted to maximize the slope of dispersion at the exit point of the dipole magnet. To see the behaviour of SR loss, slope of dispersion function and emittance, a multi-objective optimization problem can be defined in which there are three objective functions, (i)  $f_1: \left\langle \frac{\mathcal{H}(s)}{\rho^3} \right\rangle$ , (ii)  $f_2$ : derivative of dispersion function at the exit of dipole magnet and (iii)  $f_3$ : SR loss per turn. The purpose of this study to see the trade offs between conflicting objective functions. The optimization problem can be defined as

$$\text{Minimize } \vec{f}(\vec{B}) = (f_1, -f_2, f_3)$$

*with constraints*

$$\text{Variable space range } LB : 0.5 \quad \text{Tesla in each section}$$

$$UB : 2.65 \quad \text{Tesla in each section} \quad (3.7)$$

$$\Delta\theta = \left| \sum_{i=1}^{i=5} \theta_i - \theta_{original} \right| = 0,$$

$$\max(\vec{B}_i) \leq 2.65.$$

$$B_i > B_{i+1}; i = 1, 2, \dots, 4,$$

The negative sign is chosen for second objective, because it has to be maximize. The population size is chosen as 300 and number of generations is chosen as 100. Some of the optimized LGB profiles from previous studies are chosen as initial guess to give a search direction to GA. After optimization, the following trade off between first two objective with third one is found which is shown in Fig.3.23. It shows that all three objectives are conflicting. One has to choose

LGB profile judiciously. Large derivative of dispersion at the exit of dipole, which leads to large dispersion at sextupole location, comes with large SR loss per turn. In Fig. 3.24, three cases namely A, B and C are shown and corresponding parameters are compared in Table. 3.5. As value of objective function increase, SR loss also increases. Though objective function in case C is greater than the homogeneous case but emittance still reduces because radiation damping dominates.

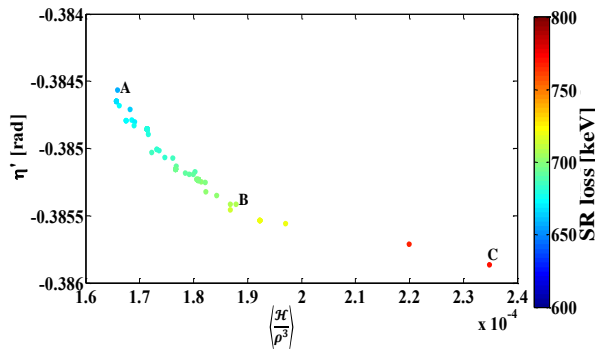


Fig. 3.23: Pareto optimal front between first and second objective. SR loss is given by color at each point of Pareto optimal front.

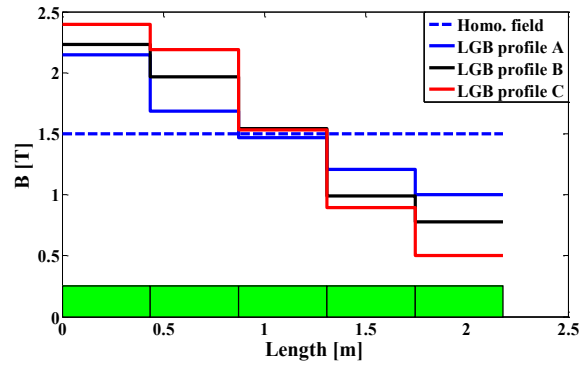


Fig. 3.24: Different LGB profiles for A, B and C.

Table 3.5: Comparison of different LGB profiles in case of MOGA.

S.No.	Parameter	A	B	C
1.	$\langle \frac{\mathcal{H}}{\rho^3} \rangle$	$1.656 \times 10^{-4}$	$1.878 \times 10^{-4}$	$2.347 \times 10^{-4}$
2.	SR loss per turn [keV]	666.8	708.2	769.1
3.	$\eta'$ [rad]	0.3846	0.3854	0.3859
4.	Emittance [nm.rad]	40.1	41.5	47.5

### 3.4 Optimization of LGB profiles in dipole for TME lattices

To study LGBs in TME lattices, a lattice based on TME is designed considering the same dipole (as in DBA lattice of Indus-2). This lattice uses same homogeneous dipole of Indus-2, i.e., length and magnetic field are same. Unit lattice cell of Indus-2 in TME configuration is shown in Fig. 3.25 with different magnetic elements and lattice functions are shown in Fig. 3.26. In TME configuration, there will be 16 super period instead of 8 to make the complete ring with circumference 172.47 m.

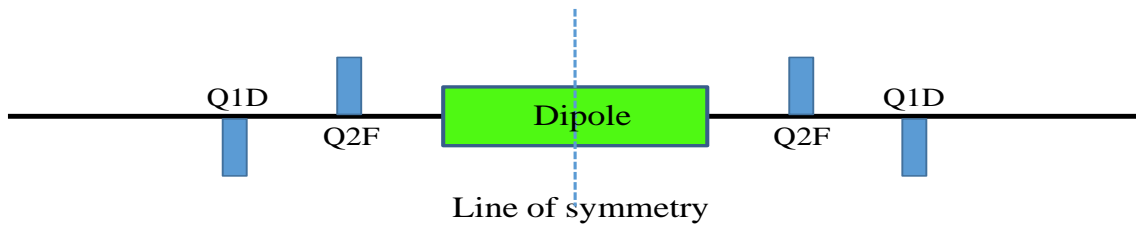


Fig. 3.25: Different magnetic elements of Indus-2 lattice in TME configuration.

Though, Indus-2 can not be operated in TME configuration, however TME is the backbone of the MBA lattices, which can be inserted between two matching cells (DBA type) to reduce the beam emittance below the limit of achromatic lattice. As shown in Fig. 3.5, LGB profile in a dipole for TME lattice is such that the magnetic field must be maximum at the center of the dipole and decreasing on either side of the dipole.

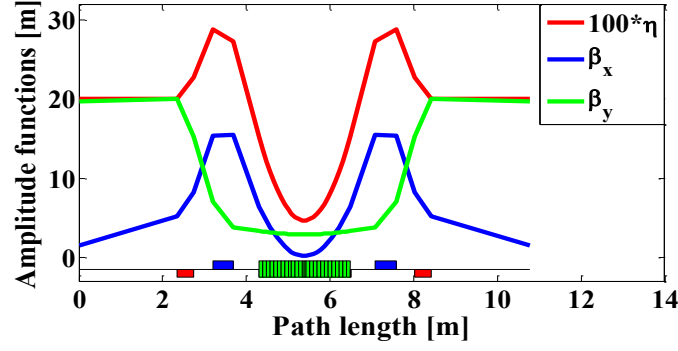


Fig. 3.26: Variation of different lattice functions.

To generate stair like LGB profile (Symmetrically decaying), dipole is divided into 25 equal sections to get more smooth LGB profile. The middle section of the dipole is further divided into 2 equal sections. Therefore, there are total 26 sections. Three cases have been studied in which, maximum magnetic field is 6 Tesla, 5 Tesla and 4 Tesla. Here, in each profile, maximum magnetic field in the center dipole section is desired.

The optimization problem for this case can be defined as

$$\text{Minimize } f(\vec{B}) = \left\langle \frac{\mathcal{H}_x}{\rho^3} \right\rangle$$

with constraints

Variable space range LB : 0.5 Tesla in each section

UB : 6.0 Tesla in each section

$$\Delta\theta = \left| \left( \sum_{i=1}^{i=26} \theta_i - \theta_{original} \right) \right| = 0, \quad (3.8)$$

$$\max(\vec{B})_i \leq 6,$$

$$(\vec{B})_i < \vec{B}_{i+1}; \quad i = 1, 2, \dots, 13,$$

$$(\vec{B})_i = (\vec{B})_{27-i}; \quad i = 1, 2, \dots, 12,$$

$$\max((\vec{B})_{13}) = 6 \text{ or } 5 \text{ or } 4$$

The CS variable at entrance, mid and exit point of the dipole are

$$\text{entrance of the dipole } (\alpha_{entr}, \beta_{entr}, \gamma_{entr.}) = (5.6372, 6.4114, 5.1124)$$

$$\text{at mid of the dipole } (\alpha_{mid}, \beta_{mid}, \gamma_{mid}) = (0, 0.1882, 5.3145) \quad (3.9)$$

$$\text{at the end of dipole } (\alpha_{end}, \beta_{end}, \gamma_{end}) = (-5.6372, 6.4115, 5.1124).$$

It can be seen that, beta function achieves minimum at the center of the dipole in TME lattice and symmetrically increases on either side. This behaviour is provided by  $\alpha$ , where at the entrance  $\alpha$  is negative, at the centre it is zero, and at the exit it achieves same value as entrance but positive.  $\gamma$  function is almost constant over the dipole.

After optimization, LGB profiles for three cases are shown in Fig. 3.27 and different parameters after including LGBs are shown in Table 3.6.

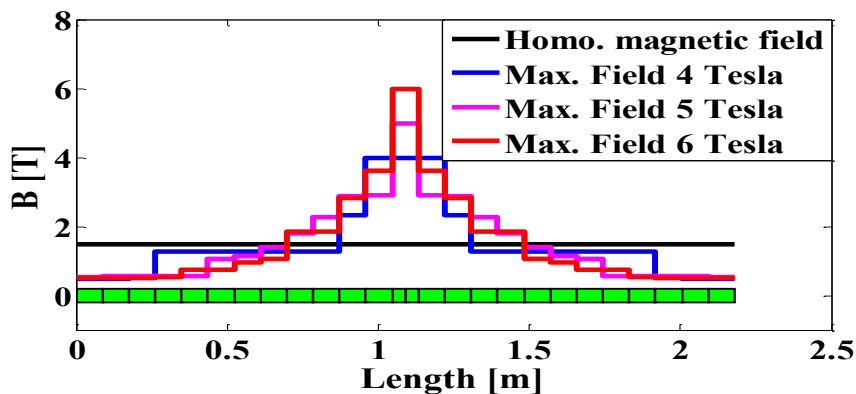


Fig. 3.27: LGB profiles for different chosen maximum magnetic field.

Table 3.6: Comparison of different parameter with original lattice in case of TME.

S.No.	Parameter	Homo. magnetic field	Max. field 4 Tesla	Max. field 5 Tesla	Max. field 6 Tesla
1.	Emittance [nm.rad]	14.14	5.365	3.8	3.27
2.	SR loss per turn [keV]	623	917	964	1111

This study shows that emittance can be reduced by less than half with dipoles having LGB than the homogeneous field dipoles, but at the cost of increased SR loss because of high magnetic field. Since magnetic field in the center dipole section is upto 6 Tesla, it can not be achieved using normal electromagnetic dipole. One has to use superconducting dipole. These dipoles with LGBs can be used in MBA lattices to reduce the beam emittance further in the same ring or one can design a storage ring with lower circumference for the same emittance, this will reduce the cost of the machine.

For the case, where magnetic field at the center is 5 Tesla, the variation of different lattice functions are shown in Fig. 3.28. At the center of the dipole, dispersion function is more minimum than the homogeneous dipole which leads to a reduction in  $\mathcal{H}$  function. Consequently, the beam emittance reduces. Also, beta functions are not changed much from the original lattice.

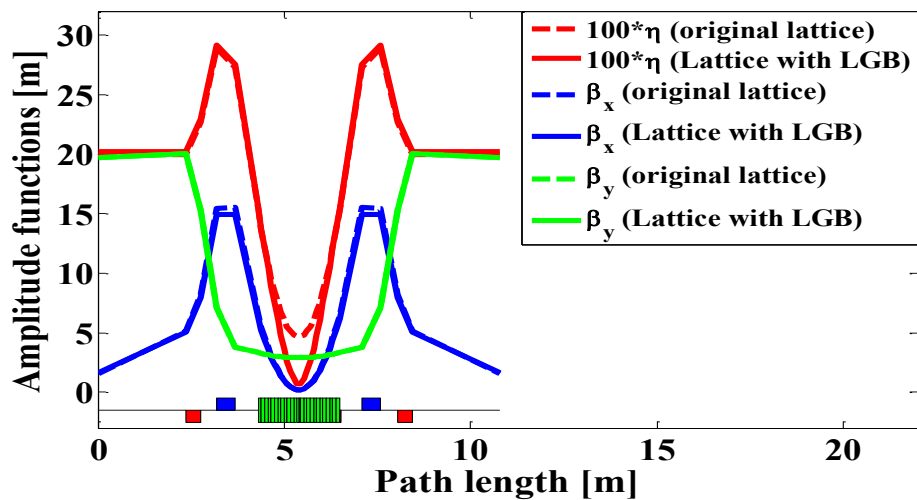


Fig. 3.28: Comparison of lattice functions with and without LGB.

In this Chapter, an extensive optimization study of LGB profiles using single and multi-objective genetic algorithms are presented. The LGB profiles of a dipole in DBA lattice case,

and for a dipole in TME lattice case are optimized. Outcome of the study is that the beam emittance reduces by  $\sim 30\%$  in DBA and less than half emittance can be reduced in TME case.

In a well design lattice, if dipoles are placed with LGBs, the distribution of dispersion over the full lattice cell will change. It is due to the fact that quadrupoles are optimized for the lattice functions with homogeneous field dipole. Further studies including optimized LGBs and tuning of quadrupoles are presented in Chapter 4 for the case of well design lattice of Indus-2 and Indus-3. The performance comparison of the lattice with and without LGBs are made.

# Chapter 4

## Indus-2 and Indus-3 storage ring lattice performance with LGBs

In Section 1.16 and 1.17, Indus-2 and proposed Indus-3 electron storage rings have been discussed. In operational storage rings, there always exists a possibility of up-gradation to improve the performance. In newly design lattices with conventional means, one can also do aggressive optimization to achieve ever improved performance by including technologically challenging quadrupole gradient and dipole fields.

The optimization studies are presented in Chapter 3 to get optimal LGB profiles in view of beam emittance and increasing the dispersion at sextupole location, to achieve efficient correction of natural chromaticity with reduced sextupole strengths. First study to reduce emittance for achromatic and TME cases are presented and comparison of emittance with nominal emittance were performed. It was also highlighted that the SR loss per turn in LGB case is always higher than the SR loss per turn from constant field dipole. In these studies, it was assumed that the lattice functions at the entrance of the dipoles are known and fixed, however, in actual lattice design with LGB profiles, the distribution of dispersion function get changed. It is

the case when quadrupoles are operating with the nominal lattice, i.e., the lattice with constant field dipoles. Therefore, re-tuning of the quadrupole strengths are required to achieve desired distribution of the lattice functions after including LGBs in place of constant field dipoles. These studies are carried out for the case of Indus-2 storage ring, which is operational in user mode, and Indus-3, which is an upcoming project at RRCAT. In Section 4.1, the optimization of quadrupoles with dipoles replaced with LGBs are performed to achieve desired distribution of lattice functions for Indus-2 storage ring lattice. The comparative study of dynamic aperture in the lattice with and without LGB are given in Section 4.2. The optimization of various objectives using MOGA are also presented in Section 4.3 to get trade off between them in a running/ designed electron storage ring in the same circumference. Similar studies for Indus-3 are performed in Section 4.4.

## **4.1 DBA lattice of Indus-2 with LGBs**

As discussed in Section 1.16, Indus-2 has been designed based on DBA configuration with ring circumference 172.47 m and beam emittance of 58 nm.rad. Positions of different magnetic elements of unit lattice are shown in Fig. 4.1. This unit lattice consist 2 dipoles, 9 quadrupoles and 4 sextupoles. Each element in the unit lattice is placed in such a way that it looks symmetric with respect to centre of quadrupole Q5D and strength of the quadrupoles are such that the lattice/ amplitude functions have distribution as shown in Fig. 4.2. The achromatic condition, i.e., dispersion and its derivative at straight sections are zero, is achieved using three quadrupoles (two Q4F and one Q5D) between dipole magnets and beta functions are controlled using all five families of quadrupoles, i.e. Q1D, Q2F, Q3D, Q4F, and Q5D.

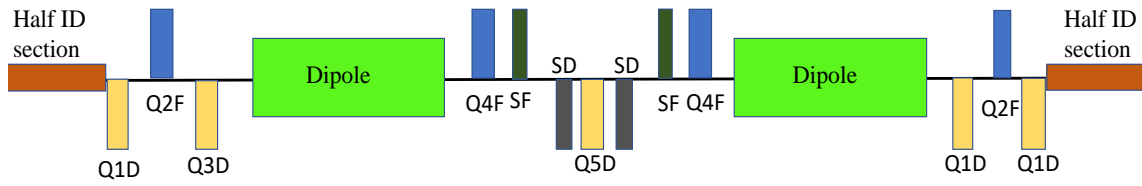


Fig. 4.1: Basic elements in Indus-2 unit lattice (not to scale). Here, QF: focusing quadrupole, QD: defocusing quadrupole, SF: focusing sextupole, SD: defocusing quadrupole. Number indicates family of that element, e.g. Q1D shows first family of defocusing quadrupoles.

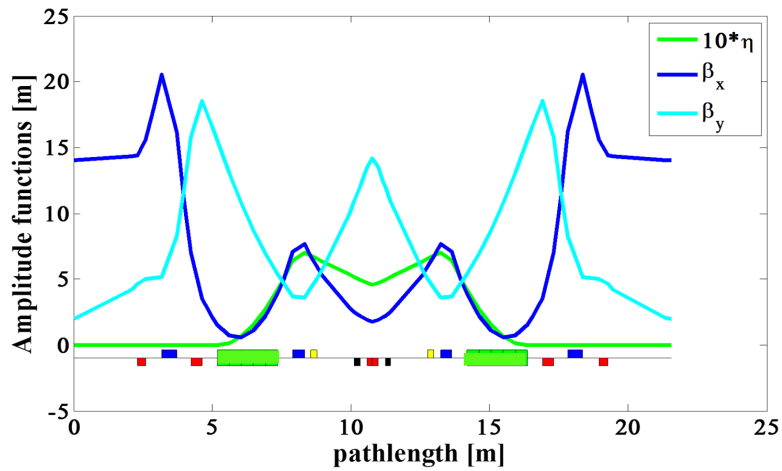


Fig. 4.2: Variation of beta and dispersion functions in Indus-2 unit lattice.

Since Indus-2 is in regular operation in user mode, ring size, length and position of any magnetic element in the machine can not be changed. In order to reduce the beam emittance further in the same ring with minimum hardware change, dipoles with LGBs can be used.

#### 4.1.1 Optimization of lattice function with LGBs

The optimization of lattice functions of an achromat (DBA or MBA) lattice with LGBs is a two step process. First, optimization of the dipole to get optimal LGB profile, which is already discussed in Chapter 3, second, optimization of strength of quadrupoles to match

lattice function to the nominal lattice.

A LGB profile has been chosen from Section 3.3.2, Chapter 3, in which dipole is divided into 5 sections and magnetic field in the first section is 2.65 Tesla. Magnetic fields in each section of the dipole are given as

$$B = [2.6500 \quad 1.5575 \quad 1.2632 \quad 1.0845 \quad 0.9575] \text{ [Tesla]}. \quad (4.1)$$

The comparison of LGB profile with homogeneous field is shown in Fig.4.3. After replacing homogeneous dipoles with dipoles with LGBs in an unit lattice, achromatic condition is lost which is shown in Fig. 4.4. This is because of unoptimized quadrupole strengths. Also, it can be seen in Fig. 4.5 and Fig. 4.6 that introduction of LGB does not change beta functions which was assumed in LGB profiles study. A small change in horizontal beta function is due to geometrical focusing in dipole magnets. But over the dipole, it is same as nominal lattice.

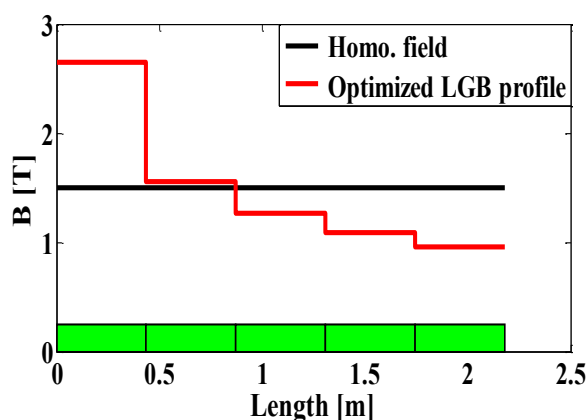


Fig. 4.3: LGB profile compared with homogeneous dipole field in the dipole magnet.

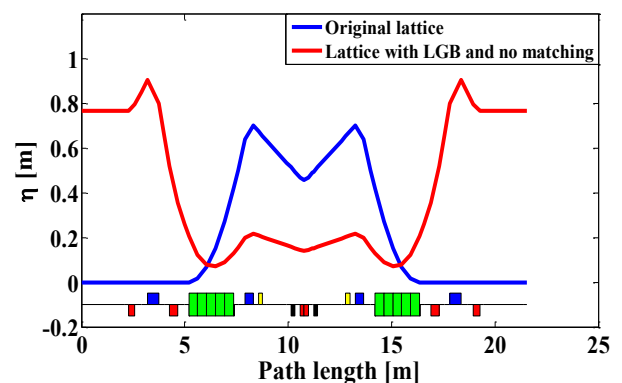


Fig. 4.4: Variation of dispersion function with LGB.

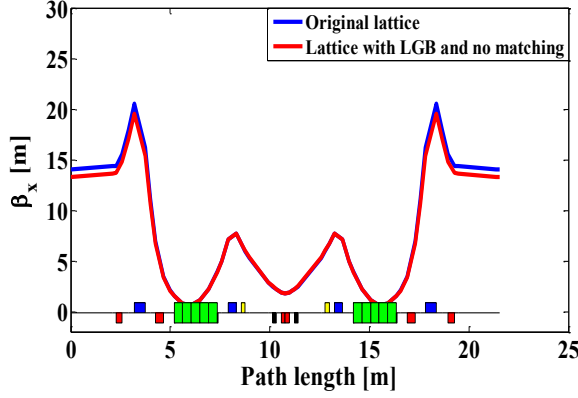


Fig. 4.5: Variation of horizontal beta function with LGB.

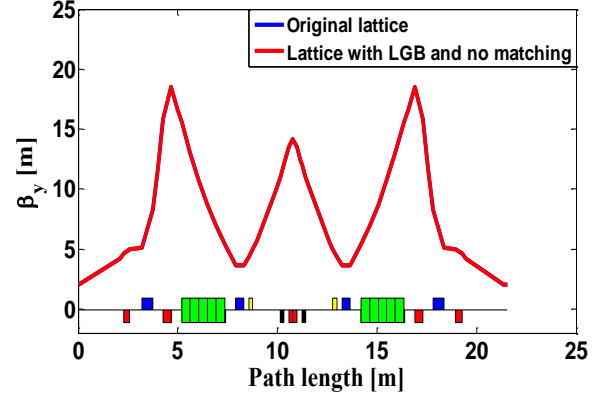


Fig. 4.6: Variation of vertical beta function with LGB.

In order to get achromatic condition and constraints on other important parameters like constraint on betatron tune, beta functions, stability conditions etc., optimization of quadrupole strengths is required. Here, all five families of quadrupoles, i.e., Q1D, Q2F, Q3D, Q4F and Q5D, have been chosen in the optimization. Here, this optimization problem is solved using single as well as multi-objective techniques. Using single objective techniques and using quadrupole strengths of nominal lattice as initial guess is described below.

In this optimization problem, there are many objective functions which are; (i)  $f_1$ : beam emittance, (ii)  $f_2$ : dispersion at straight section, (iii)  $f_3$ : slope of dispersion at straight section, (iv)  $f_4$ : derivative of beta functions at injection, (v)  $f_5$ : beta functions at injection, (vi)  $f_6$ : betatron tunes (vii)  $f_7$ : beta functions at symmetric point. Each objective function  $f_3, f_4, f_5, f_6$ , and  $f_7$  contains two objective functions for each plane. Therefore, there are 12 objective functions in total. In Indus-2, normalized strengths of quadrupoles can go upto  $2.2 \text{ m}^{-2}$ . This will put a constraint on maximum available normalized quadrupole strength. Also, lattice functions are periodic, therefore, to find a stable solution,  $|Trace(M)| \leq 2$ , where  $M$  is the transport matrix of periodic cell. In addition, maximum value of beta functions should be in limit, this will also be a constraint.

The available variables for this optimization problem are normalized strength of quadrupoles, i.e.,  $\vec{k} = (k_1, k_2, k_3, k_4, k_5)$ . In order to minimize each objective function, the objective function can be written as  $(f_i - f_i^0)^2$ ;  $i = 1, 2, \dots, 12$ . For first objective function,  $f_1^0$  can be chosen as 0, because emittance is desired as low as possible. Other  $f_i^0$  :  $i = 2, 3, \dots, 12$  can be chosen as of nominal or original lattice. The initial values of quadrupole strengths are

$$k_0 = [-0.79860 \quad 1.52949418 \quad -1.6899011 \quad 1.81969574 \quad -1.116476][\text{m}^{-2}]$$

A composite objective function with proper weight factors can be defined to convert this multi objective optimization problem into a single objective optimization problem which can be written as

$$\text{Minimize } f(\vec{k}) = \sum_{i=1}^{i=12} w_i (f_i - f_i^0)^2$$

*with constraints*

$$|(\vec{k})_i| \leq 2.2 \text{ m}^{-2}, \quad (4.2)$$

$$|\text{Trace}(M)| \leq 2,$$

$$\max(\beta_x \text{ and } \beta_y) \leq 20 \text{ m},$$

where,  $w_i (\geq 0)$  is the weight factor for  $i^{\text{th}}$  objective function and satisfy the relation  $\sum w_i = 1$ . Weight factors are chosen in such a way that it gives satisfactory optimal result. High value of weight factor is given to dispersion at straight section than the rest of the objective functions. Because requirement of achromatic condition is the first priority.

After optimization of the problem, the optimized values of quadrupole families Q1, Q2, Q3, Q4, Q5 are

$$k = [-0.8733 \quad 1.5686 \quad -1.6752 \quad 1.6591 \quad -1.0760][\text{m}^{-2}],$$

and behaviour of objective function after each iteration is shown in Fig. 4.7. With initial guess  $k_0$ , the objective function has value equal to 0.56 and after optimization, it reduces to 0.004.

The algorithm stops due to no improvement in objective function in the successive iterations. The strength of quadrupoles Q4F and Q5D are decreased from nominal lattice, which leads to reduction in natural chromaticity in the machine.

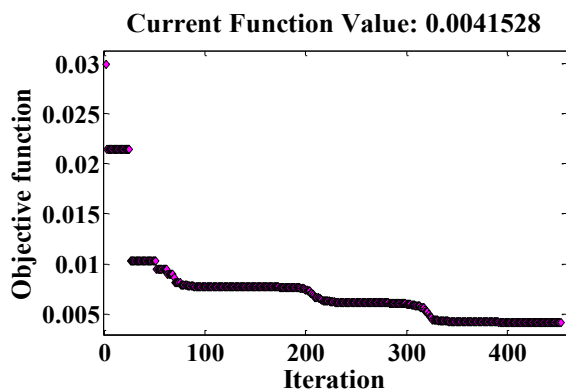


Fig. 4.7: Variation of objective function.

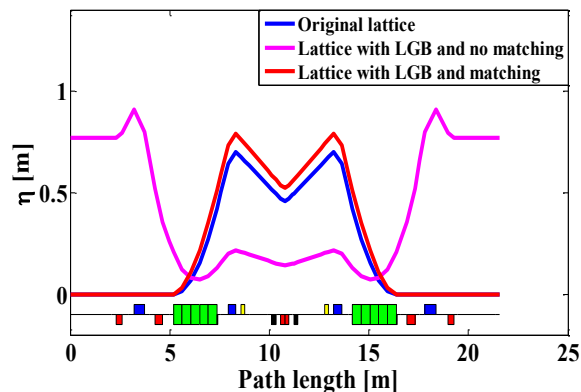


Fig. 4.8: Variation of dispersion function with LGB and matching.

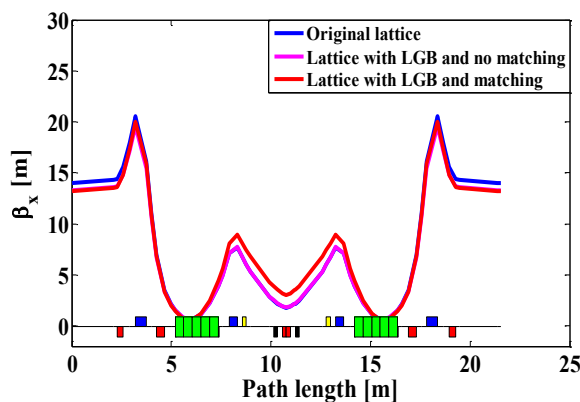


Fig. 4.9: Variation of horizontal beta function with LGB and matching.

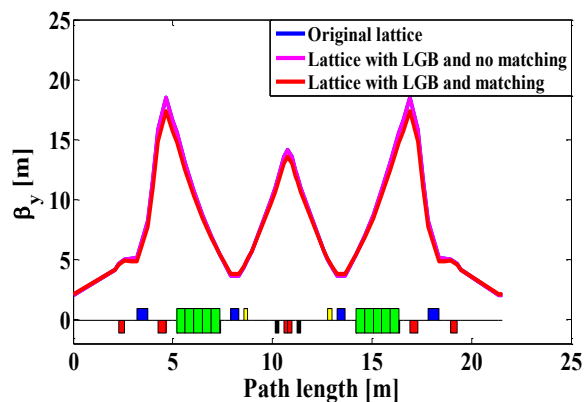


Fig. 4.10: Variation of vertical beta function with LGB and matching.

After optimization of quadrupole strengths of all five family, variation of lattice functions are shown in Fig.4.8, Fig.4.9 and Fig.4.10, which are given by lattice with LGB and matching. Achromatic condition is restored after optimization of quadrupole strengths. The small change in horizontal beta function is because of higher weight factor is given to second objective

function. But, still these changes are small. Comparison of different parameters of Indus-2 lattice with LGB and original lattice are presented in Table 4.1.

Table 4.1: Comparison of Indus-2 lattice with LGB, Indus-2 lattice with LGB and betatron tune correction and original lattice.

S.No.	Parameters	Indus-2 (Original Lattice)	Indus-2 (Lattice with LGB and matching)	Indus-2 (lattice with LGB, matching, and corrected betatron tune)
1.	Energy (GeV)	2.5	2.5	2.5
2.	Emittance (nm-rad)	58.1	38.3	43.8
3.	Energy loss per turn (keV)	623	725	725
4.	Betatron tunes $[\nu_x, \nu_y]$	[9.2 5.2]	[8.71 5.19]	[9.2 5.2]
5.	Natural chromaticity	[-19.05 -12.05]	[-19.12 -11.14]	[-14.33 -11.26]
6.	Momentum Compaction factor	0.0052	0.0051	0.0051
7.	Dispersion function at sextupole location [m]	0.68	0.76	0.76
8.	Beta function at injection [m]	[14.02 2.0]	[13.2 2.1]	[7.4 1.9]
9.	Max. Beta function [m]	[20.5 18.5 ]	[20.0 17.4]	[12.5 17.5]
10.	Beta function at symmetric point [m]	[1.8 11.2]	[3.0 13.6]	[1.88 13.1]

11.	Required sextupole strength for chromaticity correction [2,2] [m <sup>-3</sup> ]	[13.03 -11.72]	[10.85 -10.09 ]	[9.54 -9.582]
-----	--	----------------	-----------------	---------------

The brightness ratio of Indus-2 lattice with LGBs and nominal lattice is calculated using 1% coupling and  $\sigma_r = 0$ . The ratio of brightness comes out to be  $\sim 2$ . Emittance, after including LGBs in dipoles of Indus-2 lattice, reduces from 58 to 38 nm.rad with marginal change in other important parameters. As natural chromaticity of the machine is decreased and dispersion at the sextupole location is increased from 0.68 m to  $\sim 0.76$  m, sextupole strengths to correct the chromaticity to the same level of nominal lattice get reduced from  $13.03 \text{ m}^{-3}$  to  $10.85 \text{ m}^{-3}$  in horizontal and  $-11.72 \text{ m}^{-3}$  to  $-10.1 \text{ m}^{-3}$  in vertical plane. These are the major advantages of dipoles with LGB in a storage ring over storage rings with homogeneous dipoles.

Here, betatron tunes are not same as original lattice. Therefore, one has to correct betatron tune to the original lattice to see the effect of betatron tune correction on lattice functions. Therefore, betatron tune is corrected to [9.2, 5.2] using Q2F and Q3D families of quadrupoles. These quadrupoles are chosen, because they are located at zero dispersion and will not affect achromatic condition. After betatron tune correction, strengths of quadrupole Q2F changes from  $1.5686 \text{ m}^{-2}$  to  $1.6204 \text{ m}^{-2}$  and strength of quadrupole Q3D changes from  $-1.6752 \text{ m}^{-2}$  to  $-1.7003 \text{ m}^{-2}$ . The different lattice parameters after betatron tune correction are presented in the fourth column of Table 4.1 and variation of horizontal and vertical beta functions are shown in Fig. 4.11 and Fig. 4.12.

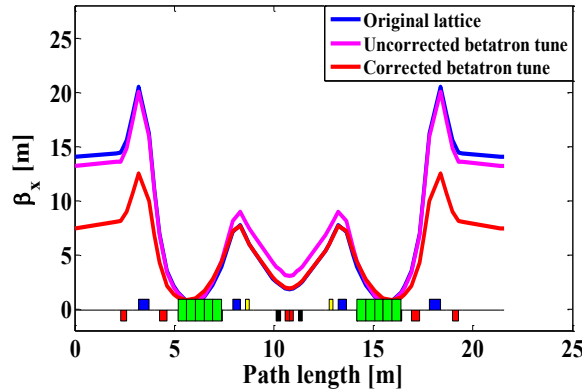


Fig. 4.11: Variation of horizontal beta function with LGB, matching, and betatron tune correction.

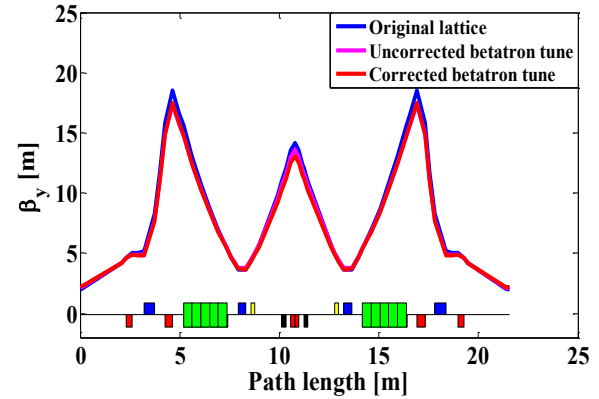


Fig. 4.12: Variation of vertical beta function with LGB, matching and betatron tune correction.

It can be seen that how betatron tune is sensitive to lattice function. After correction of betatron tune, emittance increased by 5 nm.rad and horizontal beta function at injection changes from 13.92 m to 7.4 m. This decrease in horizontal beta function will lead to more strengths of kicker to inject the beam in the storage ring, which is a disadvantage. But, low horizontal beta function at IDs location lead to low beam size in IDs which is an advantage. In practical storage ring, real effect of the change in horizontal beta function can be seen only after study of dynamic aperture, which is presented in the following Section.

#### 4.1.2 Dynamic aperture

In Section 1.10, the concept of dynamic aperture is explained. This phenomenon arises due to non linearity in the machine. As strength of sextupole for chromaticity correction is small in lattice with LGBs compared to original lattice. Hence, dynamic aperture should not change much from original lattice. After correcting chromaticity to [2, 2] (horizontal and vertical) with two families of sextupoles, for on momentum charged particles, a comparative study of dynamic aperture for three cases are compared in Fig. 4.13.

To calculate dynamic aperture, range of  $x$  is chosen from -32 mm to 32 mm in step size of 0.5 mm. On the other hand, range of  $y$  is chosen from -17 to 17 mm. The maximum range of  $x$  and  $y$  are chosen on the basis of available physical aperture of vacuum chamber. Charged particle is tracked for 1000 turns in the grids and the boundary is decided on the basis of loss, i.e., after a certain point of the grid, charged particle is lost.

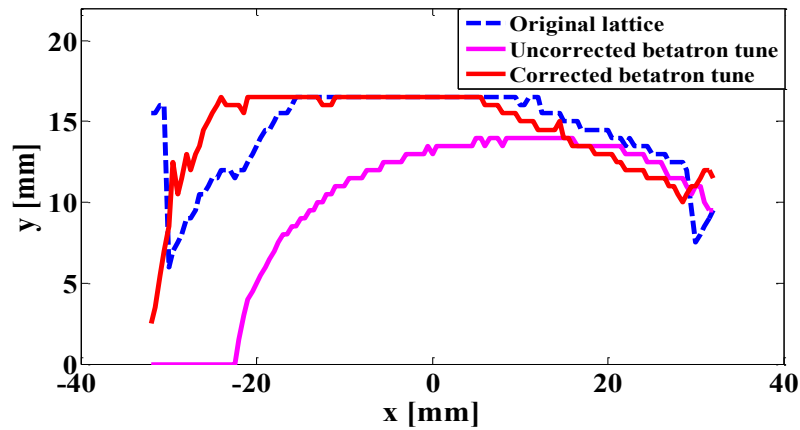


Fig. 4.13: Dynamic aperture comparison for on momentum charged particles.

Though, positive values in vertical direction are plotted, but graph of the boundary is symmetric with respect to  $x$ , i.e. a closed boundary will be there. Also, open ends at both side of  $x$  is because of fixed range of  $x$ . If range of  $x$  is allowed more, there will not be any open ends. As depicted in Fig. 4.13, if betatron tune is allowed to be relaxed then dynamic aperture shifted towards outer region in  $x$  direction. But, if we correct the betatron tune it approximately covers the same area as original lattice i.e., life time of electron beam will be same as original lattice.

In Section 4.1, quadrupole strengths are optimized using single objective algorithm. Major disadvantage of this algorithm is that the weight factors are highly sensitive and a proper choice of these weight factors is required which is a tedious task and one has to run many simulation runs to get an optimal solution. In order to avoid these difficulties, multi-objective

genetic algorithm (MOGA) can be used. A optimization study using MOGA is presented in the following Section.

## 4.2 Comparative study of beam emittance with and without LGBs

To find a trade-off between dispersion function at straight section and emittance, MOGA has been used. As optimization of quadrupole strengths of Indus-2 lattice with LGB is a multi-objective optimization problem. In this study, two objective functions, (i)  $f_1$ : emittance, and (ii)  $f_2$ : dispersion at straight section are chosen and rest of the objective functions like maximum beta functions ( $\beta_{x,max}, \beta_{y,max}$ ), betatron tunes ( $\nu_x, \nu_y$ ), beta functions at symmetric point ( $\beta_{x,sym}, \beta_{y,sym}$ ) etc., are chosen as constraints. The optimization function can be written as

$$\begin{aligned}
 & \text{Minimize } \vec{f} = (f_1, f_2), \\
 & \text{with constraints} \\
 & |(\vec{k})_i| < 2.2 \text{ m}^{-2}; i = 1, 2, \dots, 5, \\
 & |\text{Trace}(M)| \leq 2, \\
 & \max(\beta_x \text{ and } \beta_y) \leq 20\text{m}, \\
 & 0.7 \leq \text{fractional } \nu_{x,y} \leq 0.9 \quad \text{or} \quad 0.1 \leq \text{fractional } \nu_{x,y} \leq 0.25, \\
 & |\beta_{x,inj} - 14| < 1.2 \quad \text{and} \quad |\beta_{y,inj} - 2| < 0.5, \\
 & |\beta_{x,sym} - 1.8| < 1.5 \quad \text{and} \quad |\beta_{y,sym} - 14.2| < 0.2.
 \end{aligned} \tag{4.3}$$

The range of betatron tune is chosen so that fractional betatron tune is far away from dangerous resonances. Range of other constraints are chosen to get optimal solution. In Fig.4.14, a Pareto optimal front to show trade off between dispersion function at straight section and emittance is

given and it is compared with Pareto optimal front for original lattice. In Pareto optimal front, there are large number of solutions for strengths of quadrupoles.

Fig. 4.14 shows that both objectives are conflicting in nature and one must choose a solution judiciously. To get desired emittance one has to compromise dispersion at straight section. This is the major advantage of multi-objective genetic algorithm over classical methods. Beta functions at injection, natural chromaticity, betatron tune, maximum beta functions for different set of quadrupole strengths are shown in Fig.4.15, Fig.4.16, Fig.4.17, and Fig.4.18 and data of quadrupole strengths, which have dispersion at straight section less than 0.002 m are shown in numbers. There are only two data which satisfy dispersion function at straight section near to zero. For both data, emittance is nearly 38 nm.rad, other parameters can also be compared in figures.

According to ones requirement, e.g. if one wants to allow a little dispersion at straight section, then solution can be chosen such that important parameters, like betatron tune, natural chromaticity, beta functions at injection, maximum beta functions, are satisfied.

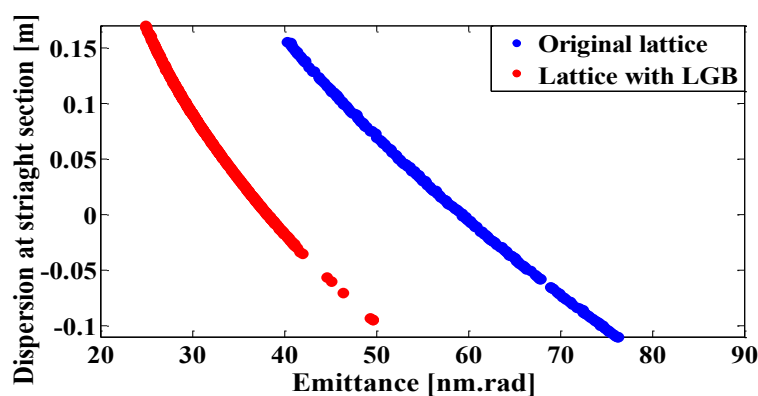


Fig. 4.14: Comparison of Pareto optimal front.

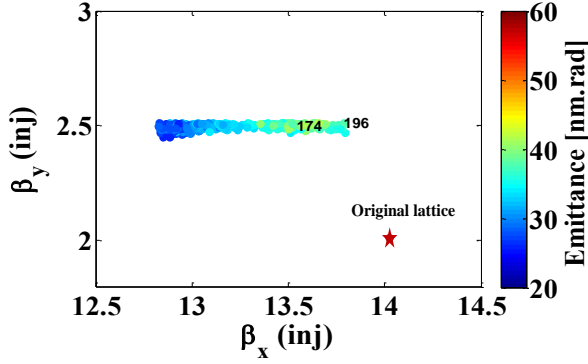


Fig. 4.15: Comparison of beta functions at injection for each solution.

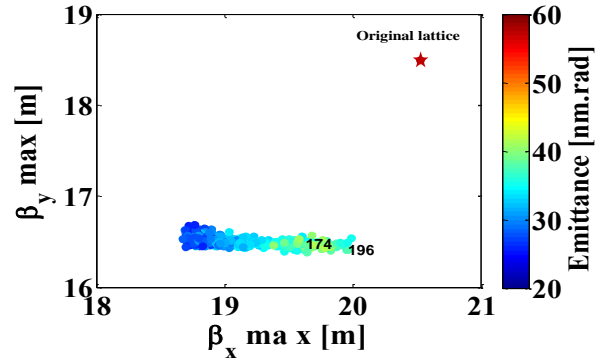


Fig. 4.16: Maximum beta functions comparison for each solution.

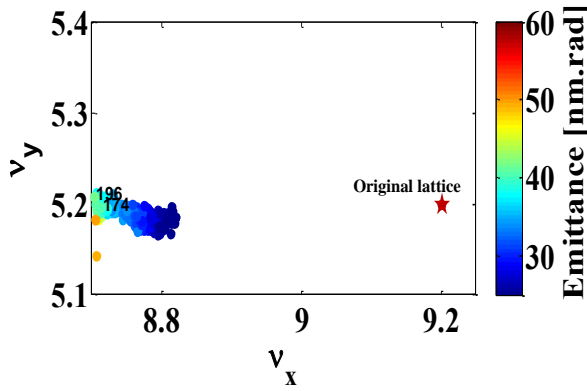


Fig. 4.17: Betatron tune comparison for each solution.

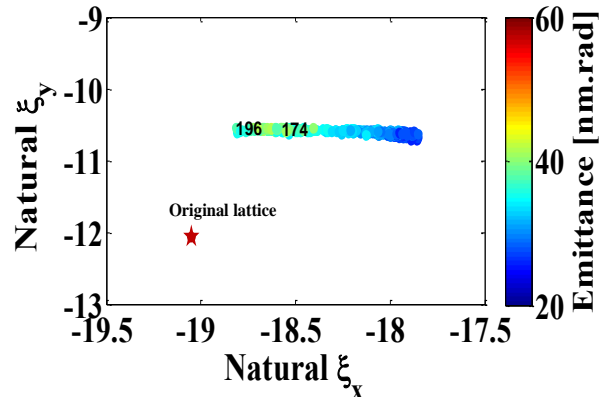


Fig. 4.18: Natural chromaticity comparison for each solution.

A similar optimization studies of LGBs are presented for Indus-3 lattice in the following Sections.

### 4.3 MBA lattice of Indus-3 with LGBs

In Section 1.17, Chapter 1, Indus-3 lattice has been discussed. Indus-3 or high brightness synchrotron radiation source (HBSRS) is a 6 GeV electron storage ring. The baseline lattice has been designed to achieve beam emittance of 150 pm.rad. Different elements of Indus-3 lattice are shown in Fig. 4.19. Magnetic elements are placed in the unit lattice in such a way

that it looks symmetric with respect to center of BM4 and strengths of quadrupoles are such that it generates lattice functions as shown in Fig. 4.20.

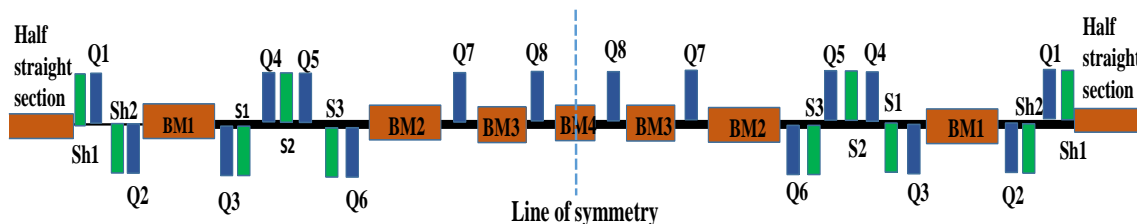


Fig. 4.19: Different magnetic elements of Indus-3 lattice (not to scale). Magnetic elements which are above base line are focusing in nature and below the base line are defocusing in nature.

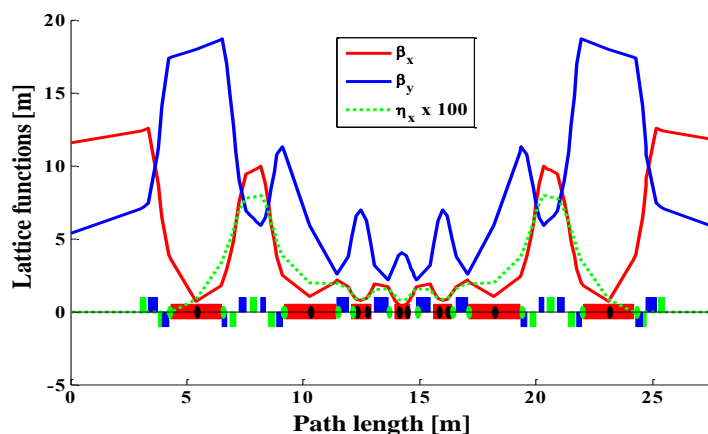


Fig. 4.20: Designed lattice functions of Indus-3 lattice.

Dipole magnets BM3 and BM4 are combined function dipole magnets, i.e., these magnets have quadrupole gradient along with dipole component. Dipole magnets BM1 and BM2 are homogeneous dipole magnets and are same. As BM3 and BM4 already have transverse gradient, hence it is difficult to include LGB because of technological challenges. Therefore, to study LGB for this lattice, dipoles BM1 and BM2 are chosen and similar logic as LGB in Indus-2 dipole can be applied. LGB profile for BM1 will be a decreasing profile. On the other hand, for BM2 it will be reversed, i.e., a increasing LGB profile to shape the dispersion function. The length of the dipoles BM3 is 2.17 m and it bends a charged particle by an angle

1.74°. In this case also, dipole magnet is divided into 5 equal sections and LGB profile is optimized using single objective genetic algorithm with maximum magnetic field 0.45 Tesla in the first section.

After optimization, magnetic fields in each section of dipole are

$$B = [0.4500 \quad 0.3167 \quad 0.2430 \quad 0.2008 \quad 0.1899][\text{Tesla}].$$

The optimized LGB profile is shown in Fig.4.21 and compared with homogeneous magnetic field, i.e., 0.28 Tesla.

This LGB profile will change the distribution of dispersion function in the lattice and the achromatic condition will be lost. Therefore, strength of quadrupoles are needed to be optimized.

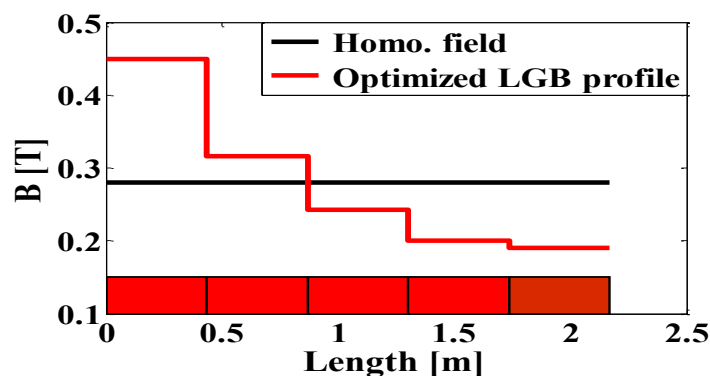


Fig. 4.21: Optimized LGB profile.

### 4.3.1 Matching of lattice function with quadrupoles

To match lattice functions and other constraints like betatron tune, stability condition, limit on maximum beta function, etc., quadrupole strengths must be optimized. This optimization problem is solved using MOGA, in which three objective functions are chosen which are: (i)  $f_1$ : emittance, (ii)  $f_2$ : dispersion function at straight section, (iii)  $f_3$ : dispersion at focusing sextupole location. Quadrupoles used in Indus-3 lattice have large gradient compared to Indus-2

lattice. Therefore, Indus-3 is a very tight focusing machine and betatron tune, lattice function etc. are much sensitive compared to Indus-2. Therefore, all quadrupole family, i.e., Q1, Q2, Q3, Q4, Q5, Q6, Q7, Q8 and quadrupole gradient in BM3 and BM4 are chosen for matching of lattice function and other important parameters. The limit on strengths of quadrupoles is chosen as  $4.2 \text{ m}^{-2}$  and for quadrupole gradient in BM3 and BM4 it is chosen as  $2.2 \text{ m}^{-2}$ .

The multi-objective optimization problem can be defined as

$$\begin{aligned}
 & \text{Minimize } \vec{f}(\vec{k}) = (f_1, f_2, -f_3), \\
 & \text{with constraints} \\
 & \quad |(\vec{k})_i| < 4.2 \text{ m}^{-2}; i = 1, 2, \dots, 8, \\
 & \quad |(\vec{k})_i| < 2.4 \text{ m}^{-2}; i = 9, 10, \\
 & \quad |\text{Trace}(M)| \leq 2, \tag{4.4} \\
 & \quad \beta_{x,y,max} \leq 20\text{m}, \\
 & \quad 0.75 \leq \text{fractional } \nu_{x,y} \leq 0.9 \quad \text{or} \quad 0.1 \leq \text{fractional } \nu_{x,y} \leq 0.3, \\
 & \quad |\beta_{x,inj} - 11.6| < 2.5 \quad \text{and} \quad |(\beta_{y,inj} - 5.34)| < 1.5, \\
 & \quad |\beta_{x,sym} - 0.4| < 1 \quad \text{and} \quad |\beta_{y,sym} - 4.3| < 1,
 \end{aligned}$$

Number of generation and number of population to run the MOGA code are 200 and 500 respectively. The large number of population are chosen to get more number of solution that satisfy constraints. To give a search direction to MOGA, initial values of strength of quadrupoles are chosen. Initial values of quadrupole strengths and quadrupole component in BM3 and BM4 are

$$\begin{aligned}
 k_0 = & [2.0369 \quad -2.1406 \quad -2.6000 \quad 2.1141 \quad 3.5617 \\
 & -2.7373 \quad 3.0327 \quad 3.6775 \quad -2.2 \quad -2.0][\text{m}^{-2}].
 \end{aligned}$$

After optimization, Pareto optimal front between emittance and dispersion at straight

section with color bar for dispersion at focusing sextupole location are shown in Fig. 4.22. It can be seen that each objective is conflicting in nature, i.e., one has to choose a solution judiciously. As dispersion at focusing sextupole increases, achromatic condition not satisfied and emittance is also increased. Emittance in each case is in the range 136 to 140 pm.rad, which shows the advantage of LGB dipoles. In MOGA, large number of solutions are generated, which are all optimal with given constraints. For each solution, beta function at injection, natural chromaticity, betatron tune and maximum beta function are calculated and are shown in Fig. 4.23, Fig. 4.24, Fig. 4.25, and Fig. 4.26.

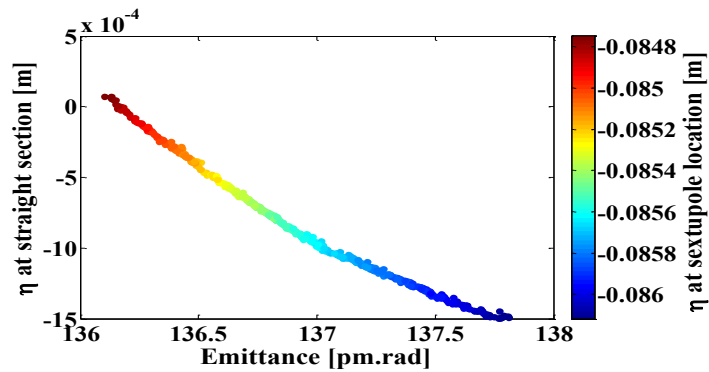


Fig. 4.22: Pareto optimal front for emittance with dispersion at straight section.

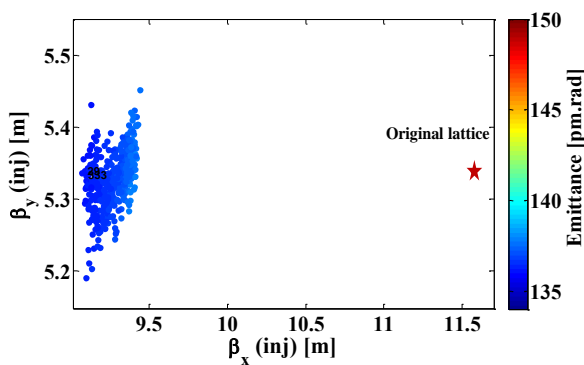


Fig. 4.23: Horizontal and vertical beta functions comparison for each solution.

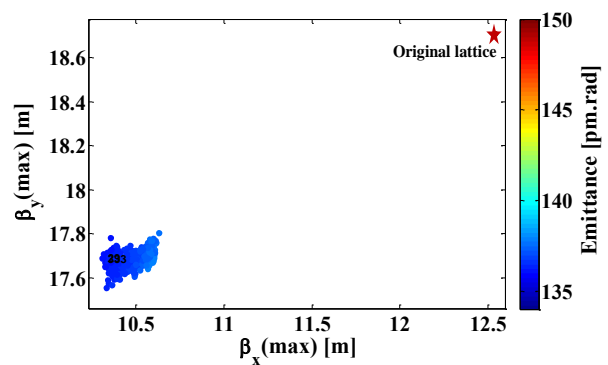


Fig. 4.24: Maximum horizontal and vertical beta functions comparison for each solution.

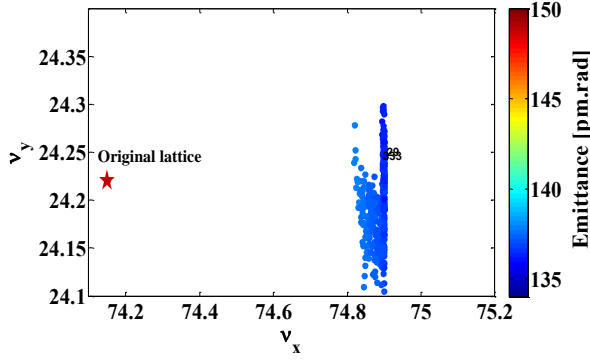


Fig. 4.25: Horizontal and vertical betatron tune comparison for each solution.

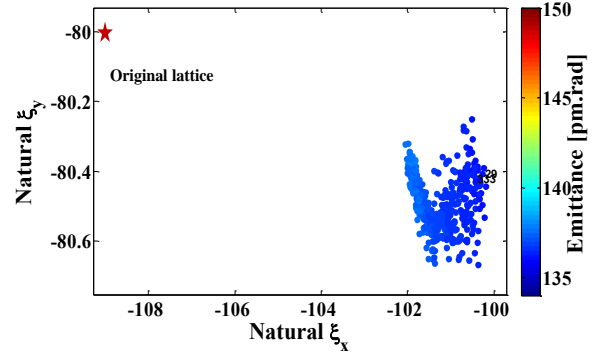


Fig. 4.26: Horizontal and vertical natural chromaticity comparison for each solution.

For each solution from MOGA, horizontal betatron tune increases from 74.2 to 74.8-74.9 which is acceptable, because it is away from resonances and vertical betatron tune is almost same to original lattice. Horizontal beta function at injection reduces from 11.5 m to 9-9.5m, which will require increase in the kicker strengths, but vertical beta function is close to original lattice. One advantage of low horizontal beta function is that beam size at IDs location will be low which is desirable. Maximum beta function is reduced for both planes by 2-2.5 m. Natural chromaticity in horizontal plane is decreased by an amount of 8, which is an advantage. Those solutions, for which dispersion at straight section is less than 0.0002 m are shown by numbers. There are only two solutions which satisfy it.

One of the solution, for which dispersion at straight section is near to zero, is given by

$$k = \begin{bmatrix} 2.1432 & -2.3929 & -1.9493 & 1.6595 & 3.8988 \\ -3.0263 & 3.1920 & 3.8916 & -2.1680 & -2.2908 \end{bmatrix} [\text{m}^{-2}].$$

For this optimized values of quadrupole strengths, betatron tune is [74.9, 24.25]. After correction of betatron tune to [75.2, 24.2] with Q1 and Q2, the strength of Q1 changes from 2.1432 to 2.1627 and strength of Q2 changes from -2.3929 to 2.4044  $\text{m}^{-2}$ , i.e., a small increase in these two quadrupole strengths. Using these strengths, variation of different lattice functions

after betatron tune correction are shown in Fig.4.27, Fig.4.28 and Fig.4.29 and comparison of different lattice parameters are shown in Table.4.2

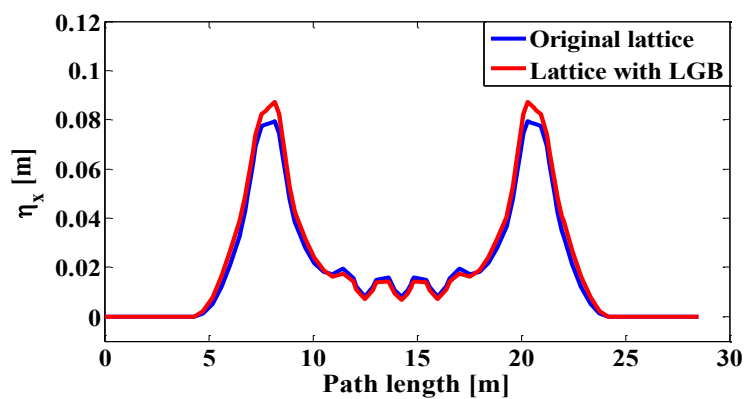


Fig. 4.27: Comparison of dispersion function.

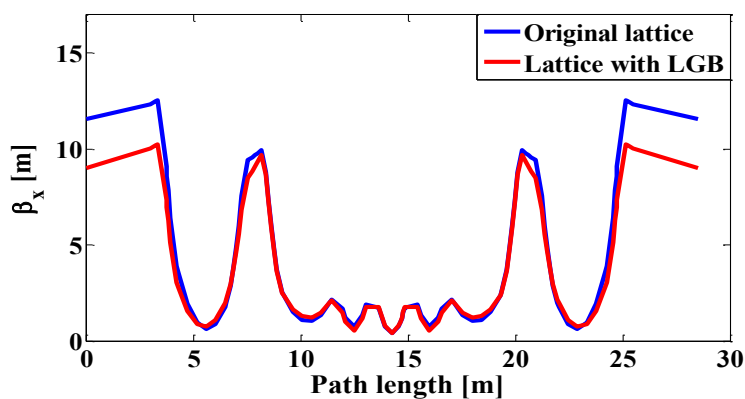


Fig. 4.28: Comparison of horizontal beta function.

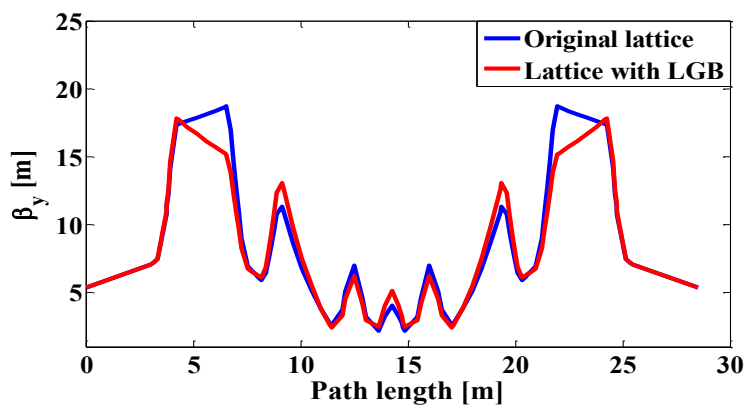


Fig. 4.29: Comparison of vertical beta function.

Though, these beta functions (lattice with LGB) are acceptable, but still there is a scope for further optimization.

Table 4.2: Comparison of Indus-3 lattice with LGB with original Indus-3 lattice.

S.No.	Parameters	Indus-3 (Original Lattice)	Indus-3 Lattice with LGB
1.	Energy (GeV)	6	6
2.	Momentum Compaction factor	$9.55 \times 10^{-5}$	$9.07 \times 10^{-5}$
3.	Emittance (nm-rad)	148.9	135.1
4.	Betatron tunes [ $\nu_x, \nu_y$ ]	[74.15 , 24.22]	[75.2 , 24.2]
5.	Natural chromaticity	[-109.15 -80.94]	[-102.52 -80.81]
6.	Energy Loss per turn (MeV)	2.46	2.57
7.	Beta function at injection [m]	[11.57 5.34]	[9.1 5.3]
8.	Max. Beta function [m]	[12.54 18.71]	[10.3 17.7]
9.	Beta function at symmetric point [m]	[0.38 4.03]	[ 0.44 5.19]
10.	Dispersion at sextupole location [m]	0.078	0.085
11.	Required sextupole strength for chromaticity correction [4, 4] [ $\text{m}^{-3}$ ]	[-89.5 118.79 -57.02]	[-90.95 118.53 -58.97]

Study of Indus-3 lattice with LGBs shows that emittance can be reduced by  $\sim 10\%$  without much affecting the lattice functions, betatron tune etc. Though natural chromaticity is reduced, but due to change in beta functions at sextupole location leads to a small increase in sextupole strength to correct the same level of chromaticity.

Though horizontal beta function is reduced at injection and sextupole strengths are increased a little bit, actual performance can only be predicted after dynamic aperture calculation which is given in the following Section.

### 4.3.2 Dynamic aperture

After correcting chromaticity to [4, 4] (horizontal and vertical) with sextupoles, dynamic aperture calculation is done by tracking of particles in the whole ring for 1000 turns. To calculate dynamic aperture, range of  $x$  is chosen from -15 mm to 15 mm in step size of 0.5 mm. On the other hand, range of  $y$  is chosen from 0 to 8 mm. The maximum range of  $x$  and  $y$  are chosen on the basis of physical aperture of vacuum chamber. Charged particle is tracked for 1000 turns in the grids and the boundary is decided on the basis of loss, i.e., after a certain point of the grid, charged particle is lost. In Fig.4.30, a comparison of dynamic aperture for Indus-3 lattice utilizing LGB dipoles and original Indus-3 lattice is shown. Nearly equal area is covered between both curves.

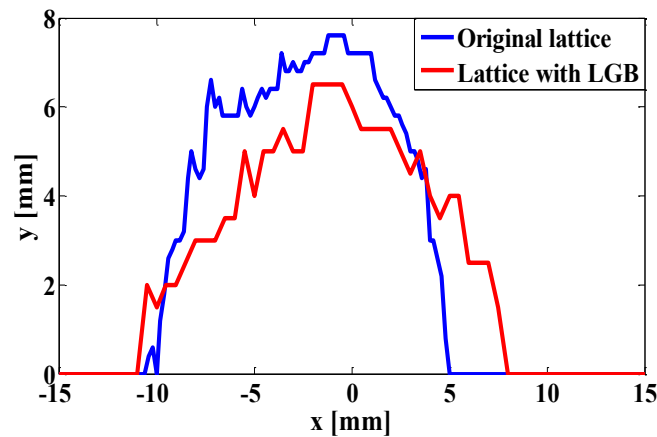


Fig. 4.30: Comparison of dynamic aperture for 1000 turns.

Though dynamic aperture is reduced a little in the vertical plane, but it is increased in the horizontal plane and this will help in off axis beam injection.

In this Chapter, Indus-2 and Indus-3 lattices which utilizes LGB dipole are optimized and different important parameters like betatron tune, lattice functions, chromaticity, dynamic aperture are analysed using single as well multi-objective techniques. The summary of this Chapter is given below.

For the case of Indus-2, using dipoles with LGB, emittance can be reduced  $\sim 33\%$  in the same ring with minimum hardware change if betatron tune is allowed to change by an integer and nearly  $25\%$  emittance reduced if same betatron tune is desired to nominal lattice. After introducing LGB brightness will increase by a factor of 2. As dispersion function at sextupole location increased from 0.7m to 0.8m, required sextupole strengths get reduced by  $16\%$  for focusing sextupole and  $13.8\%$  for defocusing sextupole for the same level of chromaticity correction, i.e., [2, 2].

For the case of Indus-3, using dipoles with LGBs, emittance can be reduced by  $\sim 10\%$  in the same circumference of the ring. Dynamic aperture area for on-momentum particles is almost the same as original lattice. Though a little decrease in vertical plane, but, there is an increase in horizontal direction which is required for off-beam injection (an advantage).

# Chapter 5

## Conclusion and future scope

Brightness of photon beam is one of the major aspect in designing or upgrading any SR source based on electron storage ring. An important beam parameter, called beam emittance, highly affects brightness of the photon beam and quality of beam, i.e., beam size. In order to increase brightness one has to improve beam emittance by some means. In recent years, advanced techniques like transverse gradient, longitudinal gradient bend (LGB), reverse or anti bend in a dipole have been studied and being used to improve the beam emittance. In this thesis work, an extensive study on optimization of LGB profiles has been presented. Further, new lattices have been designed by replacing homogeneous dipole of Indus-2 and Indus-3.

After discussing accelerator physics relevant to this thesis briefly, technologically challenging advanced methods (LGB and transverse gradient) to improve the beam emittance are discussed. In Chapter 2, the necessary numerical optimization techniques are described which are used to optimize a dipole with LGBs. In particular, single objective such as Nelder-Mead (a classical direct search method) and multi-objective optimization techniques such as genetic algorithm (GA) are discussed. Optimization studies of LGB profiles using dipole of Indus-2 are discussed in Chapter 3. Both techniques, i.e., Nelder-Mead and single objective genetic

algorithm have been used to generate different LGB profiles. New lattice for Indus-2 is designed by replacing homogeneous dipole with dipole with LGB. The introduction of LGB dipole changes the distribution of dispersion in the lattice due to unoptimized quadrupole strengths. Therefore, quadrupole strengths are optimized to match the lattice function and other important parameters. Using similar logic, dipole of Indus-3 is optimized for LGB profile and lattice functions and other important parameters are matched using all quadrupole families and quadrupole component in BM3 and BM4.

Beam emittance of Indus-2 reduced by  $\sim 30\%$  by introducing LGB in the dipole if betatron tune is allowed to change by integer and  $\sim 24\%$  with corrected betatron tune to nominal lattice. A study of Indus-2 in TME configuration is also carried out, which shows that emittance with LGB dipoles is reduced by less than half. Also, beam emittance of Indus-3 lattice reduced by  $\sim 10\%$  by introducing LGB in dipoles which shows major advantage of dipole with LGB over homogeneous dipole. In addition, LGB in dipole increases the dispersion at sextupole location, which decreases the sextupole strengths to correct the same level of chromaticity as of nominal lattice.

In this thesis, the studies of beam emittance reduction and optimization of lattice performance are presented in ideal case with LGBs. To model the LGB, we have considered the hard edge model, where fringing fields are ignored. In addition, for realistic magnetic lattice, error and analysis also need to be performed. In electron storage rings, the real advantage of LGB will be when we use anti-bends (dipoles with negative bending angles) [12]. This combination help decouple the distribution of beta and dispersion function. These studies will be carried out in future.

# Appendix A

## Derivations

### A.1 Equation of motion of an electron in a moving coordinate system

Equation of motion of a electron in a given magnetic field, in moving coordinate system can be written using Lorentz force law as

$$\frac{d\vec{P}}{dt} = e\vec{v} \times \vec{B}. \quad (\text{A.1})$$

Considering no magnetic field component in the longitudinal direction, i.e.,

$$\vec{B} = (B_x, B_y, 0).$$

Using this magnetic field and velocity  $\vec{v} = (v_x, v_y, v_s)$ ,

$$\vec{v} \times \vec{B} = -v_s B_y \hat{x} + v_s B_x \hat{y} + (v_x B_y - v_y B_x) \hat{s}.$$

Ignoring radiation generated by electron eq.(A.1) can be written as

$$\frac{d\vec{P}}{dt} = \gamma m_0 \frac{d^2 \vec{R}}{dt^2}. \quad (\text{A.2})$$

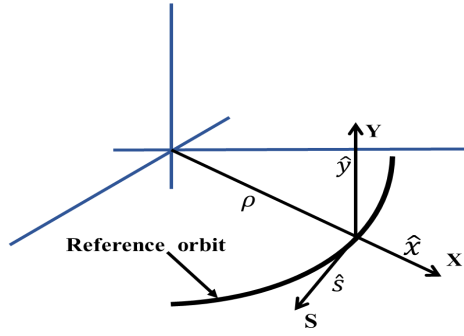


Fig. A.1: Frenet-Serret coordinate system.  $\hat{x}$ ,  $\hat{y}$  and  $\hat{s}$  are unit vectors in horizontal, vertical and longitudinal direction respectively.

Energy of the electron is constant, therefore  $\gamma$  will be a constant and  $m_0$  (a constant) is the rest mass energy of electron. Hence equation of motion becomes

$$\vec{R} = e\vec{v} \times \vec{B}.$$

$\vec{R}$  can be written as

$$\vec{R} = r\hat{x} + y\hat{y} \tag{A.3}$$

$$\vec{R} = \dot{r}\hat{x} + r\dot{\hat{x}} + \dot{y}\hat{y}. \tag{A.4}$$

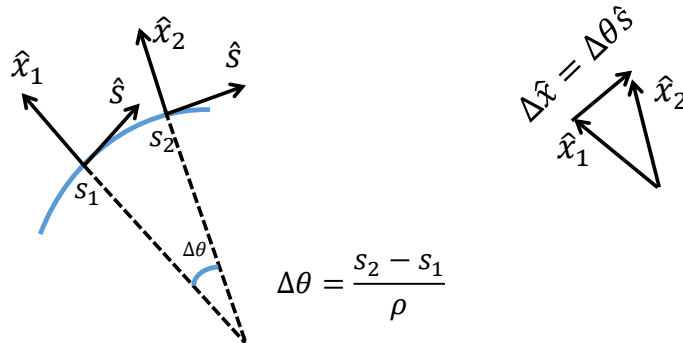


Fig. A.2: Change in unit vector in horizontal direction.

If, there is any motion in the s-direction, the unit vector  $\hat{x}$  will have a derivative, i.e.,  $\dot{\hat{x}}$ .

From Fig A.2, it can be seen that

$$\dot{\hat{x}} = \dot{\theta}\hat{s}, \quad (\text{A.5})$$

where  $\dot{\theta} = \frac{v_s}{r}$ . Therefore,

$$\dot{\vec{R}} = \dot{r}\hat{x} + r\dot{\theta}\hat{s} + \dot{y}\hat{y}, \quad (\text{A.6})$$

and differentiating one more time

$$\ddot{\vec{R}} = \ddot{r}\hat{x} + (2\dot{r}\dot{\theta} + r\ddot{\theta})\hat{s} + \ddot{y}\hat{y}. \quad (\text{A.7})$$

Using same argument as used to obtain  $\dot{\hat{x}}$ , we have

$$\dot{\hat{s}} = -\dot{\theta}\hat{x}, \quad (\text{A.8})$$

Therefore,

$$\ddot{\vec{R}} = (\ddot{r} - r\dot{\theta}^2)\hat{x} + (2\dot{r}\dot{\theta} + r\ddot{\theta})\hat{s} + \ddot{y}\hat{y}. \quad (\text{A.9})$$

Thus, equation of motion in the x-direction is

$$\ddot{r} - r\dot{\theta}^2 = -\frac{ev_s B_y}{\gamma m_0} = -\frac{ev_s^2 B_y}{\gamma m_0 v_s}. \quad (\text{A.10})$$

Since  $v_x \ll v_s$  and  $v_y \ll v_s$ , to a very good approximation, the total momentum  $p$  of the particle is  $\gamma m_0 v_s$ . So,

$$\ddot{r} - r\dot{\theta}^2 = -\frac{ev_s^2 B_y}{p}. \quad (\text{A.11})$$

Changing independent variable  $t$  to  $s$ , the derivative becomes

$$\frac{d}{dt} = \frac{ds}{dt} \frac{d}{ds}, \quad (\text{A.12})$$

Since,

$$ds = \rho d\theta = v_s dt \frac{\rho}{r}. \quad (\text{A.13})$$

Hence, assuming  $\frac{d^2 s}{dt^2} = 0$ ,

$$\frac{d^2}{dt^2} = \left(\frac{ds}{dt}\right) \frac{d^2}{ds^2} = \left(v_s \frac{\rho}{r}\right)^2 \frac{d^2}{ds^2}. \quad (\text{A.14})$$

Replacing  $r$  with  $\rho + x$ , the equation of motion becomes

$$\frac{d^2x}{ds^2} - \frac{\rho + x}{\rho^2} = -\frac{B_y}{B\rho} \left(1 + \frac{x}{\rho}\right)^2, \quad (\text{A.15})$$

where  $B\rho = \frac{p}{e}$ . A similar treatment yields for the equation of motion in the y-direction

$$\frac{d^2y}{ds^2} = \frac{B_x}{B\rho} \left(1 + \frac{x}{\rho}\right)^2. \quad (\text{A.16})$$

In general, these equations are non-linear. One can study these equation for linear case and non-linear terms can be treated as perturbation to these equations.

## A.2 Closed form solution

General equation of motion is given by

$$u'' + K(s)u = 0. \quad (\text{A.17})$$

This is the equation of harmonic oscillator with variable spring constant, i.e.,  $K = f(s)$ .

Though, spring constant is a function of independent variable  $s$ , for circular accelerators,  $K$  is periodic, i.e., there is a distance  $C$  such that

$$K(s + C) = K(s). \quad (\text{A.18})$$

The repeated distance of the hardware,  $C$ , may be as large as circumference of a synchrotron or it may be less. The general solution of equation of motion is given by

$$u(s) = A\sqrt{\beta(s)}\cos[\psi(s) + \delta], \quad (\text{A.19})$$

where  $A$  and  $\delta$  are the two constants of integration reflecting from initial conditions, and  $\beta(s)$  is also be a periodic function with periodicity  $C$ . Here, a similarity with harmonic oscillator can be noticed, when  $K$  becomes periodic function of position, the solution will differ from the

simple harmonic oscillator problem by a factor representing a spatially varying amplitude and a phase, which does not develop linearly with  $s$ .  $\beta(s)$  and  $\psi(s)$  can be found by substituting general solution into the differential equation. Differentiating  $u$  with respect to  $s$

$$u' = A \frac{\beta'}{2\sqrt{\beta}} \cos(\psi + \delta) - A\sqrt{\beta} \sin(\psi + \delta) \psi' \quad (\text{A.20})$$

and

$$u'' = A \frac{\beta\beta'' - \frac{1}{2}\beta'^2}{2\beta^{3/2}} \cos(\psi + \delta) - A \frac{\beta'}{\sqrt{\beta}} \sin(\psi + \delta) \psi' - A\sqrt{\beta} \sin(\psi + \delta) \psi'' - A\sqrt{\beta} \cos(\psi) \psi'^2. \quad (\text{A.21})$$

Inserting in eq.(A.17), we get

$$A \left[ \frac{\beta\beta'' - \frac{1}{2}\beta'^2}{2\beta^{3/2}} - \sqrt{\beta} \psi'^2 + K\sqrt{\beta} \right] \cos(\psi + \delta) - A \left[ \frac{\beta'}{\sqrt{\beta}} \psi' + \sqrt{\beta} \psi'' + \sqrt{\beta} \psi' \right] \sin(\psi + \delta) = 0. \quad (\text{A.22})$$

Since, it required that  $\beta$  and  $\psi$  are to be independent of  $\delta$ . So, coefficients of sine and cosine terms must vanish separately. Equating coefficient of sine term equal to 0, it gives

$$\beta\psi'' + \beta\psi' + \beta'\psi' = 0 \quad \text{or} \quad (\beta\psi')' = 0, \quad (\text{A.23})$$

eq.(A.23) can be solved further as

$$\psi' = \frac{Const.}{\beta(s)}, \quad (\text{A.24})$$

Where  $c$  is an arbitrary constant of integration. This arbitrary constant can be chosen as 1 for convenience.

$$\frac{1}{2}(\beta\beta'' - \frac{1}{2}\beta'^2) - \beta^2\psi'^2 + \beta^2K = 0 \quad (\text{A.25})$$

Using this relationship between  $\beta(s)$  and  $\psi$ , A.25 becomes

$$\frac{1}{2}\beta\beta' - \frac{1}{4}\beta'^2 + \beta^2K = 1. \quad (\text{A.26})$$

With the introduction of Courant-Snyder variables

$$\alpha = -\frac{1}{2}\beta' \quad \text{and} \quad \gamma = \frac{1 + \alpha^2}{\beta}, \quad (\text{A.27})$$

we can write eq.(A.25)

$$\beta'' + 2K\beta - 2\gamma = 0 \quad (\text{A.28})$$

Strictly speaking,  $\beta(s)$  need not be periodic; it only has to be a solution of the eq.(A.25). But if the motion we are trying to describe is that of a particle travelling through a periodic section of a accelerator, for instance through thousands of revolution about a circular accelerator, it is much more useful to choose the unique periodic solution for  $\beta(s)$ .

Using eq.(A.24), phase difference from a point  $s_0$  to  $s$  is given by

$$\psi = \int_{s_0}^s \frac{1}{\beta(s)} ds. \quad (\text{A.29})$$

For a complete ring, phase difference is given by

$$\mu = \psi_{ring} = \oint \frac{1}{\beta(s)} ds. \quad (\text{A.30})$$

We define betatron tune as

$$\nu = \frac{\mu}{2\pi} = \frac{1}{2\pi} \oint \frac{1}{\beta(s)} ds. \quad (\text{A.31})$$

Betatron tune tell us how many oscillation makes a charged particle in one revolution.

### A.3 Energy Loss

A relativistic electron when accelerated in a macroscopic force field will radiate electromagnetic energy. The rate of emission is proportional to the square of the accelerating force and depends on the angle between the force and the electrons velocity and is larger by the factor

$\gamma^2 = \left(\frac{E}{m_0 c^2}\right)^2$  when the force is perpendicular to the velocity than when the force is parallel to the velocity. In a circular accelerator, the typical longitudinal forces (from the accelerating system) are much smaller than the typical transverse magnetic forces. Therefore, radiation effects that accompany by the magnetic forces are needed to consider only. The rate of loss of energy,  $P_\gamma$  by radiation can be written as

$$P_\gamma = \frac{2}{3} \frac{r_e c}{(m_0 c^2)^3} E^2 F_\perp^2, \quad (\text{A.32})$$

where  $m_0, r_e$  are rest mass and classical electron radius of the electron respectively.  $F_\perp$  is the magnetic force on the electron. It is convenient to define a constant

$$C_\gamma = \frac{4\pi}{3} \frac{r_e c}{(m_0 c^2)^3} \quad (\text{A.33})$$

For electron  $C_\gamma = 8.85 \times 10^{-5} [m.GeV^{-3}]$ . Since  $F_\perp = ecB$ , the radiated power is given by

$$P_\gamma = \frac{e^2 c^3}{2\pi} C_\gamma E^2 B^2. \quad (\text{A.34})$$

This shows that instantaneous power is proportional to the square of both the energy and the local magnetic field strength. It is sometimes useful to express the magnetic force in terms of the local radius of curvature  $\rho$  of the trajectory; then

$$P_\gamma = \frac{c C_\gamma E^4}{2\pi \rho^2} \quad (\text{A.35})$$

An electron circulating on the design orbit has the nominal energy  $E_0$  and moves on the radius  $\rho = \frac{1}{G}$ . To find the energy  $U_0$  radiated in one revolution, we must integrate  $P_\gamma$  with respect to time once around the ring. Since  $dt = \frac{ds}{c}$

$$U_0 = \frac{C_\gamma E_0^4}{2\pi} \oint G^2(s) ds. \quad (\text{A.36})$$

We may write the integral as the mean of  $G^2$  multiplied by  $L = 2\pi R$ , the distance around the ring;

$$U_0 = C_\gamma^4 R \langle G \rangle. \quad (\text{A.37})$$

For an isomagnetic guide field  $G = G_0 = \frac{1}{\rho_0}$  along the curved path of the length  $2\pi\rho_0$  and zero everywhere. So,

$$\langle G^2 \rangle = \frac{G_0}{R} = \frac{1}{R\rho_0} \quad (\text{A.38})$$

and

$$U_0 = \frac{C_\gamma E_0^4}{\rho_0}. \quad (\text{A.39})$$

For a fixed radius, the energy radiated per turn varies as the fourth power of the electron energy.

# References

- [1] J. P. Blewett, Synchrotron radiation-1873 to 1947, Nuclear Instruments and methods in Physical Research A266, 1988.
- [2] H. Wiedemann, Particle Accelerator Physics, Third Edition, Spinger, 2007.
- [3] D. D. Bhawalkar, G. Singh, R. V. Nandedkar, Synchrotron radiation sources INDUS-1 and INDUS-2, Pramana-journal of physics, Vol. 50, No. 6, 1998.
- [4] Technical report of Synchrotron radiation source Indus-2, Center for Advanced Technology, Indore, India (1998).
- [5] R. Husain, Optimization and modelling of storage ring lattices: A case study of Indus-2 storage ring (PhD thesis), 2018.
- [6] T. Pulampong, Ultra low Emittance Lattice Design for Advanced Synchrotron Light Sources (PhD thesis), 2015.
- [7] L. Dallin, W. Wurtz, Towards a 4<sup>th</sup> generation storage ring at the Canadian Light Source, AIP Conference Proceedings, 2016.
- [8] S.C. Leemann, W.A. Wurtz, Pushing the MAX IV 3 GeV storage ring brightness and coherence towards the limit of its magnetic lattice, IPAC2017.

- [9] Chun-xi Wang, Minimum emittance in storage rings with uniform or nonuniform dipoles, PHYSICAL REVIEW SPECIAL TOPICS - ACCELERATORS AND BEAMS, USA, 2009.
- [10] J. Guo, T. Raubenheimer, Low emittance  $e^-/e^+$  storage ring design using bending magnets with longitudinal gradient, Proceedings of EPAC 2002, Paris, France.
- [11] A. Streun, A. Wrulich, Compact low emittance light sources based on longitudinal gradient bending magnets, Nuclear Instruments and Methods in Physics Research Section A, Vol. 770, pages 98-112, 2015.
- [12] A. Streun, The anti-bend cell for ultralow emittance storage ring lattices, Nuclear Instruments and Methods in Physics Research Section A, 2013.
- [13] Detailed Design Report on the MAX IV facility, *https://www.maxiv.lu.se/accelerators-beamlines/accelerators/accelerator-documentation/max-iv-ddr*.
- [14] J. L. Laclare, in Proceedings of Particle Accelerator Conference, Washington, DC, USA, 1427(1993).
- [15] M. Hara, Nucl. Instrum. Methods in Phys. Res. A 448, 12 (2000).
- [16] R.E. Gerig, J.M.Gibson, D.M.Mills, et al., Nucl. Instrum. Methods in Phys. Res. A 649, 1 (2011).
- [17] A. Jackson, in Proceedings of the Particle Accelerator Conference 1993, 1432(1993).

- [18] C. J. Bocchetta, D. Bulfone, F. Daclon, et al., in Proceedings of the European Particle Accelerator Conference 1994, 579 (1994)
- [19] CERN Proceedings, Vol-1, 1994.
- [20] S. Y. Lee, Accelerator Physics, Second Edition, World Scientific, 2007.
- [21] J. D. Jackson, Classical Electrodynamics, Third Edition, Wiley, 2017.
- [22] A. Wolski, Beam Dynamics in high energy particles accelerators, Imperial Collage Press, 2014.
- [23] M. Sands, The physics of electron storage rings an introduction, SLAC-121, 1970.
- [24] A. Streun, Practical Guidelines for Lattice Design, PSI, 1999.
- [25] K. Deb, Multi-Objective Using Evolutionary Algorithms, Wiley, 2018.
- [26] Michael Baudi, Nelder-Mead User's Manual, April 2010.
- [27] J. C. Lagarias, J. A. Reeds, M. H. Wright, and P. E. Wright, Convergence properties if the Nelder-Mead simplex method in low dimensions, SIAM J. OPTIM., Vol. 9, No. 1, pp. 112-147, 1998.
- [28] [http : //www.scholarpedia.org/article/Nelder – Mead – algorithm.](http://www.scholarpedia.org/article/Nelder-Mead-algorithm)
- [29] S. Kirkpatrick, C. D. Gelatt, M. P. Vecchi, Science, New Series, 220 (4598), 671(1983).
- [30] J. Kennedy, R. Eberhart, in Proceedings of the fourth IEEE International Conference on Neural Networks, Perth, Australia (1995).

- [31] S. Das, A. Abraham, A. Konar, Studies in Computational Intelligence (SCI) 116, 1(2008).
- [32] R. Storn, K. Price, Journal of Global Optimization 11, 341(1997).
- [33] A. Terebilo, Accelerator Tool Box for MATLAB, SLAC-PUB-8732, 2001.
- [34] Gaël Le Bec, Joel Chavanne, François Villar, Chamseddine Benabderrahmane, Simone Liuzzo, Jean-François Bouteille, Loys Goirand, Laurent Farvacque, Jean-Claude Biasci, and Pantaleo Raimondi, Magnets for the ESRF Diffraction-Limited Light Source Project, IEEE Transactions on applied superconductivity, VOL. 26, NO. 4, 2016.
- [35] T. Zhang, X. Huang, Numerical optimization of a low emittance lattice cell, Nuclear Instruments and Methods in Physics Research Section A, Volume 923, Pages 55-63, 2019.
- [36] D. A. Edwards, M. J. Syphers, An introduction to the physics of high energy accelerators, Wiley, 2004.
- [37] M. Aiba, M. Böge, M. Ehrlichman, A. Streun, Magnetic field of longitudinal gradient bend, Nuclear Inst. and Methods in Physics Research, A (892) 2018.

# Contents

<b>Synopsis</b>	<b>v</b>
<b>List of Figures</b>	<b>viii</b>
<b>List of Tables</b>	<b>xv</b>
<b>1 Basic Accelerator Physics</b>	<b>1</b>
1.1 Synchrotron radiation sources . . . . .	2
1.2 Coordinate system used in circular accelerators . . . . .	5
1.3 Motion of a charged particle in an electromagnetic field . . . . .	6
1.4 Basic magnetic elements used in accelerators . . . . .	8
1.4.1 Dipole magnets . . . . .	8
1.4.2 Quadrupole . . . . .	9
1.4.3 Sextupole . . . . .	11
1.5 Equation of motion of a charged particle in a given magnetic field . . . . .	12
1.5.1 Transfer matrix for a drift space . . . . .	15
1.5.2 Transfer matrix for a quadrupole . . . . .	16
1.5.3 Transfer matrix for a dipole . . . . .	17

1.6	Dispersion and trajectory of an off-momentum particle . . . . .	19
1.7	Parametric solution of equation of motion and Courant- -Snyder parameters . . . . .	21
1.8	Beam dynamics in terms of Courant-Snyder variables . . . . .	25
1.9	Betatron tune . . . . .	28
1.10	Chromaticity . . . . .	29
1.11	Momentum compaction factor . . . . .	31
1.12	Effect of synchrotron radiation on electron beam in the storage ring . . . . .	32
1.13	Different types of magnetic lattices and equilibrium emittance . . . . .	38
1.13.1	Theoretical minimum emittance (TME) lattice . . . . .	39
1.13.2	Double bend achromat (DBA)lattice . . . . .	41
1.13.3	Multi bend achromat (MBA) lattice . . . . .	42
1.14	RMS beam sizes . . . . .	43
1.15	Advance methods to improve beam emittance . . . . .	43
1.16	Indus-2 storage ring lattice . . . . .	46
1.17	Indus-3 storage ring lattice . . . . .	49
<b>2</b>	<b>Optimization techniques used in accelerators</b>	<b>53</b>
2.1	Single objective optimization problem . . . . .	54
2.1.1	Nelder-Mead method . . . . .	55
2.2	Multi-objective optimization . . . . .	60
2.3	Classical methods for multi-objective optimization problems (MOOP) . . . . .	61
2.4	Evolutionary algorithm for optimization problems . . . . .	63

2.4.1	Genetic algorithm . . . . .	64
2.4.2	Multi-objective genetic algorithm . . . . .	67
<b>3</b>	<b>Optimization of longitudinal gradient bend profiles in dipole magnet</b>	<b>70</b>
3.1	LGB profiles in dipoles for achromatic and TME lattices . . . . .	70
3.2	Objective function to generate LGB profiles . . . . .	74
3.3	Optimization of LGB profiles in dipole for achromat lattice . . . . .	75
3.3.1	Optimization using Nelder-Mead algorithm . . . . .	77
3.3.2	Optimization using genetic algorithm . . . . .	79
3.4	Optimization of LGB profiles in dipole for TME lattices . . . . .	90
<b>4</b>	<b>Indus-2 and Indus-3 storage ring lattice performance with LGBs</b>	<b>95</b>
4.1	DBA lattice of Indus-2 with LGBs . . . . .	96
4.1.1	Optimization of lattice function with LGBs . . . . .	97
4.1.2	Dynamic aperture . . . . .	104
4.2	Comparative study of beam emittance with and without LGBs . . . . .	106
4.3	MBA lattice of Indus-3 with LGBs . . . . .	108
4.3.1	Matching of lattice function with quadrupoles . . . . .	110
4.3.2	Dynamic aperture . . . . .	116
<b>5</b>	<b>Conclusion and future scope</b>	<b>118</b>
	<b>Appendix</b>	<b>120</b>
<b>A</b>	<b>Derivations</b>	<b>120</b>
A.1	Equation of motion of an electron in a moving coordinate system . . . . .	120
A.2	Closed form solution . . . . .	123

A.3 Energy Loss . . . . . 125

**References** . . . . . **128**

# Synopsis

Synchrotron light sources, based on an electron storage ring have many characteristic advantages over conventional x-ray sources such as wide energy range, higher flux, high brightness etc. The high brightness of synchrotron radiation from electron storage ring is the result of high quality of stored electron beam in the storage ring. The quality of electron beam is represented by an important figure of merit of the electron storage ring called beam emittance. The magnetic lattice of the storage ring controls the beam and the brightness of photon beam is inversely proportional to the product of two transverse beam emittances of electron beam. Beam emittance signifies how well collimated and divergent the electron beam is. Smaller its value brighter is the emitted synchrotron radiation. Thus, in storage ring lattice design, one of the important criteria for increasing the brightness is to minimize the beam emittance. The beam emittance at fixed electron energy has a cubic dependence on the bending angle. Therefore, to reduce the beam emittance, bending magnets in large numbers are required in given circumference of the storage ring.

In last few decades, several methods have been evolved to improve the beam emittance. Now a days, an innovative method using multi bend achromat (MBA) instead of double or triple bend achromat is being considered and studied, which leads to ultra low emittance. Using MBA lattice, few hundreds of pm.rad beam emittance can be achieved which leads to brightness of the photon beam of the order of  $10^{20}$  to  $10^{22}$  *photons per second per unit area per unit solid*

*angle in 0.1% bandwidth of considered wavelength* with fully loaded insertion devices. MAX IV, a 3 GeV electron storage ring, is an example of this kind of machine, which uses seven bend achromat lattice.

In order to improve beam emittance further, other technologically challenging techniques like transverse gradient, longitudinal gradient bend (LGB), introduction of anti or reverse bend in dipoles of the lattice are being used to get more aggressive design of new synchrotron radiation sources and upgrade existing/running facility to facilitate users with ever increasing brightness. Beam emittance reduction is desirable, however for successful operation of the facility, various other lattice parameters need to be optimized or constrained. For example, betatron tunes should be far away from dangerous resonances, horizontal beta function should be large at injection point and large value of dispersion is desirable at sextupole locations for effective chromaticity correction etc. These aspects make lattice design of a storage ring a complex optimization problem. In order to handle such complex optimization problem, one has to use available numerical optimization techniques.

In this thesis, extensive optimization studies to minimize the beam emittance in an electron storage ring using LGBs are discussed. We have optimized the magnetic field profile along the beam direction in a dipole magnet in general and for dipole magnet of Indus-2 storage ring, in particular. Detailed comparative studies of a storage ring lattice cell utilizing LGB and constant field dipoles are presented and merits and demerits are highlighted. The studies indicate that the beam emittance of a storage ring is much lower with dipoles utilizing LGB compared to dipoles with constant field. In addition, LGB also helps in shaping lattice parameters at sextupole location to correct chromaticity with reduced strength of sextupoles. Maintaining same circumference of the Indus-2 storage ring and matching other lattice parameters with quadrupole magnets, beam emittance can be reduced to  $\sim 40$  nm.rad with LGB compar-

ed to 58 nm.rad with constant field dipole. The studies are extended to minimize the beam emittance of baseline lattice of Indus-3, a 6 GeV electron storage ring with beam emittance 150 pm.rad. Satisfying the operational constraints, the beam emittance can further be reduced to  $\sim 135$  pm.rad by replacing four dipoles out of seven with LGBs.

This whole thesis is organized in the following way. In the first Chapter, basic physics of circular accelerators and some important parameters, such as Courant-Snyder variables, dispersion, betatron tune, chromaticity, emittance etc., are discussed, which are important in view of lattice design of a storage ring. In addition, some of the advanced techniques to reduce the beam emittance are also discussed in this Chapter. Lattice design of a storage ring and its analysis is a complex optimization problem. Different types of optimization techniques, which are capable to handle these complex optimization problem, are introduced in Chapter 2. In Chapter 3, extensive studies on optimization of LGB profiles in a dipole taking emittance and synchrotron radiation loss in consideration have been discussed. These optimization studies of LGB profiles then applied to Indus-2 storage ring lattice. The application of LGB profile changes the distribution of dispersion function which needs to be matched with original lattice. Therefore, optimization of quadrupole strengths with LGBs are carried out and important parameters are compared with original lattice of Indus-2 storage ring. Further, this study is extended to the base line design of Indus-3. These studies are presented in Chapter 4. In the last Chapter, conclusion and future scope of this thesis work has been discussed.

# List of Figures

1.1	Coordinate system used in a circular accelerators. . . . .	6
1.2	(a) Sector (black) and Rectangular (parallel edges with red color) type dipoles. (b) Vertical magnetic field along x-direction. . . . .	8
1.3	(a) Pole faces and field direction in a quadrupole magnet. A positive charged particle coming out of the page will experience a focusing force in x direction and a defocusing force in y direction. (b) Variation of vertical magnetic field along x-direction. . . . .	10
1.4	(a) Pole faces and field direction in a sextupole magnet. Force on a positively charge particle on the x axis and coming out side of the page is shown by arrow. (b) Variation of vertical magnetic field along x-direction. . . . .	12
1.5	Position and slope (with respect to longitudinal direction) of the charged particle before and after traversing the magnetic element. . . . .	15
1.6	Position and slope (with respect to longitudinal direction) of the charged particle after passing through a drift space. . . . .	16
1.7	Particle position (with respect to longitudinal direction) after passing through a focusing quadrupole. O is the centre of the quadrupole and F is focal point. . .	17

1.8	An example of arrangement of different magnetic elements. Elements 1, 3, 5, 7, 9, 11 are drift spaces. Elements 2 and 12 are focusing quadrupole, 4 and 8 are defocusing quadrupole. Elements 6 and 10 are dipole magnets. . . . .	19
1.9	Motion of different energy particles in a sector type dipole magnet. . . . .	19
1.10	Emittance as a phase space area for a single particle. Maximum position and maximum slope are also shown. . . . .	24
1.11	Position and slope of a particle after passing through a magnetic element. $(\beta_0, \alpha_0, \gamma_0)'$ and $(\beta, \alpha, \gamma)'$ are CS variables at entrance and exit of the magnetic element. . . . .	25
1.12	CS variables at the entrance and exit of the magnetic element. . . . .	27
1.13	Tune diagram for fractional betatron tune up to fourth order resonance. . . . .	28
1.14	Radiation damping phenomenon in horizontal plane. $p_x$ and $p_s$ are the momentum of electron in horizontal and longitudinal direction respectively. $p_{RF}$ is the momentum provided by RF cavity. $x'_0$ is the initial slope of electron and $x'_1$ is the slope of electron after passing through RF cavity. . . . .	33
1.15	Quantum Excitation phenomenon. . . . .	36
1.16	Variation of horizontal beta and dispersion function in case TME lattice. Both functions have minima at the centre of the bending magnet. . . . .	40
1.17	Variation of horizontal beta and dispersion function in the first dipole of DBA lattice. Dispersion and its derivative are zero at the entrance of the dipole. . . .	42
1.18	(a) Linear variation of magnetic field along x-direction (black) and compared with homogeneous field (blue). (b) Shape of dipole to get linearly decreasing magnetic field. . . . .	44
1.19	Variation of longitudinal field profile in the dipole magnet of a DBA lattice . . .	45

1.20	Variation of longitudinal field profile in the dipole of TME lattice . . . . .	46
1.21	Schematic layout of Indus Accelerator complex [3,5]. . . . .	47
1.22	Variation of beta and dispersion functions in Indus-2 unit lattice cell. Bending magnets are shown by green boxes, quadrupoles are in red and blue boxes and sextupoles are in yellow and black boxes. . . . .	48
1.23	Beta Functions of Indus-3 lattice cell. Boxes in red colour are dipole magnet, boxes in green colour are quadrupoles and boxes in blue colour are sextupole magnets. . . . .	50
2.1	Reflection (left) and expansion (right) of Nelder-Mead simplex. . . . .	59
2.2	Outside contraction (left), inside contraction (middle) and shrink (right) of Nelder-Mead simplex. . . . .	59
2.3	Various steps involved in Genetic Algorithm. . . . .	65
2.4	NSGA-II procedure for one iteration [25]. . . . .	68
3.1	Variation of dispersion function in DBA lattice. The green rectangular boxes are homogeneous dipoles, blue rectangular boxes are focusing quadrupoles, red rectangular boxes are defocusing quadrupoles, yellow ones are focusing sextupoles and the black ones are defocusing sextupoles. . . . .	71
3.2	Variation of dispersion function in TME lattice. Dispersion function is symmetric in the dipole and minima occurs at the center of the dipole. Two quadrupoles, one focusing (blue) and other defocusing (red), at both side of the dipole are used to control the lattice functions. . . . .	71
3.3	Breaking of a homogeneous dipole (left) into $n$ dipoles (right). The dipole (left) has parameters, length (L), magnetic field (B), bending angle ( $\theta$ ), local bending radius ( $\rho$ ). Same parameters can be defined for each section of dipole (right). . . . .	72

3.4	Variation of longitudinal field profile in the dipole magnet (DBA). (b) Comparison of Horizontal dispersion function for LGB dipole (solid curve) with homogeneous dipole (dashed curve). . . . .	73
3.5	(a) Variation of longitudinal field profile in the dipole magnet (TME). (b) Comparison of Horizontal dispersion function for LGB dipole (solid curve) with homogeneous dipole (dashed curve). . . . .	74
3.6	Values of CS variables at points A, B, ..., E, which are entrance of each dipole section and F is the exit of last section. . . . .	76
3.7	Variation of $\Delta\theta$ with successive simulation run. . . . .	77
3.8	LGB profiles after each simulation run using Nelder-Mead algorithm. . . . .	78
3.9	Variation of objective function after 8th simulation run. . . . .	78
3.10	Variation of $\rho$ after final simulation run. . . . .	78
3.11	Variation of dispersion function in the dipole. . . . .	78
3.12	Variation of objective function in different generations. Best fitness shows the value of objective function at current generation and maximum constraint shows how constraints are more satisfied in each generation. . . . .	81
3.13	Variation of magnetic field and $\rho$ . For homogeneous dipole magnetic field and $\rho$ are 1.503 Tesla and 5.55 m respectively. . . . .	81
3.14	Variation of dispersion function in the dipole. . . . .	81
3.15	Variation of objective function in each generation for the case where no initial guess is provided. . . . .	82
3.16	Variation of magnetic field and $\rho$ . For homogeneous dipole magnetic field and $\rho$ are 1.503 Tesla and 5.55 m respectively. . . . .	83
3.17	Variation of dispersion function in the dipole. . . . .	83

3.18	Different LGB profiles generated by genetic algorithm. . . . .	84
3.19	Emittance for different LGB profiles with objective function and SR loss (color bar). . . . .	84
3.20	Different LGB profiles using GA with maximum magnetic field in the first section 2.65 Tesla. . . . .	85
3.21	LGB profile for the 10 section case with hard constraint on maximum magnetic field. . . . .	86
3.22	LGB profile for the 15 section case with hard constraint on total magnetic field.	87
3.23	Pareto optimal front between first and second objective. SR loss is given by color at each point of Pareto optimal front. . . . .	89
3.24	Different LGB profiles for A, B and C. . . . .	89
3.25	Different magnetic elements of Indus-2 lattice in TME configuration. . . . .	90
3.26	Variation of different lattice functions. . . . .	91
3.27	LGB profiles for different chosen maximum magnetic field. . . . .	92
3.28	Comparison of lattice functions with and without LGB. . . . .	93
4.1	Basic elements in Indus-2 unit lattice (not to scale). Here, QF: focusing quadrupole, QD: defocusing quadrupole, SF: focusing sextupole, SD: defocusing quadrupole. Number indicates family of that element, e.g. Q1D shows first family of defocusing quadrupoles. . . . .	97
4.2	Variation of beta and dispersion functions in Indus-2 unit lattice. . . . .	97
4.3	LGB profile compared with homogeneous dipole field in the dipole magnet. . .	98
4.4	Variation of dispersion function with LGB. . . . .	98
4.5	Variation of horizontal beta function with LGB. . . . .	99
4.6	Variation of vertical beta function with LGB. . . . .	99

4.7	Variation of objective function. . . . .	101
4.8	Variation of dispersion function with LGB and matching. . . . .	101
4.9	Variation of horizontal beta function with LGB and matching. . . . .	101
4.10	Variation of vertical beta function with LGB and matching. . . . .	101
4.11	Variation of horizontal beta function with LGB, matching, and betatron tune correction. . . . .	104
4.12	Variation of vertical beta function with LGB, matching and betatron tune correction.	104
4.13	Dynamic aperture comparison for on momentum charged particles. . . . .	105
4.14	Comparison of Pareto optimal front. . . . .	107
4.15	Comparison of beta functions at injection for each solution. . . . .	108
4.16	Maximum beta functions comparison for each solution. . . . .	108
4.17	Betatron tune comparison for each solution. . . . .	108
4.18	Natural chromaticity comparison for each solution. . . . .	108
4.19	Different magnetic elements of Indus-3 lattice (not to scale). Magnetic elements which are above base line are focusing in nature and below the base line are defocusing in nature. . . . .	109
4.20	Designed lattice functions of Indus-3 lattice. . . . .	109
4.21	Optimized LGB profile. . . . .	110
4.22	Pareto optimal front for emittance with dispersion at straight section. . . . .	112
4.23	Horizontal and vertical beta functions comparison for each solution. . . . .	112
4.24	Maximum horizontal and vertical beta functions comparison for each solution. . . . .	112
4.25	Horizontal and vertical betatron tune comparison for each solution. . . . .	113
4.26	Horizontal and vertical natural chromaticity comparison for each solution. . . . .	113
4.27	Comparison of dispersion function. . . . .	114

4.28	Comparison of horizontal beta function. . . . .	114
4.29	Comparison of vertical beta function. . . . .	114
4.30	Comparison of dynamic aperture for 1000 turns. . . . .	116
A.1	Frenet-Serret coordinate system. $\hat{x}$ , $\hat{y}$ and $\hat{s}$ are unit vectors in horizontal, vertical and longitudinal direction respectively. . . . .	121
A.2	Change in unit vector in horizontal direction. . . . .	121

# List of Tables

1.1	Important mathematical relations [2,22]	37
1.2	Different design parameters of Indus-2 storage ring	47
1.3	Different magnetic elements of the Indus-2 storage ring.	48
1.4	Different design parameters of Indus-3 storage ring.	50
1.5	Different magnetic elements of the Indus-3 lattice.	51
3.1	Comparison of parameters with original lattice.	79
3.2	Comparison of parameters with original lattice in case of genetic algorithm.	81
3.3	Comparison of parameters with original lattice.	83
3.4	Comparison of different parameter with original lattice for 15 section case.	87
3.5	Comparison of different LGB profiles in case of MOGA.	89
3.6	Comparison of different parameter with original lattice in case of TME.	92
4.1	Comparison of Indus-2 lattice with LGB, Indus-2 lattice with LGB and betatron tune correction and original lattice.	102
4.2	Comparison of Indus-3 lattice with LGB with original Indus-3 lattice.	115

# Chapter 1

## Basic Accelerator Physics

The synchrotron radiation (SR), emitted by transverse acceleration of ultra relativistic electron under applied magnetic field, is in much demand for various science experiments due to wide photon energy range and high brightness. To achieve high brightness SR, the dedicated electron storage rings have been built and are further being designed for further enhancing it. The brightness is governed by the beam emittance, which is the design criteria for any storage ring magnetic lattice. In order to design a magnetic lattice of a electron storage ring, deep understanding of beam dynamics of circular accelerators is required. In this Chapter, beam dynamics of circular accelerators and important concepts relevant to the thesis are presented.

In Section 1.1, a brief introduction to evolution of accelerators dedicated to produce SR are discussed. Various parameters based on linear beam dynamics of circular accelerators are discussed in Sections 1.2-1.8. Important phenomenon that govern the beam emittance in a storage ring, which highly affects the brightness of SR, is introduced in Section 1.12. Various types of low emittance magnetic lattices, which are used to build storage rings, are discussed in Section 1.13. In addition, advanced methods to improve the beam emittance is described in Section 1.15. At the end, features of Indus-2 and proposed Indus-3 storage ring lattices

are discussed in Section 1.16 and 1.17. These lattices are considered to study the effect of longitudinal variation of magnetic field in the dipoles on the beam emittance.

## 1.1 Synchrotron radiation sources

E. McMillan and independently V. Veksler, invented the synchrotron in 1945 [1]. Synchrotron, basically, is a circular accelerator in which radius of the accelerating charged particle is fixed by applying magnetic field and acceleration is provided by radio frequency (RF) cavities at one or more places in the circular ring. It is well known from special relativity equations that as particle achieves higher and higher velocity, its mass increases. Therefore, under applied magnetic field, orbit of the charged particle changes. To stabilize the orbit, magnetic field has to be synchronized with energy of the charged particle. This concept is the basic principle of a synchrotron.

First synchrotron was made for the purpose of accelerating charged particle with ever increased energy for the particle physics research [1]. Electron, a very light charged particle, achieves ultrarelativistic speed in energy range of few MeV. In electron synchrotrons, at these energies electron emits SR while going through transverse acceleration under applied magnetic force in the bending magnet. The SR was first time detected at 70 MeV synchrotron at GE in the year 1947 [1].

The energy loss per turn by an electron in the form of SR increases as fourth power of energy of an electron [2], which was the main limitation in high energy circular electron accelerators and it requires very high RF power to compensate this energy loss. Soon it was realized that SR emitted from electrons has better characteristics than conventional X-rays sources like high brightness, high flux, broad energy spectrum etc., which became boon for various science experiments. At that time, scientist started to use SR produced from high energy

electron synchrotrons parasitically. These synchrotrons, where SR was used parasitically are called first generation synchrotron radiation sources (SRSs). Since then, rigorous study on the design of dedicated SRSs based on electron storage ring, in which electron beam is stored for a long time, had been carried out in various synchrotron accelerator facilities. These synchrotrons or storage rings, which were fully dedicated to produce synchrotron radiation are called second generation SRSs. In second generation SRSs, bending magnets were primary source to get uninterrupted high brightness SR for many beam line users at a time. This is the great advantage over X-rays facility where only one user at a time can use the X-ray facility. Indus-1, a 450 MeV electron storage ring located at RRCAT, is an example of second generation SRS [3]. After successful operation of second-generation electron storage rings, insertion devices (IDs) like undulators, wigglers, wavelength shifter etc. were introduced to increase brightness, flux and energy range of SR. These devices are external to the well design lattice of the storage ring. Therefore, more spaces are to be provided to install them. These spaces, i.e. magnet free zones, therefore, become part of the design of storage ring lattices. These SRSs are called third generation SRSs. Indus-2, a 2.5 GeV electron storage ring is an example of third generation SRS [3–5].

One of the main purpose of designing a new electron storage ring or upgrading an existing electron storage ring is the demand of high brightness of the photon beam. The brightness of photon beam is defined as photon flux per unit area per unit solid angle and is mathematically expressed as [6]

$$B = \frac{F}{4\pi^2 \Sigma_x \Sigma_y \Sigma_{x'} \Sigma_{y'}}, \quad (1.1)$$

where  $F$  is the flux, defined as number of photons produced per second in 0.1% bandwidth of considered wavelength.  $\Sigma_{x,y}$  and  $\Sigma_{x',y'}$  are effective beam size and divergence of photon beam,

which are related to electron beam size and divergence as [6]

$$\Sigma_{x,y} = \sqrt{\sigma_{x,y}^2 + \sigma_r^2}, \quad (1.2)$$

$$\Sigma_{x',y'} = \sqrt{\sigma_{x',y'}^2 + \sigma_{r'}^2}. \quad (1.3)$$

Here  $\sigma_{x,y}$  and  $\sigma_{x',y'}$  are horizontal and vertical electron beam size and divergence respectively, and  $\sigma_r$  and  $\sigma_{r'}$  are the photon beam size and divergence, respectively.  $\sigma_{x,y}$  and  $\sigma_{x',y'}$  are related to beam emittance of the storage ring which is an important criteria in storage ring design. Beam sizes and its relation to beam emittance is discussed in Section 1.14.

Flux of photon beam depends on number of photons produced, which depends on stored beam current. But, one cannot fill large current due to many limitations such as vacuum, load on RF, intra beam scattering issues related to lifetime etc. In addition, high current does not lead to improvement of quality of stored beam, e.g. beam size. From eq.(1.1) brightness of the photon beam is inversely proportional to product of two beam emittances in transverse plane. Therefore, as a lattice designer, one focuses on beam emittances to increase brightness with improved beam quality.

Beam emittance, roughly, scales as cubic power of bending angle, therefore more number of dipole magnets in the lattice are required to reduce the beam emittance. Now a days, scientist are focusing on fourth generation SRSs, utilizing the concept of multi bend achromat (MBA) lattice, instead of double or triple bend achromat, and IDs to build or upgrade existing storage rings to achieve ultra low emittance [7]. The requirement of more number of dipoles make storage ring large in size and consequently increases the cost of the machine. MAX IV is the first operating machine based on MBA concept [7, 8]. Further, to push beam emittance towards more lower side, technologically challenging, advanced methods were introduced such as transverse gradient [9], longitudinal gradient bend (LGB) [10, 11], reverse or anti bend [12]. LGB was first introduced by J. Gau, T. Raubenheimer in 2002 [10]. They applied the LGB

in NLC damping storage ring and found sufficient beam emittance reduction. Now a days, magnet design technology has been improved much and LGB has been widely accepted in lattice design to upgrade of an existing facility and new storage ring lattices [11]. MAX IV, a 3 GeV storage ring, is a running example of it [13]. Some examples of high energy and large circumference SRSs to produce hard X-rays are ESRF, France (6 GeV) [14], Spring-8, Japan (8 GeV) [15], APS, USA (7 GeV) [16]. Also, there are some facilities which are build to get soft X-rays like ALS, USA (1.9 GeV) [17], ELLETRA, Italy (2-2.4 GeV) [18] etc.

## 1.2 Coordinate system used in circular accelerators

It is always desirable to study the dynamics of a particle in a coordinate system in which equation of motion of the particle takes a simple form. In circular accelerators, study of charged particle dynamics is preferred in moving or Frenet-Serret coordinate system instead of conventional coordinate system.

As shown in Fig. 1.1, this coordinate system consists a designed orbit at which reference or designed charged particle moves. Coordinate axes of the coordinate system are denoted by  $X$ ,  $Y$  and  $S$  and origin is co-moving with reference charged particle which has coordinates  $(0, 0, 0)$ . Coordinates of any other charged particle is defined as deviation from the designed orbit and are denoted by  $x$ ,  $y$  and  $s$ . Here,  $x$  and  $y$  are deviations in radial and vertical direction from the designed orbit, respectively, and  $s$  is the deviation of the charged particle with respect to reference charged particle in the direction of motion. Unit vectors along  $X$ ,  $Y$  and  $S$  direction are shown in Fig. 1.1. Also, it is notable that unit vector in  $Y$  direction does not change.

Most of the large circular accelerators in the world are build to keep designed orbit in the horizontal plane. Therefore,  $X - S$  plane is known as horizontal or median plane and  $Y - S$  plane is known as vertical plane. Motion of charged particles in these two planes defines the

transverse properties of the beam of charged particles.

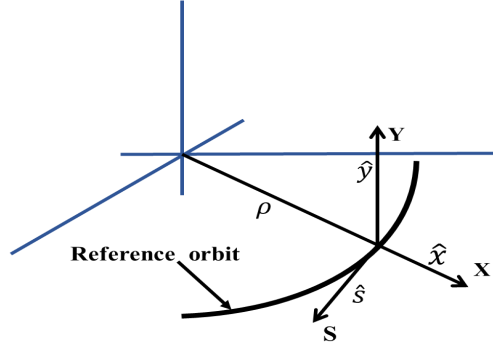


Fig. 1.1: Coordinate system used in a circular accelerators.

Local radius of curvature  $\rho$ , in general, is a function of path length  $s$ , i.e.,  $\rho = \rho(s)$ . For a straight section  $\rho = \infty$  and  $\rho$  is finite where path is curved. The  $X, Y$  and  $S$  form a right-handed coordinate system, i.e.,  $\hat{x} \times \hat{y} = \hat{s}$ . Generally, transverse deviations of a charged particle are very small, i.e.,  $x, y \ll \rho$ . Therefore, paraxial approximation can be used in study of motion of charged particle. Motion of a charged particle in an electromagnetic field is discussed in the following section.

### 1.3 Motion of a charged particle in an electromagnetic field

Motion of a charged particle in an electromagnetic field is governed by Lorentz force law and is mathematically given by [2]

$$\vec{F} = \frac{d\vec{p}}{dt} = q(\vec{E} + \vec{v} \times \vec{B}), \quad (1.4)$$

where  $\vec{p}$ ,  $q$ , and  $\vec{v}$  are momentum, charge, and velocity of the charged particle, respectively.  $\vec{E}$  and  $\vec{B}$  are electric and magnetic fields, respectively. To govern an ultrarelativistic charged particle, magnetic field is much more effective than electric field. Therefore, the transverse dynamics of the charged particle at ultrarelativistic speed can be controlled by magnetic field

only. Equation of motion for such charged particle can be written as

$$\vec{F} = \frac{d(m_0\gamma\vec{R})}{dt} = q(\vec{v} \times \vec{B}), \quad (1.5)$$

where  $m_0$  and  $\vec{R}$  are rest mass and velocity of the charged particle, respectively, and  $\gamma$  is the Lorentz factor which is given by  $\gamma = 1 + \frac{E}{E_{rest}}$ ;  $E$  and  $E_{rest}$  are the kinetic energy and rest mass energy of the charged particle respectively.

From eq.(1.5), in a normal magnetic field, one can derive following relation for a circular orbit [2]

$$\frac{p}{q} = B\rho, \quad (1.6)$$

where  $p = |\vec{p}| = \gamma m_0 |\vec{v}|$  and  $\rho$  are the momentum and bending radius of charged particle, respectively. The result in eq.(1.6) is also true for relativistic velocities. The quantity  $B\rho$ , called "Beam rigidity", is an important quantity in a circular accelerator which depends only on the momentum and given charge of the particle. For an ultrarelativistic charged particle, energy and momentum are related by  $E = cp$ ;  $c$  is the speed of light in vacuum. It means that, energy and momentum can be used interchangeably. In a storage ring, energy of reference charged particle is constant and therefore, beam rigidity of storage ring is a constant quantity.

Beam rigidity is often used to define normalized quantities for storage ring like strength of the quadrupole, sextupole etc. which are discussed in Section 1.4. For an electron storage ring  $q = e$ , eq.(1.6) can be written in terms of energy as [2]

$$B\rho(T.m) = \frac{10}{2.998}\beta E(GeV). \quad (1.7)$$

For ultrarelativistic particles, this expression is further simplified as  $\beta$  is almost equal to 1.

In a circular accelerator, magnetic fields are generated by different types of magnetic elements which are discussed in the following Section.

## 1.4 Basic magnetic elements used in accelerators

To guide the charge particles in a circular accelerator, different magnetic elements like dipoles, quadrupoles and sextupoles are used. In case of storage ring, usually a periodic unit lattice cell, an arrangement of magnetic elements in a particular fashion, is designed and is repeated to make a complete storage ring. The different magnetic elements are discussed in the following Sections [5].

### 1.4.1 Dipole magnets

An ideal dipole magnet (constant field  $\vec{B}$  in space) is used to generate a curvature (bending) in the design trajectory of an accelerator and therefore is also known as bending magnet or dipole magnet. An ideal dipole has infinite long pole faces parallel to each other and produces homogeneous (constant) field irrespective of position, i.e.,  $|\vec{B}(x, y, s)| = b$ , where  $b$  is a constant. However, practical dipole magnet has finite size. Due to finite length, fringe fields are generated which contain higher order multipoles.

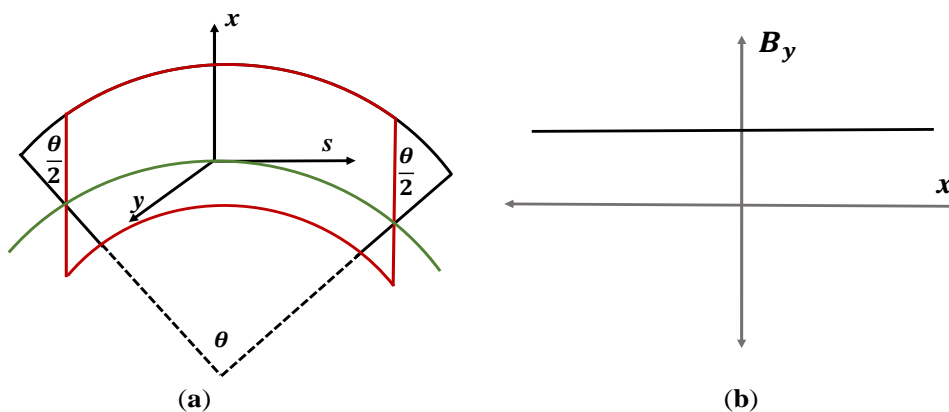


Fig. 1.2: (a) Sector (black) and Rectangular (parallel edges with red color) type dipoles.

(b) Vertical magnetic field along x-direction.

Magnetic field in a normal dipole is defined as

$$\vec{B}(x, y, s) = \pm b\hat{y}, \quad (1.8)$$

where  $\hat{y}$  is the unit vector in the vertical direction and  $b$  is a constant. However, skew dipole is defined as  $\vec{B}(x, y, s) = \pm b\hat{x}$ , where  $\hat{x}$  is the unit vector in horizontal or radial direction. It means that a normal dipole becomes a skew dipole after rotation of  $90^\circ$  about longitudinal direction.

Two types of dipole magnets are generally used in lattice design of a storage ring namely sector and rectangular, which are shown in Fig. 1.2. In a sector type dipole, the design trajectory enters and leaves the magnet edges at right angles, whereas in rectangular type, end faces are parallel to each other and design trajectory enters and leaves the magnet edges at equal angle but different from  $90^\circ$ . The transverse gradient and the longitudinal gradient can also be introduced in the bending magnets to make the size of a storage ring compact and minimise the beam emittance.

## 1.4.2 Quadrupole

A quadrupole magnet has a linearly varying magnetic field with the transverse distance ( $x$  or  $y$ ) from the design orbit, resulting in a restoring force on the charged particle passing through it, which can be used as a focusing magnet. Normal quadrupole magnet has four pole faces as shown Fig. 1.3. These pole faces are hyperbolic in shape to provide linear variation of fields with distances. Field lines originate perpendicularly from North pole and terminate on South pole. Variation of magnetic fields in a quadrupole are given as

$$B_x = gy \quad \text{and} \quad B_y = gx, \quad (1.9)$$

where  $g = \frac{dB_y}{dx}$ . At the centre of quadrupole, i.e.,  $x = 0$ ,  $y = 0$ , the net magnetic field is zero. Therefore, charged particle which passes through the centre of quadrupole does not experience

any force. Also, force on the charged particle increases with the increase of the distance from the center. Hence, more distant particle experiences more force towards or away from the centre of the quadrupole magnet. Quadrupoles are mainly used for focusing or defocusing action on the charged particles. Normalized quadrupole strength  $k$  is defined as [2]

$$k = \left(\frac{e}{p}\right) g = \frac{g}{B\rho}. \quad (1.10)$$

Eq.(1.10) can be written in terms of energy as

$$k(\text{m}^{-2}) = 0.2998 \frac{g(\text{Tm}^{-1})}{\beta E(\text{GeV})}. \quad (1.11)$$

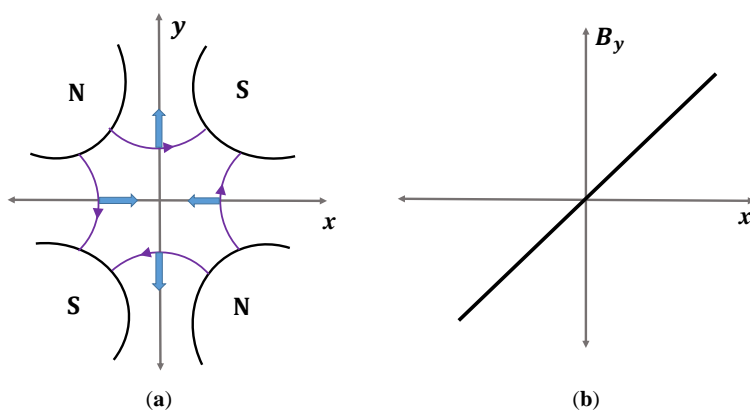


Fig. 1.3: (a) Pole faces and field direction in a quadrupole magnet. A positive charged particle coming out of the page will experience a focusing force in x direction and a defocusing force in y direction. (b)

Variation of vertical magnetic field along x-direction.

As shown in Fig. 1.3, positive charged particle coming out of the page and having different position on x-axis focuses towards centre of the quadrupole. Also, if a quadrupole focuses in one plane then in another plane it always defocuses. Therefore, to achieve overall focusing in both the transverse planes, at least two quadrupoles separated by some distance are normally used in the lattice design. Conventionally, a quadrupole focusing in horizontal plane is called focusing quadrupole and a quadrupole focusing in vertical plane is called defocusing

quadrupole. If a normal quadrupole is rotated through  $45^\circ$  about longitudinal direction, then it is called skew quadrupole. Skew quadrupoles are used to correct coupling in the machine. To build a tight focusing storage ring high gradient in the quadrupole is required.

Dipole and quadrupole magnets generate magnetic force on the particle that is either independent or linear to the charged particle position. The dynamics, which includes only dipole, quadrupole and drift space with zero magnetic fields, is known as the linear beam dynamics. Various optics characteristics and parameters of the storage rings are determined by linear beam dynamics. These parameters are introduced in Sections 1.5, 1.7 and 1.9.

### 1.4.3 Sextupole

The electron beam contains many charged particles, each may have small energy deviation from the energy of the reference or central particle. These particles when pass through the quadrupole, they focus away from the focal point. This phenomenon is known as chromatic aberration or chromaticity (discussed in Section 1.10). To correct chromaticity, the sextupole magnets are included in a storage ring and are placed near a quadrupole. A sextupole has six pole faces with North and South poles placed alternatively as shown in Fig. 1.4. The orientation of the poles are in such a way that magnetic field variation in the sextupole has following form

$$B_y = \frac{1}{2}g'(x^2 - y^2) \quad \text{and} \quad B_x = g'xy. \quad (1.12)$$

Variation of  $y$  component of magnetic field, i.e.,  $B_y$  along  $x$ -axis is shown in Fig. 1.4. The sextupole strength is defined as [2]

$$S[\text{m}^{-3}] = \frac{e}{p}g' = 0.2998 \frac{g'}{\beta E(\text{GeV})}. \quad (1.13)$$

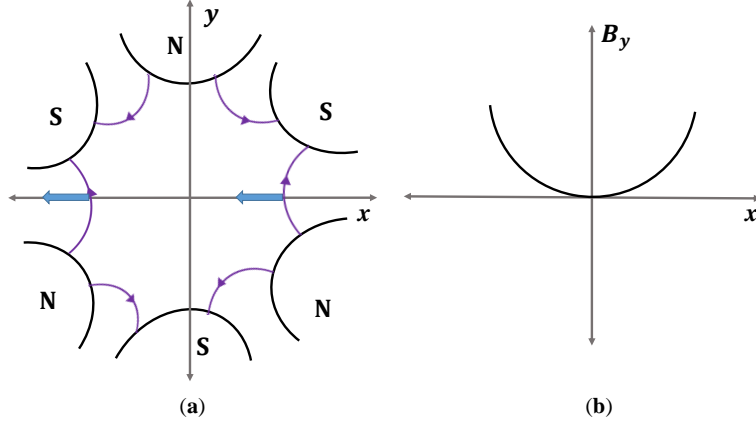


Fig. 1.4: (a) Pole faces and field direction in a sextupole magnet. Force on a positively charge particle on the  $x$  axis and coming out side of the page is shown by arrow. (b) Variation of vertical magnetic field along  $x$ -direction.

Fields in the sextupole are non-linear, as the strength of the sextupoles increase, non-linearity in the machine also increases. In addition,  $B_x$  component of sextupole field is the product of  $x$  and  $y$ , it will generate coupling in the charged particle motion.

## 1.5 Equation of motion of a charged particle in a given magnetic field

Equation of motion of a charged particle moving in a general magnetic field  $\vec{B}$  with velocity  $\vec{v}$  is given by eq.(1.5). In a storage ring, kinetic energy of the charged particle is constant, consequently,  $\gamma$  will be a constant and rest mass,  $m_0$ , is a constant, too. Therefore, eq.(1.5) becomes

$$\frac{d^2 \vec{R}}{dt^2} = q \frac{\vec{v} \times \vec{B}}{\gamma m_0}. \quad (1.14)$$

General position of the charged particle can be written as  $\vec{R} = r\hat{x} + y\hat{y}$  and general radius of curvature as  $r = \rho + x$ . Considering uncoupled motion in both transverse directions, general equation of transverse motion of a charged particle in a given magnetic field can be

written in terms of path length  $s$  as [A.1]

$$\frac{d^2x}{ds^2} - \left( \frac{\rho + x}{\rho^2} \right) = -\frac{B_y}{B\rho} \left( 1 + \frac{x}{\rho} \right)^2, \quad (1.15)$$

$$\frac{d^2y}{ds^2} = \frac{B_x}{B\rho} \left( 1 + \frac{x}{\rho} \right)^2. \quad (1.16)$$

Here, it is assumed that energy of the charged particle is constant and magnetic field component in  $s$  direction, i.e.,  $B_s$ , is zero. Magnetic field components  $B_x$  and  $B_y$  can be expanded as a Taylor's series about reference orbit as

$$B_x = B_x(0) + \frac{\partial B_x}{\partial y} y + \frac{1}{2!} \frac{\partial^2 B_x}{\partial y^2} y^2 + \dots, \quad (1.17)$$

$$B_y = B_y(0) + \frac{\partial B_y}{\partial x} x + \frac{1}{2!} \frac{\partial^2 B_y}{\partial x^2} x^2 + \dots. \quad (1.18)$$

Here,  $B_x(0)$  and  $B_y(0)$  are constant and derivatives of magnetic fields are calculated at reference orbit. For small deviations, i.e.,  $x, y \ll \rho$ , higher order terms in expansion of magnetic fields can be neglected. Using fourth Maxwell relation in the pole gap of a magnetic element where current and charges are zero, we have  $\nabla \times \vec{B} = 0 \rightarrow \frac{\partial B_x}{\partial y} = \frac{\partial B_y}{\partial x}$ . Since bending of the charged particle is considered in horizontal plane. Therefore, for horizontal motion  $B_x(0) = 0$ . Using these results, eq.(1.15) and eq.(1.16) can be further simplified as

$$\frac{d^2x}{ds^2} + \left( \frac{1}{\rho^2} + \frac{1}{B\rho} \frac{\partial B_y}{\partial x} \right) x = 0, \quad (1.19)$$

$$\frac{d^2y}{ds^2} - \left( \frac{1}{B\rho} \frac{\partial B_y}{\partial x} \right) y = 0. \quad (1.20)$$

Expression  $\frac{1}{B\rho} \frac{\partial B_y}{\partial x}$  is denoted by  $k$ . This is an important quantity which is normalized with beam rigidity and has units  $[\text{m}^{-2}]$ . In general, equation of motion in transverse planes can

be written in a single equation as

$$u'' + K(s)u = 0, \quad \text{with} \quad \begin{cases} K = \frac{1}{\rho^2} + \frac{1}{B\rho} \frac{\partial B_y}{\partial x}, & \text{for } u = x \\ K = -\frac{1}{B\rho} \frac{\partial B_y}{\partial x}, & \text{for } u = y \end{cases} \quad (1.21)$$

Eq.(1.21) is called ‘‘Hill’s equation’’ and is similar to equation of simple harmonic motion with variable spring constant. From this equation, position and slope of a charged particle can be found at any position  $s$ . In general,  $K$  is the function of path-length  $s$ . But for a magnetic element,  $K(s)$  can be treated as a constant, i.e.,  $K(s) = K$ . Assuming  $K$  positive and constant, the solution of eq.(1.21) can be written as [2, 19]

$$u(s) = A \cos(\sqrt{K}s) + B \sin(\sqrt{K}s). \quad (1.22)$$

Then slope of the particle trajectory is given by

$$u'(s) = -A\sqrt{K} \sin(\sqrt{K}s) + B\sqrt{K} \cos(\sqrt{K}s), \quad (1.23)$$

here  $A$  and  $B$  are constant. For  $K < 0$ , hyperbolic sine and cosine terms will appear instead of sine and cosine. For a given length of a magnetic element and initial position of a charged particle at the entrance of magnetic element, constants  $A$  and  $B$  can be found. After finding these two constants, eq.(1.22) and (1.23) can be written in matrix form as

$$\begin{pmatrix} u \\ u' \end{pmatrix}_{out} = \begin{pmatrix} \cos(\phi) & \frac{1}{\sqrt{K}} \sin(\phi) \\ -\sqrt{K} \sin(\phi) & \cos(\phi) \end{pmatrix} \begin{pmatrix} u \\ u' \end{pmatrix}_{in}, \quad (1.24)$$

where  $\phi = \sqrt{K}L$ . Here, *in* and *out* shows entrance and exit of the magnetic element as shown in Fig. 1.5.

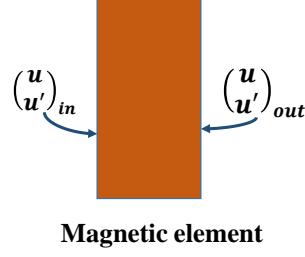


Fig. 1.5: Position and slope (with respect to longitudinal direction) of the charged particle before and after traversing the magnetic element.

The matrix

$$M = \begin{pmatrix} \cos(\phi) & \frac{1}{\sqrt{K}} \sin(\phi) \\ -\sqrt{K} \sin(\phi) & \cos(\phi) \end{pmatrix} = \begin{pmatrix} C(S) & S(s) \\ C'(s) & S'(s) \end{pmatrix} = \begin{pmatrix} M_{11} & M_{12} \\ M_{21} & M_{22} \end{pmatrix} \quad (1.25)$$

is called transfer matrix for the magnetic element, and it is different for different type of magnetic elements. Here,  $C(s) = M_{11} = \cos(\phi)$ ,  $S(s) = M_{12} = \frac{1}{\sqrt{K}} \sin(\phi)$ .  $C'(s)$  and  $S'(s)$  are derivatives of  $C(s)$  and  $S(s)$ , respectively. This transfer matrix transports position and slope of a charged particle from entrance to exit point of the magnetic element. Transfer matrix for different type of magnetic element are in following Section.

### 1.5.1 Transfer matrix for a drift space

For a drift space, i.e., no magnetic field,  $K = 0$ . Transfer matrix for a drift space is given by [19]

$$M_{Drift} = \begin{pmatrix} 1 & L \\ 0 & 1 \end{pmatrix}, \quad (1.26)$$

where  $L$  is the length of the drift space. As shown in Fig. 1.6, when a charged particle passes through a drift space its position changes, but slope remains constant.

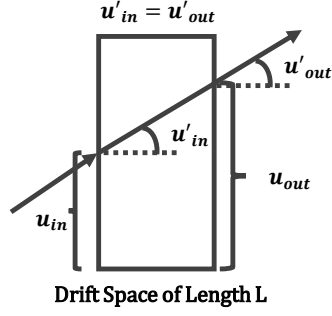


Fig. 1.6: Position and slope (with respect to longitudinal direction) of the charged particle after passing through a drift space.

Drift spaces play an important role in lattice design. Mostly all magnetic elements in the storage ring are electromagnetic in nature. Magnetic elements have coils wrapped on the iron core. One must provide some space between two magnetic element for these coils. Also, vacuum pumps and cooling systems, beam position monitors, dipole correctors, beam profile monitors require spaces. In addition, installation of IDs also require large spaces.

### 1.5.2 Transfer matrix for a quadrupole

For a pure quadrupole,  $K = k = \frac{1}{B\rho} \frac{\partial B_y}{\partial x}$  and transfer matrix for a focusing quadrupole is given by [19]

$$M_{Q, focusing} = \begin{pmatrix} \cos \phi & \frac{1}{\sqrt{|k|}} \sin \phi \\ -\sqrt{|k|} \sin \phi & \cos \phi \end{pmatrix}, \quad (1.27)$$

where  $\phi = \sqrt{k}L$  and  $k > 0$  (focusing quadrupole) and for a defocusing quadrupole transfer matrix is given by

$$M_{Q, defocusing} = \begin{pmatrix} \cosh \phi & \frac{1}{\sqrt{|k|}} \sinh \phi \\ \sqrt{|k|} \sinh \phi & \cosh \phi \end{pmatrix}, \quad (1.28)$$

where  $\phi = \sqrt{|k|}L$  and  $k < 0$  (defocusing quadrupole).

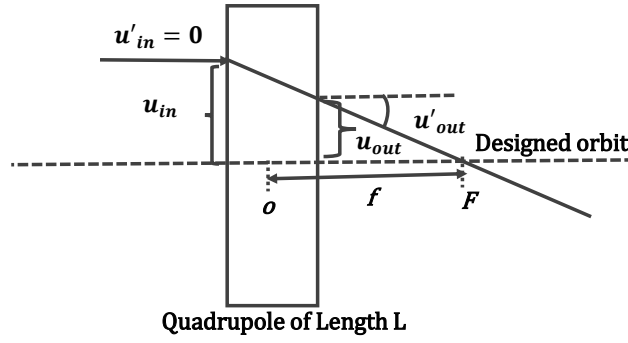


Fig. 1.7: Particle position (with respect to longitudinal direction) after passing through a focusing quadrupole. O is the centre of the quadrupole and F is focal point.

Quadrupole is a focusing element. In Fig. 1.7, action of a focusing quadrupole is shown.

Focal length of a quadrupole is given by [19]

$$f = \begin{cases} \frac{1}{\sqrt{k}L \tan(\sqrt{k}L)}, & \text{for } k > 0 \\ \frac{1}{\sqrt{-k}L \tanh(\sqrt{-k}L)}, & \text{for } k < 0 \end{cases} \quad (1.29)$$

If  $f \ll L$  (thin lens approximation), eq.(1.29) becomes

$$f = \frac{1}{kL} \quad (1.30)$$

### 1.5.3 Transfer matrix for a dipole

For a sector type dipole  $K(s) = \frac{1}{\rho^2}$ . Transfer matrix for horizontal plane is given by [19]

$$M_x = \begin{pmatrix} \cos \theta & \rho \sin \theta \\ -\frac{1}{\rho} \sin \theta & \cos \theta \end{pmatrix}, \quad (1.31)$$

where  $\theta = \frac{L}{\rho}$  is the bending angle of the dipole magnet. In vertical plane sector type dipole magnet behaves like a drift space with length  $L = \theta\rho$ , because there is no any bending in vertical plane. In thin lens approximation  $\theta \rightarrow 0$ , transfer matrix  $M_x$  can be written as

$$M_x = \begin{pmatrix} 1 & 0 \\ -\frac{L}{\rho^2} & 1 \end{pmatrix} \quad (1.32)$$

Here, one can see that dipole act as a focusing element. This focusing originates from the fact that the different energy charged particle has different  $\rho$  in the dipole. This type of focusing is called geometrical focusing.

For a rectangular type dipole magnet, transfer matrices for both transverse planes are given as [19]

$$M_x = \begin{pmatrix} 1 & \rho \sin \theta \\ 0 & 1 \end{pmatrix}, \quad M_y = \begin{pmatrix} \cos \theta & \rho \sin \theta \\ -\frac{1}{\rho} \sin \theta & \cos \theta \end{pmatrix}. \quad (1.33)$$

Transfer matrix for horizontal plane has the form like a drift space with length  $L = \rho \sin \theta$ . This is because, the weak geometrical focusing in horizontal plane is exactly compensated by the defocusing at the entrance and exit faces [2, 5].

In a magnetic lattice of a storage ring, there are large number of magnetic elements to guide a charged particle. In matrix formulation one can compute transfer matrix for a given arrangement of magnetic elements. In Fig. 1.8, an example of an arrangement of magnetic elements is shown. If transfer matrices for different magnetic elements are  $M_1, M_2, M_3, \dots, M_{12}$  and a charged particle enters from the entrance of the first element and exits from the last element, then transfer matrix for this arrangement is given by the product of individual transfer matrix as

$$M = M_{12}.M_{11}.M_{10} \dots M_2 M_1 \quad (1.34)$$

This result can be generalized for  $n$  number of magnetic elements provided transfer matrix for each element is known.

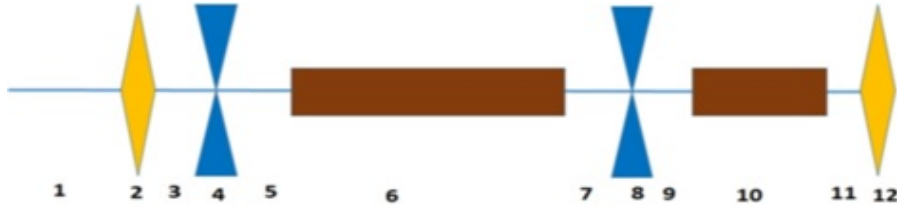


Fig. 1.8: An example of arrangement of different magnetic elements. Elements 1, 3, 5, 7, 9, 11 are drift spaces. Elements 2 and 12 are focusing quadrupole, 4 and 8 are defocusing quadrupole. Elements 6 and 10 are dipole magnets.

## 1.6 Dispersion and trajectory of an off-momentum particle

In a dipole, an off-momentum or off-energy charged particle does not follow the same path as reference charged particle even if it is launched on the designed path. This is shown in Fig. 1.9, higher energy charged particle follows longer path, however, lower energy particle follow shorter path and trajectories of different energy particles get dispersed. This phenomenon is called dispersion.

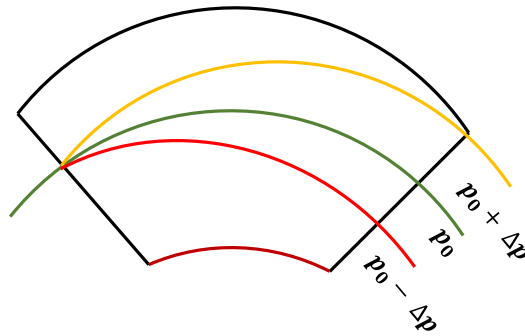


Fig. 1.9: Motion of different energy particles in a sector type dipole magnet.

Position or deviation from designed orbit of such particles is given by [2]

$$x(s) = \eta(s) \frac{\Delta p}{p_0} = \eta(s) \delta, \quad x'(s) = \eta'(s) \delta, \quad (1.35)$$

here,  $p_0$  is the momentum of reference charged particle and  $\delta p = p - p_0$  is the change in

momentum of a charged particle from reference charged particle.  $\Delta = \frac{\Delta p}{p_0}$  and  $\eta(s)$  are relative momentum deviation and dispersion function, respectively. Eq.(1.35) shows that dipole separates off different momentum or energy charged particles in position, i.e., if  $\Delta p < 0$  then  $x < 0$  and if  $\Delta p > 0$  then  $x > 0$ .

In an ideal lattice dispersion is generated by the dipole magnet in horizontal direction only. However, vertical dispersion can be present in the machine due to various errors in the machine. For example, skew quadrupole (rotated quadrupole) and rotational error in the dipole magnet can generate dispersion in vertical plane. Phenomenon of dispersion plays an important role in the consideration of lattice design of a storage ring.

Considering ideal dipole, after including dispersion and considering small momentum deviation, new equations of motion in both transverse planes can be written as [2, 19]

$$\frac{d^2x}{ds^2} + \left( \frac{1}{\rho^2} + \frac{1}{B\rho} \frac{\partial B_y}{\partial x} \right) x = \frac{\delta}{\rho}, \quad (1.36)$$

$$\frac{d^2y}{ds^2} - \left( \frac{1}{B\rho} \frac{\partial B_y}{\partial x} \right) y = 0. \quad (1.37)$$

Eq.(1.36) is an inhomogeneous differential equation while eq.(1.37) is a homogeneous differential equation. Therefore, solution of eq.(1.36) will contain homogeneous solution with particular integral and is given by [2]

$$x(s) = A.C(s) + B.S(s) + \delta.\eta(s), \quad (1.38)$$

where  $\eta(s)$  is given by

$$\eta(s) = \int_0^s \frac{1}{\rho(s')} [S(s)C(s') - C(s)S(s')] ds'. \quad (1.39)$$

After including dispersion term one can write solution of equation of motion in matrix formulation

and in terms of dispersion function as [19]

$$\begin{pmatrix} \eta \\ \eta' \\ 1 \end{pmatrix}_{out} = \begin{pmatrix} M_{11} & M_{12} & M_{13} \\ M_{21} & M_{22} & M_{23} \\ M_{31} & M_{32} & M_{33} \end{pmatrix} \begin{pmatrix} \eta \\ \eta' \\ 1 \end{pmatrix}_{in}. \quad (1.40)$$

For a sector type dipole, eq.(1.40) can be written as [19]

$$\begin{pmatrix} \eta \\ \eta' \\ 1 \end{pmatrix}_{out} = \begin{pmatrix} \cos \theta & \sin \theta & \rho(1 - \cos \theta) \\ -\frac{1}{\rho} \sin \theta & \cos \theta & \sin \theta \\ 0 & 0 & 1 \end{pmatrix} \begin{pmatrix} \eta \\ \eta' \\ 1 \end{pmatrix}_{in}, \quad (1.41)$$

Similarly for a rectangular type dipole

$$\begin{pmatrix} \eta \\ \eta' \\ 1 \end{pmatrix}_{out} = \begin{pmatrix} \cos \theta & \sin \theta & \rho(1 - \cos \theta) \\ -\frac{1}{\rho} \sin \theta & \cos \theta & 2 \tan \frac{\theta}{2} \\ 0 & 0 & 1 \end{pmatrix} \begin{pmatrix} \eta \\ \eta' \\ 1 \end{pmatrix}_{in}. \quad (1.42)$$

In Section 1.5, equation of motion is solved considering  $K$  as a constant. In the following Section, solution of equation of motion is given for a more general case, in which  $K$  is a periodic function.

## 1.7 Parametric solution of equation of motion and Courant-Snyder parameters

For circular accelerators, i.e., a periodic system, general equation of motion of a charged particle with reference energy can be written as [A.2]

$$u''(s) + K(s)u(s) = 0, \quad (1.43)$$

here  $u$  stands for  $x$  or  $y$  and  $K$  is a periodic function of path length  $s$  with period  $C$ . The period  $C$  may be either full circumference of circular accelerator or one super period in the circular

accelerator. The charged particle in the circular accelerator has to make millions of revolutions and will experience a periodic potential in every turn. Solution of such differential equation is given by Floquet's theorem and can be written in the form [2]

$$u(s) = A\sqrt{\beta(s)} \cos[\phi(s) + \phi_0], \quad (1.44)$$

here  $\phi_0$  and  $A$  are constant and  $\phi$  is the phase of the charged particle. This form of amplitude is chosen for specific problem of circular accelerators. Any general function which depends on  $s$  can be chosen for amplitude function. Amplitude function  $\beta(s)$  is also a periodic function with same period of  $K$ , i.e.,  $C$ . Solution in eq.(1.44) confirms that after each turn charged particle acquires a positive phase, which means, particle will not have same position after travelling a complete turn or a super period.

After substituting solution in eq.(1.43), an equation in terms of sine and cosine can be obtained. After equating the coefficient of sine and cosine terms equal to zero, two equations can be obtained as [A.2]

$$\frac{1}{2} \left( \beta\beta'' - \frac{1}{2}(\beta'')^2 \right) - \beta^2(\phi')^2 + k\beta^2 = 0 \quad (1.45)$$

$$\beta'\phi' + \beta\phi'' = 0. \quad (1.46)$$

Eq.(1.46) can be rearranged as  $(\beta\phi')' = 0$  or  $\beta\phi' = \text{Constant}$ . Value of this constant is just a scaling factor and can be chosen as 1 for simplicity. Further,

$$\phi'(s) = \frac{1}{\beta(s)} \rightarrow \phi(s) = \int_0^s \frac{ds'}{\beta(s')}. \quad (1.47)$$

In a circular accelerator, one is free to choose our reference point of integration from 0 to  $s$ . Therefore, integration constant is chosen as 0 for simplicity.  $\phi(s)$  is called phase advance of charged particle after travelling a distance  $s$  and it depends on amplitude function  $\beta(s)$ . Using result for phase advance, eq.(1.45) becomes

$$\frac{1}{2}\beta\beta'' - \frac{1}{4}(\beta')^2 + \beta^2k = 1. \quad (1.48)$$

This is an important relation called envelope equation. Because it represent the envelope of the beam. Also, it may happen that for some values of quadrupole strength  $k$ , solution of envelope equation may not exist. This leads to resonances for such values of  $k$ .

With the introduction of new variables, which are given as

$$\alpha = -\frac{1}{2}\beta', \quad \gamma = \frac{1 + \alpha^2}{\beta} \quad (1.49)$$

eq.(1.45) becomes

$$\alpha' = k\beta - \gamma. \quad (1.50)$$

The variables  $\alpha(s), \beta(s), \gamma(s)$  are called Courant-Snyder variables or Twiss parameters. Twiss parameters and the phase function  $\phi(s)$  are called betatron functions or lattice functions and oscillatory motion of a charged particle along longitudinal direction or beam line is called the betatron oscillation [2].

One can find an invariant of motion between solution  $u(s)$  and Courant-Snyder variables by eliminating  $(\phi(s) + \phi_0)$  from solution  $u(s)$ , which is given by

$$\gamma u^2 + 2\alpha u u' + \beta u'^2 = A^2. \quad (1.51)$$

A quantity  $\epsilon$ , called emittance, is defined as  $A^2 = \epsilon$ . Relation in eq.(1.51) is the equation of general ellipse with area  $\pi\epsilon$ , i.e., emittance is directly related to the phase space area. General ellipse as shown in Fig.1.10, denotes motion of single particle in phase space. After passing through different magnetic elements this ellipse will change its shape and size but area will remain constant if forces are conservative and linear. In circular accelerators, there are large number of charged particles and form the beam. Charged particles having same emittance but different in phase will lie on this ellipse at different locations. If this is the ellipse for outermost charged particle which survives i.e. stable in the storage ring, then all charged particles whose emittance are lower than outermost charged particle will surely survive.

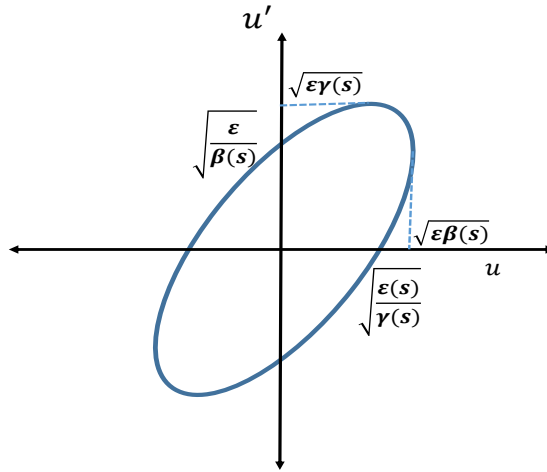


Fig. 1.10: Emittance as a phase space area for a single particle. Maximum position and maximum slope are also shown.

The beam emittance of whole beam can equivalently be describe by the emittance of the outermost charged particle in a beam. Trajectories of charged particles on the ellipse is described by

$$u_i(s) = \sqrt{\epsilon} \sqrt{\beta(s)} \cos[\phi(s) + \phi_{0i}], \quad (1.52)$$

where  $\phi_{0i}$  is an arbitrary phase constant of the  $i^{th}$  charged particle. Selecting every point along the beam line for which  $\cos[\phi(s) + \phi_{0i}] = \pm 1$ , one can get an envelope of the beam containing all charged particles as

$$u_{max} = \pm \sqrt{\epsilon \beta(s)}. \quad (1.53)$$

This is the maximum amplitude that a charged particle can have at any position  $s$ . Beam envelope changes with path length  $s$  and depends only on beam emittance and betatron functions.

Courant-Snyder variables plays important role in beam dynamics and one can study beam dynamics in terms of Courant-Snyder variables.

## 1.8 Beam dynamics in terms of Courant-Snyder variables

If, initial position and slope at the entrance of a magnetic element are known, then position and slope can be found at the exit of the magnetic element provided that Courant-Snyder (CS) are known at entrance and exit of the magnetic element. one can write matrix equation for position and slope of a charged particle in term of CS variables as [20]

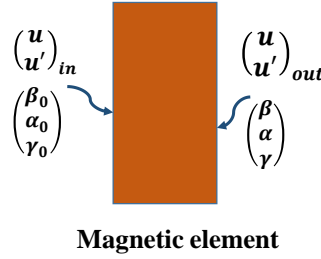


Fig. 1.11: Position and slope of a particle after passing through a magnetic element.  $(\beta_0, \alpha_0, \gamma_0)'$  and  $(\beta, \alpha, \gamma)'$  are CS variables at entrance and exit of the magnetic element.

$$\begin{pmatrix} u \\ u' \end{pmatrix}_{out} = \begin{pmatrix} \sqrt{\frac{\beta}{\beta_0}}(\cos \phi + \alpha_0 \sin \phi) & \sqrt{\beta\beta_0} \sin \phi \\ \frac{(\alpha_0 - \alpha) \cos \phi - (1 + \alpha\alpha_0) \sin \phi}{\sqrt{\beta\beta_0}} & \frac{\beta_0}{\beta} (\cos \phi - \alpha \sin \phi) \end{pmatrix} \begin{pmatrix} u \\ u' \end{pmatrix}_{in}. \quad (1.54)$$

Here, *in* and *out* denote entrance and exit of the magnetic element. Eq.(1.54) is true for any charged particle trajectory. CS variables are properties of magnetic element and each charged particle having different position and slope will experience same values of these variables.

For a periodic system  $\beta = \beta_0$  and  $\alpha = \alpha_0$ , eq.(1.54) reduces to

$$\begin{pmatrix} u \\ u' \end{pmatrix}_{out} = M \begin{pmatrix} u \\ u' \end{pmatrix}_{in}, \quad (1.55)$$

where matrix  $M$  is the transfer matrix which is given by

$$M = \begin{pmatrix} \cos \mu + \alpha \sin \mu & \beta \sin \mu \\ \gamma \sin \mu & \cos \mu - \alpha \sin \mu \end{pmatrix}, \quad (1.56)$$

here  $\mu$  is the phase advance for one turn or one super period [A.2]. This  $2 \times 2$  matrix is called one turn or one period matrix and further, it can be written as

$$M = I \cos \mu + J \sin \mu, \quad (1.57)$$

where  $I$  is the  $2 \times 2$  identity matrix and  $J$  is given by

$$J = \begin{pmatrix} \alpha & \beta \\ -\gamma & -\alpha \end{pmatrix}; \quad \text{with property } J^2 = -I. \quad (1.58)$$

Transfer matrix in this form has an advantage that it can be written as  $M = \exp(J\mu)$ .

If charged particle makes  $n$  turns in the ring then for stability of this charged particle in the whole ring, there must be a stability criteria. In any large circular accelerator, a unit periodic structure is repeatedly used to make complete structure of circular accelerator. Number of repetition of this periodic structure is called super period. If  $M_p$  is the transfer matrix for one super period and charged particles makes  $n$  turns in a storage ring then transfer matrix for  $p$  super period and  $n$  turns is given as follows

$$M = ((M_p)^p)^n = (M_p)^{np} = \exp(npJ\mu). \quad (1.59)$$

To ensure stability of particles after  $n$  turns,  $\mu$  must be real and matrix element of  $M$  must be finite. From eq.(1.56), a necessary condition for stability of charged particles can be derived as [20]

$$|\text{Trace}(M)| = |2 \cos \mu| \leq 2. \quad (1.60)$$

In addition, CS variables at the entrance and exit can be related for a magnetic element if transfer matrix  $M$  for a magnetic element is known. Consider CS variables at the entrance

of the magnetic element, are  $(\beta, \alpha, \gamma)_{in} = (\beta_0, \alpha_0, \gamma_0)$ , then CS variables at the exit is given by [19]

$$\begin{pmatrix} \beta \\ \alpha \\ \gamma \end{pmatrix}_{in} = \begin{pmatrix} M_{11}^2 & -2M_{11}M_{12} & M_{12}^2 \\ -M_{11}M_{21} & M_{11}M_{22} + M_{12}M_{21} & -M_{12}M_{22} \\ M_{21}^2 & -2M_{21}M_{22} & M_{22}^2 \end{pmatrix} \begin{pmatrix} \beta_0 \\ \alpha_0 \\ \gamma_0 \end{pmatrix} \quad (1.61)$$

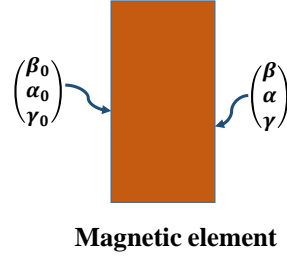


Fig. 1.12: CS variables at the entrance and exit of the magnetic element.

Eq.(1.61) is an important relation to see the behaviour of CS variables in different magnetic elements e.g. for a drift space, the transfer matrix  $M$  can be given in terms of path length,  $s$ , as

$$M = \begin{pmatrix} 1 & s \\ 0 & 1 \end{pmatrix}. \quad (1.62)$$

Therefore,

$$\begin{pmatrix} \beta \\ \alpha \\ \gamma \end{pmatrix} = \begin{pmatrix} 1 & -2s & s^2 \\ 0 & 1 & -s \\ 0 & 0 & 1 \end{pmatrix} \begin{pmatrix} \beta_0 \\ \alpha_0 \\ \gamma_0 \end{pmatrix}. \quad (1.63)$$

Hence,

$$\begin{aligned} \beta(s) &= \beta_0 - 2\alpha_0 s + s^2 \gamma_0 \\ \alpha(s) &= \alpha_0 - s \gamma_0 \\ \gamma(s) &= \gamma_0. \end{aligned} \quad (1.64)$$

From eq.(1.64),  $\beta(s)$  follows a parabolic nature in drift space,  $\alpha(s)$  is linear with  $s$  and  $\gamma(s)$  is constant throughout drift space.

Some concepts like betatron tune, chromaticity, momentum compaction factor play important role in operation of practical storage ring. These are discussed in the Sections 1.9, 1.10 and 1.11.

## 1.9 Betatron tune

Off axis particle oscillates about designed orbit due to focusing nature of the quadrupoles. The number of oscillations per revolution is called betatron tune and denoted by  $\nu_x$  for horizontal plane and  $\nu_y$  in vertical plane. Expression for betatron tune is given by [A.2]

$$\nu_{x,y} = \frac{\mu_{x,y}}{2\pi} = \frac{1}{2\pi} \oint \frac{1}{\beta_{x,y}(s)} ds, \quad (1.65)$$

where  $\mu_{x,y} = \oint \frac{1}{\beta_{x,y}(s)} ds$  is the phase advance for complete ring.

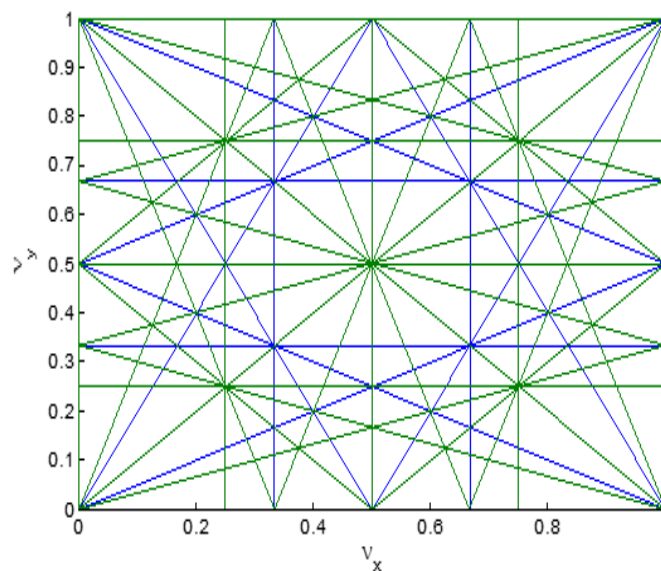


Fig. 1.13: Tune diagram for fractional betatron tune up to fourth order resonance.

Any practical storage ring is not ideal, errors, either systematic or random, always are present in the practical machine. Imperfections in the machine, e.g. dipolar error, quadrupolar

error, sextupolar error, excite resonances in the storage ring. Therefore, for stable oscillations, there are restriction on the betatron tunes. For example betatron tune should not be integer or half integer or one third integer. Dipolar error generates first order resonances or integer tune resonances, quadrupolar error generates second order or half integer tune resonances and sextupole error generates third order resonances. General condition for resonance can be written as  $m\nu_x + n\nu_y = l$ , where  $m, n, l$  are integers. This is the equation of straight line in a 2-D plane, called tune space. This is shown in Fig.1.13 up to fourth order. Each line is a resonance line and  $|m| + |n|$  is called order of resonance. In order to operate a storage ring, the fractional betatron tunes in both planes should be far away from the resonance lines.

## 1.10 Chromaticity

Generally, in a storage ring there are bunches instead of a single charged particle and these bunches have large number of charged particles. In addition, single bunch has spread in energy, i.e., each charged particle has small energy deviation from the reference charged particle. After passing through the quadrupole, these different energy charged particles experience different focusing force, and as a result, they focus at different points. This phenomenon is called chromaticity.

Momentum dependent quadrupole strength is given as [2]

$$k(p) = \frac{e}{p}g, \quad (1.66)$$

here  $e$  is the charge on charged particle. Then change in quadrupole strength will be

$$\Delta k = \frac{dk}{dp}\Delta p = \frac{eg}{p_0} \left( \frac{\Delta p}{p_0} \right) = -k\delta \quad (1.67)$$

$$\Delta k = \begin{cases} k\delta, & \text{for horizontal motion } (k > 0) \\ -k\delta, & \text{for vertical motion } (k < 0) \end{cases} \quad (1.68)$$

For horizontal focusing quadrupole, higher momentum charged particle experiences weaker quadrupole strength and vice versa for lower momentum charged particles. These effects introduce shift in betatron tune, which may cross the resonance line and may lead to loss of the beam. Total betatron tune shift can be given as [5, 6]

$$\Delta\nu_{x,y} = \frac{1}{4\pi} \int \beta_{x,y}(s) \Delta k_{x,y}(s) ds = \mp \frac{1}{4\pi} \int \beta_{x,y} \frac{\Delta p}{p_0} k(s) ds. \quad (1.69)$$

Taking  $k$  positive, naturally occurring chromaticities for both planes of the machine are defined as [5]

$$\xi_{x,y} = \frac{\Delta\nu_{x,y}}{\frac{\Delta p}{p_0}} = -\frac{1}{4\pi} \oint \beta_{x,y} k(s) ds. \quad (1.70)$$

For a strong focusing machine, natural chromaticity is always negative [5]. Natural chromaticity depends on betatron function and strength of the quadrupoles only, i.e., higher strength quadrupole placed at higher beta functions will lead to higher natural chromaticity. Correction of natural chromaticity is done by using sextupoles. Expression for chromaticity correction for horizontal and vertical planes are given by [5]

$$\xi_{x,y} = -\frac{1}{4\pi} \oint \beta_{x,y}(s) [k(s) \mp S(s)\eta(s)] ds, \quad (1.71)$$

where  $S(s)$  is the sextupole strength. Using appropriate strength of the sextupole, one can achieve desired value of chromaticity in the machine. To efficiently correct the chromaticity in each plane, chromatic sextupoles should be placed at the location where dispersion is non-zero and betatron functions are well separated. Horizontal chromaticity correction needs large horizontal and small vertical beta function and vice versa for the vertical chromaticity correction. Sextupole having a strength  $S$ , compensate the focusing error by deflecting higher momentum charged particle and lower momentum charged particle towards the focusing point.

In a storage ring, there are two types of aperture: (i) physical aperture, which is defined by boundary of vacuum chamber, and (ii) dynamic aperture, which is a completely theoretical

phenomenon. Dynamic aperture is defined as "stable area of a boundary under non-linear forces". Non-linear forces arises due to non-linear magnetic fields e.g. fields of sextupoles, octupoles and multipoles due to errors in the practical electron storage ring. Multipole fields excite various higher order resonances and leads to particle loss in the beam. Therefore, area available for stable oscillation of charged particles gets reduced.

Dynamic aperture of an electron beam in the storage ring is a hypothetical aperture beyond which any charged particle will not survive. This means that if a charged particle is inside of dynamic aperture, then it has stable oscillations for sufficient number of turns. It is always experienced that large dynamic aperture provides good operating condition for a any electron storage ring. It is very challenging to increase the dynamic aperture. Dynamic aperture can be calculated by tracking of charged particle through the storage ring. The plot of all maximum stable initial amplitude gives dynamic aperture boundary.

## 1.11 Momentum compaction factor

The path length of a closed off-momentum charged particle will differ from the path length of the reference charged particle (which is defined to be the circumference,  $C$ ). Momentum compaction is defined as relative change in circumference per unit relative momentum off-set and denoted by  $\alpha_c$  [2].

$$\alpha_c = \frac{\frac{\Delta L}{L}}{\frac{\Delta p}{p}} = \frac{\Delta L}{L} \frac{p}{\delta}. \quad (1.72)$$

This quantity tells us about how orbits are closely packed for different off-energy charged particles.  $\alpha_c$  can be negative, positive or zero depending on the energy deviation of the particle.

$\alpha_c$  is related with dispersion as

$$\alpha_c = \frac{1}{C} \oint \frac{\eta(s)}{\rho(s)} ds. \quad (1.73)$$

In a storage ring, a low value of  $\alpha$  is desired to make beam close to reference orbit, which is also a challenging task for a storage ring lattice designer.

In an electron storage ring, emission of synchrotron radiation affects the dynamics of electron beam which is discussed below.

## 1.12 Effect of synchrotron radiation on electron beam in the storage ring

A relativistic charged particle when accelerated in a macroscopic electromagnetic field emits radiation which is called synchrotron radiation (SR). Instantaneous power radiated by such a charged particle is given by [21]

$$P = \frac{2e^2}{3c} \gamma^6 \left( (\dot{\vec{\beta}})^2 - (\vec{\beta} \times \dot{\vec{\beta}})^2 \right), \quad (1.74)$$

where  $e$  is the charge of the charged particle,  $\gamma$  is the Lorentz factor,  $c$  is the speed of the light,  $\vec{\beta} = \frac{\vec{v}}{c}$  is the velocity and  $\dot{\vec{\beta}} = \frac{\dot{\vec{v}}}{c}$  is the acceleration of the charged particle. In terms of accelerating forces, the rate of radiated energy is proportional to the square of the accelerating force. Also, the rate depends on the angle between the force and the charged particle's velocity and is larger by the factor  $\gamma^2 = \left( \frac{E}{m_0 c^2} \right)^2$  when the force is perpendicular to the velocity than when the force is parallel to the velocity. In a circular accelerator the typical longitudinal forces (from the accelerating system) are much weaker than the typical transverse magnetic forces. Therefore, one needs to consider the radiation effects that accompanied by the magnetic forces only.

Energy lost by an electron, having energy  $E$ , in one turn in an electron storage ring is given by [22]

$$U = \frac{C_\gamma \beta_0 E^4}{2\pi} \oint \frac{ds}{[\rho(s)]^2} = \frac{c_\gamma E^4}{2\pi} \oint \frac{ds}{[\rho(s)]^2}, \quad (1.75)$$

here  $\beta_0 = 1$  (at ultrarelativistic speed),  $C_\gamma = \frac{e^2}{3\epsilon_0(m_0c^2)^4}$  is a constant and for electrons this constant has a numerical value equal to  $8.846 \times 10^{-5}$  [m.GeV<sup>-3</sup>].  $I_2$  is the second radiation integral and is defined as [22]

$$I_2 = \oint \frac{ds}{[\rho(s)]^2} \quad (1.76)$$

Second radiation integral is inversely proportional to square of the local radius of curvature and for an isomagnet (constant field dipole), it is a constant and has value  $\frac{2\pi}{\rho}$ . Thus, for an isomagnet energy loss per turn can be given as [A.3]

$$U_0 = 88.575 \frac{[E(\text{GeV})]^4}{\rho}. \quad (1.77)$$

Eq.(1.77) shows that, electron storage rings with small radius of curvature (high magnetic field) have higher energy loss per turn.

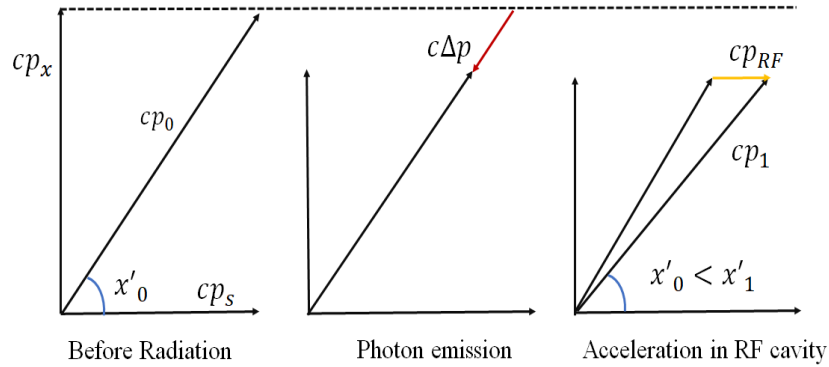


Fig. 1.14: Radiation damping phenomenon in horizontal plane.  $p_x$  and  $p_s$  are the momentum of electron in horizontal and longitudinal direction respectively.  $p_{RF}$  is the momentum provided by RF cavity.  $x'_0$  is the initial slope of electron and  $x'_1$  is the slope of electron after passing through RF cavity.

In an electron storage ring, emission of SR has damping effect on betatron oscillations as well as synchrotron oscillations (oscillations in longitudinal direction). This damping effect is called radiation damping. Fig.1.14 explains the phenomenon of radiation damping in the horizontal plane. To understand this, consider an electron oscillating about a closed orbit in horizontal plane having momentum  $p_0$ , after emission of SR in bending magnet, the momentum

of an electron reduced by  $\Delta p$  in the direction of SR emission. The loss of momentum is compensated by RF cavity. But, as shown in Fig. 1.14, after passing through the RF cavity only longitudinal component of momentum,  $p_s$ , is compensated and energy is restored. As a result, slope of the electron is decreased. As electron moves in the ring, slope of electron decreases turn by turn. This radiation damping phenomenon is true for each electron in the beam which emits radiation and it leads to reduction in beam emittance. Also, this radiation damping happens in each plane, i.e., horizontal, vertical and longitudinal planes. The rate equation of damping of horizontal beam emittance is given by [22]

$$\frac{d\epsilon_x}{dt} = -\frac{2}{\tau_x}\epsilon_x. \quad (1.78)$$

Similarly, for vertical beam emittance

$$\frac{d\epsilon_y}{dt} = -\frac{2}{\tau_y}\epsilon_y. \quad (1.79)$$

Damping times in horizontal, vertical and longitudinal planes are given by [22]

$$\tau_x = \frac{2E_0}{j_x U_0} T_0, \quad (1.80)$$

$$\tau_y = \frac{2E_0}{j_y U_0} T_0, \quad (1.81)$$

$$\tau_s = \frac{2E_0}{j_s U_0} T_0, \quad (1.82)$$

where  $T_0$  is the time period for one revolution and  $j_{i=x,y,s}$  is called damping partition number and are given as [22]

$$j_x = 1 - \frac{I_4}{I_2}, \quad j_y = 1, \quad j_s = 2 + \frac{I_4}{I_2}. \quad (1.83)$$

Here,  $j_x$ ,  $j_y$ , and  $j_s$  are called horizontal, vertical and longitudinal damping partition number, respectively.  $I_4$  is the fourth radiation integral and is defined as [22]

$$I_4 = \oint \frac{\eta_x(s)}{\rho(s)} \left( \frac{1}{[\rho(s)]^2} + 2k_1 \right) ds, \quad (1.84)$$

where  $k_1$  is the normalized quadrupole strength in the dipole magnet. This type of magnets are called combined function magnet. For a homogeneous field dipole magnet  $k_1$  becomes zero. The damping partition numbers satisfy an important relation called Robinson theorem which is given as [22]

$$j_x + j_y + j_s = 4. \quad (1.85)$$

Significance of Robinson theorem is this, damping in a particular plane can be influenced by damping in the other planes, because total damping number must be constant.

After so many turns, slope of electrons in the beam must go to zero, consequently beam emittance will reduce to zero if only radiation damping phenomenon occurs. However, there exist finite value of beam emittance called equilibrium or natural beam emittance. This is because of counter effect that occurs in the electron storage ring, called quantum excitation.

It is well established that emission of SR radiation is discrete and quantum in nature. As shown in Fig.1.15, after emission of photon from an on energy closed orbit electron, there is a sudden change in energy of the electron and it oscillates about an off-energy closed energy. In addition, electron beam consist of large number of electrons in the form of bunches. There is energy spread in these electron bunches. Therefore, photons emitted from different electrons are of different energy and also, random in nature [22, 23]. These sudden change in energies of electrons act as noise or fluctuation source in the phase space and act opposite to the radiation damping, which prevent the betatron amplitude of oscillations to be damped to zero. Due to quantum excitation, oscillations grow up unless they are balanced by radiation damping. Including these two phenomena a rate equation for horizontal emittance can be written as [22]

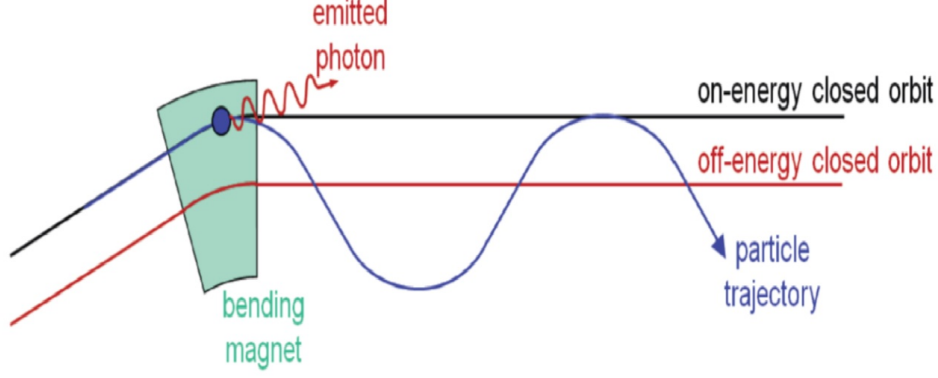


Fig. 1.15: Quantum Excitation phenomenon.

$$\frac{d\epsilon_x}{dt} = -\frac{2}{\tau_x}\epsilon_x + \frac{2}{\tau_x}C_q\gamma^2\frac{I_5}{j_x I_2}. \quad (1.86)$$

In eq.(1.86), first term arises from radiation damping and second term arises from quantum excitation. In the equilibrium condition,  $\frac{d\epsilon_x}{dt} = 0$ , and emittance is given by

$$\epsilon_{x0} = C_q\gamma^2\frac{I_5}{j_x I_2}. \quad (1.87)$$

$\epsilon_{x0}$  is called natural emittance and  $C_q = \frac{55}{32\sqrt{3}}\frac{\hbar}{m_0c}$ ,  $\hbar$  is the Plank constant divided by  $2\pi$ . For electron storage rings, its value is equal to  $C_q = 3.832 \times 10^{-12}\text{m}$ .  $I_5$  is the fifth radiation integral and is defined as [22]

$$I_5 = \oint \frac{\mathcal{H}_x(s)}{[\rho(s)]^3} ds. \quad (1.88)$$

$I_5$  depends on  $\mathcal{H}$  function and inversely proportional to cubic power of local radius of curvature.

The  $\mathcal{H}$  function is defined as [22]

$$\mathcal{H}_x = \gamma_x\eta_x^2 + 2\alpha_x\eta_x\eta_x' + \beta_x\eta_x'^2. \quad (1.89)$$

The  $\mathcal{H}_x(s)$  function depends on twiss parameters, dispersion and its derivative. There are two more radiation integral which are defined as [22]

$$I_1 = \oint \frac{\eta_x(s)}{\rho(s)} ds, \quad (1.90)$$

$$I_3 = \oint \frac{ds}{|\dot{\rho}(s)|^3}. \quad (1.91)$$

$I_1$  is related to the momentum compaction factor  $\alpha_c$ , which plays an important role in the longitudinal dynamics and  $I_3$  is related to equilibrium energy spread in a bunch, which is given by

$$\sigma_{\delta 0} = C_q \gamma^2 \frac{I_3}{j_s I_2}. \quad (1.92)$$

For y-direction, ideally there should not be any dispersion. Therefore,  $\mathcal{H}$  and hence fifth radiation integral must be zero. This implies that the vertical emittance must be zero. However, in deriving equation for the natural emittance, it is assumed that all photons were emitted directly along the instantaneous direction of motion of electron. In fact, photons are emitted with a distribution with angular width  $\frac{1}{\gamma}$  about the direction of motion of the electron [22]. This leads to some vertical recoil that excite vertical betatron motion, resulting a non-zero vertical emittance. An expression for lower limit of the vertical beam emittance, called quantum limit, is given by [22].

$$\epsilon_{y,min} = \frac{12}{55} \frac{C_q}{I_2} \oint \frac{\beta_y(s)}{|\dot{\rho}(s)|^3} ds. \quad (1.93)$$

Though vertical beam emittance has finite value, but, still it is much smaller than the natural beam emittance. Also, errors and betatron coupling in the practical electron storage ring, increase the vertical beam emittance. It is always desirable to make errors in the practical machine as small as possible to achieve quantum limit of vertical beam emittance.

Important mathematical relations are summarized in Table 1.1.

Table 1.1: Important mathematical relations [2, 22]

Radiation integral $I_1$	$\oint \frac{\eta_x(s)}{\rho(s)} ds$
Radiation integral $I_2$	$\oint \frac{ds}{[\rho(s)]^2}$

Radiation integral $I_3$	$\oint \frac{1}{ \rho^3 }$
Radiation integral $I_4$	$\oint \frac{\eta_x(s)}{\rho(s)} \left( \frac{1}{[\rho(s)]^2} + 2k_1 \right) ds$
Radiation integral $I_5$	$\oint \frac{\mathcal{H}_x(s)}{[\rho(s)]^3} ds$
Energy loss per turn	$88.575 \frac{[E(\text{GeV})]^4}{\rho}$
Natural emittance $\epsilon_x$	$C_q \gamma^2 \frac{I_5}{j_x I_2}$
Damping partition numbers	$j_x = 1 - \frac{I_4}{I_2}, j_y = 1, j_s = 2 + \frac{I_4}{I_2}$
Horizontal damping time $\tau_x$	$\frac{2E_0}{j_x U_0} T_0$
Vertical damping time $\tau_y$	$\frac{2E_0}{j_y U_0} T_0$
Longitudinal damping time $\tau_s$	$\frac{2E_0}{j_s U_0} T_0$
Robinson's theorem	$j_x + j_y + j_s = 4$
$\mathcal{H}$ function	$\gamma\eta^2 + 2\alpha\eta\eta' + \beta\eta'^2$
Equilibrium energy spread $\sigma_{\delta 0}$	$C_q \gamma^2 \frac{I_3}{j_s I_2}$

## 1.13 Different types of magnetic lattices and equilibrium emittance

In order to achieve low emittance different type of lattices are proposed such as theoretical minimum emittance (TME), double bend achromat (DBA), and triple bend achromat (TBA),

a combination of TME and DBA. Now a days multi bend achromat (MBA) lattice are used to achieve ultra low emittance in electron storage rings. Natural beam emittance can be written as averaged quantities as [20]

$$\epsilon_{x0} = C_q \gamma^2 \frac{I_5}{j_x I_2} = C_q \gamma^2 \frac{\langle \frac{\mathcal{H}_x(s)}{\rho^3(s)} \rangle}{\langle \frac{1}{\rho^2(s)} \rangle}. \quad (1.94)$$

For a lattice which utilizes isomagnetic dipole,  $\rho$  is constant and beam emittance is given by

$$\epsilon_{x0} = C_q \gamma^2 \frac{I_5}{j_x I_2} = C_q \gamma^2 \frac{\langle \mathcal{H}_x(s) \rangle}{j_x \rho}. \quad (1.95)$$

Storage ring having isomagnetic dipoles, the horizontal damping partition number  $j_x \sim 1$  and  $\langle \mathcal{H}_x \rangle$  is the average over the dipoles [20]. Therefore, to minimize emittance is equivalent to minimize  $\langle \mathcal{H}_x \rangle$  over the dipole with respect to  $\eta_x$  and  $\beta_x$ .

The theoretical minimum beam emittance in the isomagnetic lattice is given by [5]

$$\epsilon_{x,min} = F_{lat} C_q \gamma^2 \theta^3, \quad (1.96)$$

where  $\theta$  is the bending angle of the dipole.  $F_{lat}$  is called form factor, which depends on the particular magnetic cell structure. From eq.(1.96), it can be seen that beam emittance depends on third power of the bending angle. For a fixed energy electron storage ring  $C_q \gamma^2$  is constant. Therefore, emittance in a given storage ring with fixed energy can be reduced with dipoles with smaller bending angle. But small bending will lead to large number of dipoles to bend the electron by 360 deg and this leads to large size of storage ring, consequently cost of the storage ring will increase.

### 1.13.1 Theoretical minimum emittance (TME) lattice

In a TME lattice, there is a single dipole in the unit lattice cell. Dispersion and beta functions are symmetric with respect to centre of the dipole magnet as shown in Fig.1.16. After

minimizing  $\mathcal{H}_x$  with respect to horizontal beta function and horizontal dispersion function  $\eta_x$  over the dipole, the minimum of the average of  $\mathcal{H}_x$  function is given by [5, 20]

$$\langle \mathcal{H}_x \rangle = \frac{1}{12\sqrt{15}} \rho \theta^3, \quad (1.97)$$

where  $\rho$  and  $\theta$  are the radius of curvature and bending angle of the dipole. Values of  $\beta_x$  and  $\eta_x$  at the entrance and at centre of the dipole magnet are given as

$$\text{at the entrance of the dipole : } (\beta_0, \alpha_0, \eta_0, \eta'_0) = \left( \frac{8}{\sqrt{15}}L, \sqrt{15}, 6L\theta, -2\theta \right), \quad (1.98)$$

$$\text{at the centre of the dipole : } (\beta_c, \eta_c)_{TME} = \left( \frac{1}{\sqrt{60}}L, \frac{L\theta}{24} \right), \quad (1.99)$$

here  $L$  is the length of the dipole. Theoretical minimum emittance is given by

$$\epsilon_{x,TME} = \frac{1}{12\sqrt{15}} C_q \frac{\gamma^2 \theta^3}{j_x}. \quad (1.100)$$

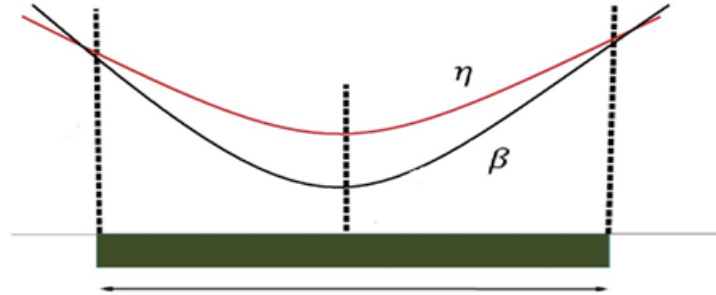


Fig. 1.16: Variation of horizontal beta and dispersion function in case TME lattice. Both functions have minima at the centre of the bending magnet.

For a TME lattice form factor is taken as 1. Though TME lattice has lowest minimum emittance. But they cannot be used for third generation synchrotron radiation sources due to requirement of zero dispersion at the location of IDs. Both horizontal beta function and dispersion function attain higher value in the quadrupoles, therefore, generate large negative

natural chromaticity. Therefore, much stronger sextupoles are required to correct the chromaticity. In addition, dispersion is nonzero at the ID straight section, which is not desirable. Hence, TME lattice is not the proper choice for the storage ring lattice. Therefore, a lattice called DBA is used which provide zero dispersion at location of IDs.

### 1.13.2 Double bend achromat (DBA)lattice

This type of lattice consists two bending magnets in the unit lattice cell to make an achromat. If dispersion and it derivative are zero at the entrance of the dipole magnet, it is called achromatic condition and lattice which provide achromatic condition is called achromat. The dispersion free region is utilized for installation of IDs. This type of lattice is most widely used in electron storage rings. In Fig.1.17, part of the achromat is shown. In this type of lattice minimum of beta function is not at the centre of the bending magnet. After minimizing  $\langle \mathcal{H}_x(s) \rangle$  with respect to  $\beta_x$  and  $\alpha_x$ , minimum of  $\langle \mathcal{H}_x \rangle$  is given by [20]

$$\langle \mathcal{H}_x \rangle_{MEDBA} = \frac{1}{4\sqrt{15}} \rho \theta^3, \quad (1.101)$$

with the condition on  $\beta_x$  and  $\alpha_x$  at the entrance as [20]

$$\beta_0 = \frac{6}{\sqrt{15}} L \quad \alpha_0 = \sqrt{15} \quad \gamma_0 = \frac{8\sqrt{5}}{\sqrt{3}}. \quad (1.102)$$

Minimum beam emittance is given by [5, 20]

$$\epsilon_{x,DBA} = \frac{1}{4\sqrt{15}} C_q \frac{\gamma^2 \theta^3}{j_x}. \quad (1.103)$$

After choosing optimum values of  $\beta_0 = \frac{6}{\sqrt{15}} L$  and  $\alpha_0 = \sqrt{15}$  at the entrance of the dipole, beta function achieves minimum value  $\beta_{x,minimum} = \frac{3}{4\sqrt{60}} L$  at  $s_0 = \frac{3}{8} L$  in the dipole magnet. From eq.(1.100) and eq.(1.103) we found that

$$\epsilon_{x,DBA} = 3\epsilon_{x,TME} \quad (1.104)$$

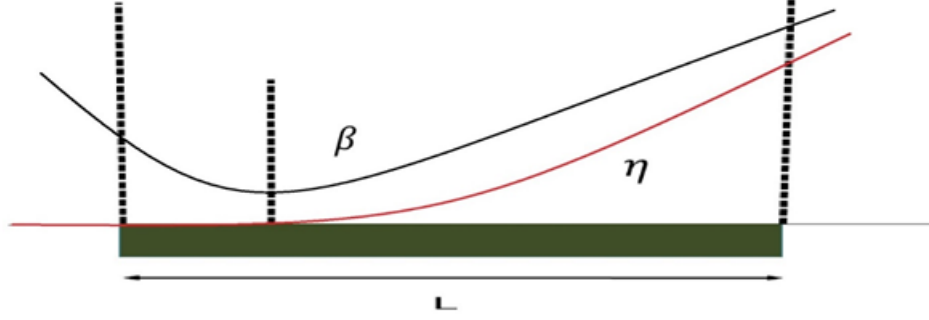


Fig. 1.17: Variation of horizontal beta and dispersion function in the first dipole of DBA lattice.

Dispersion and its derivative are zero at the entrance of the dipole.

Though form factor for DBA is three time higher than the TME, a practical storage ring in DBA configuration acquires even higher form factor than 3, generally, in the range of 3-10 [24]. For some storage rings, it may be higher than 10.

### 1.13.3 Multi bend achromat (MBA) lattice

To achieve much lower natural emittance, concept of MBA lattice was introduced. In MBA lattice more than two dipole magnets are normally used. In a MBA lattice, more number of TME dipoles are introduced between the two dipoles of DBA lattice. The minimum emittance in a MBA lattice is given by [5]

$$\epsilon_{x,MBA} = \frac{1}{12\sqrt{15}} \left( \frac{M+1}{M-1} \right) C_q \frac{\gamma^2 \theta^3}{j_x}, \quad (1.105)$$

where  $M$  is the number of dipole in the MBA lattice and for equal bending angle in all dipole used,  $\theta$  is the average angle of all dipoles. Now a days, MBA lattice is more preferred to achieve ultra low emittance in the electron storage rings.

## 1.14 RMS beam sizes

In dispersion free region, the RMS beam sizes and beam divergences in the transverse plane are defined by only betatron function and are given as [22]

$$\text{Horizontal plane: } \sqrt{\epsilon_x \beta_x(s)}, \quad \sqrt{\epsilon_x \gamma_x(s)}, \quad (1.106)$$

$$\text{Vertical plane: } \sqrt{\epsilon_y \beta_y(s)}, \quad \sqrt{\epsilon_y \gamma_y(s)}, \quad (1.107)$$

For a region where dispersion is finite, the RMS beam sizes and divergences are given by

$$\text{Horizontal plane: } \sqrt{\epsilon_x \beta_x(s) + (\eta_x \sigma_\delta)^2}, \quad \sqrt{\epsilon_x \gamma_x(s) + (\eta'_x \sigma_\delta)^2}, \quad (1.108)$$

$$\text{Vertical plane: } \sqrt{\epsilon_y \beta_y(s) + (\eta_y \sigma_\delta)^2}, \quad \sqrt{\epsilon_y \gamma_y(s) + (\eta'_y \sigma_\delta)^2}, \quad (1.109)$$

where  $\epsilon_x$  and  $\sigma_\delta$  are RMS beam emittance and RMS momentum spread.

## 1.15 Advance methods to improve beam emittance

In last few decades, new advance methods were introduced to reduce the beam emittance further, like transverse gradient, longitudinal gradient bend (LGB), and anti bend etc. in the dipole magnet. Here, we have discussed transverse gradient and LGB in a dipole.

Natural horizontal beam emittance as given in eq.(1.87) is

$$\epsilon_{x0} = C_q \gamma^2 \frac{I_5}{j_x I_2}. \quad (1.110)$$

Here, the first term  $C_q$  is constant and second term  $\gamma^2$  is also a constant as energy in the storage ring is fixed. Therefore, in order to reduce the beam emittance, only radiation integrals and horizontal damping partition number are to be optimized. This can be done in following two ways.

**Maximize  $j_x$ :** From eq.(1.84), if we introduce negative quadrupole gradient in dipole magnet in such a way that the quantity  $\frac{I_4}{I_2}$  becomes  $-ve$ , then  $j_x$  can be made greater than 1 and beam emittance will reduce. As Robinson's theorem puts a limit on  $j_x$ , the value of  $j_x$  can be increased up to 2 only. Also, if one increase the  $j_x$  above 2 by increasing  $k_1$ , the dipole will loose its dipole nature and behaves like a pure quadrupole and it is also difficult task to provide such gradient in the dipole magnet. It means, improving horizontal damping partition number, one can reduce beam emittance by a factor of 2. Physically, increasing horizontal damping partition number means rate of radiation damping will increase, i.e., electron beam will damp fast for the same quantum excitation.

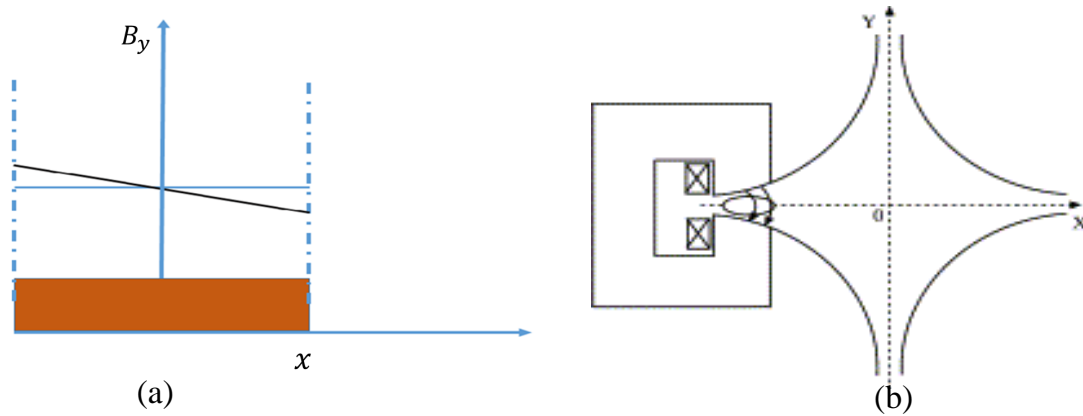


Fig. 1.18: (a) Linear variation of magnetic field along x-direction (black) and compared with homogeneous field (blue). (b) Shape of dipole to get linearly decreasing magnetic field.

Since bending of electron is in horizontal plane, there will not be any effect on  $j_y$ . Therefore,  $j_s$  will increase due to Robinson theorem. Also,  $j_s$  is inversely proportional to energy spread in the bunch [24], energy spread of bunch will increase and this leads to increase in bunch length that is not desirable in electron storage rings. In Fig. 1.18, a linearly decreasing magnetic field compared with homogeneous magnetic field is shown. At the center of dipole both have same value of field. The linearly decreasing magnetic field will provide quadrupole gradient in the dipole. Also, a curved shape of dipole is shown to produce linearly decreasing

magnetic field.

**Minimize the term  $\frac{I_5}{I_2}$ :**  $I_5$  contains  $\mathcal{H}$  function in the numerator which is defined in eq.(1.89) and  $\rho^3$  in the denominator. If, one is able to reduce the  $\mathcal{H}$  function or increase the radius of curvature or both in the dipole magnet, emittance will decreased naturally. To achieve this goal, a longitudinal variation in dipole field profile was introduced [10]. These dipoles then termed as longitudinal gradient bend (LGB). The LGB field profile instead of homogeneous magnetic field in the dipole causes  $\mathcal{H}$  function and radius of curvature to vary differently. In recent studies, it was established that LGB profile follows parabolic decay [24] of the magnetic field over the length of the dipole magnet. For achromat case, magnetic field decreases from high value at one end to low value at other end as shown in Fig. 1.19 [24]. This LGB profile helps in providing two major beam dynamical advantages: (i) reduction of beam emittance, and (ii) large dispersion at the sextupole location.

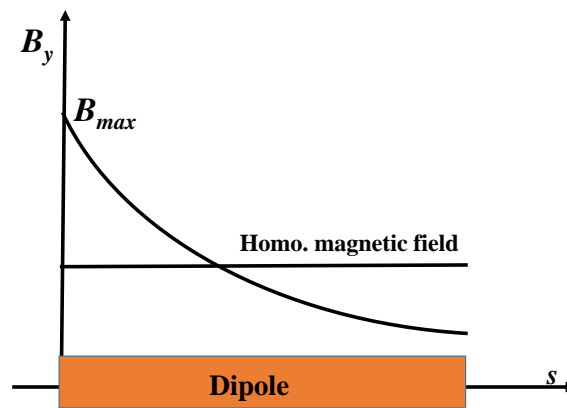


Fig. 1.19: Variation of longitudinal field profile in the dipole magnet of a DBA lattice

For a TME lattice, the magnetic field profile is such that its maximum occurs at the center of the dipole and field reduces symmetrically to lower value on either side as shown in Fig. 1.20 [24]. This LGB profile satisfy only one purpose, i.e., reduction of beam emittance.

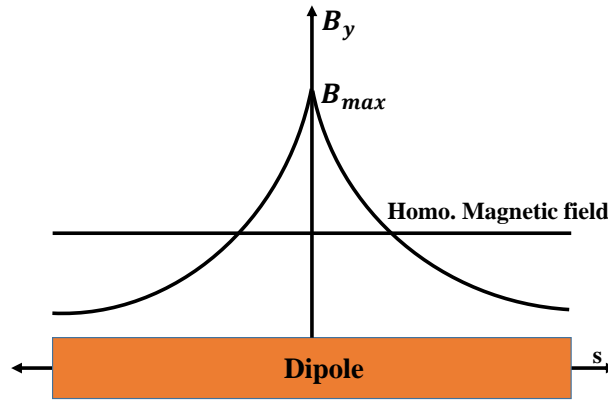


Fig. 1.20: Variation of longitudinal field profile in the dipole of TME lattice

Using this type of LGB profile dispersion will reduce at the centre of dipole and consequently  $\mathcal{H}$  function will reduce. This leads to reduction in beam emittance. Physically in both cases i.e achromat and TME, we are reducing the quantum excitation in the dipole magnet.

## 1.16 Indus-2 storage ring lattice

In India, there are two electron storage ring based SRSs namely Indus-1 and Indus-2, located at RRCAT, Indore. Indus-1, a 450 MeV energy synchrotron radiation source has circumference of 18 m, which provides SR in the vacuum ultraviolet range. Indus-2, which is a third generation electron storage ring, has energy 2.5 GeV and provides synchrotron radiation in the hard x-rays regime [3,4]. This radiation is very useful for variety of material study. A schematic layout of Indus-1 and Indus-2 synchrotron radiation source facility is shown in Fig. 1.21. The base line lattice of Indus-2 was designed for beam emittance of 58 nm.rad.

Both storage rings share a common injector system consisting of a 20 MeV microtron and 20-450/550 MeV booster synchrotron [3–5]. Unit lattice cell of Indus-2 is based on DBA or Chessman Green lattice. In unit lattice cell, there are 2 dipole magnets for bending of beam, 9 quadrupoles (4 focusing type and 5 defocusing type) for focusing and defocusing action of beam, 4 sextupoles (2 focusing and 2 defocusing) for chromaticity correction.

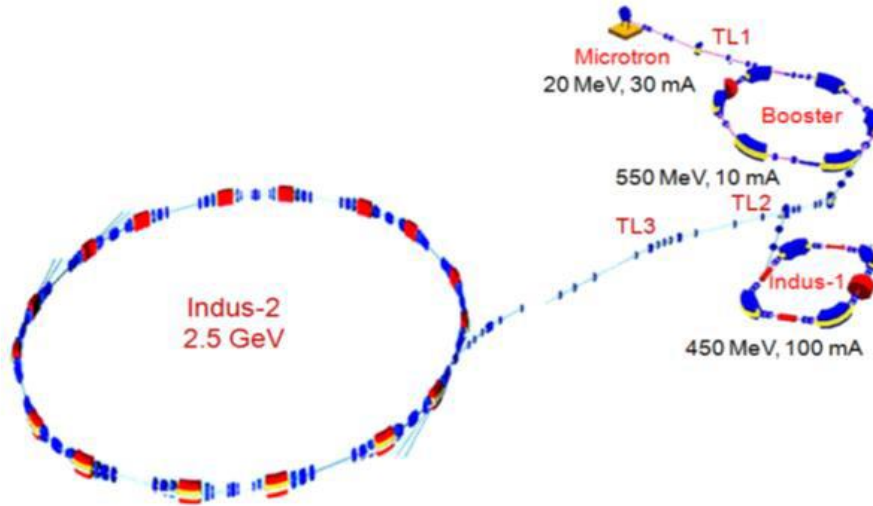


Fig. 1.21: Schematic layout of Indus Accelerator complex [3, 5].

In Table 1.2 different designed parameters of Indus-2 lattice are given and different magnetic elements with their maximum available strength are shown in Table 1.3.

Table 1.2: Different design parameters of Indus-2 storage ring

Beam Energy	2.5 GeV
Beam current	200-300 mA
Circumference	172.47 m
Beam Emittance, $\epsilon_x$	58 nm.rad
Betatron tune [ $\nu_x, \nu_y$ ]	[9.2, 5.2]
Natural chromaticity [ $\xi_x, \xi_y$ ]	[-19, -12]
Corrected chromaticity [ $\xi_x, \xi_y$ ]	[2, 2]
Momentum compaction factor, $\alpha_c$	$5.2 \times 10^{-3}$
Energy spread, $\sigma_\delta$	$9 \times 10^{-4}$
Damping time [ $\tau_x, \tau_y, \tau_s$ ]	[4.74, 4.62, 2.28] ms
Energy loss per turn	623 keV
Power loss	186.6 kW(BM)@ 300 mA

Table 1.3: Different magnetic elements of the Indus-2 storage ring.

S.No.	Name	Type	Length [m]	Max. Available Field	Total Number
1.	BM	Dipole (Rectangular type)	2.18	1.503 T	16
2.	Q1D	Defocusing Quadrupole	0.30	16 T m <sup>-1</sup>	16
3.	Q2F	Focusing Quadrupole	0.55	16 T m <sup>-1</sup>	16
4.	Q3D	Defocusing Quadrupole	0.40	16 T m <sup>-1</sup>	16
5.	Q4F	Focusing Quadrupole	0.40	16 T m <sup>-1</sup>	16
6.	Q5D	Defocusing Quadrupole	0.40	16 T.m <sup>-1</sup>	8
7.	SF	Focusing Sextupole	0.2	400 T m <sup>-2</sup>	16
8.	SD	Defocusing Sextupole	0.2	400 T m <sup>-2</sup>	16

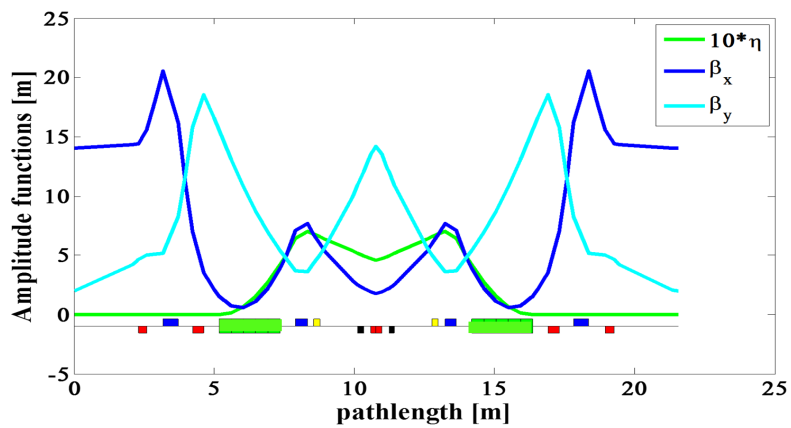


Fig. 1.22: Variation of beta and dispersion functions in Indus-2 unit lattice cell. Bending magnets are shown by green boxes, quadrupoles are in red and blue boxes and sextupoles are in yellow and black boxes.

Lattice functions for one unit lattice cell of Indus-2 are shown in Fig.1.22. This lattice is designed in such a way that dispersion acquires high value at sextupole location, maximum beta functions are less than 21 m through out the lattice cell.

Indus-2 is in regular operation. Therefore no changes in position and lengths of any magnetic element of Indus-2 lattice can be done. Beam emittance of Indus-2 lattice can be reduced by replacing homogeneous dipole with dipoles with LGBs. In this thesis work, studies with LGB in the dipole magnet has been done with two purposes, (i) lower the beam emittance, (ii) increase dispersion at sextupole location. In addition, building constraints are to be satisfied, i.e. all other hardware need not be shifted.

## 1.17 Indus-3 storage ring lattice

Indus-3, a 6 GeV electron storage ring, is a proposed high brightness synchrotron radiation source (HBSRS) at RRCAT. Baseline lattice has been designed to achieve emittance of  $\sim 150$  pm.rad. Indus-3 uses hybrid seven bend achromat lattice cell with ring circumference  $\sim 911.7$  m. The ultra low emittance of Indus-3 leads to brightness of the order of  $10^{20} - 10^{22}$  photons per second per unit angle per unit area in 0.1% bandwidth of considered wavelength with fully loaded IDs. In Fig. 1.23, the lattice functions for one unit lattice cell are shown with position of different magnetic elements. In the Table 1.4, different designed parameters are shown and the Table 1.5 shows numbers and strengths of different magnetic elements in Indus-3 lattice. A transverses quadrupole gradient have been provided in BM3 and BM4. That is why this lattice is a hybrid lattice. The strengths of quadrupoles are quite high. This leads to tight focusing of beam in the machine. The aperture size of Indus-3 is quite small compared to Indus-2 lattice.

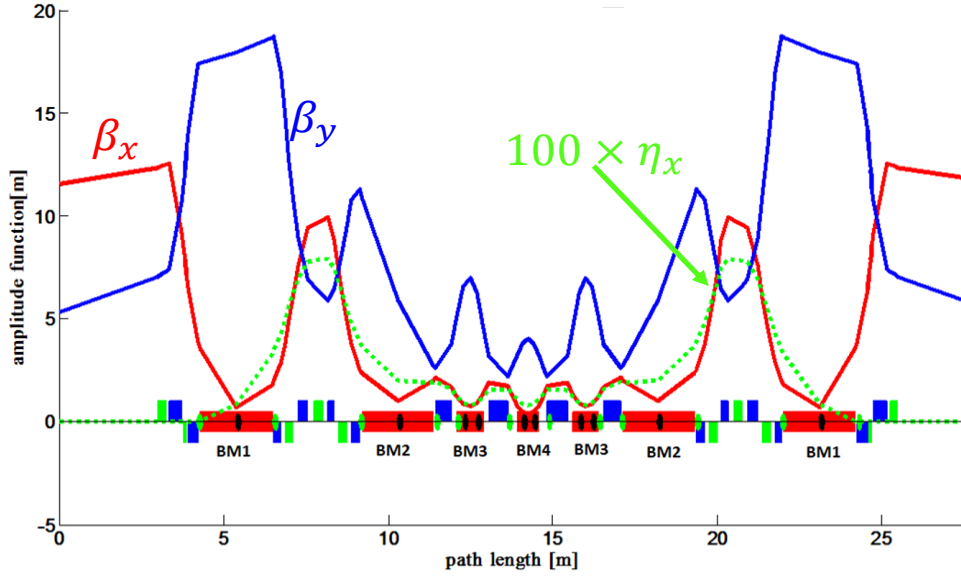


Fig. 1.23: Beta Functions of Indus-3 lattice cell. Boxes in red colour are dipole magnet, boxes in green colour are quadrupoles and boxes in blue colour are sextupole magnets.

Table 1.4: Different design parameters of Indus-3 storage ring.

Beam Energy	6.0 GeV
Beam current	200 mA
Circumference	911.798 m
Beam Emittance, $\epsilon_x$	149 pm.rad
Betatron tune $[\nu_x, \nu_y]$	[74.15, 24.22]
Natural chromaticity $[\xi_x, \xi_y]$	[-109.6, -80.9]
Corrected chromaticity $[\xi_x, \xi_y]$	[4, 4]
Momentum compaction factor, $\alpha_c$	$1 \times 10^{-4}$
Energy spread, $\sigma_\delta$	$1.02 \times 10^{-3}$
Damping time $[\tau_x, \tau_y, \tau_s]$	[8.72, 14.84, 11.44] ms
Energy loss per turn	2.46 MeV
Power loss per turn	491.7 kW(BM)@ 200 mA

Table 1.5: Different magnetic elements of the Indus-3 lattice.

S.No.	Name	Element	Length [m]	Required Field	Total Number
1.	BM1	Dipole	2.17	0.28 T	64
2.	BM2	Dipole	2.17	0.28 T	64
3.	BM3	Dipole	0.4	0.63 T	64
4.	BM4	Dipole	0.325	0.75 T	32
5.	Q1F	Quadrupole	0.40	40.8 T m <sup>-1</sup>	16
6.	Q2D	Quadrupole	0.30	42.8 T m <sup>-1</sup>	64
7.	Q3D	Quadrupole	0.20	42.2 T m <sup>-1</sup>	64
8.	Q4F	Quadrupole	0.30	71.2 T m <sup>-1</sup>	64
9.	Q5F	Quadrupole	0.20	54.8 T m <sup>-1</sup>	64
10.	Q6D	Quadrupole	0.25	60.6 T m <sup>-1</sup>	64
11.	Q7D	Quadrupole	0.50	36.4 T m <sup>-1</sup>	64
12.	Q8F	Quadrupole	0.60	73.6 T m <sup>-1</sup>	64
14.	S1 (D)	Sextupole	0.25	3580 T m <sup>-2</sup>	64
15.	S2 (F)	Sextupole	0.25	4752 T m <sup>-2</sup>	64
16.	S3 (D)	Sextupole	0.250	2880 T m <sup>-2</sup>	64
17.	SH1 (F)	Harmonic Sextupole	0.25	1462 T m <sup>-2</sup>	64
18.	SH2 (D)	Harmonic Sextupole	0.1	2748 T m <sup>-2</sup>	64

F: Focusing, D: Defocusing

As there are transverse gradient in BM3 and BM4, therefore, only BM1 and BM2 are left which have homogeneous field. These dipoles can be chosen to study LGB profiles.

In this Chapter, a brief introduction of accelerator physics relevant to this thesis work is presented which are very important in storage ring design. Many concepts like, lattice functions, betatron tune, beam emittance, chromaticity etc are discussed. In addition, effect of SR on the beam emittance and concept of radiation damping and quantum excitation which leads to equilibrium emittance are also discussed. Different types of low emittance lattice cell and advanced method to reduce the beam emittance are also described. Though, beam emittance reduction is desirable in any storage ring, however for successful operation of the facility, various other lattice parameters need to be optimized or constrained. For example, betatron tunes should be far away from dangerous resonances, horizontal beta function should be large at injection point, large value of dispersion is desirable at sextupole locations for effective chromaticity correction, large dynamic aperture for good beam life time and injection efficiency etc. These aspects make lattice design of a storage ring a complex optimization problem. This requires a better understanding of optimization techniques. Various optimization techniques are discussed in Chapter 2 and optimized result for Indus-2 and Indus-3 are presented in Chapter 3 and 4.

## **Chapter 2**

# **Optimization techniques used in accelerators**

As discussed in Chapter 1, in lattice design of a storage ring, many conflicting objectives like beam emittance, dynamic aperture, desired lattice parameters, with large number of variables such as strengths of different magnetic elements, position of different magnetic elements etc., and many constraints like maximum achievable strengths of magnetic elements, constraints on lattice functions, betatron tune etc., are needed to be optimized. These aspects make the storage ring lattice design a complicated multi-objective optimization problem. Therefore, numerical techniques that can handle these complicated optimization problem are required. In recent past, classical, like simplex method, as well as modern methods, which are evolutionary methods, were used to handle these optimization problems. Evolutionary algorithms were introduced in the field of accelerator design in recent years [5]. These evolutionary methods found to be very efficient in designing of lattice of storage ring and set a new trend in optimizing the accelerator performance in simulations as well as in real operation. In this Chapter, two non gradient optimization methods, Nelder-Mead algorithm, a classical method and genetic

algorithm, an evolutionary method are discussed in detail. These methods will be used to perform numerical optimization of LGB profiles in a dipole magnet and the studies are presented in Chapter 3.

The meaning of optimization of an objective function, which depends on one or more independent variables, is to find the values of the independent variables for which the objective function has extremum (either minima or maxima). If there is only one objective function that needs to be optimized, then this optimization problem is called **single objective optimization problem** [25], which is discussed in Section 2.1. On the other hand, if there are more than one objective function that need to be optimized, then this optimization problem is called **multi-objective optimization problem**, which is discussed in Section 2.2.

## 2.1 Single objective optimization problem

In a single objective optimization problem, an objective function  $f(\vec{x})$ , is needed to be optimized which depends on one or more independent variables  $\vec{x} = (x_1, x_2, x_3, \dots, x_n) = x_i$ ; where  $i = 1, 2, 3, \dots, n$ ;  $n$  is the number of independent variables. Single objective optimization problem can be written, mathematically, as [25]

$$\begin{aligned}
 & \text{Minimize or Maximize } f(\vec{x}) \\
 & \text{Subject to } \quad g_j(\vec{x}) \geq 0, \quad j = 1, 2, 3, \dots, J, \\
 & \quad \quad \quad h_k(\vec{x}) = 0, \quad k = 1, 2, 3, \dots, K, \\
 & \quad \quad \quad x_i^L \leq x_i \leq x_i^U, \quad i = 1, 2, 3, \dots, n,
 \end{aligned} \tag{2.1}$$

where  $g_j$ 's are  $J$  inequality constraints,  $h_k$ 's are  $K$  equality constraints,  $x_i^L$  and  $x_i^U$  are lower and upper bound for  $i^{\text{th}}$  independent variable, respectively. To optimize such single objective function  $f(\vec{x})$ , one needs to find those values of independent variables for which  $f(\vec{x})$  has extremum (maximum or minimum) value. Most of the algorithms were developed to solve

either minimization or maximization of objective functions. Hence, it was a difficult task to handle mixed optimization problems. Therefore, to handle such optimization problems, duality principle [25] was introduced, where any maximization problem can be converted into minimization problem by multiplying the objective function by -1.

To solve single objective optimization problems, various classical methods, also called derivative based methods, like Newton's method, steepest descent method, and quasi-Newton's method, were developed [5]. In these methods, the objective function must be differentiable upto first order (gradient) and sometimes, second partial derivatives (hessian) are required. But in most of the real world problem, the first or second partial derivatives of the objective functions are not always possible. Therefore, other methods called direct search methods, were developed to solve single optimization problem.

The simplest direct search method is the "Brute Force Method". Here, the search domain is divided into grids, which are visited point by point, and whenever best one is found, best found minimizer is updated. This method is also called sampling method. But this method has several drawbacks like there is strong dependence of grid size on the problem and exponential growth with grid size. Also search time increases exponentially. Another search method that tries to avoid these difficulties is **Nelder-Mead method**. In the following Section, the Nelder-Mead algorithm is discussed.

### 2.1.1 Nelder-Mead method

Nelder-Mead algorithm is designed to solve the classical unconstrained single objective optimization problem. It uses a variable shape simplex. A simplex in  $\mathbb{R}^n$  space is a convex hull of  $n + 1$  vertices, for example, in two dimensions, the simplex is a triangle and in three dimensions, it is a tetrahedron.

A simplex based direct search method begins with a set of  $n+1$  points  $\vec{x}_1, \vec{x}_2, \dots, \vec{x}_{n+1} \in$

$\mathbb{R}^n$  that are considered as the vertices of working simplex  $S$ . Here, each  $\vec{x}_i; i = 1, 2, \dots, n + 1$  is an initial solution of objective function. There are many methods to create initial simplex like Spendley's et al regular simplex, axis by axis simplex, Pfeffer's method etc [26]. Pfeffer's method for generating initial simplex is described below.

In the Pfeffer's method, two positive quantity  $\tau_u$  and  $\tau_z$  are defined, where  $\tau_u$  is used for usual components of  $\vec{x}_0$ , where  $\vec{x}_0$  is the user defined initial guess of solutions, and  $\tau_z$  is used for the case where one component of  $\vec{x}_0$  is zero. The standard values of  $\tau_u$  and  $\tau_z$  are

$$\tau_u = 0.05 \quad \text{and} \quad \tau_z = 0.00025.$$

The first vertex of the initial simplex is chosen as initial guess  $\vec{x}_0$  and can be written as

$$\vec{x}_1 = \vec{x}_0. \tag{2.2}$$

The other vertices are defined as

$$(\vec{x}_i)_j = \begin{cases} (\vec{x}_0)_j + \tau_u(\vec{x}_0), & \text{if } j = i - 1 \quad \text{and} \quad (\vec{x}_0)_j \neq 0, \\ \tau_z, & \text{if } j = i - 1 \quad \text{and} \quad (\vec{x}_0)_j = 0, \\ (\vec{x}_0)_j, & \text{if } j \neq i - 1, \end{cases} \tag{2.3}$$

for vertices  $i = 2, \dots, n + 1$  and components of initial guess  $j = 1, \dots, n$ . After calculating initial simplex, this algorithm perform some operation for one iteration which are discussed below [5, 27]

1. **Ordering:** In order to perform the algorithm, the vertices of  $S$  are ordered with respect to the function values as

$$f(\vec{x}_1) \leq f(\vec{x}_2) \leq f(\vec{x}_3) \leq \dots \leq f(\vec{x}_n) \leq f(\vec{x}_{n+1}).$$

Objective function values  $f(\vec{x}_{n+1})$ ,  $f(\vec{x}_n)$  and  $f(\vec{x}_1)$  are called worst, second worst and best points.

2. **Centroid:** After ordering function values at vertices, centroid  $\vec{c}$  of all vertices, except worst vertex, is calculated.

$$\vec{c} = \frac{1}{n} \sum_{i=1}^n \vec{x}_i. \quad (2.4)$$

3. **Transformation:** After calculating centroid, new working simplex is found from the current one by replacing only the worst vertex  $\vec{x}_{n+1}$  with a better point by using reflection, expansion and contraction. If iteration succeeds, the accepted point becomes the new vertex of the working simplex. If this fails, shrink the simplex towards the best vertex  $\vec{x}_1$ . In this case,  $n$  new vertices are computed.

- **Reflection:** In reflection, reflection point,  $\vec{x}_r$ , is calculated as

$$\vec{x}_r = \vec{c} + \alpha(\vec{c} - \vec{x}_{n+1}), \quad \text{and} \quad f_r = f(\vec{x}_r). \quad (2.5)$$

Here,  $\alpha$  is reflection coefficient. If  $f_1 \leq f(\vec{x}_r) < f(\vec{x}_n)$ , accept point  $\vec{x}_r$  and terminate the iteration here and go to the step 1 for next iteration.

- **Expansion:** If  $f_r < f_1$ , i.e., objective function has lower value at reflection point than the best point, then expansion operation is performed and expansion point  $\vec{x}_e$  is calculated as

$$\vec{x}_e = \vec{c} + \gamma(\vec{x}_r - \vec{c}) = \vec{c} + \alpha\gamma(\vec{c} - \vec{x}_{n+1}) \quad \text{and} \quad f_e = f(\vec{x}_e). \quad (2.6)$$

Here,  $\gamma$  is expansion coefficient. If  $f_e < f_r$ , accept  $\vec{x}_e$  and terminate the iteration. Otherwise, if  $f_e \geq f_r$ , accept  $\vec{x}_r$  and terminate the iteration here and go to the step 1 for next iteration. The expansion of the simplex is applied only if  $f_e < f_r < f_1$ .

- **Contraction:** if  $f_r \geq f_n$ , contraction is performed between best point and better of  $\vec{c}$  and  $\vec{x}_{n+1}$ , then contraction point,  $\vec{x}_c$  is calculated, which can be either outside or inside.

– **Outside:** If  $f_n \leq f_r < f_{n+1}$  (i.e.,  $\vec{x}_r$  is strictly better than  $\vec{x}_{n+1}$ ). In this case, outside contraction is performed and contraction point,  $\vec{x}_c$ , is calculated as

$$\vec{x}_c = \vec{c} + \beta(\vec{x}_r - \vec{c}) = \vec{c} + \beta\alpha(\vec{c} - \vec{x}_{n+1}) \quad \text{and} \quad f_c = f(\vec{x}_c). \quad (2.7)$$

Here,  $\beta$  is contraction coefficient. If  $f_c \leq f_r$ , accept  $\vec{x}_c$  and terminate the iteration and go to the step 1 for next iteration. Otherwise, shrink operation is performed.

– **Inside:** If  $f_r \geq f_{n+1}$ , inside contraction is performed and calculated as

$$\vec{x}_c = \vec{c} - \beta(\vec{c} - \vec{x}_{n+1}) \quad \text{and} \quad f_c = f(\vec{x}_c). \quad (2.8)$$

If  $f_c < f_{n+1}$ ,  $\vec{x}_c$  is accepted and terminate the iteration. Otherwise, perform the shrink operation.

• **Shrink:** In this operation,  $n$  vertices are computed as

$$\vec{x}_j = \vec{x}_l + \delta(\vec{x}_j - \vec{x}_l) \quad \text{and} \quad f_j = f(\vec{x}_j), \text{ for } j = 1, 2, \dots, n + 1 \text{ with } j \neq 1. \quad (2.9)$$

Here,  $\delta$  is shrink coefficient. The shrink transformation was introduced to prevent the algorithm from failing in the following case.

A failed contraction is much rarer, but it can occur when a valley is curved and one point of the simplex is much farther from the valley bottom than the others. Contraction may then cause the reflected point to move away from the valley bottom instead of towards it. Further contractions are then useless. The action proposed, contracts the simplex towards the lowest point, and will eventually bring all points into the valley.

In Fig. 2.1 and Fig. 2.2, different operation of Nelder-Mead algorithm for 2-D case are shown. In these figures,  $\vec{x}_3$  is the worst vertex for the simplex.

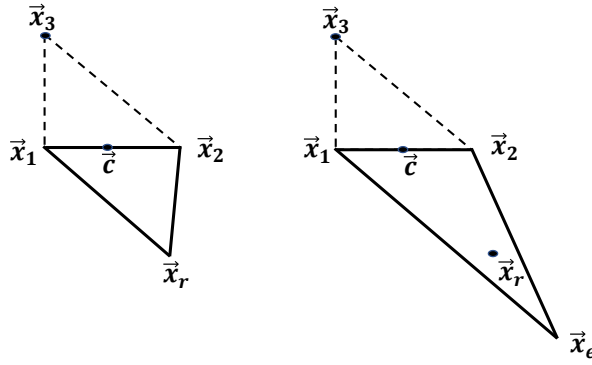


Fig. 2.1: Reflection (left) and expansion (right) of Nelder-Mead simplex.

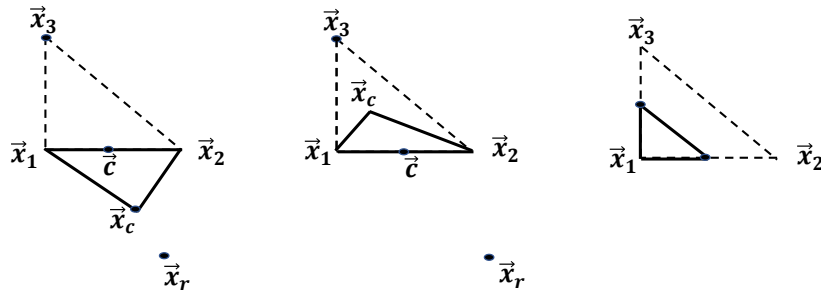


Fig. 2.2: Outside contraction (left), inside contraction (middle) and shrink (right) of Nelder-Mead simplex.

Different coefficients should satisfy the following constraints [27]

$$\alpha > 0, \gamma > 1, \gamma > \alpha, 0 < \beta < 1, 0 < \delta < 1.$$

The standard values of these parameters are

$$\alpha = 1, \gamma = 2, \beta = \frac{1}{2}, \delta = \frac{1}{2}.$$

For a practical implementation of the Nelder-Mead algorithm, it must include a test that ensures termination in a finite amount of time [28]. (i) Domain convergence or termination test: It becomes true when the working simplex  $S$  is sufficiently small in some sense. (ii) Function value convergence test: It become true when function values  $f_j$  are close enough in

some sense. (iii) No convergence test: It become true if the number of iteration or function evaluation exceeds some prescribed maximum allowed value.

In MATLAB, Nelder-Mead algorithm is coded with the name *fminsearch* and has been used in the present thesis for the optimization of LGB profile in a dipole magnet of a low emittance lattice cell.

## 2.2 Multi-objective optimization

In multi-objective optimization problems, a set of objective functions,  $f_m$ ;  $m = 1, 2, 3, \dots$ ,  $M$ , need to be optimized simultaneously. These objective functions can be defined in a vector form as

$$\vec{f}(\vec{x}) = (f_1, f_2, f_3, \dots, f_M), \quad (2.10)$$

here  $M$  is the number of objective function. Each  $f_m$  is a function of  $\vec{x} = (x_1, x_2, x_3, \dots, x_n)$ . Vector objective function  $\vec{f}$  has to be optimized with linear or non-linear constraints within variable bounds [25]. In mathematical form, optimization problem becomes

$$\begin{aligned} \text{Minimize} \quad & f_m(\vec{x}), \quad m = 1, 2, 3, \dots, M, \\ \text{Subject to} \quad & g_j(\vec{x}) \geq 0, \quad j = 1, 2, 3, \dots, J, \\ & h_k(\vec{x}) = 0, \quad k = 1, 2, 3, \dots, K, \\ & x_i^L \leq x_i \leq x_i^U, \quad i = 1, 2, 3, \dots, n, \end{aligned} \quad (2.11)$$

$J$  and  $K$  are the number of inequality and equality constraints respectively.  $x_i^L$  and  $x_i^U$  are lower and upper bounds for  $i^{th}$  independent variable. One must find vector  $\vec{x}$  such that each objective function achieves minimum value.

In real world multi-objective optimization, there may be conflicting nature of objective functions, i.e., one function can only be improved at the cost of deteriorating the other functions. In such cases, there does not exist unique optimal solution. There exist a number of solutions

which all are optimal. But, for a practical point of view user always needs a single optimal solution, no matter whether the associated optimization problem is single objective or multi-objective. Therefore, in multi-objective problem one must find a set of all optimal solution by considering all objectives equally important. After a set of all optimal solution is found, one can use higher level qualitative information associated with each objective to make a choice. Therefore, there is a two step process for an ideal multi-objective optimization procedure [25].

**Step 1** Find multiple trade-off optimal solutions with a wide range of values for objectives.

**Step 2** Choose one of the obtained solution using higher level information.

But, if for a particular problem a preference factor is known for each objective, then, there is no need to follow above two step process. One can assign preference factor to each objective and form a composite single objective [see Section 2.3]. This procedure is called a preference based multi-objective optimization. Using different preference vector, one can find many optimal solutions. But, it is important to realize that the trade-off solution is largely sensitive to preference vector used in forming composite function. A change in preference vector will result in a different trade-off solution and any arbitrary preference vector may not result in a trade-off optimal solution to all problems. Besides this difficulty, finding a relative preference vector itself is highly subjective and not straightforward. One of the classical method to solve multi-objective optimization problem is discussed in the following Section.

## **2.3 Classical methods for multi-objective optimization problems (MOOP)**

Many classical methods were developed to solve MOOP like weighted sum method, epsilon constraint Method, weighted matrix methods, rotated matrix methods etc. [25]. Weighted sum method, a preference based approach for solving MOOP, is described here.

Weighted sum method is useful if one knows about weight factors that must be given to each objective function. One can write optimization problem with composite function as [25]

$$\begin{aligned}
 f(\vec{x}) &= \sum_{m=1}^M w_m f_m \\
 \text{Subject to } \quad g_j(\vec{x}) &\geq 0, \quad j = 1, 2, 3, \dots, J, \\
 h_k(\vec{x}) &= 0, \quad k = 1, 2, 3, \dots, K, \\
 x_i^L &\leq x_i \leq x_i^U, \quad i = 1, 2, 3, \dots, n,
 \end{aligned} \tag{2.12}$$

where  $\sum_{m=1}^M w_m = 1$  and  $w_m$  is the weight factor for  $m^{\text{th}}$  objective function, which satisfy

$$0 \leq w_m \leq 1.$$

This method is the simplest way to solve MOOP. In this method, each objective  $f_m$  must have same functional behaviour, i.e., each function must have minima. Otherwise this method will not work.

Most of the classical methods use a deterministic procedure for approaching the optimum solution. These classical algorithms start from a random guess solution. After that, based on pre-specified transition rules, the algorithm finds a search direction, which is often arrived at by considering local information. Now, an unidirectional search is performed along the search direction to find the best solution. This best solution becomes the new solution and the above procedure is continued for a number of times. These methods are fast converging, however, they may converge to local minima. It is, therefore, recommended to run the method for few times to achieve a reasonable solution. In addition, these methods have many user defined parameters, for example in weighted sum method each weight factor,  $w_i$  must be defined and it is difficult to decide for an arbitrary optimization problem.

To avoid these difficulties, the evolutionary algorithms (EA) were introduced in MOOP. One of the most striking difference between classical search and EA is that in each iteration,

EA uses a population or set of random solutions. Therefore, the outcome of an EA is also a population of solution. If there is a single optimum in an optimization problem, all EA population will converge to that optimum solution. However, if there are multiple optimal solution for an optimization problem, then EA can capture all optimal solution in its final population. This ability makes EA an unique method in solving multi-objective optimization problem.

## **2.4 Evolutionary algorithm for optimization problems**

In 1975, Holland introduced the genetic algorithms (GA), a modern optimization method, to handle MOOP which allows optimization algorithm to find global optimal solutions [25]. After that many methods were developed. In 1983, the simulated annealing algorithm was introduced by Kirkpatrick et al. [29] and in 1995, Kennedy and Eberhart introduces another recipe in the optimization, a particle swarm optimization (PSO) [30, 31]. In 1995, differential evolution (DE) algorithm was introduced by Storn and Price [32]. These advance optimization methods belong to population based optimization methods, which are a class of evolutionary algorithms. These methods for optimization have proven their effectiveness in real world problem where the objective functions and the constraints are discontinuous and non differentiable.

The working of GA is based on the natural evolution and governed by Darwin's principle of survival of fittest which says that [5]

1. If above-average offspring is generated by genetic processing, usually it survives longer than an ordinary individuals survives. Therefore, it has more chances to produce offspring which have some of its qualities better than an average individual.
2. On the other hand, if a below-average offspring is created by a genetic processing, it

generally does not survive longer and eliminated quickly from the population.

This suggest that individuals in the population that are most fit amongst all others will survive in the next generation. This is the principle of genetic algorithm which is implemented in mathematical form and used as the global search algorithms and is discussed below.

### **2.4.1 Genetic algorithm**

The genetic algorithm (GA) is well established in the field of accelerator design. Since, GA uses population based approach, therefore, constraints can be handle in much better way than classical methods.

In all real optimization problems, there may be the case where domain of the problem is not known. In that case, GA initiates its search from a random population of the solution. If a termination criterion is not satisfied, different operators like reproduction, crossover and mutation are applied to update solutions. One iteration of these operators is called one generation. A flow chart for one iteration of genetic algorithm is shown in the Fig. 2.3 and various steps involved in genetic algorithm is discussed in the following Sections [5]

#### **1. Population initialization (P)**

According to the problem range and constraints at any generation, initial population is initialized. Familiar way to generate initial population is uniform distribution or Gaussian distribution of the variables. This distribution must be generated within the upper and lower limits of the variables. After the first population is created, GA assign fitness to each solution. If the termination criteria is not satisfied then GA performs reproduction, crossover and mutation operations to create population, called children or offsprings, for the next generation which are discussed below.

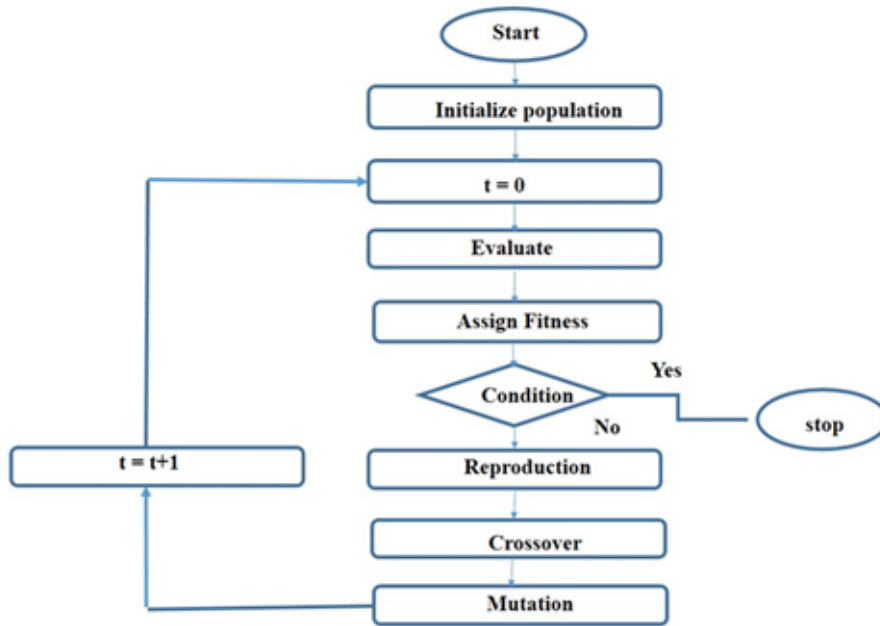


Fig. 2.3: Various steps involved in Genetic Algorithm.

## 2. **Reproduction or selection**

In the reproduction or selection method, more copies of a solution, which has highest fitness, are reproduced. There are many selection methods for example tournament selection, roulette wheel selection, ranking selection etc. Tournament selection is more popular among other selection methods due to its simple implementation. In this selection method  $n$  number of solutions are picked randomly and they compete with each other. The solution which has highest fitness, wins. This solution goes into next generation. The number of solutions which compete each other in the tournament is called as tournament size. Normally, the tournament size is taken to be two and the tournament selection method is called a binary tournament selection.

## 3. **Crossover**

Crossover operator in GA utilizes two or more parent solutions to generate offspring of the reproduced population which is based on selection method. Simulated binary crossover (SBX) is widely used among the available crossover operators [25]. Two

offspring  $(x_{o1}, x_{o2})$  solutions from two distinct parent solution  $(x_{p1}, x_{p2})$  are generate by SBX method using following set of equations [25]

$$\begin{aligned} x_{o1} &= \frac{1}{2}[(1 + \beta_i)x_{p1} + (1 - \beta_i)x_{p2}], \\ x_{o2} &= \frac{1}{2}[(1 - \beta_i)x_{p1} + (1 + \beta_i)x_{p2}], \end{aligned} \quad (2.13)$$

where  $\beta_i$  can be calculated using following relation [5]

$$\beta_i = \begin{cases} (2q_i)^{-(\eta_c+1)} & ; \quad q_i \leq 0.5, \\ \left(\frac{1}{2-2q_i}\right)^{-(\eta_c+1)} & ; \quad \text{otherwise,} \end{cases} \quad (2.14)$$

where  $q_i \in (0, 1)$  is a random number.  $\eta_c$  is a parameter that controls the crossover process. Generated offspring solution are close to the parent solution if value of  $\eta_c$  is high, and a small value of  $\eta_c$  allows the distant solution to be selected as offspring.

#### 4. Mutation

Mutation in GA has same meaning as in natural evolution, i.e., changes in genes. Here, a small change in a solution is done to mutate it. Mutation operation is performed after selection and crossover operations. One of the mutation method is polynomial mutation. It is given as [25]

$$x_{om} = x_o + \Delta_{max}\bar{\delta}_i, \quad (2.15)$$

where  $\Delta_{max} = (x_i^{(U)} - x_i^{(L)})$  and parameter  $\bar{\delta}_i$  is calculated as

$$\bar{\delta}_i = \begin{cases} (2r_i)^{-(\eta_m+1)} & ; \quad r_i < 0.5, \\ 1 - [2(1 - r_i)]^{-(\eta_m+1)} & ; \quad r_i \geq 0.5, \end{cases} \quad (2.16)$$

where  $r_i \in (0, 1)$  is a random number and  $\eta_m$  is a parameter that controls the mutation process. If  $\eta_m = 0$ , the independent variation  $-\Delta_{max}\bar{\delta}_i$  are uniformly distributed between  $\Delta_{max}$  to  $\Delta_{max}$ . As  $\eta_m$  is increased largely,  $\bar{\delta}_i$  approaches towards zero. It means that no mutation is applied. Therefore  $x_{0m} = x_0$

These operations generates the population for the next generation  $t + 1$ . This process continues until the stopping criteria is satisfied.

Genetic algorithms can be used to solve single as well as multi-objective optimization problems. Single objective optimization problem is defined in Section 2.1. In MATLAB, single objective genetic algorithm is implemented as a code "ga" and widely used in accelerator design.

## 2.4.2 Multi-objective genetic algorithm

Most of the multi-objective optimization problem contains conflicting objectives, for example, in lattice design of a storage ring one need small beam emittance and sizeable dynamic aperture. These two objectives are example of conflicting objectives. one cannot achieve lower emittance without worsening the dynamic aperture [5].

One of the goal of an ideal multi-objective is to find many trade-off solutions. Solutions which satisfy all constraints and non dominated by each others are called Pareto optimal solution and trade-off of Pareto optimal solutions is called Pareto optimal front [25]. A single objective GA can be converted into a multi-objective optimizer with following steps: (i) emphasize is given to the non-dominated solution in order to progress the solution towards the optimal solution, (ii) to maintain diversity in the solution, emphasize is given to less-crowded solution, (iii) to achieve fast convergence close to the true Pareto optimal front, emphasize is given to best solutions.

To address these three issues, elitist non dominated sorting GA is developed to convert single objective GA to multi-objective GA [5, 25]. Its working principle is shown in Fig. (2.4). The parent population ( $P_t$ ) of size  $N$  is generated randomly and off-springs ( $Q_t$ ) of size  $N$  are generated using GA operators at generation  $t$ . Together  $P_t$  and  $Q_t$  makes a population  $R_t$  of size  $2N$ . This combined population is sorted into number of Pareto optimal fronts using non

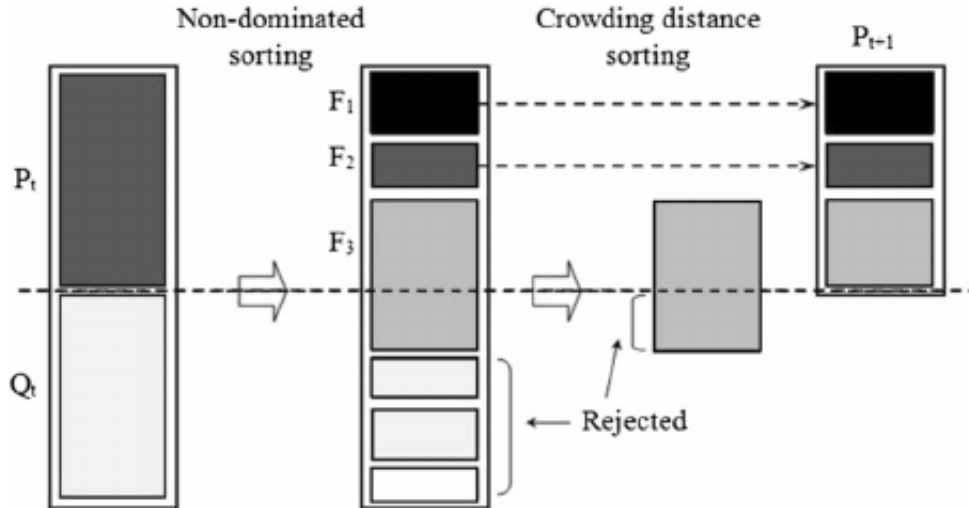


Fig. 2.4: NSGA-II procedure for one iteration [25].

dominated sorting. The first front  $F_1$  is completely non dominated set. The second front  $F_2$  is dominated by members of  $F_1$  only. This process is continued to get more and more optimal fronts. We assign fitness value 1 to  $F_1$ , fitness value 2 to  $F_2$ , and so on. A new parameter known as crowding distance, which measures how close the individual is to its neighbour individual, is calculated for each individuals. Large value of crowding distance provides better diversity in the population [5].

The parent population  $P_{t+1}$  of size  $N$  in the next generation are selected from non dominated solution starting from the best solutions or best optimal fronts and so on. When the number of population become  $N$ , rest of the solutions are simply rejected. This process of selecting parent population from previous generation continued until termination criteria is not satisfied. In MATLAB multi-objective GA is implemented with the code name *gamultiobj*.

In MATLAB, a complete package of simulation code with name Accelerator Toolbox (AT) [33], has been developed at SLAC worldwide. This code calculates all lattice parameters of a storage ring like emittance, momentum compaction factor, damping times, damping partition numbers, energy loss per turn etc. Also transfer matrix for an element or whole ring can be calculated. A program using AT can be written for a lattice design. AT generates data for plot

of beta function, dispersion function etc. and tracking can also be done to calculate dynamic aperture.

In this Chapter, different optimization techniques, in particular Nelder-Mead algorithm and genetic algorithm, have been discussed. These optimization techniques are very useful in handling optimization problems where derivatives of objective function are not possible. These techniques can handle complex optimization problems and are widely used in accelerator design. Both algorithms have been used in the study of optimization of LGB profiles in a dipole, which is presented in Chapter 3.

## Chapter 3

# Optimization of longitudinal gradient bend profiles in dipole magnet

As discussed in Chapter 1, longitudinal gradient bend (LGB) is an advance technique to reduce the beam emittance. First study of LGB in a storage ring was presented by J. Guo and T. Raubenheimer in 2002. In their paper [10], they applied the LGB in NLC damping storage ring and found a satisfactory reduction of beam emittance than the homogeneous dipoles. Now a days, magnet design technology has been improved much and most of the storage ring lattice designer are using LGB in place of constant filed dipoles to reduce beam emittance further. In this Chapter, optimization studies of LGB profiles in a dipole for two type of lattices namely achromat and theoretical minimum emittance (TME) is presented which is discussed in the following Section.

### 3.1 LGB profiles in dipoles for achromatic and TME lattices

In storage rings, mostly achromat type lattices are used, for example, double bend achromat (DBA), triple bend achromat (TBA) or multi bend achromat (MBA), due to requirement

of horizontal dispersion,  $\eta$ , and its derivative,  $\eta'$ , to be zero at the locations of IDs. A unit cell of a DBA lattice, similar to Indus-2 storage ring, is shown in Fig. 3.1. It consists of two homogeneous dipole magnets to bend the electron, nine quadrupoles to control lattice functions and four sextupoles to correct chromaticity in both transverse planes. Using combination of quadrupoles between the two dipoles, one can achieve achromatic condition, i.e.,  $\eta$  and  $\eta'$  are zero at the entrance of the first dipole and symmetrically at the exit of the second dipole. This lattice is designed to get large dispersion at sextupole locations.

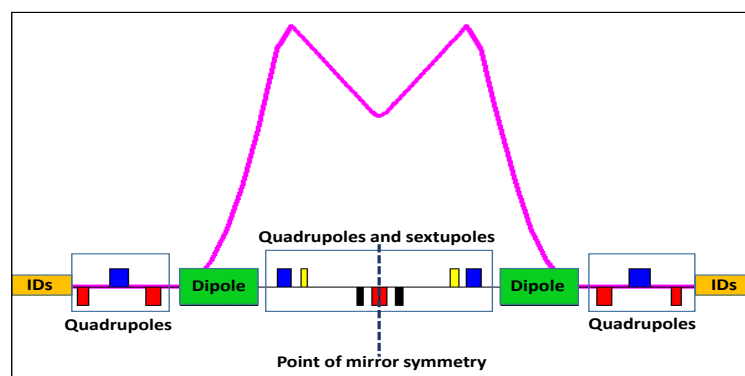


Fig. 3.1: Variation of dispersion function in DBA lattice. The green rectangular boxes are homogeneous dipoles, blue rectangular boxes are focusing quadrupoles, red rectangular boxes are defocusing quadrupoles, yellow ones are focusing sextupoles and the black ones are defocusing sextupoles.

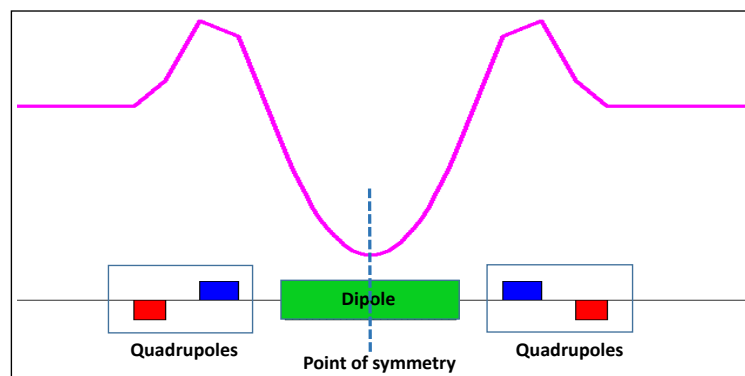


Fig. 3.2: Variation of dispersion function in TME lattice. Dispersion function is symmetric in the dipole and minima occurs at the center of the dipole. Two quadrupoles, one focusing (blue) and other defocusing (red), at both sides of the dipole are used to control the lattice functions.

In Fig. 3.2, an unit cell of TME lattice with homogeneous dipoles is shown. Here, achromatic condition is not satisfied. Though, TME lattice can not be used for third generation storage rings due to requirement of zero dispersion at location of IDs, but, it is useful in designing of TBA or MBA lattices, where more than one dipole satisfying TME condition are used. In order to reduce beam emittance further in the same lattice, the homogeneous dipoles can be replaced with dipoles having LGB profile in both type of lattices. LGB profiles for DBA and TME lattices have been discussed in Section 1.15, Chapter 1. For a DBA lattice, a parabolic decaying LGB profile is required. On the other hand, for a TME lattice, LGB profile is such that its maxima occurs at centre of the dipole and reduces symmetrically on either side. Though, continuous LGB field profile are desirable, but, design of continuous decay profile is very complicated [11, 34]. Therefore, stair like parabolic decay profile is modeled instead of continuous parabolic decay profile.



Fig. 3.3: Breaking of a homogeneous dipole (left) into  $n$  dipoles (right). The dipole (left) has parameters, length ( $L$ ), magnetic field ( $B$ ), bending angle ( $\theta$ ), local bending radius ( $\rho$ ). Same parameters can be defined for each section of dipole (right).

In order to generate stair like LGB profile, dipole magnet is divided into  $n$  sections (Fig. 3.3) in such a way that total length is same as homogeneous dipole. After that, magnetic field in each section is chosen in such a way that, it fits the continuous parabolic decay profile with the condition that total bending angle must be same as homogeneous dipole. For DBA and TME lattices, stair like parabolic decay profiles are shown in Fig. 3.4 and Fig. 3.5.

As shown in Fig. 3.4, magnetic field in the first section is high (low local radius of curvature  $\rho$ ), which generates higher slope of horizontal dispersion,  $\eta'_x$ , than the homogeneous dipole, but almost same horizontal dispersion,  $\eta_x$ . In the next dipole section, magnetic field is lower than the first section, but still higher than the homogeneous dipole, it will also generate higher  $\eta'_x$  and  $\eta_x$  will have higher value than homogeneous dipole. This behaviour of  $\eta_x$  is shown in Fig. 3.4. Also, at the exit of the dipole,  $\eta_x$  and  $\eta'_x$  are higher than the homogeneous dipole, which leads to high dispersion at sextupole location. In each section,  $\mathcal{H}$  function and bending radius,  $\rho$ , will have different values than the homogeneous dipole. This leads to different values of  $I_5 \left( = \left\langle \frac{\mathcal{H}}{\rho^3} \right\rangle; \mathcal{H} = \gamma_x \eta_x^2 + 2\alpha_x \eta_x \eta'_x + \beta_x \eta_x'^2 \right)$  in each section and average of  $I_5$  will have smaller value than the homogeneous dipole magnet due to dominating nature of  $\rho^3$  in sections having magnetic field lower than the homogeneous dipole fields. In this way, emittance will reduce.

After introducing LGB in the dipole magnet, one can achieve lower emittance in the same circumference of the storage ring or one can design a compact ring for the same emittance. Also, large dispersion at the sextupole location leads to low sextupole strength to correct the same level of chromaticity in the machine. These are the major advantage of LGBs.

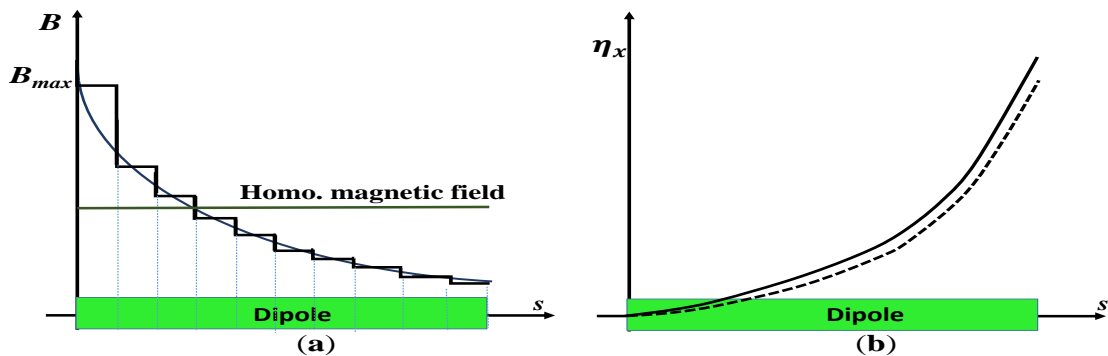


Fig. 3.4: Variation of longitudinal field profile in the dipole magnet (DBA). (b) Comparison of Horizontal dispersion function for LGB dipole (solid curve) with homogeneous dipole (dashed curve).

For a TME lattice, purpose of introducing LGB is to minimize beam emittance only. As shown in Fig. 3.5, a symmetric decaying LGB profile reduces the dispersion at the center of the dipole. Therefore, area under the curve, i.e.,  $\langle \frac{\mathcal{H}}{\rho^3} \rangle$  reduces, which leads to lower emittance. But, higher magnetic field will increase the SR loss, i.e., in order to reduce beam emittance, one has to compromise high SR loss.

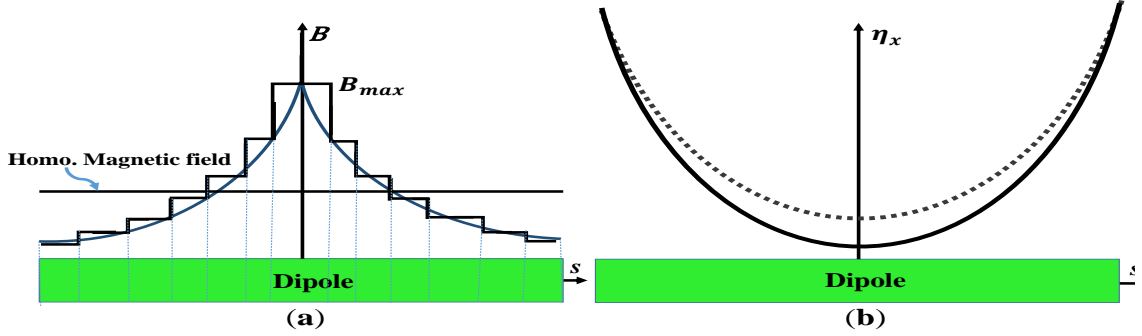


Fig. 3.5: (a) Variation of longitudinal field profile in the dipole magnet (TME). (b) Comparison of Horizontal dispersion function for LGB dipole (solid curve) with homogeneous dipole (dashed curve).

## 3.2 Objective function to generate LGB profiles

Expression for the horizontal natural beam emittance is given by eq.(1.95) as

$$\epsilon_{x0} = C_q \gamma^2 \frac{\langle \frac{\mathcal{H}_x(s)}{\rho^3(s)} \rangle}{\langle \frac{1}{\rho^2} \rangle}, \quad (3.1)$$

here,  $\mathcal{H}_x = \gamma_x \eta_x^2 + 2\alpha_x \eta_x \eta_x' + \beta_x \eta_x'^2$ , i.e.,  $\mathcal{H}_x = f(\alpha_x, \beta_x, \gamma_x, \eta_x, \eta_x')$  and  $\rho$  is the local radius of curvature of the dipole. For a storage ring with fixed energy, one can choose

$$f = \left\langle \frac{\mathcal{H}_x(s)}{\rho^3(s)} \right\rangle / \left\langle \frac{1}{\rho^2} \right\rangle, \quad (3.2)$$

as an objective function which, in principle, is a function of magnetic field and length in each section of dipole. Therefore, optimization problem will be; minimize  $f(\vec{B}, \vec{L})$  with constraints on total length, total bending angle and maximum magnetic field. One more constraint on

magnetic field in each section is that magnetic field should be of decreasing nature, i.e.,  $B_i > B_{i+1}$ ;  $i = 1, 2 \dots, n - 1$ ;  $n$  is the number of dipole sections. If dipole is divided into equal sections such that total length is equal to length of homogeneous dipole magnet, then objective function will be a function of magnetic fields only.

Variation in Courant-Snyder (CS) variables  $\alpha_x$ ,  $\beta_x$  and  $\gamma_x$  is governed by quadrupole strengths. Therefore, LGB profile will introduce only marginal change (due to geometrical focusing in dipoles) in these variables and CS variables of original lattice can be taken in calculation of  $\mathcal{H}_x$  function. It means that,  $\mathcal{H}_x$  is independent of CS variables and only function of  $\eta_x$  and  $\eta'_x$ . A case study, where dipole magnet is divided into 5 equal sections, is discussed in the following Section.

### 3.3 Optimization of LGB profiles in dipole for achromat lattice

To study LGB profiles for an achromat lattice, dipole of Indus-2 (a DBA lattice) is taken. The length of the dipole is 2.175 m and maximum magnetic field is 1.503 Tesla. This dipole magnet bends a charged particle by  $22.5^\circ$  with  $\rho = 5.55$  m. To generate LGB profiles, dipole is divided into 5 equal section such that total length of the dipole is unchanged. The objective function to minimize beam emittance can be chosen as

$$f = \left\langle \frac{\mathcal{H}_x(s)}{\rho^3(s)} \right\rangle. \quad (3.3)$$

The  $\langle \frac{1}{\rho^2} \rangle$  term will be taken care by the  $\rho^3$  in the  $\langle \frac{\mathcal{H}_x}{\rho^3} \rangle$ .

Let  $\theta_i$  and  $L_i$  are the angle length of  $i^{th}$  section of dipole magnet, where  $i = 1, 2, \dots, 5$ .

Therefore, optimization problem becomes

$$\begin{aligned}
 & \text{Minimize } f(\vec{B}) = \left\langle \frac{\mathcal{H}_x}{\rho^3} \right\rangle \\
 & \text{with constraints } \Delta\theta = \left| \sum_{i=1}^{i=5} \theta_i - \theta_{original} \right| = 0, \\
 & \max(\vec{B})_i < 2.65. \\
 & (\vec{B})_i > (\vec{B})_{i+1}; \quad i = 1, 2, \dots, 4,
 \end{aligned} \tag{3.4}$$

here  $\vec{B} = (B_1, B_2, B_3, B_4, B_5)$ ,  $\theta_{original} = 22.5^\circ$  and length,  $L = 2.1795$  m. The maximum magnetic field, 2.65 T, is chosen based on SR loss and emittance reduction. Since  $\Delta\theta$  can not be made to zero, therefore, if  $\Delta\theta$  is less than  $10^{-3}$ , then solution can be acceptable.

	Point A	Point B	Point C	Point D	Point E	Point F
$\alpha$	1.2462	0.5308	-0.1976	-0.9213	-1.6222	-2.2832
$\beta$ [m]	1.5357	0.7595	0.6139	1.1027	2.2136	3.9195
$\gamma$ [m <sup>-1</sup> ]	1.6625	1.6877	1.6924	1.6766	1.6405	1.5851

Fig. 3.6: Values of CS variables at points A, B, ..., E, which are entrance of each dipole section and F is the exit of last section.

In Fig. 3.6, values of CS variables are given at points A, B, ..., F. At each point,  $\mathcal{H}$ -function is calculated. After that, taking average of the  $\mathcal{H}$  function at entrance and exit of each dipole section,  $\mathcal{H}$  function is calculated at the centre of each dipole section. Then objective function can be calculated as

$$f = \frac{1}{5} \sum_{i=1}^5 \frac{\mathcal{H}_{xi}}{(\rho_i)^3}. \tag{3.5}$$

Here, hard edge model of dipole [2] is assumed, i.e. fringe fields between two dipole sections are completely ignored. Two optimization methods, Nelder-Mead algorithm and single objective genetic algorithm, have been used to generate LGB profiles.

### 3.3.1 Optimization using Nelder-Mead algorithm

The optimization problem is defined in eq. (3.4). The primary requirement of Nelder Mead method is that it requires an initial guess to create initial simplex. Therefore, 1.5 Tesla in each section of dipole magnet, which is the field of a homogeneous dipole, is chosen as an initial guess. For this initial guess, the value of objective function is  $2.07 \times 10^{-4}$ . Here, default stopping criteria of the algorithm are chosen, i.e., the algorithm will be stopped if objective function does not change in successive iteration or the objective function is less than  $10^{-4}$ . Though initial guess is provided for the first simulation run, but, it requires more relaxation on the constraint of total angle to run the program. In the second simulation run, optimized values of magnetic field from first simulation run can be used as initial guess and constraint on total angle is made more tight than the first simulation run.

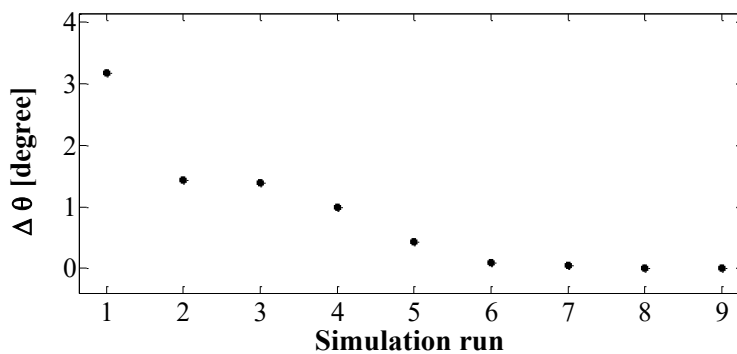


Fig. 3.7: Variation of  $\Delta\theta$  with successive simulation run.

After 9 successive simulation runs, a solution for which  $\Delta\theta$  is  $6.4 \times 10^{-4}$  is achieved, and solution is accepted. Variation of  $\Delta\theta$  for different simulation runs is shown in Fig 3.7 which shows that using improved initial guess, constraint on  $\Delta\theta$  can be satisfied in few simulation

runs. Different LGB profiles after each simulation run are shown in Fig. 3.8 and Variation of objective function for 9<sup>th</sup> simulation run is shown in Fig.3.11.

After final simulation run, optimized values of magnetic fields in each section are

$$B = [2.0991 \quad 1.6772 \quad 1.4414 \quad 1.2539 \quad 1.0740][\text{Tesla}],$$

with objective function value  $1.64 \times 10^{-4}$ .

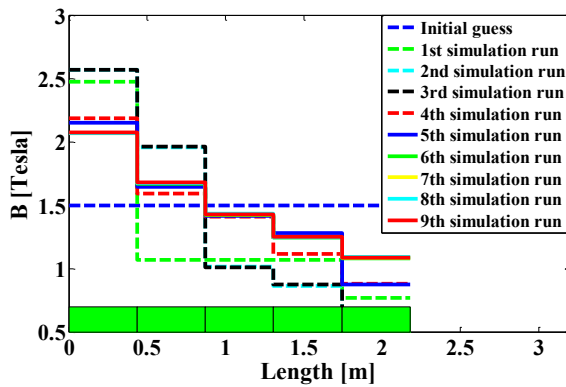


Fig. 3.8: LGB profiles after each simulation run using Nelder-Mead algorithm.

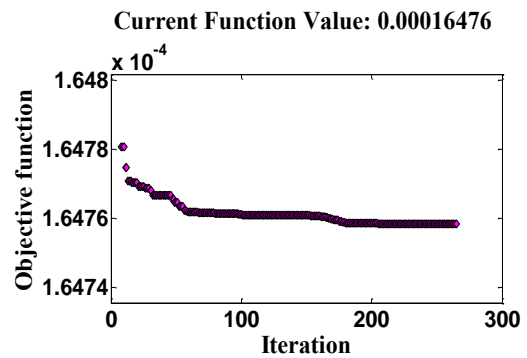


Fig. 3.9: Variation of objective function after 8th simulation run.

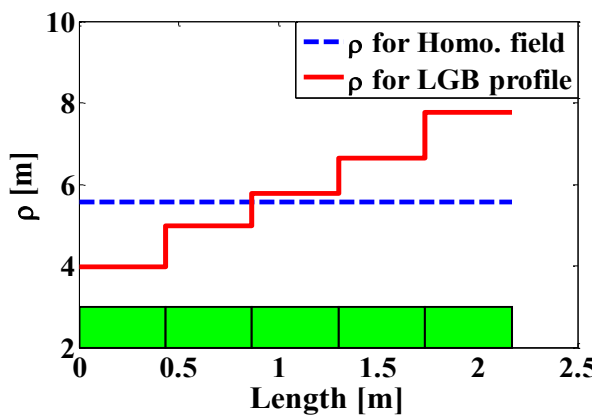


Fig. 3.10: Variation of  $\rho$  after final simulation run.

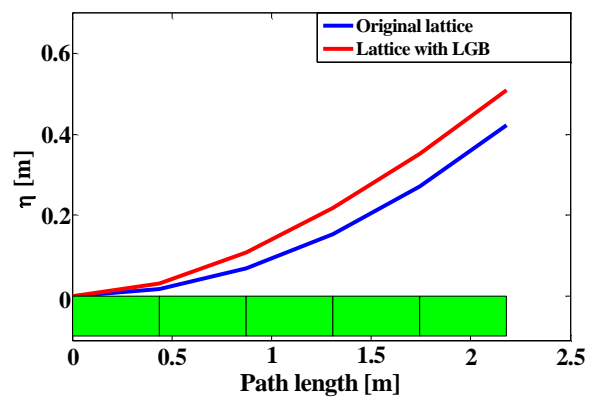


Fig. 3.11: Variation of dispersion function in the dipole.

After assuming LGB profile in all dipole magnets of Indus-2 lattice, different parameters in achromatic condition are shown in Table 3.1. In calculating the beam emittance (using

eq.(3.1)), electron energy is considered to be 2.5 GeV, which is the designed energy for Indus-2. For calculation of SR loss per turn, it is assumed that there are total 16 dipoles (each 22.5 deg) to complete the full storage ring i.e. ring of Indus-2.

Table 3.1: Comparison of parameters with original lattice.

S.No.	Parameter	original lattice	Lattice with LGB and achromatic condition
1.	Emittance [nm.rad]	58	41.5
2.	SR loss per turn [keV]	623	656

The emittance for this case is less than  $\sim 30\%$  from the nominal lattice, i.e., lattice with constant field dipole with a little increase in SR loss (30 keV).

This study shows that Nelder-Mead algorithm requires good initial guess to find an optimal solution in reasonable simulation runs. If initial guess is not good, it will need more relaxation on the constraints and requires more simulation runs to find an optimal solution. This is the major drawback of this method. To avoid these difficulties posed by Nelder-Mead method, GA technique can be used. In the Section below, a study with GA is presented.

### 3.3.2 Optimization using genetic algorithm

The genetic algorithm uses a random population of initial solutions. In successive generation, it try find a search direction in which solutions satisfy more constraints. The objective function for this case can be defined in a similar way as,

$$\text{Minimize } f(\vec{B}) = \left\langle \frac{\mathcal{H}_x}{\rho^3} \right\rangle$$

with constraints

Variable space range  $LB : 0.5$  Tesla in each section

$UB : 2.65$  Tesla in each section (3.6)

$$\Delta\theta = \left| \sum_{i=1}^{i=5} \theta_i - \theta_{original} \right| \leq 10^{-3},$$

$$\max(\vec{B})_i \leq 2.65.$$

$$(\vec{B})_i > (\vec{B})_{i+1}; \quad i = 1, 2, \dots, 4,$$

here,  $UB$  and  $LB$  are lower and upper bounds of independent variables.

### 3.3.2.1 Optimization using GA with initial guess

In order to provide a search direction to GA, initial guess for this method is provided same as in previous case, i.e., 1.5 Tesla in each section of the dipole. The number of generation and population size are chosen as 50 and 100, respectively. In a single simulation run, GA gives result with satisfying all constraints which is shown in Fig. 3.12.

After optimization the optimized values of the magnetic fields in each section of the dipole are

$$B = [2.0982 \quad 1.6111 \quad 1.4742 \quad 1.2926 \quad 1.0676][\text{Tesla}],$$

which is shown in the Fig.3.13. The obtained LGB profile is almost similar to the profile obtained using Nelder-Mead algorithm. The variation of dispersion function in the dipole is shown in Fig. 3.14. The calculated values of the beam emittance and SR loss per turn are also equivalent.

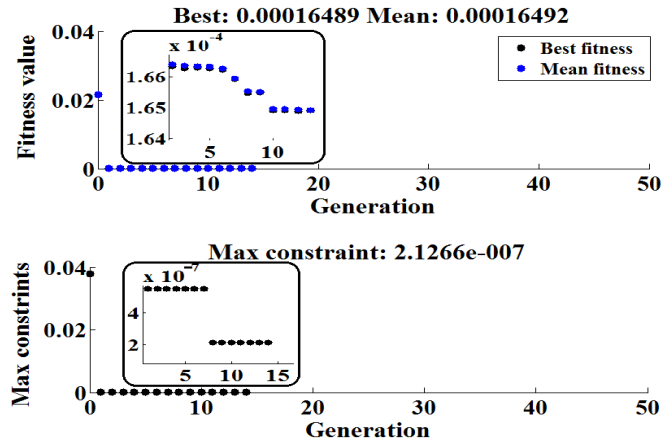


Fig. 3.12: Variation of objective function in different generations. Best fitness shows the value of objective function at current generation and maximum constraint shows how constraints are more satisfied in each generation.

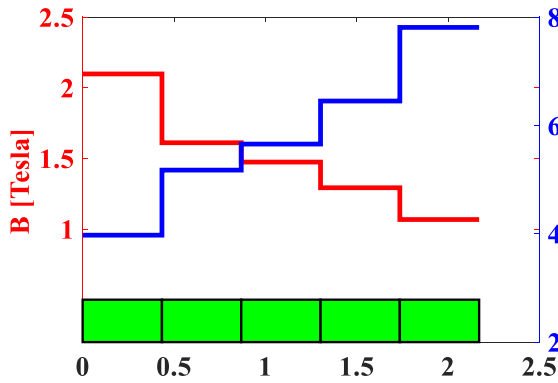


Fig. 3.13: Variation of magnetic field and  $\rho$ .

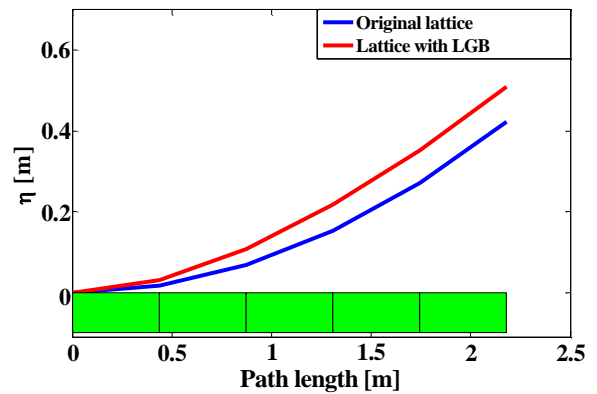


Fig. 3.14: Variation of dispersion function in the dipole.

For homogeneous dipole magnetic field and  $\rho$  are 1.503 Tesla and 5.55 m respectively.

Table 3.2: Comparison of parameters with original lattice in case of genetic algorithm.

S.No.	Parameter	original lattice	Lattice with LGB and achromatic condition
1.	Emittance [nm.rad]	58	42
2.	SR loss per turn [keV]	623	655

Though, an initial guess is provided here (a bad solution for GA), GA can give results without any initial guess in a single simulation run. This is the great advantage of GA over Nelder-Mead method. One result without any initial guess is presented in the following Section.

### 3.3.2.2 Optimization using GA without initial guess

For this case, GA algorithm is used with same objective function defined in eq.(3.6) without any initial guess. The variation of objective function and LGB profile are shown in Fig. 3.15 and Fig. 3.16. The objective function reduces to almost same value as previous case and a similar LGB profile is also generated. Emittance and SR loss are compared in Table 3.3, which shows almost same result i.e. there is no need to provide initial guess to run the GA code. After optimization the optimized values of the magnetic field in each section of the dipole are

$$B = [2.1701 \quad 1.6630 \quad 1.4979 \quad 1.0912 \quad 1.0904][\text{Tesla}]$$

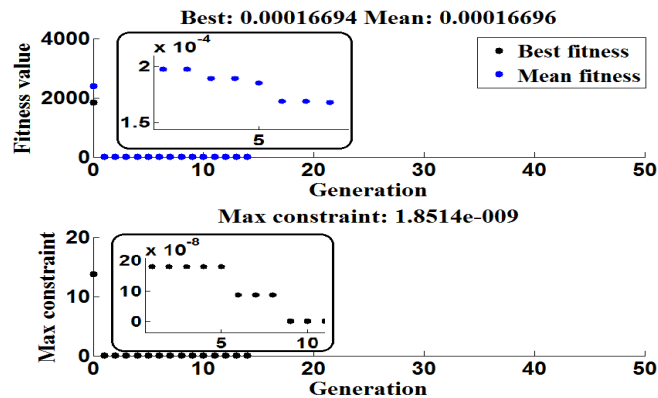


Fig. 3.15: Variation of objective function in each generation for the case where no initial guess is provided.

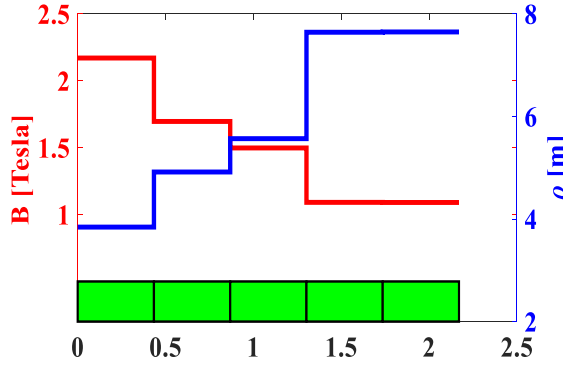


Fig. 3.16: Variation of magnetic field and  $\rho$ .  
For homogeneous dipole magnetic field and  $\rho$   
are 1.503 Tesla and 5.55 m respectively.

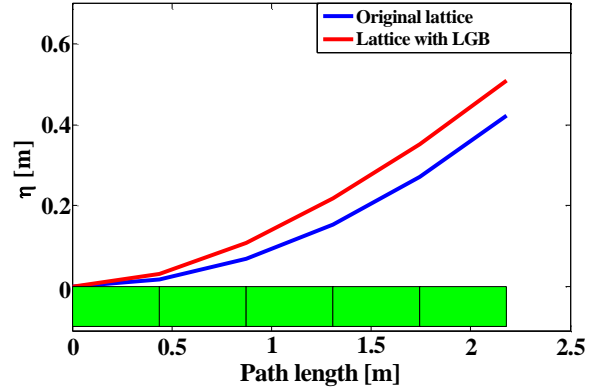


Fig. 3.17: Variation of dispersion function in  
the dipole.

Table 3.3: Comparison of parameters with original lattice.

S.No.	Parameter	original lattice	Lattice with LGB and achromatic condition
1.	Emittance [nm.rad]	58	41
2.	SR loss per turn [keV]	623	667.7

Based on these studies, it can be concluded that GA produces much better results compared to Nelder-Mead algorithm in view of getting optimal solution in a single run of the simulation. It can also be highlighted that the over all emittance in both the optimization is almost similar. Emittance in each case reduced to  $\sim 41 - 42$  nm.rad from 58 nm.rad and SR loss per turn is almost same.

### 3.3.2.3 Convergence test of GA

Simulation studies to test the convergence of GA algorithm in producing the LGB profiles and the objective function is also carried out. The results of generated LGB profiles for

fourteen simulation runs considering same lower and upper bounds of the magnetic fields are shown in Fig.3.18. The objective function converges to the same value almost in all simulation runs. There are very small variations in each profile except 13<sup>th</sup> and 14<sup>th</sup> profile. The small variation in the profile is due to randomness in the initial population in each GA simulation run.

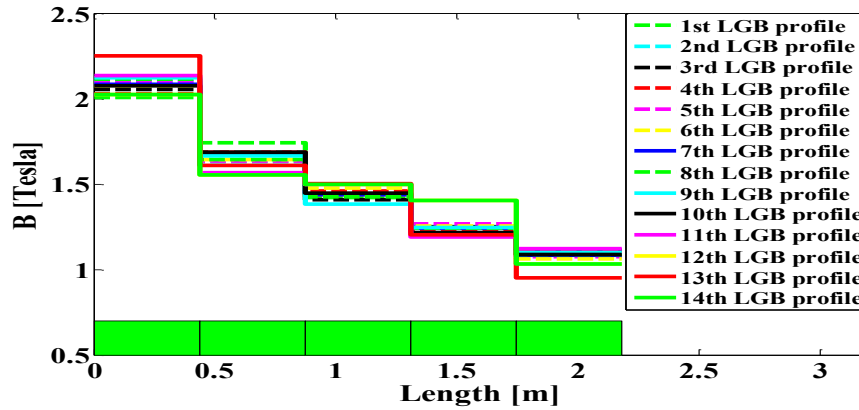


Fig. 3.18: Different LGB profiles generated by genetic algorithm.

As shown in Fig. 3.19, though, there is a little variation in the field profiles and objective functions in each case, but emittance is almost same which is  $\sim 40-42$  nm.rad. In addition, SR loss in each case is also same except one case (13<sup>th</sup> LGB profile), in which SR loss is  $\sim 675$  keV. It is because of increased magnetic field in the first section. This shows the advantage of LGB dipole over homogeneous dipole, i.e., using dipoles with LGB, one can significantly reduce beam emittance in the same circumference of storage ring.

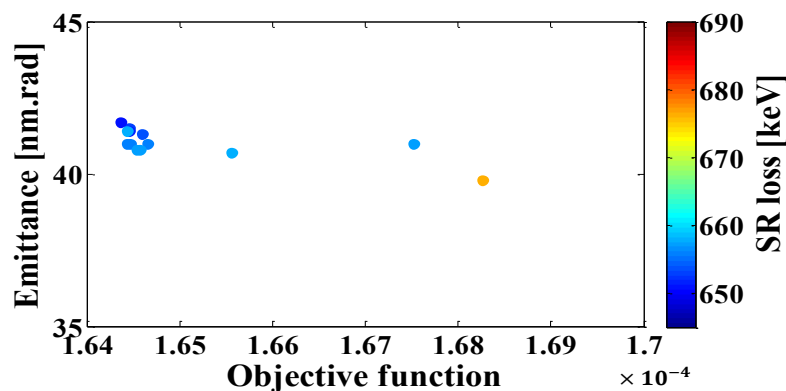


Fig. 3.19: Emittance for different LGB profiles with objective function and SR loss (color bar).

### 3.3.2.4 Optimization using GA with hard constraint

Another study with hard constraint on maximum field is also presented, in which maximum field in first section is strictly desired to be 2.65 Tesla. This maximum field will shift the critical wavelength of SR towards much harder X-rays [2], which is the requirement of many material research. Using objective function of eq.(3.6) with one more constraint, i.e.,  $max(\vec{B})_1 = 2.65$  Tesla, different LGB profiles have been generated which are shown in Fig.3.20.

In this case, the value of objective function after optimization are  $1.840 \times 10^{-4} - 1.879 \times 10^{-4}$  and emittance in achromatic condition are 38 – 39 nm.rad. Though, value of objective function is increased, emittance in achromatic condition get reduced a little bit more than previous cases, i.e.,  $\sim 38 - 39$  nm.rad, due to increased SR loss, which is increased from 623 keV to  $\sim 720 - 727$  keV, because of increased magnetic field. The increase in SR loss enhances the radiation damping which ultimately reduce the beam emittance. The increased SR loss can be compensated by increasing the RF power.

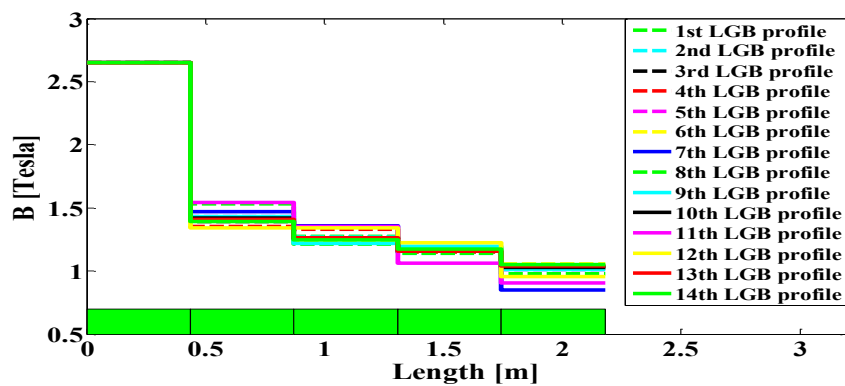


Fig. 3.20: Different LGB profiles using GA with maximum magnetic field in the first section 2.65 Tesla.

In the previous studies, dipole magnet is divided into 5 sections. In the following Section, we will explore the effect on beam emittance and SR loss by optimizing the LGB

profiles in a dipole magnet, divided in more number of sections. Motivation of this case is to achieve LGB profile close to true parabolic profile, and to see the effect on beam emittance. In the following Section, studies with dipole divided into 10 and 15 sections are presented.

### 3.3.2.5 Selection of number of dipole sections

If a dipole is divided into 10 or 15 sections, the number of independent variables will be 10 or 15 respectively. Here, same objective function with more number of variables and hard constrains on maximum magnetic field in first section has been used.

**Case I:** Dipole magnet is divided into 10 sections.

Optimization problem is given in eq.(3.6) and hard constraint on the magnetic field in first section is taken. After optimization, optimized LGB profile is shown in Fig.3.21.

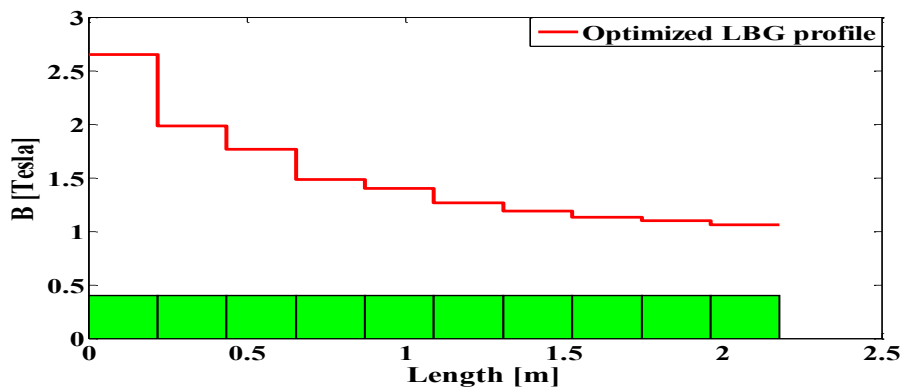


Fig. 3.21: LGB profile for the 10 section case with hard constraint on maximum magnetic field.

**Case II:** Dipole magnet is divided into 15 sections.

In a similar way, dipole can be divided into 15 sections to get more converged profile towards parabola. After optimization, the optimized profile is shown in Fig. 3.22.

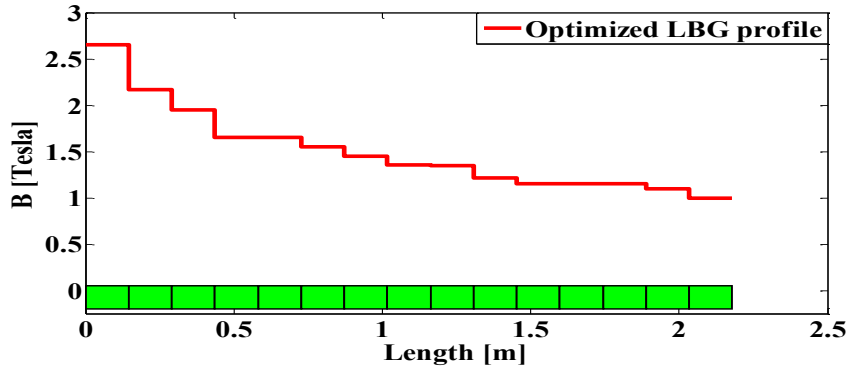


Fig. 3.22: LGB profile for the 15 section case with hard constraint on total magnetic field.

In Table 3.4, different parameters are compared for both the cases with 5 sections case.

Table 3.4: Comparison of different parameter with original lattice for 15 section case.

S.No.	Parameter	5 section case	10 section case	15 section case
1.	Emittance [nm.rad]	38.5	38.8	39.5
2.	SR loss per turn [keV]	722	685	677

In both cases, emittance reduces from 58 to  $\sim 39$  nm.rad. This study shows that more number of section in dipole does not lead to considerable reduction in beam emittance. It is also challenging to design and manufacture the dipole with LGB profile for more and small lengths of the sections, and it will increase the cost of magnet. For further studies, the case in which dipole is divided into 5 sections is considered, which is an acceptable trend in low emittance ring designs [34].

So far we have discussed the optimization of LGB profiles to minimize the beam emittance based on single objective Nelder-Mead and GA algorithm. Various other objectives are considered as the constraints. In the following Section, the optimization of the LGB profiles using MOGA to minimize the beam emittance, maximize the dispersion at sextupole location,

and minimize the SR loss will be discussed.

### 3.3.2.6 Optimization using multi objective genetic algorithm (MOGA)

The LGB profile optimization considering three conflicting objectives is performed using MOGA algorithm. First objective is to minimize emittance (minimize  $I_5$ ), maximize the dispersion at sextupole (in chromatic section) and minimize the SR loss. The second objective of maximizing the dispersion can be converted to maximize the slope of dispersion at the exit point of the dipole magnet. To see the behaviour of SR loss, slope of dispersion function and emittance, a multi-objective optimization problem can be defined in which there are three objective functions, (i)  $f_1: \left\langle \frac{\mathcal{H}(s)}{\rho^3} \right\rangle$ , (ii)  $f_2$ : derivative of dispersion function at the exit of dipole magnet and (iii)  $f_3$ : SR loss per turn. The purpose of this study to see the trade offs between conflicting objective functions. The optimization problem can be defined as

$$\text{Minimize } \vec{f}(\vec{B}) = (f_1, -f_2, f_3)$$

*with constraints*

$$\text{Variable space range } LB : 0.5 \quad \text{Tesla in each section}$$

$$UB : 2.65 \quad \text{Tesla in each section} \quad (3.7)$$

$$\Delta\theta = \left| \sum_{i=1}^{i=5} \theta_i - \theta_{original} \right| = 0,$$

$$\max(\vec{B}_i) \leq 2.65.$$

$$B_i > B_{i+1}; i = 1, 2, \dots, 4,$$

The negative sign is chosen for second objective, because it has to be maximize. The population size is chosen as 300 and number of generations is chosen as 100. Some of the optimized LGB profiles from previous studies are chosen as initial guess to give a search direction to GA. After optimization, the following trade off between first two objective with third one is found which is shown in Fig.3.23. It shows that all three objectives are conflicting. One has to choose

LGB profile judiciously. Large derivative of dispersion at the exit of dipole, which leads to large dispersion at sextupole location, comes with large SR loss per turn. In Fig. 3.24, three cases namely A, B and C are shown and corresponding parameters are compared in Table. 3.5. As value of objective function increase, SR loss also increases. Though objective function in case C is greater than the homogeneous case but emittance still reduces because radiation damping dominates.

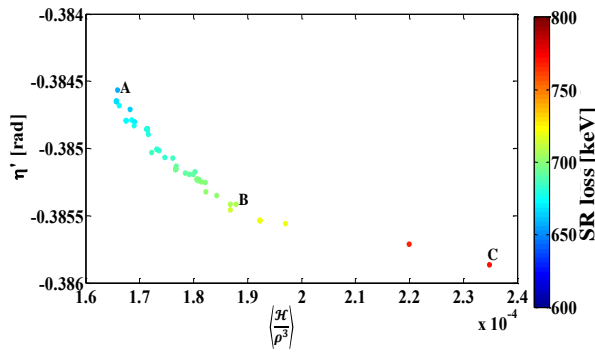


Fig. 3.23: Pareto optimal front between first and second objective. SR loss is given by color at each point of Pareto optimal front.

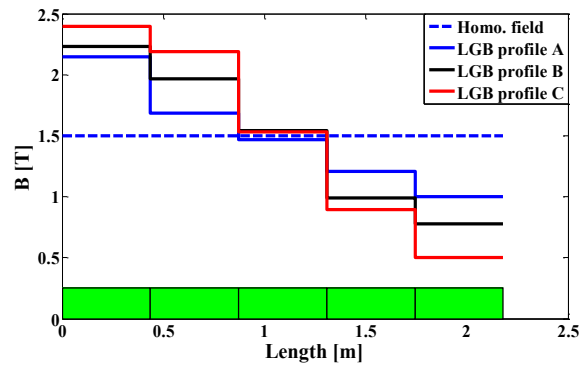


Fig. 3.24: Different LGB profiles for A, B and C.

Table 3.5: Comparison of different LGB profiles in case of MOGA.

S.No.	Parameter	A	B	C
1.	$\langle \frac{\mathcal{H}}{\rho^3} \rangle$	$1.656 \times 10^{-4}$	$1.878 \times 10^{-4}$	$2.347 \times 10^{-4}$
2.	SR loss per turn [keV]	666.8	708.2	769.1
3.	$\eta'$ [rad]	0.3846	0.3854	0.3859
4.	Emittance [nm.rad]	40.1	41.5	47.5

### 3.4 Optimization of LGB profiles in dipole for TME lattices

To study LGBs in TME lattices, a lattice based on TME is designed considering the same dipole (as in DBA lattice of Indus-2). This lattice uses same homogeneous dipole of Indus-2, i.e., length and magnetic field are same. Unit lattice cell of Indus-2 in TME configuration is shown in Fig. 3.25 with different magnetic elements and lattice functions are shown in Fig. 3.26. In TME configuration, there will be 16 super period instead of 8 to make the complete ring with circumference 172.47 m.

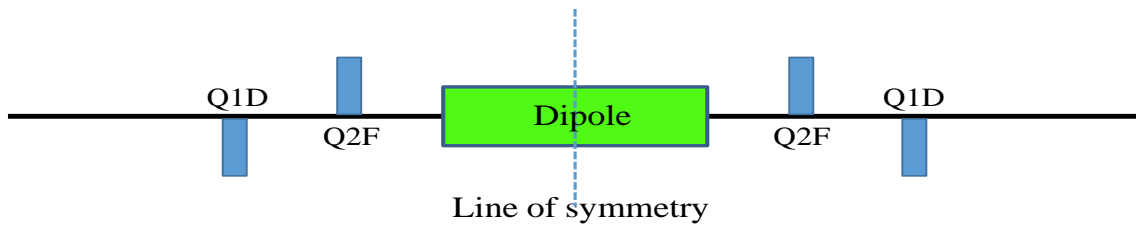


Fig. 3.25: Different magnetic elements of Indus-2 lattice in TME configuration.

Though, Indus-2 can not be operated in TME configuration, however TME is the backbone of the MBA lattices, which can be inserted between two matching cells (DBA type) to reduce the beam emittance below the limit of achromatic lattice. As shown in Fig. 3.5, LGB profile in a dipole for TME lattice is such that the magnetic field must be maximum at the center of the dipole and decreasing on either side of the dipole.

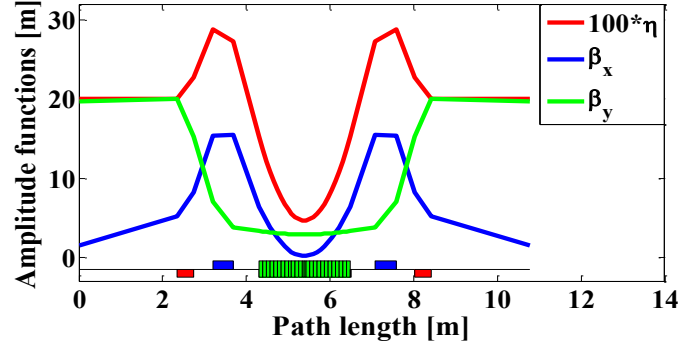


Fig. 3.26: Variation of different lattice functions.

To generate stair like LGB profile (Symmetrically decaying), dipole is divided into 25 equal sections to get more smooth LGB profile. The middle section of the dipole is further divided into 2 equal sections. Therefore, there are total 26 sections. Three cases have been studied in which, maximum magnetic field is 6 Tesla, 5 Tesla and 4 Tesla. Here, in each profile, maximum magnetic field in the center dipole section is desired.

The optimization problem for this case can be defined as

$$\text{Minimize } f(\vec{B}) = \left\langle \frac{\mathcal{H}_x}{\rho^3} \right\rangle$$

with constraints

Variable space range LB : 0.5 Tesla in each section

UB : 6.0 Tesla in each section

$$\Delta\theta = \left| \left( \sum_{i=1}^{i=26} \theta_i - \theta_{original} \right) \right| = 0, \quad (3.8)$$

$$\max(\vec{B})_i \leq 6,$$

$$(\vec{B})_i < \vec{B}_{i+1}; \quad i = 1, 2, \dots, 13,$$

$$(\vec{B})_i = (\vec{B})_{27-i}; \quad i = 1, 2, \dots, 12,$$

$$\max((\vec{B})_{13}) = 6 \text{ or } 5 \text{ or } 4$$

The CS variable at entrance, mid and exit point of the dipole are

$$\text{entrance of the dipole } (\alpha_{entr}, \beta_{entr}, \gamma_{entr.}) = (5.6372, 6.4114, 5.1124)$$

$$\text{at mid of the dipole } (\alpha_{mid}, \beta_{mid}, \gamma_{mid}) = (0, 0.1882, 5.3145) \quad (3.9)$$

$$\text{at the end of dipole } (\alpha_{end}, \beta_{end}, \gamma_{end}) = (-5.6372, 6.4115, 5.1124).$$

It can be seen that, beta function achieves minimum at the center of the dipole in TME lattice and symmetrically increases on either side. This behaviour is provided by  $\alpha$ , where at the entrance  $\alpha$  is negative, at the centre it is zero, and at the exit it achieves same value as entrance but positive.  $\gamma$  function is almost constant over the dipole.

After optimization, LGB profiles for three cases are shown in Fig. 3.27 and different parameters after including LGBs are shown in Table 3.6.

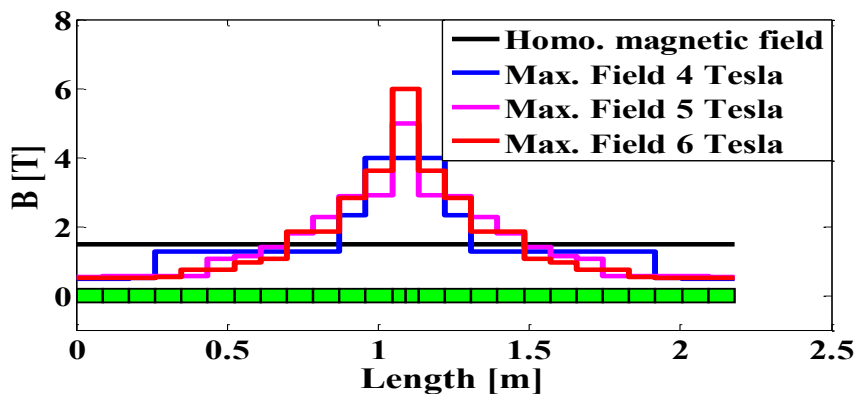


Fig. 3.27: LGB profiles for different chosen maximum magnetic field.

Table 3.6: Comparison of different parameter with original lattice in case of TME.

S.No.	Parameter	Homo. magnetic field	Max. field 4 Tesla	Max. field 5 Tesla	Max. field 6 Tesla
1.	Emittance [nm.rad]	14.14	5.365	3.8	3.27
2.	SR loss per turn [keV]	623	917	964	1111

This study shows that emittance can be reduced by less than half with dipoles having LGB than the homogeneous field dipoles, but at the cost of increased SR loss because of high magnetic field. Since magnetic field in the center dipole section is upto 6 Tesla, it can not be achieved using normal electromagnetic dipole. One has to use superconducting dipole. These dipoles with LGBs can be used in MBA lattices to reduce the beam emittance further in the same ring or one can design a storage ring with lower circumference for the same emittance, this will reduce the cost of the machine.

For the case, where magnetic field at the center is 5 Tesla, the variation of different lattice functions are shown in Fig. 3.28. At the center of the dipole, dispersion function is more minimum than the homogeneous dipole which leads to a reduction in  $\mathcal{H}$  function. Consequently, the beam emittance reduces. Also, beta functions are not changed much from the original lattice.

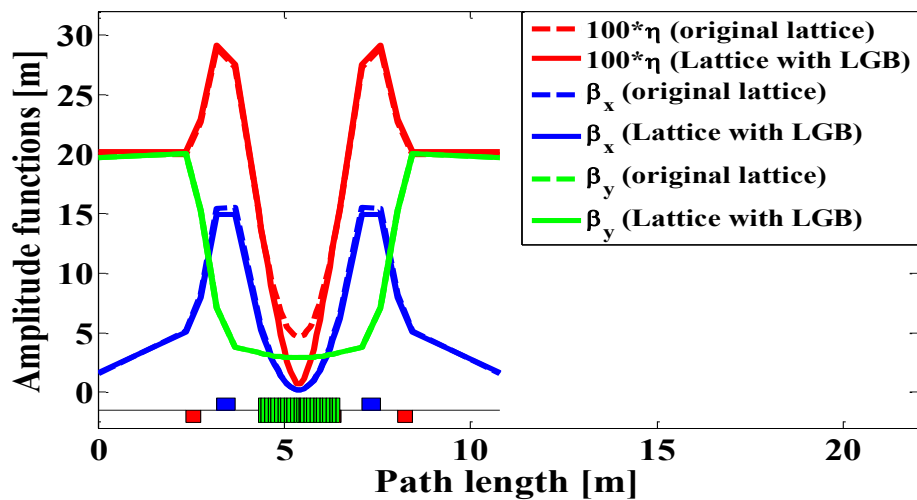


Fig. 3.28: Comparison of lattice functions with and without LGB.

In this Chapter, an extensive optimization study of LGB profiles using single and multi-objective genetic algorithms are presented. The LGB profiles of a dipole in DBA lattice case,

and for a dipole in TME lattice case are optimized. Outcome of the study is that the beam emittance reduces by  $\sim 30\%$  in DBA and less than half emittance can be reduced in TME case.

In a well design lattice, if dipoles are placed with LGBs, the distribution of dispersion over the full lattice cell will change. It is due to the fact that quadrupoles are optimized for the lattice functions with homogeneous field dipole. Further studies including optimized LGBs and tuning of quadrupoles are presented in Chapter 4 for the case of well design lattice of Indus-2 and Indus-3. The performance comparison of the lattice with and without LGBs are made.

# Chapter 4

## Indus-2 and Indus-3 storage ring lattice performance with LGBs

In Section 1.16 and 1.17, Indus-2 and proposed Indus-3 electron storage rings have been discussed. In operational storage rings, there always exists a possibility of up-gradation to improve the performance. In newly design lattices with conventional means, one can also do aggressive optimization to achieve ever improved performance by including technologically challenging quadrupole gradient and dipole fields.

The optimization studies are presented in Chapter 3 to get optimal LGB profiles in view of beam emittance and increasing the dispersion at sextupole location, to achieve efficient correction of natural chromaticity with reduced sextupole strengths. First study to reduce emittance for achromatic and TME cases are presented and comparison of emittance with nominal emittance were performed. It was also highlighted that the SR loss per turn in LGB case is always higher than the SR loss per turn from constant field dipole. In these studies, it was assumed that the lattice functions at the entrance of the dipoles are known and fixed, however, in actual lattice design with LGB profiles, the distribution of dispersion function get changed. It is

the case when quadrupoles are operating with the nominal lattice, i.e., the lattice with constant field dipoles. Therefore, re-tuning of the quadrupole strengths are required to achieve desired distribution of the lattice functions after including LGBs in place of constant field dipoles. These studies are carried out for the case of Indus-2 storage ring, which is operational in user mode, and Indus-3, which is an upcoming project at RRCAT. In Section 4.1, the optimization of quadrupoles with dipoles replaced with LGBs are performed to achieve desired distribution of lattice functions for Indus-2 storage ring lattice. The comparative study of dynamic aperture in the lattice with and without LGB are given in Section 4.2. The optimization of various objectives using MOGA are also presented in Section 4.3 to get trade off between them in a running/ designed electron storage ring in the same circumference. Similar studies for Indus-3 are performed in Section 4.4.

## **4.1 DBA lattice of Indus-2 with LGBs**

As discussed in Section 1.16, Indus-2 has been designed based on DBA configuration with ring circumference 172.47 m and beam emittance of 58 nm.rad. Positions of different magnetic elements of unit lattice are shown in Fig. 4.1. This unit lattice consist 2 dipoles, 9 quadrupoles and 4 sextupoles. Each element in the unit lattice is placed in such a way that it looks symmetric with respect to centre of quadrupole Q5D and strength of the quadrupoles are such that the lattice/ amplitude functions have distribution as shown in Fig. 4.2. The achromatic condition, i.e., dispersion and its derivative at straight sections are zero, is achieved using three quadrupoles (two Q4F and one Q5D) between dipole magnets and beta functions are controlled using all five families of quadrupoles, i.e. Q1D, Q2F, Q3D, Q4F, and Q5D.

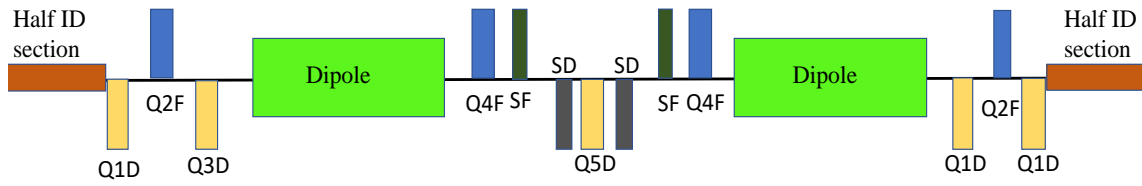


Fig. 4.1: Basic elements in Indus-2 unit lattice (not to scale). Here, QF: focusing quadrupole, QD: defocusing quadrupole, SF: focusing sextupole, SD: defocusing quadrupole. Number indicates family of that element, e.g. Q1D shows first family of defocusing quadrupoles.

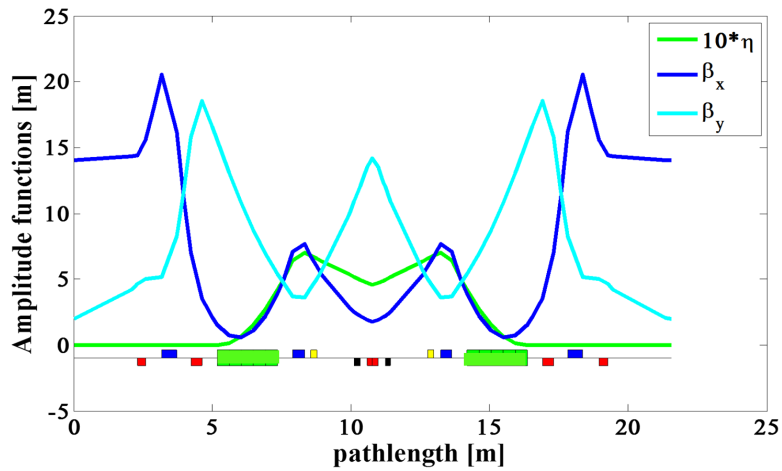


Fig. 4.2: Variation of beta and dispersion functions in Indus-2 unit lattice.

Since Indus-2 is in regular operation in user mode, ring size, length and position of any magnetic element in the machine can not be changed. In order to reduce the beam emittance further in the same ring with minimum hardware change, dipoles with LGBs can be used.

#### 4.1.1 Optimization of lattice function with LGBs

The optimization of lattice functions of an achromat (DBA or MBA) lattice with LGBs is a two step process. First, optimization of the dipole to get optimal LGB profile, which is already discussed in Chapter 3, second, optimization of strength of quadrupoles to match

lattice function to the nominal lattice.

A LGB profile has been chosen from Section 3.3.2, Chapter 3, in which dipole is divided into 5 sections and magnetic field in the first section is 2.65 Tesla. Magnetic fields in each section of the dipole are given as

$$B = [2.6500 \quad 1.5575 \quad 1.2632 \quad 1.0845 \quad 0.9575] \text{ [Tesla]}. \quad (4.1)$$

The comparison of LGB profile with homogeneous field is shown in Fig.4.3. After replacing homogeneous dipoles with dipoles with LGBs in an unit lattice, achromatic condition is lost which is shown in Fig. 4.4. This is because of unoptimized quadrupole strengths. Also, it can be seen in Fig. 4.5 and Fig. 4.6 that introduction of LGB does not change beta functions which was assumed in LGB profiles study. A small change in horizontal beta function is due to geometrical focusing in dipole magnets. But over the dipole, it is same as nominal lattice.

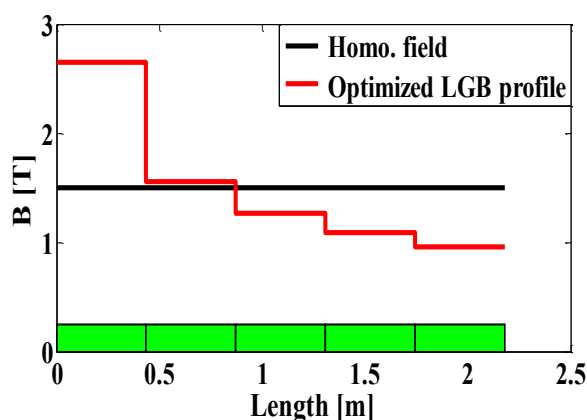


Fig. 4.3: LGB profile compared with homogeneous dipole field in the dipole magnet.

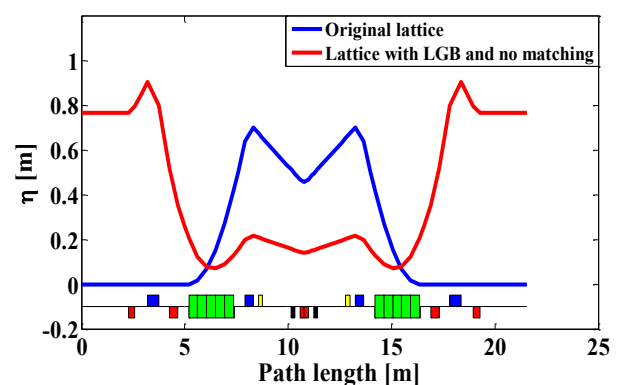


Fig. 4.4: Variation of dispersion function with LGB.

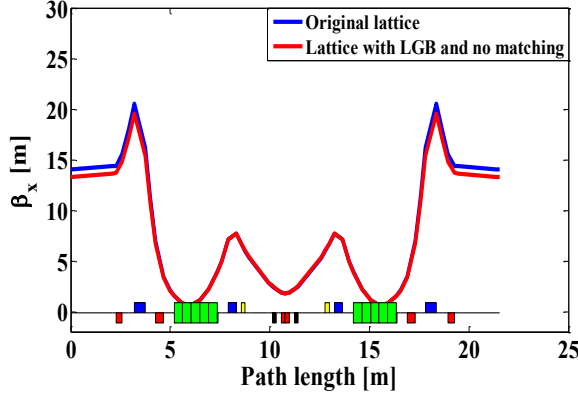


Fig. 4.5: Variation of horizontal beta function with LGB.

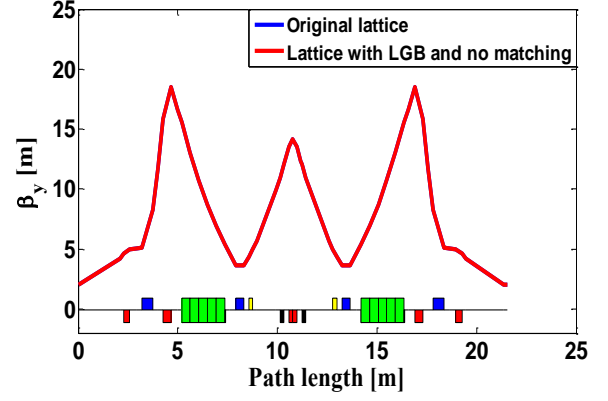


Fig. 4.6: Variation of vertical beta function with LGB.

In order to get achromatic condition and constraints on other important parameters like constraint on betatron tune, beta functions, stability conditions etc., optimization of quadrupole strengths is required. Here, all five families of quadrupoles, i.e., Q1D, Q2F, Q3D, Q4F and Q5D, have been chosen in the optimization. Here, this optimization problem is solved using single as well as multi-objective techniques. Using single objective techniques and using quadrupole strengths of nominal lattice as initial guess is described below.

In this optimization problem, there are many objective functions which are; (i)  $f_1$ : beam emittance, (ii)  $f_2$ : dispersion at straight section, (iii)  $f_3$ : slope of dispersion at straight section, (iv)  $f_4$ : derivative of beta functions at injection, (v)  $f_5$ : beta functions at injection, (vi)  $f_6$ : betatron tunes (vii)  $f_7$ : beta functions at symmetric point. Each objective function  $f_3, f_4, f_5, f_6$ , and  $f_7$  contains two objective functions for each plane. Therefore, there are 12 objective functions in total. In Indus-2, normalized strengths of quadrupoles can go upto  $2.2 \text{ m}^{-2}$ . This will put a constraint on maximum available normalized quadrupole strength. Also, lattice functions are periodic, therefore, to find a stable solution,  $|Trace(M)| \leq 2$ , where  $M$  is the transport matrix of periodic cell. In addition, maximum value of beta functions should be in limit, this will also be a constraint.

The available variables for this optimization problem are normalized strength of quadrupoles, i.e.,  $\vec{k} = (k_1, k_2, k_3, k_4, k_5)$ . In order to minimize each objective function, the objective function can be written as  $(f_i - f_i^0)^2$ ;  $i = 1, 2, \dots, 12$ . For first objective function,  $f_1^0$  can be chosen as 0, because emittance is desired as low as possible. Other  $f_i^0$  :  $i = 2, 3, \dots, 12$  can be chosen as of nominal or original lattice. The initial values of quadrupole strengths are

$$k_0 = [-0.79860 \quad 1.52949418 \quad -1.6899011 \quad 1.81969574 \quad -1.116476][\text{m}^{-2}]$$

A composite objective function with proper weight factors can be defined to convert this multi objective optimization problem into a single objective optimization problem which can be written as

$$\text{Minimize } f(\vec{k}) = \sum_{i=1}^{i=12} w_i (f_i - f_i^0)^2$$

*with constraints*

$$|(\vec{k})_i| \leq 2.2 \text{ m}^{-2}, \quad (4.2)$$

$$|\text{Trace}(M)| \leq 2,$$

$$\max(\beta_x \text{ and } \beta_y) \leq 20 \text{ m},$$

where,  $w_i (\geq 0)$  is the weight factor for  $i^{\text{th}}$  objective function and satisfy the relation  $\sum w_i = 1$ . Weight factors are chosen in such a way that it gives satisfactory optimal result. High value of weight factor is given to dispersion at straight section than the rest of the objective functions. Because requirement of achromatic condition is the first priority.

After optimization of the problem, the optimized values of quadrupole families Q1, Q2, Q3, Q4, Q5 are

$$k = [-0.8733 \quad 1.5686 \quad -1.6752 \quad 1.6591 \quad -1.0760][\text{m}^{-2}],$$

and behaviour of objective function after each iteration is shown in Fig. 4.7. With initial guess  $k_0$ , the objective function has value equal to 0.56 and after optimization, it reduces to 0.004.

The algorithm stops due to no improvement in objective function in the successive iterations. The strength of quadrupoles Q4F and Q5D are decreased from nominal lattice, which leads to reduction in natural chromaticity in the machine.

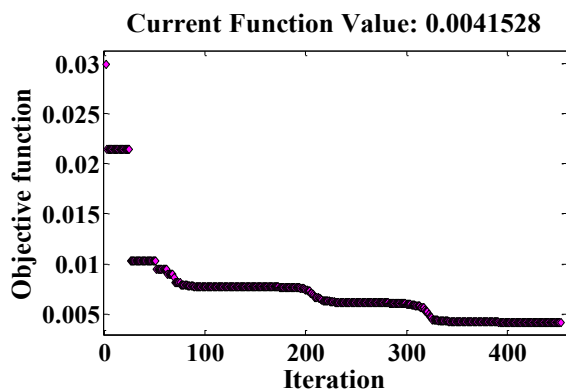


Fig. 4.7: Variation of objective function.

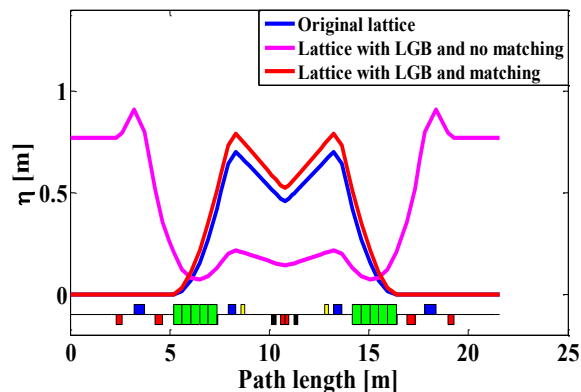


Fig. 4.8: Variation of dispersion function with LGB and matching.

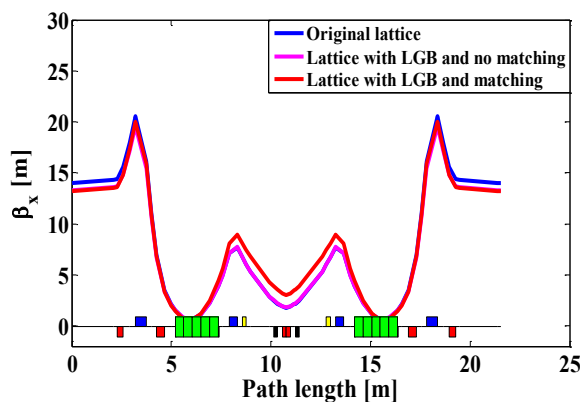


Fig. 4.9: Variation of horizontal beta function with LGB and matching.

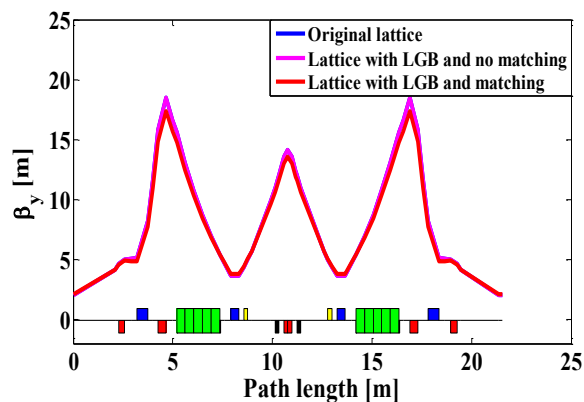


Fig. 4.10: Variation of vertical beta function with LGB and matching.

After optimization of quadrupole strengths of all five family, variation of lattice functions are shown in Fig.4.8, Fig.4.9 and Fig.4.10, which are given by lattice with LGB and matching. Achromatic condition is restored after optimization of quadrupole strengths. The small change in horizontal beta function is because of higher weight factor is given to second objective

function. But, still these changes are small. Comparison of different parameters of Indus-2 lattice with LGB and original lattice are presented in Table 4.1.

Table 4.1: Comparison of Indus-2 lattice with LGB, Indus-2 lattice with LGB and betatron tune correction and original lattice.

S.No.	Parameters	Indus-2 (Original Lattice)	Indus-2 (Lattice with LGB and matching)	Indus-2 (lattice with LGB, matching, and corrected betatron tune)
1.	Energy (GeV)	2.5	2.5	2.5
2.	Emittance (nm-rad)	58.1	38.3	43.8
3.	Energy loss per turn (keV)	623	725	725
4.	Betatron tunes $[\nu_x, \nu_y]$	[9.2 5.2]	[8.71 5.19]	[9.2 5.2]
5.	Natural chromaticity	[-19.05 -12.05]	[-19.12 -11.14]	[-14.33 -11.26]
6.	Momentum Compaction factor	0.0052	0.0051	0.0051
7.	Dispersion function at sextupole location [m]	0.68	0.76	0.76
8.	Beta function at injection [m]	[14.02 2.0]	[13.2 2.1]	[7.4 1.9]
9.	Max. Beta function [m]	[20.5 18.5 ]	[20.0 17.4]	[12.5 17.5]
10.	Beta function at symmetric point [m]	[1.8 11.2]	[3.0 13.6]	[1.88 13.1]

11.	Required sextupole strength for chromaticity correction [2,2] [m <sup>-3</sup> ]	[13.03 -11.72]	[10.85 -10.09 ]	[9.54 -9.582]
-----	--	----------------	-----------------	---------------

The brightness ratio of Indus-2 lattice with LGBs and nominal lattice is calculated using 1% coupling and  $\sigma_r = 0$ . The ratio of brightness comes out to be  $\sim 2$ . Emittance, after including LGBs in dipoles of Indus-2 lattice, reduces from 58 to 38 nm.rad with marginal change in other important parameters. As natural chromaticity of the machine is decreased and dispersion at the sextupole location is increased from 0.68 m to  $\sim 0.76$  m, sextupole strengths to correct the chromaticity to the same level of nominal lattice get reduced from  $13.03 \text{ m}^{-3}$  to  $10.85 \text{ m}^{-3}$  in horizontal and  $-11.72 \text{ m}^{-3}$  to  $-10.1 \text{ m}^{-3}$  in vertical plane. These are the major advantages of dipoles with LGB in a storage ring over storage rings with homogeneous dipoles.

Here, betatron tunes are not same as original lattice. Therefore, one has to correct betatron tune to the original lattice to see the effect of betatron tune correction on lattice functions. Therefore, betatron tune is corrected to [9.2, 5.2] using Q2F and Q3D families of quadrupoles. These quadrupoles are chosen, because they are located at zero dispersion and will not affect achromatic condition. After betatron tune correction, strengths of quadrupole Q2F changes from  $1.5686 \text{ m}^{-2}$  to  $1.6204 \text{ m}^{-2}$  and strength of quadrupole Q3D changes from  $-1.6752 \text{ m}^{-2}$  to  $-1.7003 \text{ m}^{-2}$ . The different lattice parameters after betatron tune correction are presented in the fourth column of Table 4.1 and variation of horizontal and vertical beta functions are shown in Fig. 4.11 and Fig. 4.12.

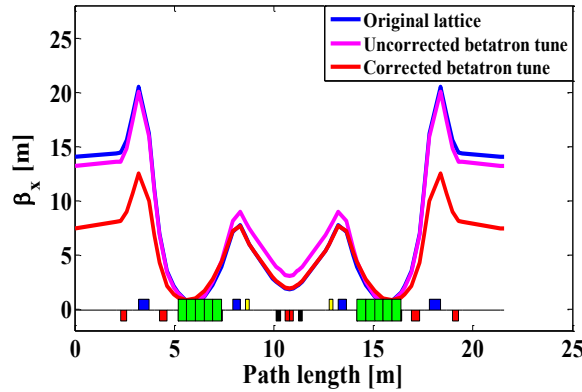


Fig. 4.11: Variation of horizontal beta function with LGB, matching, and betatron tune correction.

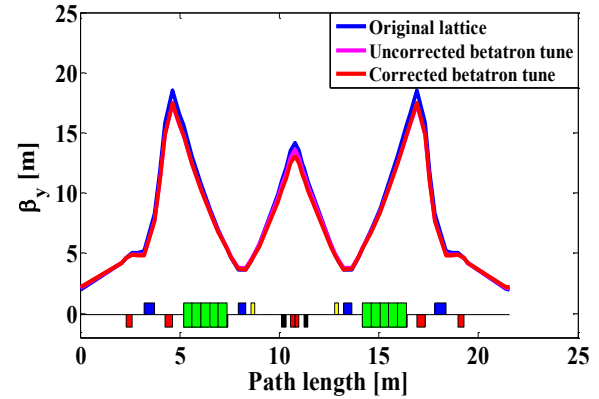


Fig. 4.12: Variation of vertical beta function with LGB, matching and betatron tune correction.

It can be seen that how betatron tune is sensitive to lattice function. After correction of betatron tune, emittance increased by 5 nm.rad and horizontal beta function at injection changes from 13.92 m to 7.4 m. This decrease in horizontal beta function will lead to more strengths of kicker to inject the beam in the storage ring, which is a disadvantage. But, low horizontal beta function at IDs location lead to low beam size in IDs which is an advantage. In practical storage ring, real effect of the change in horizontal beta function can be seen only after study of dynamic aperture, which is presented in the following Section.

### 4.1.2 Dynamic aperture

In Section 1.10, the concept of dynamic aperture is explained. This phenomenon arises due to non linearity in the machine. As strength of sextupole for chromaticity correction is small in lattice with LGBs compared to original lattice. Hence, dynamic aperture should not change much from original lattice. After correcting chromaticity to [2, 2] (horizontal and vertical) with two families of sextupoles, for on momentum charged particles, a comparative study of dynamic aperture for three cases are compared in Fig. 4.13.

To calculate dynamic aperture, range of  $x$  is chosen from -32 mm to 32 mm in step size of 0.5 mm. On the other hand, range of  $y$  is chosen from -17 to 17 mm. The maximum range of  $x$  and  $y$  are chosen on the basis of available physical aperture of vacuum chamber. Charged particle is tracked for 1000 turns in the grids and the boundary is decided on the basis of loss, i.e., after a certain point of the grid, charged particle is lost.

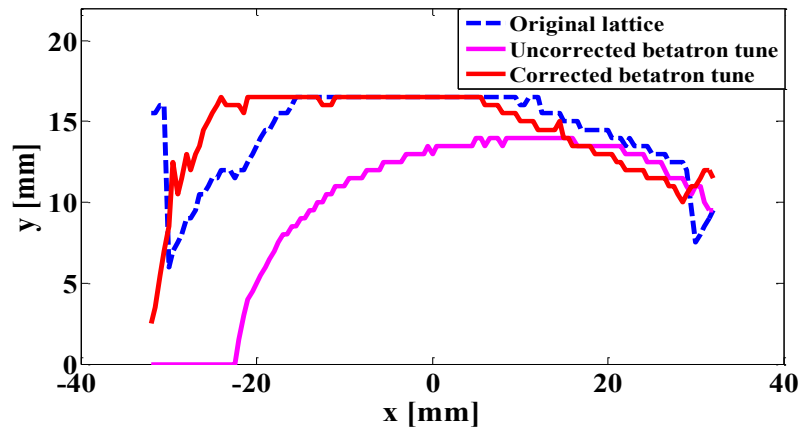


Fig. 4.13: Dynamic aperture comparison for on momentum charged particles.

Though, positive values in vertical direction are plotted, but graph of the boundary is symmetric with respect to  $x$ , i.e. a closed boundary will be there. Also, open ends at both side of  $x$  is because of fixed range of  $x$ . If range of  $x$  is allowed more, there will not be any open ends. As depicted in Fig. 4.13, if betatron tune is allowed to be relaxed then dynamic aperture shifted towards outer region in  $x$  direction. But, if we correct the betatron tune it approximately covers the same area as original lattice i.e., life time of electron beam will be same as original lattice.

In Section 4.1, quadrupole strengths are optimized using single objective algorithm. Major disadvantage of this algorithm is that the weight factors are highly sensitive and a proper choice of these weight factors is required which is a tedious task and one has to run many simulation runs to get an optimal solution. In order to avoid these difficulties, multi-objective

genetic algorithm (MOGA) can be used. A optimization study using MOGA is presented in the following Section.

## 4.2 Comparative study of beam emittance with and without LGBs

To find a trade-off between dispersion function at straight section and emittance, MOGA has been used. As optimization of quadrupole strengths of Indus-2 lattice with LGB is a multi-objective optimization problem. In this study, two objective functions, (i)  $f_1$ : emittance, and (ii)  $f_2$ : dispersion at straight section are chosen and rest of the objective functions like maximum beta functions ( $\beta_{x,max}, \beta_{y,max}$ ), betatron tunes ( $\nu_x, \nu_y$ ), beta functions at symmetric point ( $\beta_{x,sym}, \beta_{y,sym}$ ) etc., are chosen as constraints. The optimization function can be written as

$$\begin{aligned}
 & \text{Minimize } \vec{f} = (f_1, f_2), \\
 & \text{with constraints} \\
 & |(\vec{k})_i| < 2.2 \text{ m}^{-2}; i = 1, 2, \dots, 5, \\
 & |\text{Trace}(M)| \leq 2, \\
 & \max(\beta_x \text{ and } \beta_y) \leq 20\text{m}, \\
 & 0.7 \leq \text{fractional } \nu_{x,y} \leq 0.9 \quad \text{or} \quad 0.1 \leq \text{fractional } \nu_{x,y} \leq 0.25, \\
 & |\beta_{x,inj} - 14| < 1.2 \quad \text{and} \quad |\beta_{y,inj} - 2| < 0.5, \\
 & |\beta_{x,sym} - 1.8| < 1.5 \quad \text{and} \quad |\beta_{y,sym} - 14.2| < 0.2.
 \end{aligned} \tag{4.3}$$

The range of betatron tune is chosen so that fractional betatron tune is far away from dangerous resonances. Range of other constraints are chosen to get optimal solution. In Fig.4.14, a Pareto optimal front to show trade off between dispersion function at straight section and emittance is

given and it is compared with Pareto optimal front for original lattice. In Pareto optimal front, there are large number of solutions for strengths of quadrupoles.

Fig. 4.14 shows that both objectives are conflicting in nature and one must choose a solution judiciously. To get desired emittance one has to compromise dispersion at straight section. This is the major advantage of multi-objective genetic algorithm over classical methods. Beta functions at injection, natural chromaticity, betatron tune, maximum beta functions for different set of quadrupole strengths are shown in Fig.4.15, Fig.4.16, Fig.4.17, and Fig.4.18 and data of quadrupole strengths, which have dispersion at straight section less than 0.002 m are shown in numbers. There are only two data which satisfy dispersion function at straight section near to zero. For both data, emittance is nearly 38 nm.rad, other parameters can also be compared in figures.

According to ones requirement, e.g. if one wants to allow a little dispersion at straight section, then solution can be chosen such that important parameters, like betatron tune, natural chromaticity, beta functions at injection, maximum beta functions, are satisfied.

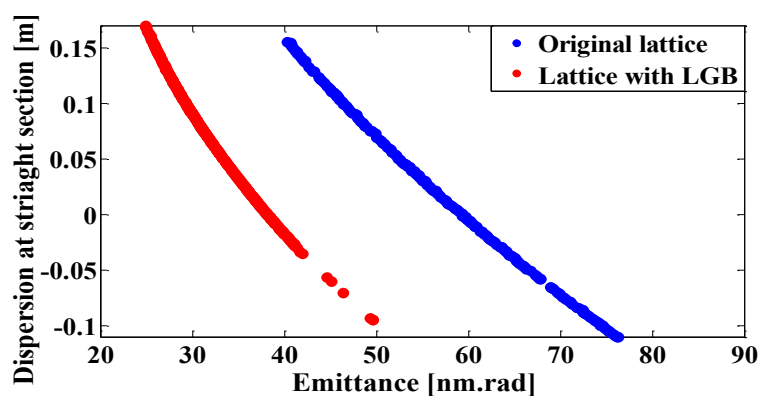


Fig. 4.14: Comparison of Pareto optimal front.

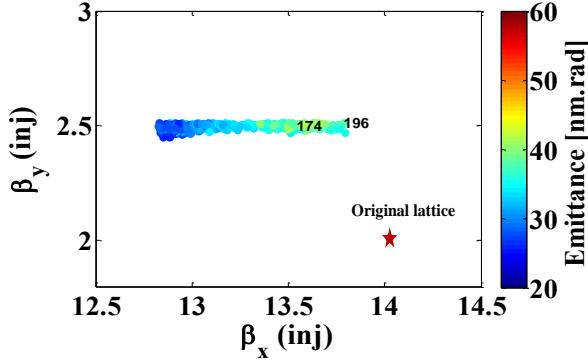


Fig. 4.15: Comparison of beta functions at injection for each solution.

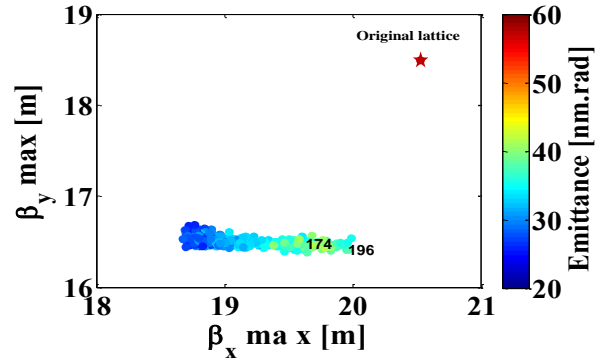


Fig. 4.16: Maximum beta functions comparison for each solution.

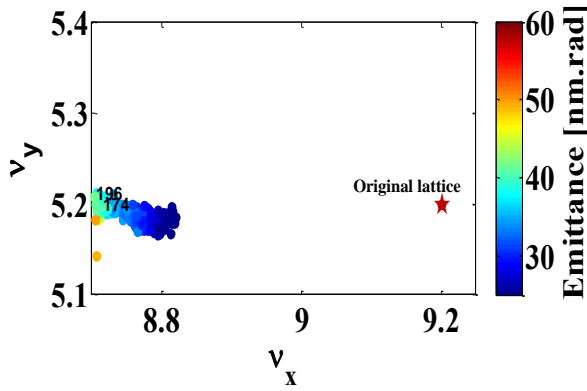


Fig. 4.17: Betatron tune comparison for each solution.

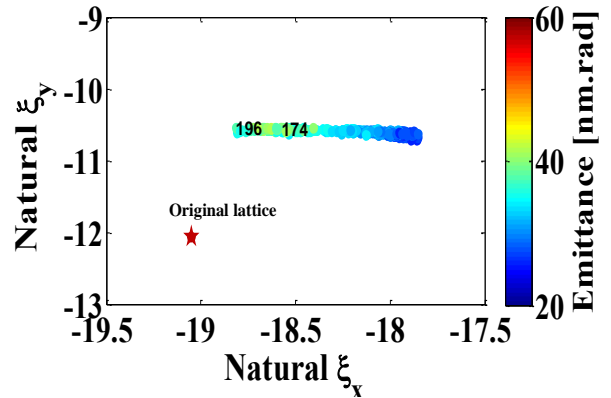


Fig. 4.18: Natural chromaticity comparison for each solution.

A similar optimization studies of LGBs are presented for Indus-3 lattice in the following Sections.

### 4.3 MBA lattice of Indus-3 with LGBs

In Section 1.17, Chapter 1, Indus-3 lattice has been discussed. Indus-3 or high brightness synchrotron radiation source (HBSRS) is a 6 GeV electron storage ring. The baseline lattice has been designed to achieve beam emittance of 150 pm.rad. Different elements of Indus-3 lattice are shown in Fig. 4.19. Magnetic elements are placed in the unit lattice in such a way

that it looks symmetric with respect to center of BM4 and strengths of quadrupoles are such that it generates lattice functions as shown in Fig. 4.20.

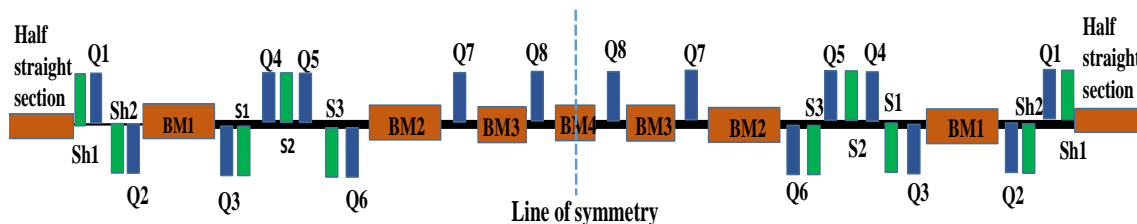


Fig. 4.19: Different magnetic elements of Indus-3 lattice (not to scale). Magnetic elements which are above base line are focusing in nature and below the base line are defocusing in nature.

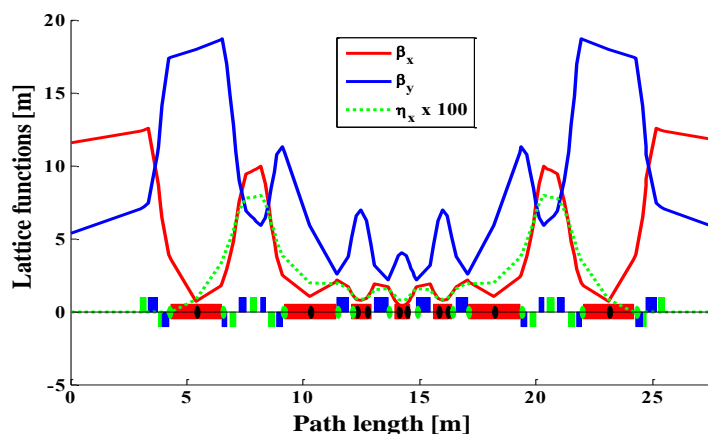


Fig. 4.20: Designed lattice functions of Indus-3 lattice.

Dipole magnets BM3 and BM4 are combined function dipole magnets, i.e., these magnets have quadrupole gradient along with dipole component. Dipole magnets BM1 and BM2 are homogeneous dipole magnets and are same. As BM3 and BM4 already have transverse gradient, hence it is difficult to include LGB because of technological challenges. Therefore, to study LGB for this lattice, dipoles BM1 and BM2 are chosen and similar logic as LGB in Indus-2 dipole can be applied. LGB profile for BM1 will be a decreasing profile. On the other hand, for BM2 it will be reversed, i.e., a increasing LGB profile to shape the dispersion function. The length of the dipoles BM3 is 2.17 m and it bends a charged particle by an angle

1.74°. In this case also, dipole magnet is divided into 5 equal sections and LGB profile is optimized using single objective genetic algorithm with maximum magnetic field 0.45 Tesla in the first section.

After optimization, magnetic fields in each section of dipole are

$$B = [0.4500 \quad 0.3167 \quad 0.2430 \quad 0.2008 \quad 0.1899][\text{Tesla}].$$

The optimized LGB profile is shown in Fig.4.21 and compared with homogeneous magnetic field, i.e., 0.28 Tesla.

This LGB profile will change the distribution of dispersion function in the lattice and the achromatic condition will be lost. Therefore, strength of quadrupoles are needed to be optimized.

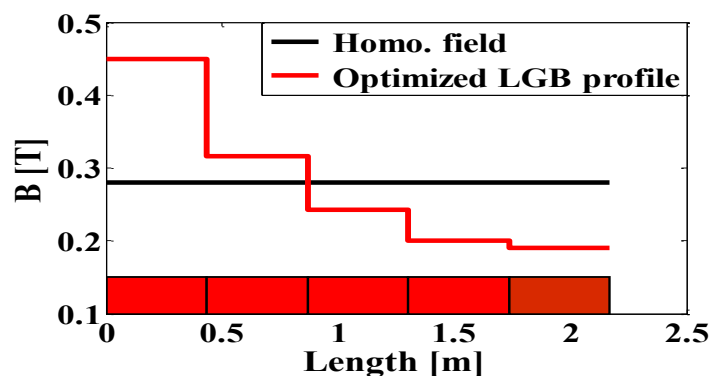


Fig. 4.21: Optimized LGB profile.

### 4.3.1 Matching of lattice function with quadrupoles

To match lattice functions and other constraints like betatron tune, stability condition, limit on maximum beta function, etc., quadrupole strengths must be optimized. This optimization problem is solved using MOGA, in which three objective functions are chosen which are: (i)  $f_1$ : emittance, (ii)  $f_2$ : dispersion function at straight section, (iii)  $f_3$ : dispersion at focusing sextupole location. Quadrupoles used in Indus-3 lattice have large gradient compared to Indus-2

lattice. Therefore, Indus-3 is a very tight focusing machine and betatron tune, lattice function etc. are much sensitive compared to Indus-2. Therefore, all quadrupole family, i.e., Q1, Q2, Q3, Q4, Q5, Q6, Q7, Q8 and quadrupole gradient in BM3 and BM4 are chosen for matching of lattice function and other important parameters. The limit on strengths of quadrupoles is chosen as  $4.2 \text{ m}^{-2}$  and for quadrupole gradient in BM3 and BM4 it is chosen as  $2.2 \text{ m}^{-2}$ .

The multi-objective optimization problem can be defined as

$$\begin{aligned}
 & \text{Minimize } \vec{f}(\vec{k}) = (f_1, f_2, -f_3), \\
 & \text{with constraints} \\
 & \quad |(\vec{k})_i| < 4.2 \text{ m}^{-2}; i = 1, 2, \dots, 8, \\
 & \quad |(\vec{k})_i| < 2.4 \text{ m}^{-2}; i = 9, 10, \\
 & \quad |\text{Trace}(M)| \leq 2, \\
 & \quad \beta_{x,y,max} \leq 20\text{m}, \\
 & \quad 0.75 \leq \text{fractional } \nu_{x,y} \leq 0.9 \quad \text{or} \quad 0.1 \leq \text{fractional } \nu_{x,y} \leq 0.3, \\
 & \quad |\beta_{x,inj} - 11.6| < 2.5 \quad \text{and} \quad |(\beta_{y,inj} - 5.34)| < 1.5, \\
 & \quad |\beta_{x,sym} - 0.4| < 1 \quad \text{and} \quad |\beta_{y,sym} - 4.3| < 1,
 \end{aligned} \tag{4.4}$$

Number of generation and number of population to run the MOGA code are 200 and 500 respectively. The large number of population are chosen to get more number of solution that satisfy constraints. To give a search direction to MOGA, initial values of strength of quadrupoles are chosen. Initial values of quadrupole strengths and quadrupole component in BM3 and BM4 are

$$\begin{aligned}
 k_0 = & [2.0369 \quad -2.1406 \quad -2.6000 \quad 2.1141 \quad 3.5617 \\
 & -2.7373 \quad 3.0327 \quad 3.6775 \quad -2.2 \quad -2.0][\text{m}^{-2}].
 \end{aligned}$$

After optimization, Pareto optimal front between emittance and dispersion at straight

section with color bar for dispersion at focusing sextupole location are shown in Fig. 4.22. It can be seen that each objective is conflicting in nature, i.e., one has to choose a solution judiciously. As dispersion at focusing sextupole increases, achromatic condition not satisfied and emittance is also increased. Emittance in each case is in the range 136 to 140 pm.rad, which shows the advantage of LGB dipoles. In MOGA, large number of solutions are generated, which are all optimal with given constraints. For each solution, beta function at injection, natural chromaticity, betatron tune and maximum beta function are calculated and are shown in Fig. 4.23, Fig. 4.24, Fig. 4.25, and Fig. 4.26.

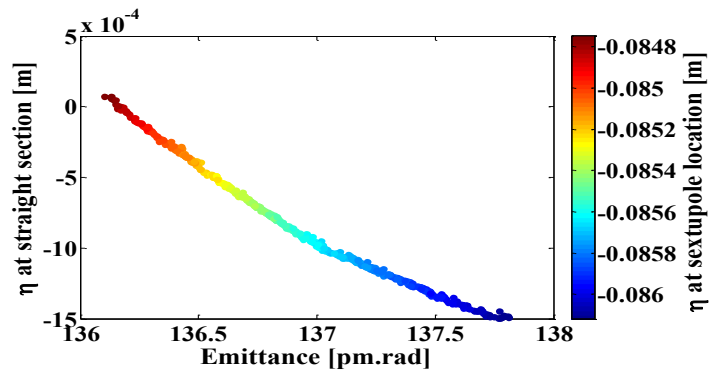


Fig. 4.22: Pareto optimal front for emittance with dispersion at straight section.

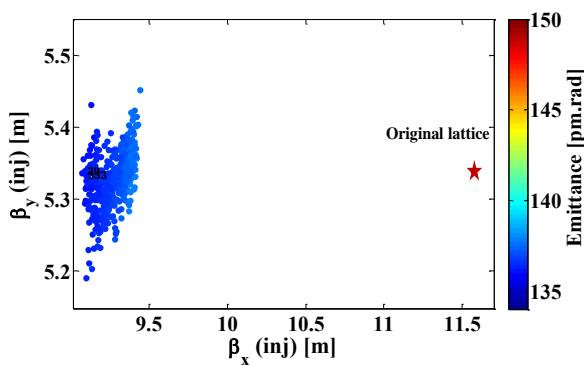


Fig. 4.23: Horizontal and vertical beta functions comparison for each solution.

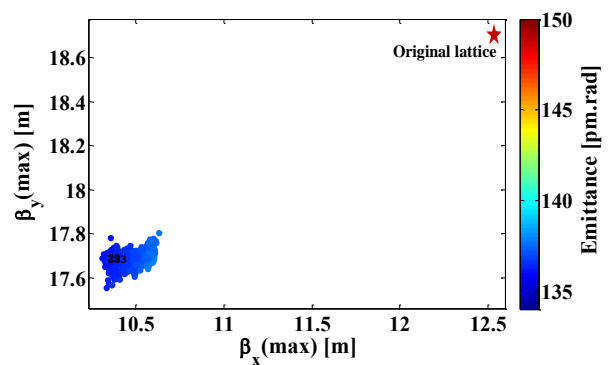


Fig. 4.24: Maximum horizontal and vertical beta functions comparison for each solution.

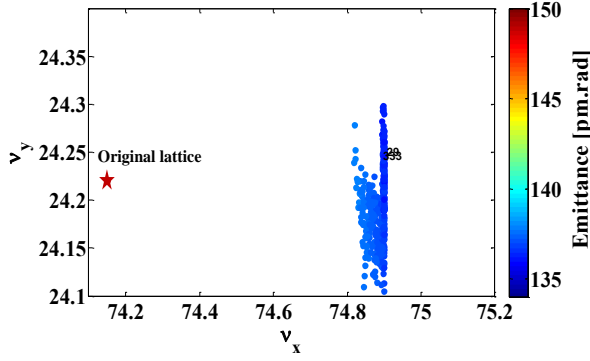


Fig. 4.25: Horizontal and vertical betatron tune comparison for each solution.

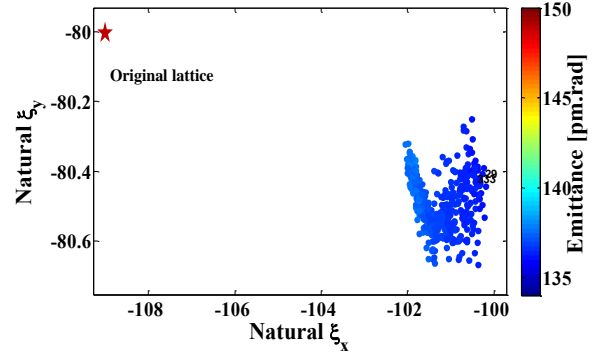


Fig. 4.26: Horizontal and vertical natural chromaticity comparison for each solution.

For each solution from MOGA, horizontal betatron tune increases from 74.2 to 74.8-74.9 which is acceptable, because it is away from resonances and vertical betatron tune is almost same to original lattice. Horizontal beta function at injection reduces from 11.5 m to 9-9.5m, which will require increase in the kicker strengths, but vertical beta function is close to original lattice. One advantage of low horizontal beta function is that beam size at IDs location will be low which is desirable. Maximum beta function is reduced for both planes by 2-2.5 m. Natural chromaticity in horizontal plane is decreased by an amount of 8, which is an advantage. Those solutions, for which dispersion at straight section is less than 0.0002 m are shown by numbers. There are only two solutions which satisfy it.

One of the solution, for which dispersion at straight section is near to zero, is given by

$$k = \begin{bmatrix} 2.1432 & -2.3929 & -1.9493 & 1.6595 & 3.8988 \\ -3.0263 & 3.1920 & 3.8916 & -2.1680 & -2.2908 \end{bmatrix} [\text{m}^{-2}].$$

For this optimized values of quadrupole strengths, betatron tune is [74.9, 24.25]. After correction of betatron tune to [75.2, 24.2] with Q1 and Q2, the strength of Q1 changes from 2.1432 to 2.1627 and strength of Q2 changes from -2.3929 to 2.4044  $\text{m}^{-2}$ , i.e., a small increase in these two quadrupole strengths. Using these strengths, variation of different lattice functions

after betatron tune correction are shown in Fig.4.27, Fig.4.28 and Fig.4.29 and comparison of different lattice parameters are shown in Table.4.2

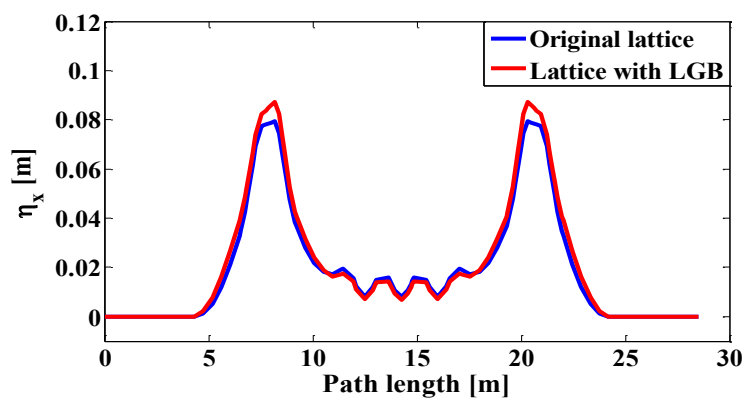


Fig. 4.27: Comparison of dispersion function.

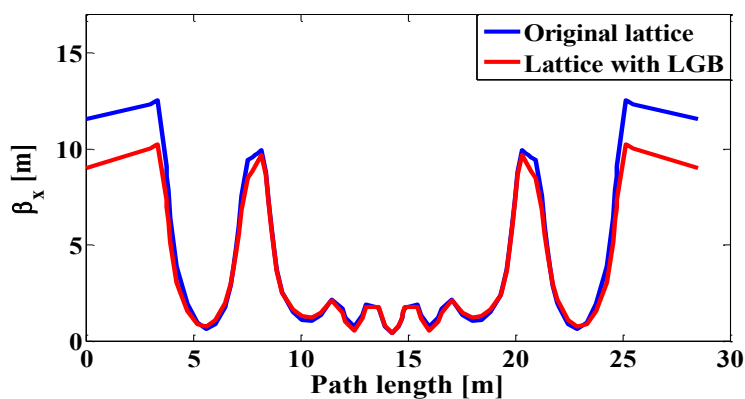


Fig. 4.28: Comparison of horizontal beta function.

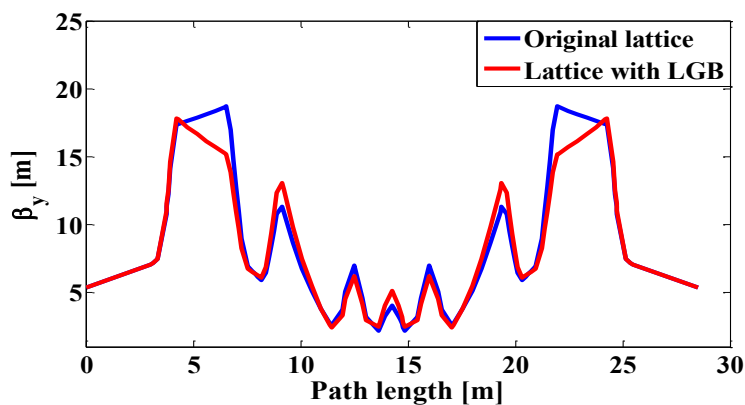


Fig. 4.29: Comparison of vertical beta function.

Though, these beta functions (lattice with LGB) are acceptable, but still there is a scope for further optimization.

Table 4.2: Comparison of Indus-3 lattice with LGB with original Indus-3 lattice.

S.No.	Parameters	Indus-3 (Original Lattice)	Indus-3 Lattice with LGB
1.	Energy (GeV)	6	6
2.	Momentum Compaction factor	$9.55 \times 10^{-5}$	$9.07 \times 10^{-5}$
3.	Emittance (nm-rad)	148.9	135.1
4.	Betatron tunes $[\nu_x, \nu_y]$	[74.15 , 24.22]	[75.2 , 24.2]
5.	Natural chromaticity	[-109.15 -80.94]	[-102.52 -80.81]
6.	Energy Loss per turn (MeV)	2.46	2.57
7.	Beta function at injection [m]	[11.57 5.34]	[9.1 5.3]
8.	Max. Beta function [m]	[12.54 18.71]	[10.3 17.7]
9.	Beta function at symmetric point [m]	[0.38 4.03]	[ 0.44 5.19]
10.	Dispersion at sextupole location [m]	0.078	0.085
11.	Required sextupole strength for chromaticity correction [4, 4] $[m^{-3}]$	[-89.5 118.79 -57.02]	[-90.95 118.53 -58.97]

Study of Indus-3 lattice with LGBs shows that emittance can be reduced by  $\sim 10\%$  without much affecting the lattice functions, betatron tune etc. Though natural chromaticity is reduced, but due to change in beta functions at sextupole location leads to a small increase in sextupole strength to correct the same level of chromaticity.

Though horizontal beta function is reduced at injection and sextupole strengths are increased a little bit, actual performance can only be predicted after dynamic aperture calculation which is given in the following Section.

### 4.3.2 Dynamic aperture

After correcting chromaticity to [4, 4] (horizontal and vertical) with sextupoles, dynamic aperture calculation is done by tracking of particles in the whole ring for 1000 turns. To calculate dynamic aperture, range of  $x$  is chosen from -15 mm to 15 mm in step size of 0.5 mm. On the other hand, range of  $y$  is chosen from 0 to 8 mm. The maximum range of  $x$  and  $y$  are chosen on the basis of physical aperture of vacuum chamber. Charged particle is tracked for 1000 turns in the grids and the boundary is decided on the basis of loss, i.e., after a certain point of the grid, charged particle is lost. In Fig.4.30, a comparison of dynamic aperture for Indus-3 lattice utilizing LGB dipoles and original Indus-3 lattice is shown. Nearly equal area is covered between both curves.

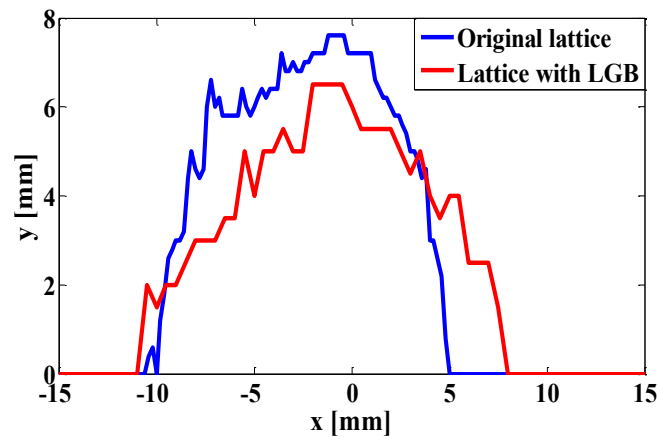


Fig. 4.30: Comparison of dynamic aperture for 1000 turns.

Though dynamic aperture is reduced a little in the vertical plane, but it is increased in the horizontal plane and this will help in off axis beam injection.

In this Chapter, Indus-2 and Indus-3 lattices which utilizes LGB dipole are optimized and different important parameters like betatron tune, lattice functions, chromaticity, dynamic aperture are analysed using single as well multi-objective techniques. The summary of this Chapter is given below.

For the case of Indus-2, using dipoles with LGB, emittance can be reduced  $\sim 33\%$  in the same ring with minimum hardware change if betatron tune is allowed to change by an integer and nearly  $25\%$  emittance reduced if same betatron tune is desired to nominal lattice. After introducing LGB brightness will increase by a factor of 2. As dispersion function at sextupole location increased from 0.7m to 0.8m, required sextupole strengths get reduced by  $16\%$  for focusing sextupole and  $13.8\%$  for defocusing sextupole for the same level of chromaticity correction, i.e., [2, 2].

For the case of Indus-3, using dipoles with LGBs, emittance can be reduced by  $\sim 10\%$  in the same circumference of the ring. Dynamic aperture area for on-momentum particles is almost the same as original lattice. Though a little decrease in vertical plane, but, there is an increase in horizontal direction which is required for off-beam injection (an advantage).

# Chapter 5

## Conclusion and future scope

Brightness of photon beam is one of the major aspect in designing or upgrading any SR source based on electron storage ring. An important beam parameter, called beam emittance, highly affects brightness of the photon beam and quality of beam, i.e., beam size. In order to increase brightness one has to improve beam emittance by some means. In recent years, advanced techniques like transverse gradient, longitudinal gradient bend (LGB), reverse or anti bend in a dipole have been studied and being used to improve the beam emittance. In this thesis work, an extensive study on optimization of LGB profiles has been presented. Further, new lattices have been designed by replacing homogeneous dipole of Indus-2 and Indus-3.

After discussing accelerator physics relevant to this thesis briefly, technologically challenging advanced methods (LGB and transverse gradient) to improve the beam emittance are discussed. In Chapter 2, the necessary numerical optimization techniques are described which are used to optimize a dipole with LGBs. In particular, single objective such as Nelder-Mead (a classical direct search method) and multi-objective optimization techniques such as genetic algorithm (GA) are discussed. Optimization studies of LGB profiles using dipole of Indus-2 are discussed in Chapter 3. Both techniques, i.e., Nelder-Mead and single objective genetic

algorithm have been used to generate different LGB profiles. New lattice for Indus-2 is designed by replacing homogeneous dipole with dipole with LGB. The introduction of LGB dipole changes the distribution of dispersion in the lattice due to unoptimized quadrupole strengths. Therefore, quadrupole strengths are optimized to match the lattice function and other important parameters. Using similar logic, dipole of Indus-3 is optimized for LGB profile and lattice functions and other important parameters are matched using all quadrupole families and quadrupole component in BM3 and BM4.

Beam emittance of Indus-2 reduced by  $\sim 30\%$  by introducing LGB in the dipole if betatron tune is allowed to change by integer and  $\sim 24\%$  with corrected betatron tune to nominal lattice. A study of Indus-2 in TME configuration is also carried out, which shows that emittance with LGB dipoles is reduced by less than half. Also, beam emittance of Indus-3 lattice reduced by  $\sim 10\%$  by introducing LGB in dipoles which shows major advantage of dipole with LGB over homogeneous dipole. In addition, LGB in dipole increases the dispersion at sextupole location, which decreases the sextupole strengths to correct the same level of chromaticity as of nominal lattice.

In this thesis, the studies of beam emittance reduction and optimization of lattice performance are presented in ideal case with LGBs. To model the LGB, we have considered the hard edge model, where fringing fields are ignored. In addition, for realistic magnetic lattice, error and analysis also need to be performed. In electron storage rings, the real advantage of LGB will be when we use anti-bends (dipoles with negative bending angles) [12]. This combination help decouple the distribution of beta and dispersion function. These studies will be carried out in future.

# Appendix A

## Derivations

### A.1 Equation of motion of an electron in a moving coordinate system

Equation of motion of a electron in a given magnetic field, in moving coordinate system can be written using Lorentz force law as

$$\frac{d\vec{P}}{dt} = e\vec{v} \times \vec{B}. \quad (\text{A.1})$$

Considering no magnetic field component in the longitudinal direction, i.e.,

$$\vec{B} = (B_x, B_y, 0).$$

Using this magnetic field and velocity  $\vec{v} = (v_x, v_y, v_s)$ ,

$$\vec{v} \times \vec{B} = -v_s B_y \hat{x} + v_s B_x \hat{y} + (v_x B_y - v_y B_x) \hat{s}.$$

Ignoring radiation generated by electron eq.(A.1) can be written as

$$\frac{d\vec{P}}{dt} = \gamma m_0 \frac{d^2 \vec{R}}{dt^2}. \quad (\text{A.2})$$

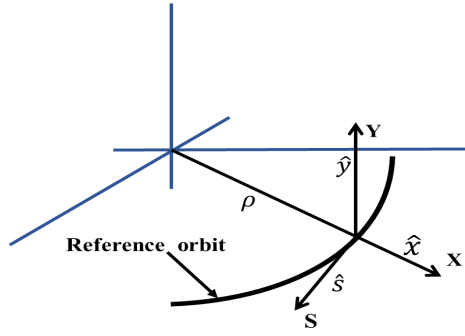


Fig. A.1: Frenet-Serret coordinate system.  $\hat{x}$ ,  $\hat{y}$  and  $\hat{s}$  are unit vectors in horizontal, vertical and longitudinal direction respectively.

Energy of the electron is constant, therefore  $\gamma$  will be a constant and  $m_0$  (a constant) is the rest mass energy of electron. Hence equation of motion becomes

$$\vec{R} = e\vec{v} \times \vec{B}.$$

$\vec{R}$  can be written as

$$\vec{R} = r\hat{x} + y\hat{y} \tag{A.3}$$

$$\vec{R} = \dot{r}\hat{x} + r\dot{\hat{x}} + \dot{y}\hat{y}. \tag{A.4}$$

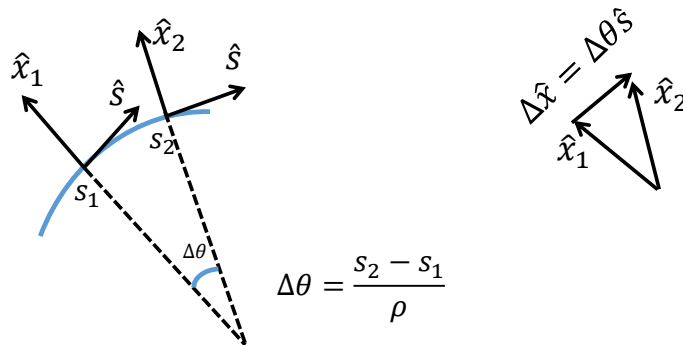


Fig. A.2: Change in unit vector in horizontal direction.

If, there is any motion in the s-direction, the unit vector  $\hat{x}$  will have a derivative, i.e.,  $\dot{\hat{x}}$ .

From Fig A.2, it can be seen that

$$\dot{\hat{x}} = \dot{\theta}\hat{s}, \quad (\text{A.5})$$

where  $\dot{\theta} = \frac{v_s}{r}$ . Therefore,

$$\dot{\vec{R}} = \dot{r}\hat{x} + r\dot{\theta}\hat{s} + \dot{y}\hat{y}, \quad (\text{A.6})$$

and differentiating one more time

$$\ddot{\vec{R}} = \ddot{r}\hat{x} + (2\dot{r}\dot{\theta} + r\ddot{\theta})\hat{s} + \ddot{y}\hat{y}. \quad (\text{A.7})$$

Using same argument as used to obtain  $\dot{\hat{x}}$ , we have

$$\dot{\hat{s}} = -\dot{\theta}\hat{x}, \quad (\text{A.8})$$

Therefore,

$$\ddot{\vec{R}} = (\ddot{r} - r\dot{\theta}^2)\hat{x} + (2\dot{r}\dot{\theta} + r\ddot{\theta})\hat{s} + \ddot{y}\hat{y}. \quad (\text{A.9})$$

Thus, equation of motion in the x-direction is

$$\ddot{r} - r\dot{\theta}^2 = -\frac{ev_s B_y}{\gamma m_0} = -\frac{ev_s^2 B_y}{\gamma m_0 v_s}. \quad (\text{A.10})$$

Since  $v_x \ll v_s$  and  $v_y \ll v_s$ , to a very good approximation, the total momentum  $p$  of the particle is  $\gamma m_0 v_s$ . So,

$$\ddot{r} - r\dot{\theta}^2 = -\frac{ev_s^2 B_y}{p}. \quad (\text{A.11})$$

Changing independent variable  $t$  to  $s$ , the derivative becomes

$$\frac{d}{dt} = \frac{ds}{dt} \frac{d}{ds}, \quad (\text{A.12})$$

Since,

$$ds = \rho d\theta = v_s dt \frac{\rho}{r}. \quad (\text{A.13})$$

Hence, assuming  $\frac{d^2 s}{dt^2} = 0$ ,

$$\frac{d^2}{dt^2} = \left(\frac{ds}{dt}\right) \frac{d^2}{ds^2} = \left(v_s \frac{\rho}{r}\right)^2 \frac{d^2}{ds^2}. \quad (\text{A.14})$$

Replacing  $r$  with  $\rho + x$ , the equation of motion becomes

$$\frac{d^2x}{ds^2} - \frac{\rho + x}{\rho^2} = -\frac{B_y}{B\rho} \left(1 + \frac{x}{\rho}\right)^2, \quad (\text{A.15})$$

where  $B\rho = \frac{p}{e}$ . A similar treatment yields for the equation of motion in the y-direction

$$\frac{d^2y}{ds^2} = \frac{B_x}{B\rho} \left(1 + \frac{x}{\rho}\right)^2. \quad (\text{A.16})$$

In general, these equations are non-linear. One can study these equation for linear case and non-linear terms can be treated as perturbation to these equations.

## A.2 Closed form solution

General equation of motion is given by

$$u'' + K(s)u = 0. \quad (\text{A.17})$$

This is the equation of harmonic oscillator with variable spring constant, i.e.,  $K = f(s)$ .

Though, spring constant is a function of independent variable  $s$ , for circular accelerators,  $K$  is periodic, i.e., there is a distance  $C$  such that

$$K(s + C) = K(s). \quad (\text{A.18})$$

The repeated distance of the hardware,  $C$ , may be as large as circumference of a synchrotron or it may be less. The general solution of equation of motion is given by

$$u(s) = A\sqrt{\beta(s)}\cos[\psi(s) + \delta], \quad (\text{A.19})$$

where  $A$  and  $\delta$  are the two constants of integration reflecting from initial conditions, and  $\beta(s)$  is also be a periodic function with periodicity  $C$ . Here, a similarity with harmonic oscillator can be noticed, when  $K$  becomes periodic function of position, the solution will differ from the

simple harmonic oscillator problem by a factor representing a spatially varying amplitude and a phase, which does not develop linearly with  $s$ .  $\beta(s)$  and  $\psi(s)$  can be found by substituting general solution into the differential equation. Differentiating  $u$  with respect to  $s$

$$u' = A \frac{\beta'}{2\sqrt{\beta}} \cos(\psi + \delta) - A\sqrt{\beta} \sin(\psi + \delta) \psi' \quad (\text{A.20})$$

and

$$u'' = A \frac{\beta\beta'' - \frac{1}{2}\beta'^2}{2\beta^{3/2}} \cos(\psi + \delta) - A \frac{\beta'}{\sqrt{\beta}} \sin(\psi + \delta) \psi' - A\sqrt{\beta} \sin(\psi + \delta) \psi'' - A\sqrt{\beta} \cos(\psi) \psi'^2. \quad (\text{A.21})$$

Inserting in eq.(A.17), we get

$$A \left[ \frac{\beta\beta'' - \frac{1}{2}\beta'^2}{2\beta^{3/2}} - \sqrt{\beta} \psi'^2 + K\sqrt{\beta} \right] \cos(\psi + \delta) - A \left[ \frac{\beta'}{\sqrt{\beta}} \psi' + \sqrt{\beta} \psi'' + \sqrt{\beta} \psi' \right] \sin(\psi + \delta) = 0. \quad (\text{A.22})$$

Since, it required that  $\beta$  and  $\psi$  are to be independent of  $\delta$ . So, coefficients of sine and cosine terms must vanish separately. Equating coefficient of sine term equal to 0, it gives

$$\beta\psi'' + \beta\psi' + \beta'\psi' = 0 \quad \text{or} \quad (\beta\psi')' = 0, \quad (\text{A.23})$$

eq.(A.23) can be solved further as

$$\psi' = \frac{Const.}{\beta(s)}, \quad (\text{A.24})$$

Where  $c$  is an arbitrary constant of integration. This arbitrary constant can be chosen as 1 for convenience.

$$\frac{1}{2}(\beta\beta'' - \frac{1}{2}\beta'^2) - \beta^2\psi'^2 + \beta^2K = 0 \quad (\text{A.25})$$

Using this relationship between  $\beta(s)$  and  $\psi$ , A.25 becomes

$$\frac{1}{2}\beta\beta' - \frac{1}{4}\beta'^2 + \beta^2K = 1. \quad (\text{A.26})$$

With the introduction of Courant-Snyder variables

$$\alpha = -\frac{1}{2}\beta' \quad \text{and} \quad \gamma = \frac{1 + \alpha^2}{\beta}, \quad (\text{A.27})$$

we can write eq.(A.25)

$$\beta'' + 2K\beta - 2\gamma = 0 \quad (\text{A.28})$$

Strictly speaking,  $\beta(s)$  need not be periodic; it only has to be a solution of the eq.(A.25). But if the motion we are trying to describe is that of a particle travelling through a periodic section of a accelerator, for instance through thousands of revolution about a circular accelerator, it is much more useful to choose the unique periodic solution for  $\beta(s)$ .

Using eq.(A.24), phase difference from a point  $s_0$  to  $s$  is given by

$$\psi = \int_{s_0}^s \frac{1}{\beta(s)} ds. \quad (\text{A.29})$$

For a complete ring, phase difference is given by

$$\mu = \psi_{ring} = \oint \frac{1}{\beta(s)} ds. \quad (\text{A.30})$$

We define betatron tune as

$$\nu = \frac{\mu}{2\pi} = \frac{1}{2\pi} \oint \frac{1}{\beta(s)} ds. \quad (\text{A.31})$$

Betatron tune tell us how many oscillation makes a charged particle in one revolution.

### A.3 Energy Loss

A relativistic electron when accelerated in a macroscopic force field will radiate electromagnetic energy. The rate of emission is proportional to the square of the accelerating force and depends on the angle between the force and the electrons velocity and is larger by the factor

$\gamma^2 = \left(\frac{E}{m_0c^2}\right)^2$  when the force is perpendicular to the velocity than when the force is parallel to the velocity. In a circular accelerator, the typical longitudinal forces (from the accelerating system) are much smaller than the typical transverse magnetic forces. Therefore, radiation effects that accompany by the magnetic forces are needed to consider only. The rate of loss of energy,  $P_\gamma$  by radiation can be written as

$$P_\gamma = \frac{2}{3} \frac{r_e c}{(m_0c^2)^3} E^2 F_\perp^2, \quad (\text{A.32})$$

where  $m_0, r_e$  are rest mass and classical electron radius of the electron respectively.  $F_\perp$  is the magnetic force on the electron. It is convenient to define a constant

$$C_\gamma = \frac{4\pi}{3} \frac{r_e c}{(m_0c^2)^3} \quad (\text{A.33})$$

For electron  $C_\gamma = 8.85 \times 10^{-5} [m.GeV^{-3}]$ . Since  $F_\perp = ecB$ , the radiated power is given by

$$P_\gamma = \frac{e^2 c^3}{2\pi} C_\gamma E^2 B^2. \quad (\text{A.34})$$

This shows that instantaneous power is proportional to the square of both the energy and the local magnetic field strength. It is sometimes useful to express the magnetic force in terms of the local radius of curvature  $\rho$  of the trajectory; then

$$P_\gamma = \frac{cC_\gamma}{2\pi} \frac{E^4}{\rho^2} \quad (\text{A.35})$$

An electron circulating on the design orbit has the nominal energy  $E_0$  and moves on the radius  $\rho = \frac{1}{G}$ . To find the energy  $U_0$  radiated in one revolution, we must integrate  $P_\gamma$  with respect to time once around the ring. Since  $dt = \frac{ds}{c}$

$$U_0 = \frac{C_\gamma E_0^4}{2\pi} \oint G^2(s) ds. \quad (\text{A.36})$$

We may write the integral as the mean of  $G^2$  multiplied by  $L = 2\pi R$ , the distance around the ring;

$$U_0 = C_\gamma^4 R \langle G \rangle. \quad (\text{A.37})$$

For an isomagnetic guide field  $G = G_0 = \frac{1}{\rho_0}$  along the curved path of the length  $2\pi\rho_0$  and zero everywhere. So,

$$\langle G^2 \rangle = \frac{G_0}{R} = \frac{1}{R\rho_0} \quad (\text{A.38})$$

and

$$U_0 = \frac{C_\gamma E_0^4}{\rho_0}. \quad (\text{A.39})$$

For a fixed radius, the energy radiated per turn varies as the fourth power of the electron energy.

# References

- [1] J. P. Blewett, Synchrotron radiation-1873 to 1947, Nuclear Instruments and methods in Physical Research A266, 1988.
- [2] H. Wiedemann, Particle Accelerator Physics, Third Edition, Spinger, 2007.
- [3] D. D. Bhawalkar, G. Singh, R. V. Nandedkar, Synchrotron radiation sources INDUS-1 and INDUS-2, Pramana-journal of physics, Vol. 50, No. 6, 1998.
- [4] Technical report of Synchrotron radiation source Indus-2, Center for Advanced Technology, Indore, India (1998).
- [5] R. Husain, Optimization and modelling of storage ring lattices: A case study of Indus-2 storage ring (PhD thesis), 2018.
- [6] T. Pulampong, Ultra low Emittance Lattice Design for Advanced Synchrotron Light Sources (PhD thesis), 2015.
- [7] L. Dallin, W. Wurtz, Towards a 4<sup>th</sup> generation storage ring at the Canadian Light Source, AIP Conference Proceedings, 2016.
- [8] S.C. Leemann, W.A. Wurtz, Pushing the MAX IV 3 GeV storage ring brightness and coherence towards the limit of its magnetic lattice, IPAC2017.

- [9] Chun-xi Wang, Minimum emittance in storage rings with uniform or nonuniform dipoles, PHYSICAL REVIEW SPECIAL TOPICS - ACCELERATORS AND BEAMS, USA, 2009.
- [10] J. Guo, T. Raubenheimer, Low emittance  $e^-/e^+$  storage ring design using bending magnets with longitudinal gradient, Proceedings of EPAC 2002, Paris, France.
- [11] A. Streun, A. Wrulich, Compact low emittance light sources based on longitudinal gradient bending magnets, Nuclear Instruments and Methods in Physics Research Section A, Vol. 770, pages 98-112, 2015.
- [12] A. Streun, The anti-bend cell for ultralow emittance storage ring lattices, Nuclear Instruments and Methods in Physics Research Section A, 2013.
- [13] Detailed Design Report on the MAX IV facility, *https://www.maxiv.lu.se/accelerators-beamlines/accelerators/accelerator-documentation/max-iv-ddr*.
- [14] J. L. Laclare, in Proceedings of Particle Accelerator Conference, Washington, DC, USA, 1427(1993).
- [15] M. Hara, Nucl. Instrum. Methods in Phys. Res. A 448, 12 (2000).
- [16] R.E. Gerig, J.M.Gibson, D.M.Mills, et al., Nucl. Instrum. Methods in Phys. Res. A 649, 1 (2011).
- [17] A. Jackson, in Proceedings of the Particle Accelerator Conference 1993, 1432(1993).

- [18] C. J. Bocchetta, D. Bulfone, F. Daclon, et al., in Proceedings of the European Particle Accelerator Conference 1994, 579 (1994)
- [19] CERN Proceedings, Vol-1, 1994.
- [20] S. Y. Lee, Accelerator Physics, Second Edition, World Scientific, 2007.
- [21] J. D. Jackson, Classical Electrodynamics, Third Edition, Wiley, 2017.
- [22] A. Wolski, Beam Dynamics in high energy particles accelerators, Imperial Collage Press, 2014.
- [23] M. Sands, The physics of electron storage rings an introduction, SLAC-121, 1970.
- [24] A. Streun, Practical Guidelines for Lattice Design, PSI, 1999.
- [25] K. Deb, Multi-Objective Using Evolutionary Algorithms, Wiley, 2018.
- [26] Michael Baudi, Nelder-Mead User's Manual, April 2010.
- [27] J. C. Lagarias, J. A. Reeds, M. H. Wright, and P. E. Wright, Convergence properties if the Nelder-Mead simplex method in low dimensions, SIAM J. OPTIM., Vol. 9, No. 1, pp. 112-147, 1998.
- [28] [http : //www.scholarpedia.org/article/Nelder – Mead – algorithm.](http://www.scholarpedia.org/article/Nelder-Mead-algorithm)
- [29] S. Kirkpatrick, C. D. Gelatt, M. P. Vecchi, Science, New Series, 220 (4598), 671(1983).
- [30] J. Kennedy, R. Eberhart, in Proceedings of the fourth IEEE International Conference on Neural Networks, Perth, Australia (1995).

- [31] S. Das, A. Abraham, A. Konar, Studies in Computational Intelligence (SCI) 116, 1(2008).
- [32] R. Storn, K. Price, Journal of Global Optimization 11, 341(1997).
- [33] A. Terebilo, Accelerator Tool Box for MATLAB, SLAC-PUB-8732, 2001.
- [34] Gaël Le Bec, Joel Chavanne, François Villar, Chamseddine Benabderrahmane, Simone Liuzzo, Jean-François Bouteille, Loys Goirand, Laurent Farvacque, Jean-Claude Biasci, and Pantaleo Raimondi, Magnets for the ESRF Diffraction-Limited Light Source Project, IEEE Transactions on applied superconductivity, VOL. 26, NO. 4, 2016.
- [35] T. Zhang, X. Huang, Numerical optimization of a low emittance lattice cell, Nuclear Instruments and Methods in Physics Research Section A, Volume 923, Pages 55-63, 2019.
- [36] D. A. Edwards, M. J. Syphers, An introduction to the physics of high energy accelerators, Wiley, 2004.
- [37] M. Aiba, M. Böge, M. Ehrlichman, A. Streun, Magnetic field of longitudinal gradient bend, Nuclear Inst. and Methods in Physics Research, A (892) 2018.